DEVELOPING NOVEL MANNOSE-BINDING LECTIN THERAPIES TO PREVENT, DIAGNOSE AND TREAT INFECTIONS IN CHILDREN

THESIS FOR THE DEGREE OF

DOCTOR OF PHILOSOPHY

UCL

KERRY-ANNE KITE

INFECTION, IMMUNITY, AND INFLAMMATION

UCL INSTITUTE OF CHILD HEALTH

DECLARATION:

The following people contributed to the work presented in this thesis:

In Part I, the FcMBL beads were designed and manufactured at the Wyss institute, Harvard, USA and shipped to use for the purpose of this study. Heat map and cluster analysis of the FcMBL spectra were performed by Sahil Loomba and Dr Thomas Elliott; Appendix B, which details the methods used for this, was written by them as part of a forthcoming publication on the FcMBL bead method and reproduced here with their consent. Clinical Sepsityper samples were performed as part of routine diagnostics by the Great Ormond Street Hospital (GOSH) clinical microbiology staff.

In Part II, Chapter seven, the biofilms samples were prepared for SEM imaging by Dr Mark Turmaine of UCL.

Patients used in Chapter eight were recruited by the DIAMONDS study staff. Serum samples were aliquoted for this study by the DIAMONDS study staff. Clinical information including patient demographics were collected for this study by the DIAMONDS staff. For the patients that were recruited from GOSH, their clinical information was collected and provided by Dr Gabriella Shanks, Dr Louis Grandjean and Dr Justin Penner. In Chapter eight the design of the MBL neutralisation assays for SARS-CoV-2 were designed by myself, from discussions with Dr Dagmar Alber, Professor Nigel Klein, Dr Claire Smith, and Dr Sam Ellis. The neutralisation experiments were carried out in the Royal Free Category Three Laboratory by Dr Sam Ellis and myself. The neutralisation data was analysed by myself. Statistical analysis was performed with help from Dr Thomas Elliott.

I, Kerry-Anne Kite confirm that the work presented in this thesis is my own. Where information has been derived from other sources, I confirm that this has been indicated in the thesis.

Signed:

Kerry-Anne Kite

ABSTRACT:

This thesis concerns the extensive properties of the immune molecule mannose-binding lectin (MBL). The work centres around the broad-range sugar recognition properties of MBL for microbes, with an emphasis on bacterial, yeast and viral infections. This thesis focuses on translational research in particular on the integration of MBL into the clinic to provide more effective diagnostic tools and therapies for childhood diseases.

In Part I of this thesis, we utilise the properties of MBL to bind, concentrate and rapidly diagnose infections using mass spectrometry. We found that MBL molecules conjugated to magnetic beads are effective at binding a wide range of different pathogens within blood samples. We further found that the beads are able to enrich the samples by significantly increasing concentrations and reducing host background. We compared this approach with the rapid diagnosis method currently in use at GOSH's clinical microbiology. We observe that the MBL-based method is more successful at identifying yeast infections than the current standard and is equally as effective at detecting bacterial infections.

Part II addresses the potential of MBL therapy to prevent and treat chronic infections, particularly biofilms. Biofilms are associated with increased mortality and morbidity rates, as well as an increased risk of antimicrobial resistance development. We show that MBL is able to bind bacteria and reduce the formation of these biofilms, and also enhances the immune response to established biofilm infections. The final chapter of this thesis focuses on the role of MBL in protection against the novel severe-acute respiratory syndrome coronavirus 2 (SARS-CoV-2). In particular we show that MBL deficiency or low MBL serum levels may be a risk factor in the development of paediatric multisystem inflammatory syndrome temporally associated with SARS-CoV-2 (PIMS-TS), an inflammatory syndrome appearing in response to SARS-CoV-2 infection observed in children. We observed significant reductions in SARS-CoV-2 binding to lung epithelium when using MBL mixtures previously prepared and tested in the clinic.

IMPACT STATEMENT:

This thesis has impact that spans several fields of academic and clinical medicine, covering the rapid diagnosis of infections and the prevention and treatment of viral and bacterial infections. Paediatric infections are difficult to diagnose and treat due the diverse and broad range of infections children can acquire. Moreover, in the clinic, sample size can be small and decreases the chances of a diagnosis with current microbiology laboratory methods. Compared to adults, children can become severely ill from low levels of pathogen, and in the case of blood stream infections bacteraemias in children can be too minute for conventional testing. Removing the host debris and blood for analysis of the pathogen is the major crux in rapid diagnosis using mass spectrometry. This thesis introduces a novel method to clean and enrich samples whilst simultaneously binding a broad range of microbes. This concentrating of microbes allows for rapid detection of infection in small samples with potential impacts on mortality rates as well as infection control.

We also demonstrated a novel treatment for chronic established infections i.e., biofilms which are a major issue, particularly in paediatric health care settings. The severe financial burden, increased resistance rates, and frequency of biofilm associated infections means that new alternative and adjunct antibiofilm therapies are urgently needed. We showed that use of a naturally produced protein of the innate immune system, mannose-binding lectin (MBL), can enhance the hosts immune system toward chronic infections and improve treatment. We also showed that MBL can aid in the prevention of the development of such infections.

The role of MBL in SARS-CoV-2 infection, particularly in a case study of children who become seriously ill after SARS-CoV-2 contact with a multi-organ inflammatory syndrome (now known as PIMS-TS) similar to Kawasaki disease was investigated. We found that MBL deficiency and low MBL levels were a potential risk factor in the development of PIMS-TS.

We have demonstrated that MBL is a potent and important regulator of homeostasis in humans. This thesis has thus demonstrated MBL may be suitable for rapid clinical diagnosis of infection and is a potential therapy for vulnerable children.

To Max, Coco, Boris, Bobbie, Basket, Billy, Minnie, Charlie, Dudley,

Maui, Thomas, Corkey, Barbie and all the other special ones

ACKNOWLEDGEMENTS:

I would like to thank the following people, without whom this thesis would not have been possible.

Firstly, the BENECARE Foundation, Liechtenstein, who provided generously to this project and to its continuation throughout the pandemic, alongside Luca and Pauline Albertini who have supported the continuation of MBL research.

My supervisor Professor Nigel Klein who always had kind words, anecdotes, and advice throughout and who continued to supervise his students even during the most difficult of times, for which we are extremely grateful and lucky. Dr Michael Super, his wife and family, and his team who greeted me so warmly and provided advice and support throughout this project. Thank you to Dr Dagmar Alber who supported all aspects of this thesis and provided invaluable technical support, especially for the biofilm and viral chapters. To Dr Elaine Cloutman-Green who took me under her wing and gave invaluable advice and opportunities which made this thesis possible. To Dr Sean Nair for his support and encouragement. Professor Steffen Thiel and his team at Aarhus, who provided reagents and advice which allowed this project to go the extra mile. Francis Yongblah and all of the Microbiology team at GOSH for teaching me invaluable microbiology techniques and providing me with samples which made this project possible. Erika Tranfield who provided invaluable MALDI-TOF MS technical support for this project. Dr Lizzie Robinson for her dedication to supporting me through tough times and always having a friendly face to run to. Sunando Roy, Ronan Doyle, Thomas Elliott and Lily Gates for regular pub trips and good times. To Wendy and Dave Elliott and the rest of the Chesterfield family for all of their love and support.

A special thank you to Dr Lily Gates who went from colleague to friend to bridesmaid providing endless support, friendship, and good times throughout my time at ICH which I will forever treasure. My husband Thomas Elliott whose dedicated support and patience whilst teaching me the statistics (and mathematics as a whole) necessary for this thesis as well as his continued love made this possible. Whose time in hospital during this PhD personally highlighted the need to continue building more efficient and effective tools for rapid diagnosis of blood stream infections for healthcare providers.

This thesis wouldn't have been possible without the continued and unwavering support of my father, mother, brother, and sister.

Finally, thank you to anyone and everyone who ever took the time to read this thesis.

Table of Contents

ABBREVIATIONS

ACN	Acetonitrile
BHI	Brain Heart Infusion
BSI	Blood Stream Infections
CFU	Colony forming units
CHCA	Cyano-4-Hydroxycinnamic Acid
CRD	Carbohydrate Recognition Domain
DHB	2,5-Dihydroxybenzoic acid
dH_2O	Distilled H_2O
ELISA	Enzyme-Linked Immunosorbent Assay
ELLecSA	Enzyme-Linked Lectin-Sorbent Assay
FA	Formic Acid
FcMBL	Fragment Crystallisable Region conjugated to Mannose-Binding Lectin
GlcNAc	N-acetylglucosamine
HBSS	Hank's Buffered Salt Solution
HCCA	α-Cyano-4-hydroxycinnamic acid
I/R	Ischemia/Reperfusion
LB	Luria Broth
MAC	Membrane Attack Complex
MALDI	Matrix-Assisted Laser Desorption Ionisation
MBL	Mannose-Binding Lectin
MIC	Minimum Inhibitory Concentration
MS	Mass Spectrometry
MAp	MBL-Associated Protein
MASP	MBL-Associated Serine Protease
m/z	Mass-To-Charge Ratio
PAMP	Pathogen-Associated Molecular Pattern
PB	Peripheral blood
PBS	Phosphate Buffered Saline
PCR	Polymerase Chain Reaction
pdMBL	Plasma-Derived Human Mannose-Binding Lectin
PFA	Paraformaldehyde
PFU	Plaque Forming Units
PMF	Peptide Mass Fingerprint
PRM	Pattern Recognition Molecules
rMBL	Recombinant Human Mannose-Binding Lectin
RPM	Revolutions per minute
RT	Room temperature
SEM	Scanning electron microscopy
SNP	Single Nucleotide Polymorphism
TBST	Tris Buffered Saline with Tween
TFA	Trifluoroacetic Acid
TOF	Time-of-flight
TTP	Time To Positivity

LIST OF FIGURES:

LIST OF TABLES:

CHAPTER ONE

INTRODUCTION

1.1. BACKGROUND TO THIS THESIS

Blood stream infections (BSIs) are a major burden in the paediatric population and are a leading cause of infant mortality [1]. Due to advances in treatment therapies there is an increasing patient population of children who are at risk of nosocomial infections from which they suffer significant morbidity and mortality [2]. Resistant bacteria are found with increasing frequency in children including methicillin-resistant *Staphylococcus aureus* (MRSA). Resistant infections arise more frequently in the oncology and intensive care units due to the empirical use of broad-spectrum antibiotics and current difficulties in rapid and accurate diagnosis [3]. Co-infections or secondary infections due to viruses are a major problem in the paediatric community resulting in severe respiratory infections and septicaemia [4]. Within the lung and other areas of the host, bacteria can form biofilms, particularly in those with compromised barriers or reduced ciliary clearance such as cystic fibrosis (CF). Biofilms are notoriously difficult-to-treat communities of pathogens which encase themselves in a self-produced matrix [5]. Some can require up to three orders of magnitude more antibiotic to clear, resulting in an increased risk of resistance if too low a dose is prescribed [6]. Rapid diagnosis of vulnerable individuals is crucial and can provide quick, effective, and more targeted treatments with narrow-spectrum therapies, as well as easing economic burden. Diagnosing and clearing these infections in the paediatric community is a perennial problem and an increasing concern with the rise in bacterial resistance within these communities. There is a growing urgency for rapid diagnosis and alternative treatments to fight these infections and understanding the host immune responses to pathogens can help provide insight into more effective therapies for these patients. This is also the case with novel viruses which we have experienced during this project. The spread of SARS-CoV-2 and the associated novel disease PIMS-TS has shed light on the importance of innate immunity and its key role in control of viral infections. This thesis is centred around the broad range recognition capability of mannose-binding lectin (MBL) and its potential to assist healthcare providers in tackling the above problems. This thesis is divided in two: firstly, examining genetically-engineered MBL as a potential diagnostic tool to capture and enrich clinical samples; secondly to evaluate the use of MBL as an alternative or adjunct to antimicrobial therapy in childhood infections, with a focus on bacterial biofilms and viral infections in childhood.

1.2. THIS THESIS

The work in this thesis centres on the broad range recognition properties of MBL which ties together all of the work undertaken in each of the research chapters. This covers translation research, taking the science behind MBL binding and translating this into clinical impact. Some of the projects undertaken in this thesis focus on MBL in the rapid diagnosis of infection, and others on MBL therapy to prevent and treat infections, two distinct areas. Thus, we have divided this thesis in two; Part I explores the utilisation of FcMBL beads to enhance rapid diagnosis of infections in children. Part II investigates the role and potential use of MBL reconstitution in the prevention and treatment of bacterial and viral infections (Figure 1).

- Chapter two introduces the requisite background to MBL and discusses the relevant research history.

Part I: FcMBL in clinical microbiology

- Chapter three describes the current methodologies used in clinical microbiology.
- Chapter four details the methodology of Part I and experimental protocols for FcMBL.
- Chapters five describes the optimisation of FcMBL for the diagnosis of blood stream infections.
- Chapter six investigates the implementation of FcMBL beads into clinical diagnostics, focusing on positive blood cultures and comparing the FcMBL beads to the standard diagnostic techniques.

Part II: MBL as a therapeutic

- Chapter seven studies the use of MBL in the prevention and treatment of MRSA biofilms *in vitro*.
- Chapter eight investigates the relative MBL serum levels of patients with and without PIMS-TS as well as the role of MBL in the neutralisation of SARS-CoV-2 *in vitro*.

We conclude in Chapter nine with a final discussion of the implications of these results regarding the clinical impact of MBL in diagnosis and its potential as a novel therapeutic in the treatment of paediatric infections.

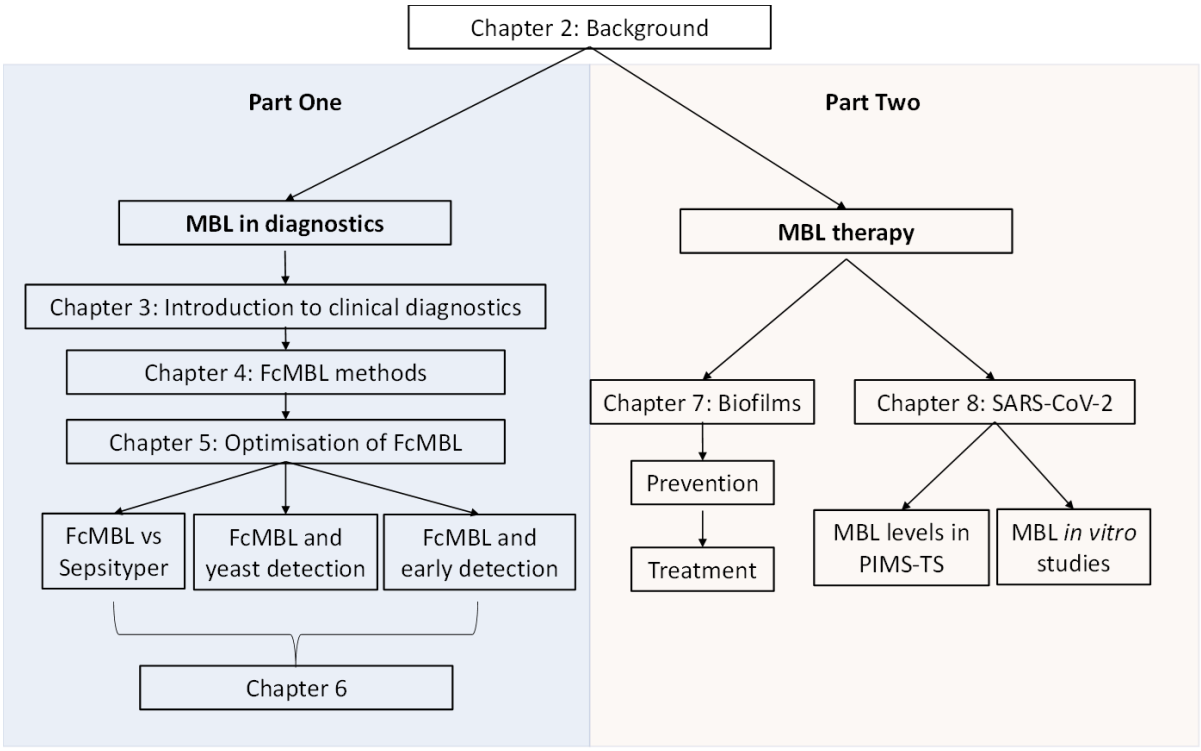

Figure 1: Thesis structure

CHAPTER TWO

BACKGROUND

2.1. IMMUNITY AND MEDIATORS OF THE HOST IMMUNE RESPONSE

The immune system defends the host from foreign (e.g., infection) and endogenous (e.g., cancer) noxious agents and to do this it needs the ability to distinguish between self and non-self or aberrant patterns. Once the distinction between self and non-self has been made, cells of the immune system known as lymphocytes are activated, which in turn activate antibody production to eventually destroy the target (Figure 2). Other lymphocytes can recognise the target directly and induce destruction. Thus, there are two major branches of the immune system, known as cell-mediated immunity and antibody-mediated immunity (humoral immunity), respectively. Advancements in the understanding of the immune system have been fuelled by the desire to prevent and treat the unwell.

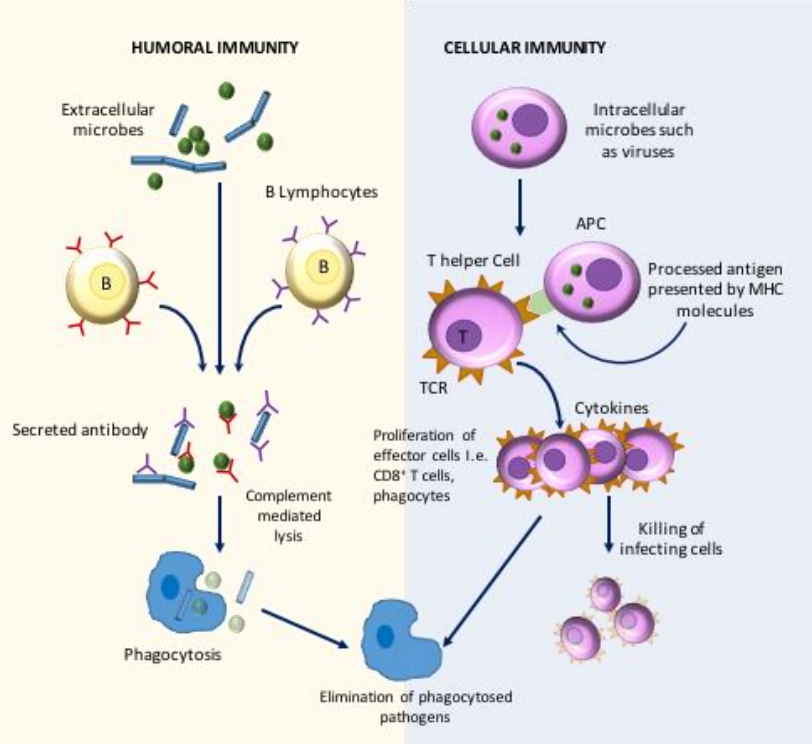

Figure 2: A representation of the differences between the humoral (left) and cellular immunity (right) pathways. APC=Antigen presenting cell.

2.2. INNATE IMMUNITY

The innate immune response is complex, and one of the oldest components of the immune system. It consists of barriers against pathogens including epithelia, antimicrobial peptides, humoral components (i.e., complement) and cells (i.e., neutrophils, monocytes, macrophages, and dendritic cells). It is the first line of defence against infection, responding rapidly to conserved regions expressed on pathogens whilst tolerating normal host flora. The innate immune system is important for the initiation and development of the adaptive immune response, which has many differences (Table 1). Though there are major differences between innate and adaptive immunity, crosstalk between them is crucial for our health.

Table 1 The properties of the innate and adaptive immune response

Innate Immunity	**Adaptive immunity**
Rapid	Lag phase – response is not immediate
Differentiates self and non-self	Differentiates self and non-self
Broad range specificity	High specificity (limited range)
Lacks memory	Subsequent exposure results in an enhanced response

2.3. THE COMPLEMENT SYSTEM

The complement system is one of the most ancient forms of innate immunity that has three main arms to defend the host against infection. The complement system consists of a wide range of proteins in the blood, which circulate as zymogens. Complement can recognise both damaged cells and pathogens, and facilitates their safe clearance by either direct killing or stimulating phagocytosis [7]. The initiation of the complement cascade is broken down into three pathways: the classical, the lectin and the alternative pathways. All three pathways generate a C3 convertase which triggers the termination arm of the complement pathway (Figure 3).

2.3.1. THE CLASSICAL PATHWAY

The classical pathway is initiated by antibody-antigen complexes. The C1 complex consists of a single C1q, two C1r and two C1s subunits (Figure 3). C1r cleaves and activates the C1s which then allows for cleavage of C4 and C2 into the C3 convertase (C2aC4b) which cleaves C3. The C1q molecule is expressed by monocytes, macrophages and dendritic cells, as well as endothelial and epithelial cells [8]. It can be expressed as a cell membrane associated ligand or can be secreted by the cell. The C1q complex is a 460kDa collagen-like hexameric glycoprotein. C1q has six globular heads which are attached to a central fibril-like region by six collagen–like stalks. The C1q family of globular heads is attached to a central domain by collagen-like stalks which is seen in other proteins such as MBL which is important in the lectin pathway of complement.

2.3.2. THE LECTIN PATHWAY

It was originally believed there were only two arms of the complement pathway, the classical and alternative. The discovery of the lectin arm of the complement pathway in humans was made at the UCL Institute of Child Health (ICH) with the discovery of a lack of MBL in a cohort of chronically ill children [9]. The lectin pathway is similar to the classical pathway, though differing in the molecules involved (Figure 3). The lectin pathway is initiated by mannose-binding lectin (MBL), ficolins and other lectins such as surfactants found in the lung [10]. There are three main ficolins; the most common in circulation is H-ficolin, with M-ficolin and L-ficolin the other two forms [11]. The lectin family of proteins recognise different sugars and thus span a large range of microbial sugars which they can recognise, complimenting each other. The lectins all bind to MASPs with varying degrees of competition. Yet, it was shown that both free and ficolin bound MASPs will bind preferentially to MBL [12, 13].

2.3.3. THE ALTERNATIVE PATHWAY

Unlike the classical and the lectin pathways which require recognition of a specific target to activate, the alternative pathway is activated by spontaneous hydrolysis of the internal thioester bond in the C3 (Figure 3). C3 then splits into C3a and C3b, and the C3b binds to the microbe directly which facilitates the binding of Factor B. The C3bFactorB complex allows Factor D to cleave Factor B into smaller fragments Ba and Bb. C3bBb remains bound to the membrane and becomes the alternative pathway's C3 convertase [14]. Under homeostasis C3b remains bound to properdin. Properdin is a serum protein that is expressed by several immune cells and is regulated by inflammatory agonists such as TNFα, C5α and FMLP [15]. This release into the environment allows for local alternative pathway activation. Due to the spontaneous hydrolysis of C3, the alternative pathway needs to be tightly controlled [16].

2.3.4. THE TERMINAL LYTIC PATHWAY

The terminal lytic pathway refers to the formation of the membrane attack complex (MAC), also known as the soluble terminal complement complex (TCC). The first step of the pathway is the formation of the C5 convertase which is formed either by the classical and the lectin pathway (C4bC2aC3b) or the alternative pathway (C3bBbP). These cleave the C5 protein into C5a, which is a potent anaphylatoxin, and C5b, which is the initial component of the MAC (Figure 3). To form the transmembrane MAC lesion C5b then binds C6, C7, C8 and then C9 (Up to 18 C9 molecules can be used to form the MAC; not shown). It is only when C6 and C7 bind that the conformational change allows for the complex to be inserted into the membrane. This complex forms a pore in the cell membrane or wall of the target cell, which destroys the cell [17].

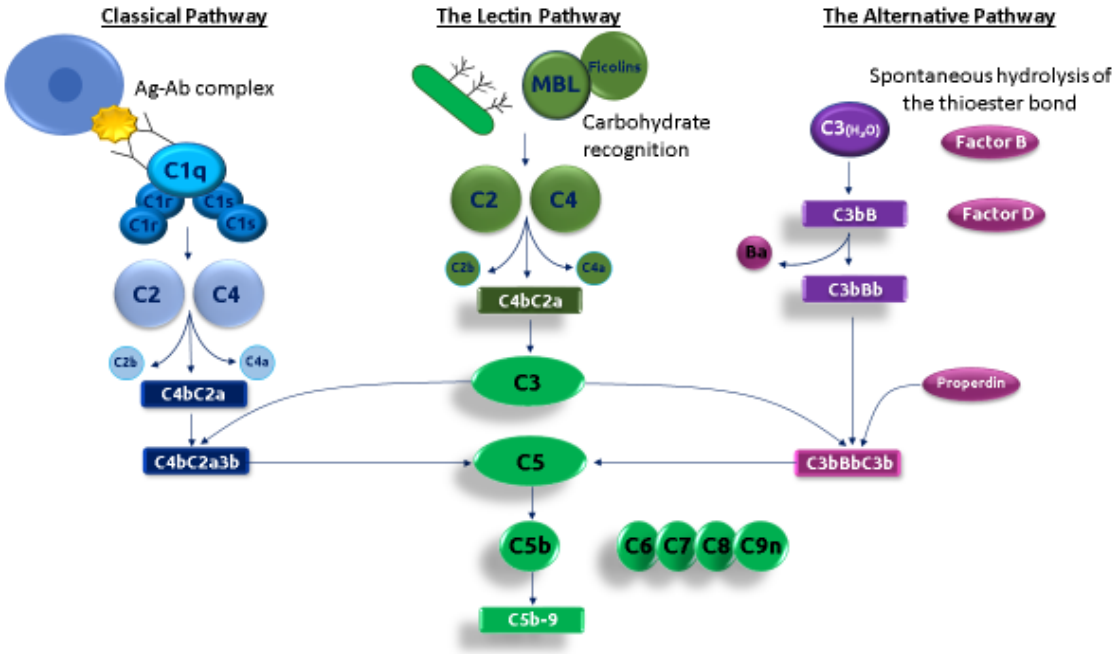

Figure 3: The three arms of the complement pathway: the classical (blue), lectin (green) and alternative (purple) pathways. The classical pathway is activated via antigen-antibody binding. The lectin pathway depends on microbial or aberrant carbohydrate recognition. The alternative pathway is activated without recognition of antigen or carbohydrate but instead by spontaneous hydrolysis of the C3 thioester bond.

2.4. MANNOSE-BINDING LECTIN

MBL is an important protein of the innate immune defence produced in the liver, achieving its function by enabling the deposition of complement on the surface of microbes [18]. MBL belongs to the C-type lectin family of collectins which function as pattern recognition molecules (PRMs) which play a pivotal role in our innate immunity and require calcium to function. MBL can recognise carbohydrate structures on the surface of a wide range of pathogens including bacteria, fungi, viruses, and protozoa, as well as pathogen-associated molecules such as endotoxins [19, 20]. Binding of MBL to cognate carbohydrate moieties results in activation of the lectin complement pathway and target destruction. Moreover, MBL is an important opsonin of the immune response, enhancing phagocytosis by neutrophils and macrophages thus playing a key role in clearing infection [21].

2.4.1. MANNOSE-BINDING LECTIN GENE STRUCTURE

In 1989 the gene structure of MBL was identified in chromosome 10q11.1-q21 (Figure 4) [22]. The human MBL gene (*MBL2*) encodes four exons interrupted by three introns 600, 1350 and 800 base pairs in size [23]. Exon 1 encodes for the signal peptide, a cysteine rich domain, and seven copies of a repeated glycine-Xaa-Yaa motif essential for the triple helix formation of collagen structures (Xaa and Yaa indicate any amino acid). Exon 2 also contains 12 glycine-Xaa-Yaa repeats and exon 3 encodes for the neck region. Exon 4 codes for the carbohydrate-recognition domain (CRD). There are three main single nucleotide polymorphisms (SNPs) in exon 1 of the *MBL2* gene found at codon 54 (rs1800450), 57 (rs1800451) and 52 (rs5030737), known as the B, C and D alleles respectively, with the wildtype allele (A). These mutations disrupt the collagen domain and affect MBLs ability to oligomerise [24]. Within the promoter region there are two main SNPs at -550 (H/L) (rs11003125) and -221bp (Y/X) (rs7096206), along with a SNP in the 5' UTR (+4P/Q). These promotor polymorphisms affect the secretion and plasma concentration levels of MBL (Figure 4). The combination of promoter and exon 1 polymorphisms form seven well-characterised secretor haplotypes (HYPA, LYPA, LYQA, LXPA, HYPD, LYPB, LYQC). The HYPA and LYQA haplotypes are associated with high MBL production, LYPA with intermediate-production, LXPA with low production, and LYPB, LYQC and HYPD defective or deficient haplotypes. Typical plasma levels of MBL varies between 10ng/ml and 10,000ng/ml and is largely determined genetically however, individuals with identical haplotypes can have an up to 10-fold difference in their plasma concentrations [25].

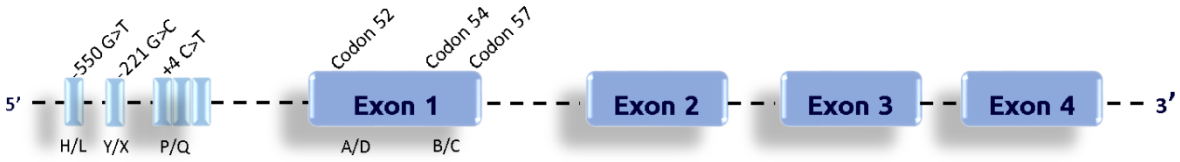

Figure 4: Structure of the *MBL2* gene. Dark blue indicates the exons and light blue represents the promoter mutations.

2.4.2. MANNOSE-BINDING LECTIN STRUCTURE

MBL is synthesised as a single polypeptide which forms homodimers via its collagen-like domain of 32 kDa size (Figure 5). The protein circulates as oligomers of homotrimers forming higher order oligomers ranging from dimers to hexamers. Patients with recurrent infections were found to have one of three SNPs in exon 1 of *MBL2* (Figure 4) [26]. These SNPs were shown to disrupt the collagen helix and prevent its ability to form homotrimers and ultimately higher order oligomers (Figure 5). The ligand for MBL binding is dictated by the spatial orientation of the CRD, which differs between oligomers and suggests a reason for why different orders of oligomers circulate naturally i.e., to enhance the range of recognition. The micro-pattern and spatial geometry of the macro-patterns are what allows MBL to distinguish between host and infected or transformed cells [27]. MBL can activate complement by acting as a structural support between aberrant carbohydrate structures and MBL-associated serine protease (MASP) activation. When MBL binds abnormal carbohydrate patterns, it takes a new conformation enabling attached homodimers of MASP-1 to activate MASP-2 and initiate the complement pathway. MASP-2 is capable of causing the cleavage of C4 and C2 as well as MASP-1, MASP-3 and MAp19, and has been shown to enhance the pathway. It has also been shown that larger oligomers such as tetramers are superior in complement activation compared to trimers due to their stronger interactions with MASPs and MAp44 and also due to enhanced binding properties [12].

2.4.3. MBL-ASSOCIATED SERINE PROTEASES (MASPS)

MBL-associated serine proteases are essential for complement activation of the lectin pathways. They are secreted into the blood stream and bind the collagenous regions of MBL and other lectins. MASP-2 is expressed in the liver, regulated by STAT3, IL-1β and IL-6. It binds in a calcium-dependant manner to MBL and ficolins as a homodimer and has an epidermal growth factor-like domain through which it binds [28, 29]. Though MASP-2 is capable of activating the lectin complement pathway, MASP-1 is needed for MASP-2 activation in physiological conditions and thus MASP-1 is also essential for activation of the lectin pathway [30-33]. Complement activation is induced after binding of the lectin and conformational changes in its structure [34]. This in turn

activates MASP-1, a zymogen that allows for the activation of MASP-2 which then cleave the C4 complement protein. Both MASP-1 and MASP-2 bind and cleave C2, which permits the formation of the C3 convertase (Figure 3) [35-37]. MASP-2 also has a key role in the coagulation cascade by cleaving prothrombin [38]. Levels of 400-500ng/ml are found in healthy individuals and have been shown to stay stable; however, levels lower than 100ng/ml are considered deficient [39-41]. Interestingly, despite its clear role in complement activation, high levels of MASP-2 have been associated with severe infections in adult patients undergoing chemotherapy for haematological cancer [42]. MASPs also play a key role in the coagulation pathway by activating platelets and inducing coagulation and thrombosis. This is seen in acute respiratory failure observed in severe disease cases [43],which has been observed in COVID-19 and with high levels of MASPs found in the lung during post-mortem (PM), this has led scientists to investigate the roles of MASPs in SARS-CoV-2 in more detail. MAp19 on the other hand is a truncated form of MASP-2 produced due to alternative slicing of the *MASP2* gene, lacking the serine protease activity. Secreted into the plasma from the liver and expressed at similar levels to MASP-2, only a small portion of Map19 is associated with MBL and ficolins, with a 10 times lower binding affinity compared with MASP-2 [44]. MAp19 has also been hypothesised to play a role in the prevention of renal stone formation via inhibition of calcium oxalate [44, 45]. Surprisingly, MAp19 interacts with the nucleocapsid of SARS-CoV-1, though the significance of this binding has yet to be determined [46].

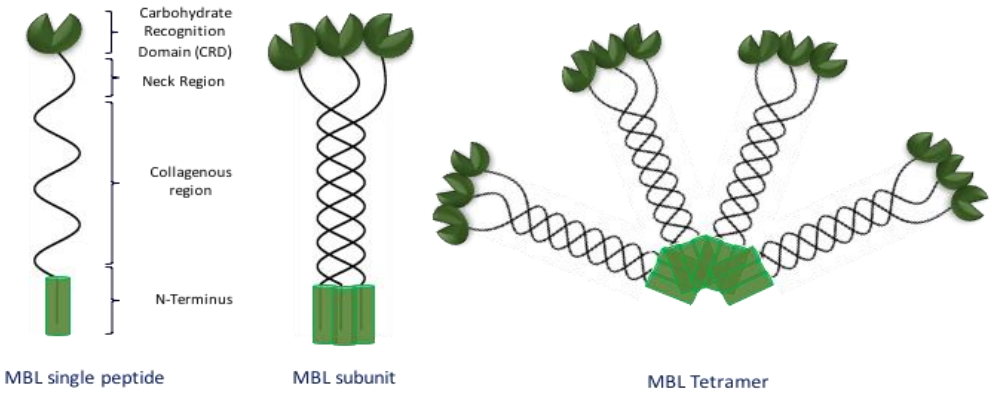

Figure 5: Mannose-binding lectin structure; MBL is synthesised as a single peptide (left) which forms homotrimers via interactions at the collagen region (middle). These homodimers go on to form higher-order oligomers ranging from dimers to hexamers (right).

2.4.4. MANNOSE-BINDING LECTIN FUNCTION

MBL is a potent activator of the lectin pathway of complement and an important opsonin. MBL has a particular affinity for polymeric sugars which are present on the surface of pathogens. The CRD has a single binding site for monosaccharides such as mannan, fucose or *N*-Acetylglucosamine (GlcNAc). This small interaction between the sugar and MBL is what enables MBL to recognise a broad range of targets [47]. Binding to cognate antigen induces a conformational change allowing for the activation of the MASP complexes, which in turn initiates the complement cascade and MAC formation. The production of C4a and C2b induces priming of phagocytic cells and enhances pathogen uptake and elimination. However, though it has been shown that MBL can function as an opsonin in the absence of complement proteins such as C3, the exact identity of the cellular receptors for the collagenous region are yet to be fully determined. One suggestion is that the complement receptor CD91 can recognise MBL as well as C1q [48]. Calreticulin and CD93 have also been suggested as potential receptors for MBL as well as complement receptor 1 [48-50].

2.4.5. MANNOSE-BINDING LECTIN DEFICIENCY

The threshold for MBL deficiency presently lacks a standard definition in the literature. Furthermore, MBL is still produced (albeit in very small amounts) in those with deficiency related mutations, though they are usually unable to form oligomers and instead circulate only as single peptides. Extreme deficiency is typically defined by serum levels <100ng/ml [51], though deficiency in general lacks such a consistent characterisation in the literature. Levels below 400ng/ml have been shown to be unable to activate the complement pathway [52]. Nevertheless, different thresholds have been used in various studies, ranging from as low as <50ng/ml, up to <1300ng/ml [53]. The mutations discussed, which affect the circulating and functional levels of MBL, correlate closely with the serum levels produced allowing genotype to be identified by phenotype [54].

2.4.6. GLOBAL MANNOSE-BINDING LECTIN LEVELS

Since the discovery of human MBL in 1989, a variety of different promoter and gene mutations have been discovered. These variations are found more frequently in different regions, suggesting selective pressure for the differences (Figure 6). One study found that the concentration of MBL was 5 times lower in Africans than in Eskimos and showed that deficient or low MBL levels are found in approximately 30% of the African population compared to 5-7% in the Caucasian population [55].

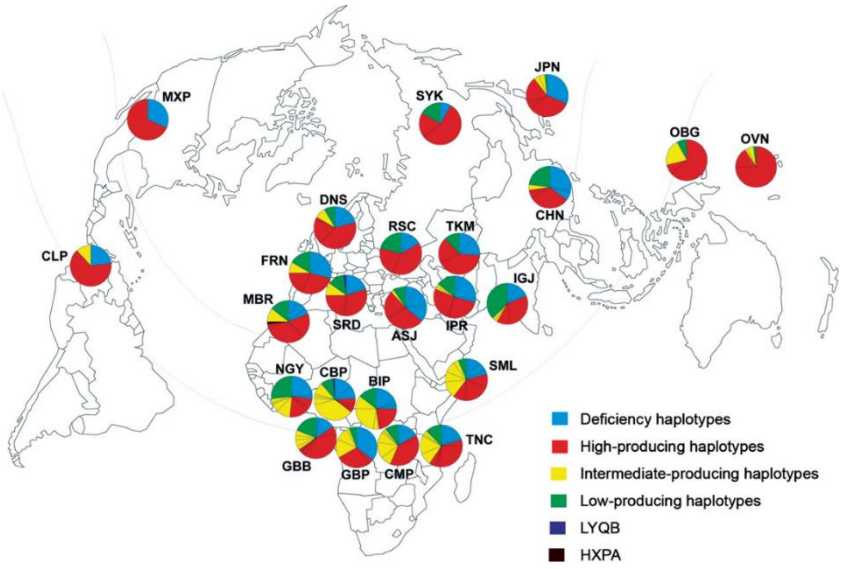

Figure 6: Worldwide distribution of *MBL2* haplotypes (taken from Verdu et al 2006)

2.4.7. MANNOSE-BINDING LECTIN IN CHILDREN

Maternal IgG is passed to the child during the final trimester of the pregnancy via the placenta (Figure 7). Serum immunoglobulins quickly wane after birth, leaving a gap between the development of the child's own antibody responses and the protection from their mothers' antibodies. This leaves the child vulnerable to infection; MBL is believed to play its main role by bridging this gap. Correspondingly, children born with low or deficient MBL levels may become sick more often, usually not severely, though they may require prophylactic antibiotics during the winter up until school age [56]. The majority of children will have no issues regarding their MBL status after developing a mature adaptive immune system, though children with other health complications can become increasingly vulnerable.

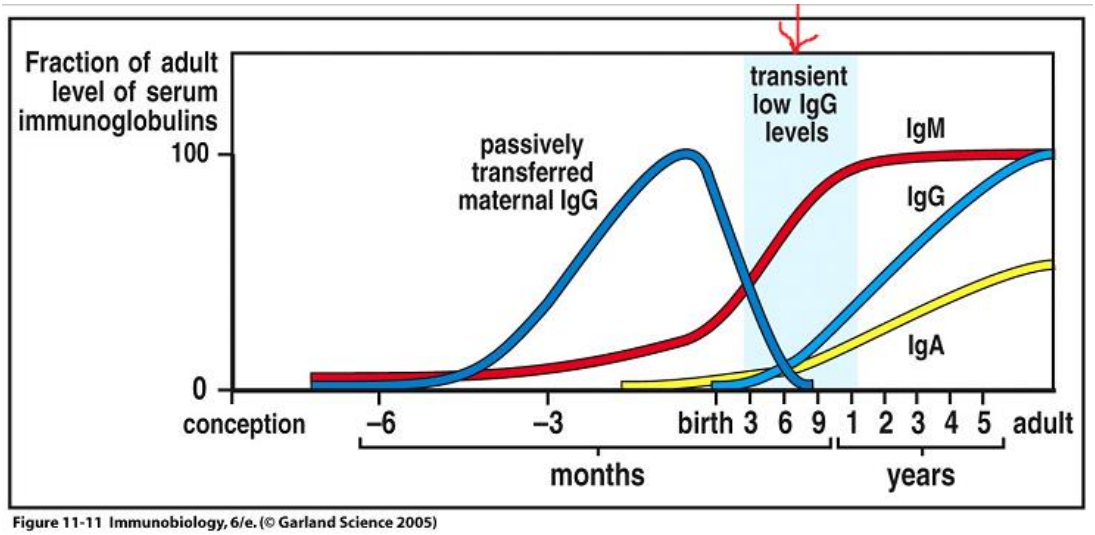

Figure 7: Levels of maternal IgG antibody which are passed to the child via the placenta during the final 3 months of pregnancy (Immunobiology, Garland Science 2005). Maternal IgG begins to wane around 3 months after birth with the child needing to rely on their own immune system for protection. MBL bridges this gap during the antibody development stage.

2.4.8. MANNOSE-BINDING LECTIN IN HEALTH AND DISEASE

MBL deficiency is the most common immunodeficiency known to date and is associated with susceptibility to a variety of pathogens, more severe infection, shorter life expectancy of patients with compromised mucosal barriers such as CF and contributes to higher morbidity of autoimmune diseases [57, 58]. MBL deficiency has been implicated in an increased infection risk particularly in children and neonates. Two studies demonstrated that MBL levels increased over 5 days in term neonates but that MBL levels at term were only one third the levels seen at 3 months [59, 60]. A study by Dzwonek showed that MBL levels below 400ng/ml trebled the chance of developing sepsis in neonates. It was shown that MBL levels below 400ng/ml did not activate complement and therefore did not enhance opsonophagocytosis [54]. Low MBL levels are associated with an increased risk in Gram-negative bacterial sepsis and nosocomial sepsis in neonates [61]. Deficient or low MBL levels are associated with more severe pneumococcal infection and pneumococcal meningitis, respiratory complications, and increased risk for higher frequency infections in children with malignancies [62][63]. Studies in MBL-null mice show a decreased clearance of

bacteria, particularly *Staphylococcus aureus*. Neutropenic and MBL-null mice demonstrate higher bacterial accumulations in the organs compared with wildtype [64]. It has also been demonstrated that MBL aggregates bacteria and yeast, allowing for enhanced recognition and phagocytosis via the immune cells. Though MBL deficiency is commonly associated with an increased risk in bacterial and fungal infection more recent *in vitro* and genetic studies have demonstrated MBL deficiency a risk for certain viral infections. In blood borne infections such as Ebola and HIV, MBL has been shown to have a neutralising affect against the virus [65-68]. Mice treated with high level MBL therapy were able to survive an otherwise-fatal Ebola virus dose [67]. Moreover, an *in vitro* model using MBL therapy was demonstrated to protect T cells from HIV infection [69]. However, there has been some controversy over these results due to the super physiological concentration of 50,000ng/ml MBL required for 100% viral inhibitions. Nevertheless, respiratory viruses are of particular interest due to the debate over the role of MBL in the lung. Although it was previously believed that MBL was not found in the lungs, and that the surfactant members of the lectin family were responsible for control of infection in the airways, its presence in the lung during infection was documented in 2005 [70]. *In vitro* assays have demonstrated the neutralising effect of both recombinant and plasma-derived MBL against influenza A (IAV) at physiological levels [71, 72]. Enhancement of IAV uptake via neutrophils is observed with a brief incubation of MBL and it has been shown that MBL binds the glycoproteins neuraminidase (NA) and haemagglutinin (HA). These studies have focused on both the MBL phenotypes in the clinic as well as the neutralising effects of MBL *in vitro*. Yet, studies with H1N1 IAV showed that MBL knockout mice have milder disease and reduced cytokine production [73]. Interestingly, in 2004 with the outbreak of the Coronavirus SARS-CoV-1, MBL was shown to have a neutralising effect on the virus and the prevalence of defective MBL genotypes were found to be higher in the more severely affected patients [74-76]. The median MBL serum levels of 733ng/ml were seen in severely affected patients compared to controls of 1369ng/ml. The role of MBL in the responses to SARS-CoV-2 infection in children is reviewed in Part II Chapter eight of this thesis.

Conversely, while the link between low levels of MBL and infection susceptibility is well-established in the literature, there have also been studies suggesting that high levels of MBL may contribute to tissue injury in inflammatory diseases such as

ischemic reperfusion (IR). This potentially induces a selective pressure that would explain the wide range of different haplotypes observed, and their globally-varying distribution [77, 78]. There are several theories as to the prevalence of MBL deficiency. One of these is that MBL deficiency is protective in areas with high tuberculosis levels, as MBL may allow access for tuberculosis by mediated phagocytosis of the bacterium which can withstand the highly acidic nature of the lysosomes. Another is its apparent role in IR related damage: the first responding opsonins to IR are IgM antibodies, which mediate the removal of necrotic tissue [79]; however, patients with high levels of functional MBL have been shown to have a worse prognosis after IR due to increased complement deposition [78]. An IR model study in adult rats demonstrated a more favourable outcome in rats whose MBL pathway was inhibited using monoclonal anti-MBL [80]. Another more recent (and unfavourable) association of MBL is in excessive thrombosis and coagulopathy seen in COVID-19 patients [81].

Though both *in vitro* and *in vivo* experiments seem to cast MBL therapy in a promising light, one must consider the reasons for why MBL is such a common immunodeficiency and what such selective pressures have led to it becoming the most common immunodeficiency despite its apparent protective role in infection. This is likely due to MBL having an initial protective role during early infection but resulting in increased damage when hyper-inflammation is sustained.

2.4.9. MANNOSE-BINDING LECTIN: A MODULATOR OF INFLAMMATION

Over the recent decades increasing evidence has demonstrated an extended role for MBL in the regulation of inflammation, certainly in diseases presenting in response to infection or trauma such as sepsis and systemic inflammatory response syndrome (SIRS). Polymorphisms in the exon 1 region have been associated with a greater increase in the development of SIRS as well as the progression to sepsis or septic shock in paediatric ICU patients [82]. Yet, a study in 2005 found that for postoperative patients, complications, particularly SIRS, were more likely to occur in patients expressing high MBL levels with low MBL levels adding protection [83]. Garred et al showed that MBL was capable of controlling systemic spread of infectious agents during illness or after surgery [84]. The study genotyped MBL in 272 patients with

SIRS. They found that MBL variants were associated with the development of sepsis and septic shock, as well as an increased mortality risk. Yet, it has been shown that MBL results in a worse prognosis after myocardial ischemic reperfusion injury [85]. Mice deficient for MBL were protected from severe cardiac IR injury but mice reconstituted with recombinant human MBL (rMBL) had significant injury. It was suggested that MBL can regulate cytokine release. A study in 2001 showed that MBL also regulates inflammatory cytokine release by monocytes in response to meningococci. MBL concentrations of 6µg/ml, levels seen during an acute phase response, were shown to significantly reduce the release of interleukin (IL)-6, IL-1β and tumour necrosis factor-alpha (TNFα). Interestingly, low MBL levels enhanced IL-6, IL-1β and TNFα concentrations [86]. Sprong et al subsequently demonstrated that MBL plays a role in the production of IL-10 and IL1β by PMBCs in response to non-LPS meningococci [87]. Chaka also found that TNF-α was induced in PBMCs by MBL after incubation with *Cryptococcus neoformans* at concentrations of 0.31 to 1.25pg/ml, yet declined at increased concentrations [88].

2.4.10. MANNOSE-BINDING THERAPY: THEN AND NOW

MBL therapy began unwittingly in 1968 when a patient described with a familial disorder of phagocytosis presented with the inability to phagocytose yeast [89]. The patient was a 3-month-old Caucasian female who suffered with eczema, intermittent diarrhoeal episodes, and failure to thrive as well as recurrent infections. Whilst in hospital she later developed enteritis*, Escherichia coli* and *Klebsiella aerobacter* infection and Staphylococcal septicaemia. Similar defective opsonisation was found in her mother and other family members who remained well. Weekly infusions with fresh heterologous plasma were shown to correct the defect by *in vitro* assays and provided effective treatment for the dermatitis, and she remained infection free even once treatments ceased. The investigators were unaware at the time the defect was MBL; it was only later appreciated when it was compared to a similar cohort of children investigated in 1989 at the UCL Institute of Child Health who were also found to be lacking MBL. Subsequent studies of cohorts with different childhood diseases began to reveal an important role of MBL in disease modification, and suggestions for MBL reconstitution therapy were discussed. Plasma derived (pdMBL) and recombinant MBL (rMBL) have both been tested in clinical trials that demonstrated safe and long-

lasting results, with no known lasting results demonstrated [58, 90]. A case study was carried out in Denmark using pdMBL on a 21-year-old woman who was MBL deficient and awaiting a double lung transplant due to CF [58]. She received three months of therapy in the hope of prolonging her life until a donor could be found. Her condition did not improve but was stabilised and her lung function correlated significantly with her MBL serum levels (Figure 8). There was also an inverse correlation with the levels of C-reactive protein (CRP) and IL-6 to her MBL serum levels. The patient received three months of MBL treatment before it was discontinued, and the patient died two months later before a donor was found. Moreover, recombinant MBL showed significant protection against systemic spread of *Pseudomonas* in mice during post burn injury (Figure 9) [51].

Over the recent decades many functions of MBL have been uncovered, from opsonophagocytosis to the modulation of inflammation. A push to market pdMBL and rMBL was made in 2006 by the company Enzon; no successful attempts have been made since. Many concerns were addressed in the clinical trials of 2006. MBL was deemed safe with no side effects nor any anti-MBL antibody production in deficient volunteers. One concern was that patients with deficient genotypes could produce antibodies to the foreign agent however, as discussed above MBL is secreted in very small amounts in deficient genotypes with the lack of oligomer formation being the substantive issue. A clinical trial was carried out in 2006-2009 on young patients with MBL deficiency (<300ng/ml) and neutropenia and looked at the safety and efficacy of rMBL therapy [91]. Despite demonstrating the safety of rMBL, the study did not yield significant results. Though, the study design for this trial can be criticised. Firstly, the children eligible for this trial were undergoing cytologic chemotherapy for haematological or oncological disease and must have been receiving broad-spectrum antibiotics as a study requirement. This requirement is believed to be why no significant results were seen in this trial, as the antibiotics would have already reduced the infection and inflammation; thus, MBL therapy would be somewhat redundant with no significant or striking results being gathered. A more suitably selected cohort could have given more clear insight into the potential benefits of MBL reconstitution.

In chapter seven we investigate the novel use of both plasma derived and recombinant MBL as therapy in the prevention and eradication of MRSA biofilms. Chapter eight looks at the capabilities of both rMBL and pdMBL to neutralise SARS-CoV-2 infection.

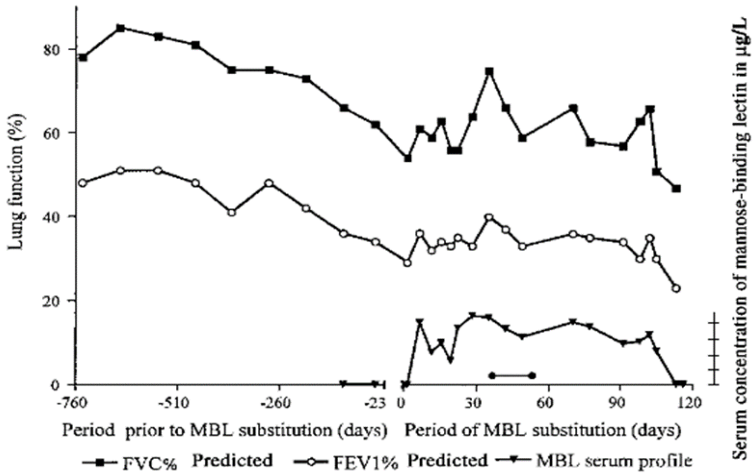

Fig. 2. FVC% and FEV_1% predicted values in the 2 years (days) prior to MBL treatment (mean of 3-month periods are indicated) and the corresponding data during MBL substitution are indicated. Serum levels of MBL when assessed at the same time as the lung functions are indicated. MBL measurements reflect MBL level just prior to a new infusion. During a 2-week period (from days 35–49), alternative doses of MBL (3 and 6 mg) were given.

Figure 8: Measuring the lung function and MBL serum levels of a 21-year-old CF patient receiving infusions of pdMBL whilst awaiting a double lung transplant. FVC and FEV show a clear correlation with MBL serum levels (Taken from Garred et al 2002)

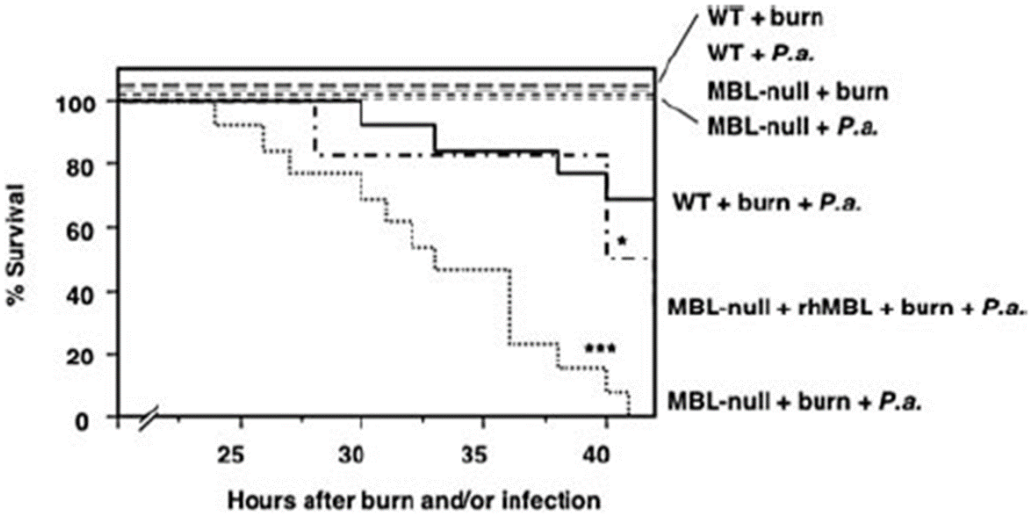

Figure 9: Recombinant MBL reduces the mortality rate of mice infected with P. aeruginosa post-surgery by 50% (taken from Moller-Kristensen et al 2006). MBL-null mice are unable to survive over 40 hours post-infection whereas MBL-null mice who received therapy with recombinant MBL had an increased survival of 50%.

2.4.11. THE DEVELOPMENT OF FCMBL

Recently, a genetically engineered MBL known as Fc-mannose-binding lectin (FcMBL) was created by the team of Dr Michael Super at the Wyss Institute, Harvard, USA (Figure 10). FcMBL is a fusion protein which is composed of an IgG1 Fc domain attached to the neck at its C-terminus and two MBL carbohydrate recognition domains at its N-terminus (accession code KJ710775). The IgG Fc is positioned 'backwards' in the molecule, with its N-terminus being expressed at the C-terminus of the complete fusion protein. The N-terminus of the molecule is biotinylated and bound to streptavidin coated magnetic Dynabeads (Thermofisher). Approximately 7,000 molecules are bound per bead increasing the binding affinity (Figure 10). The IgG Fc domain is inactivated by de-glycosylation of the fragment. This has been used to capture pathogens from small amounts of blood to confirm sepsis, and further, has been coated onto dialysis tubes and successfully used to purify septic blood of pigs [19, 20, 92].

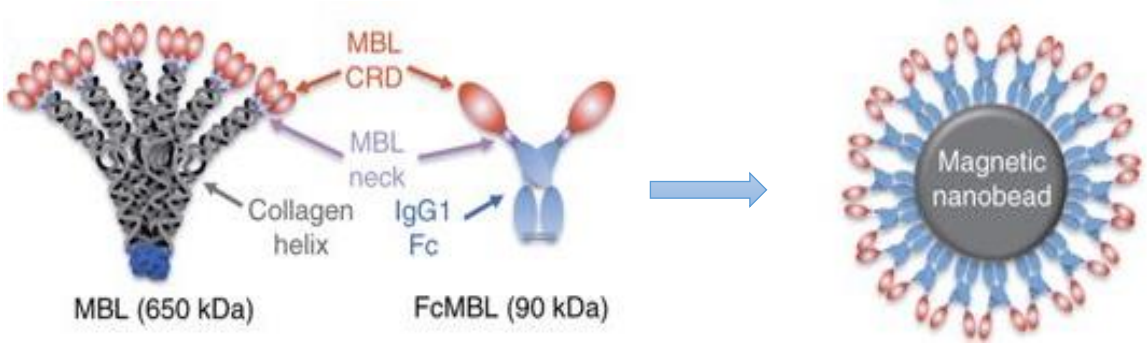

Figure 10: The FcMBL molecule structure. Natural plasma derived MBL on the left and the FcMBL molecule in the middle. On the right a diagram of the FcMBL-conjugated beads (Taken from the Wyss Institute website).

Interestingly, MBL does not typically recognise human cells, as the sugars MBL recognises are found at the C-terminus of surface expressed proteins on the human cell and not readily exposed to the immune system. However, tumour cells express aberrant sugar profiles, allowing FcMBL beads to capture circulating tumour cells responsible for disseminating primary tumours to distant organs [93]. The beads not only bind microbes and aberrant sugars of living cells, but also have a high affinity for fragmented microbes as well as endotoxin (Figure 11) [19]. This led to the

development of an enzyme-linked lectin sorbent assay (ELLecSA) capable of binding pathogen-associated molecular pattens (PAMPs) found on bacteria and fungi. This method can rapidly detect both live and fragmented pathogen in blood samples (<1 hour), confirming infection (sepsis) or SIRS or other sterile inflammatory issues [94]. In a human study of suspected sepsis patients, the FcMBL ELLecSA was able to detect PAMPs in 80% of samples irrespective of antibiotic therapy. In contrast only 18% of the same patient samples had positive blood cultures, the current gold standard diagnostic tool. The FcMBL beads have demonstrated the ability to bind over 200 isolates and 95 different species. However, the beads only bound 38% of live *E. coli* isolates, increasing to 92% upon fragmentation and release of PAMPs [19]. The beads were able to rapidly isolate *S. aureus* from infected synovial clinical samples. Though originally the binding yields were disappointing (<5%), pre-treatment of the samples with hypotonic washes and protease cocktails increased the efficacy to 76%. MBL has been shown to have a higher affinity in children compared to adults due to the lower presence of anti-wall teichoic acid (WTA) antibodies, likely why treatment increased the efficacy of the FcMBL beads [95]. This is due to the stripping of antibodies on the surface of the bacteria. Despite the broad range detection and high sensitivity of this technique, it does not provide an identification of the underlying microbe.

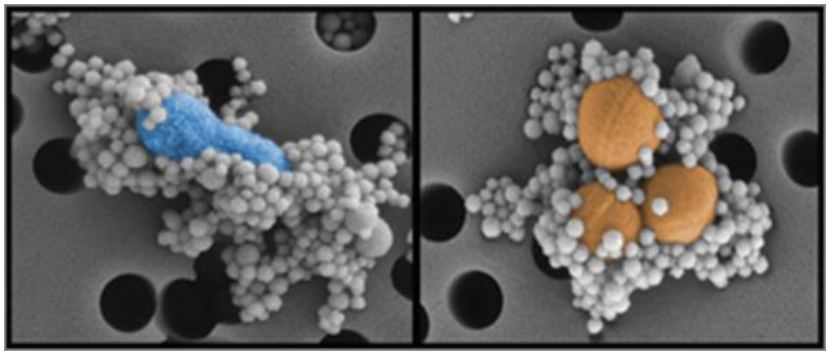

Figure 11: SEM imaged of FcMBL beads binding the clinically relevant pathogens *E. coli* (blue) and *S. aureus* (yellow) (Image was taken from the Wyss Institute website).

In China a similar FcMBL molecule was designed. The group demonstrated a shorter turnaround time in *Candida* infected blood by capturing fungi using genetically engineered-MBL conjugated beads direct from plasma samples and plating directly on to solid agar. Time until colonies were produced by the genetically engineered method and the standard blood culture method of positively flagged cultures, sub culturing and subsequent mass spectrometry (MS) analysis was reduced by an average of 29 hours. Another publication in 2020 described using FcMBL conjugated magnetic beads similar to Harvard's [96]. The group designed an in-lab chip which could simultaneously capture and filter bacteria from human serum/plasma and identify via PCR amplification using the FcMBL beads. The assay allowed for the capture of as little as 5 colony forming units per ml (CFU/ml) and amplification and detection of sepsis with approximately 85% capture efficiency and within 90 minutes.

Due to the broad range binding capabilities of the FcMBL beads including binding to fragmented microbes we proposed that FcMBL could be utilised in the rapid diagnosis of infections in children. The advantage over standard culturing techniques, which require live pathogen (and thus with success rates that drop significantly after antibiotic therapy), is that FcMBL can detect dead or fragmented microbes. As MALDI-TOF MS is a rapidly increasingly-prevalent technology responsible for cheap and rapid identification in diagnosis laboratories worldwide we proposed that FcMBL could be used in conjugation with MALDI-TOF MS.

In Part I we investigate the use of FcMBL beads in the rapid diagnosis of paediatric infections. Chapter five focuses specifically on the optimisation of these beads, determining the optimal protocol for the identification of blood stream infections (BSIs). Chapter six is a comparative study of the FcMBL method with the rapid diagnostic method currently used at GOSH and assesses the clinical power of the FcMBL method.

2.5. PAEDIATRIC INFECTIONS

2.5.1.1. BLOOD STREAM INFECTIONS IN CHILDREN

Systemic infections usually stem from a primary infection site allowing entry to the blood. Bacteraemias are a common occurrence, with low levels of bacteria entering the blood after minor events such as brushing teeth [97]. Septicaemia, however, is a more severe form of BSI. Left untreated septicaemia can lead to sepsis, a more devasting and crippling disease, though it is worth noting that not all BSIs lead to sepsis. Sepsis can be caused by a range of microbes including Gram-negative and Gram-positive bacteria, as well as fungi and viruses. Sepsis bears a very high mortality rate, in particular candidemia which carries a 50% mortality rate [98]. The word sepsis comes from the Greek word “sipsi” meaning “make rotten” and was first used to describe the disease by Hippocrates. An improved understanding of the disease has led to various updated definitions, the most recent being described by Singer et al, 2016. According to the study the new definition of sepsis is evidence of infection as well as life-threatening organ dysfunction which is characterised as 2 points or greater by the organ failure assessment score (SOFA) [99]. In children, two of the leading causes of Gram-negative bacteraemias are *Escherichia coli* and *Neisseria meningitidis* which accounted for approximately 5% of paediatric bacteraemias in 2007 [100]. Data from 2007 in England and Wales showed that four groups of bacteria accounted for approximately 50% of bacteraemias in children in 2007: coagulase-negative Staphylococci (28%), *Staphylococcus aureus* (10%), non-pyogenic Streptococci (9%) and *Streptococcus pneumoniae* (7%). Though, other studies have suggested that *Escherichia coli* is the leading cause of BSIs in children [101]. The discrepancy is likely due to demographic differences and study numbers. Moreover, decreases in *Haemophilus influenzae*, *S. pneumoniae* and *N. meningitis* were seen due to the wide scale introduction of vaccine programs against these pathogens. BSI rates drop significantly in healthy children after the first few months of life with the most common pathogens occurring after this being *S. aureus* and *S. pneumoniae* from community-acquired pneumonia as well as *N. meningitis*. An issue for paediatrics is the collection of large volumes of blood required for culture. It has been demonstrated that an increase in blood volume correlates directly with a reduction in the time until detection [102]. One study showed that less than 1ml was insufficient for detection of

pathogens less than <4 CFU/ml and that 2-6ml of blood is required for the detection of less than ≤10 CFU/ml [103]. Moreover, it is reported that low-level bacteraemias are common in the paediatric population, occurring in 38-68% of all patients with positive blood cultures [104]. A study in 1997 found that over two-thirds of children under 2-months of age with BSIs had an average of ≤10 CFU/ml [103, 105]. Children up to the age of 15 years had ≤10 CFU/ml in 60% of cases and 23% were present at ≤1 CFU/ml [104]. The combined issues of low blood culture volume and high frequency of low-level bacteraemia has led to severe difficulties in diagnosis for the paediatric population.

2.5.1.2. INCIDENCE OF BLOOD STREAM INFECTIONS IN CHILDREN

Hospital-acquired BSIs (HA-BSI) are associated with significant morbidity and mortality as well as significant economic burden, with young children and older adults having been shown to have higher rates of HA-BSIs [106]. A study by the Health Protection Agency in 2011 showed that the highest rates of healthcare associated infections were in children aged between one month and two years old (8.2%). A study in 2011 also showed that patients on an intensive care unit (ICU) are some of the most vulnerable to BSIs with 23.4% of patients acquiring healthcare associated infections compared to 6.4% from other wards [107]. This leads to the increased antimicrobial use on the ICU (60.8%), almost twice as high as other wards (34.7%). Sudhir et al showed that the majority of sepsis infection sources were respiratory tract infections, urinary tract infections and gastrointestinal tract infections [108]. Studies also show that in the ICU, respiratory tract infections followed by genitourinary infections, are the most common sources of sepsis [109].

2.5.1.3. TREATMENT OF BLOOD STREAM INFECTIONS

Empirical antibiotic therapy is recommended by the International Committee on Surviving Sepsis (SCC), to be administered within the first hour of diagnosis [110]. Empirical antimicrobials are broad-spectrum therapies covering the majority of common microorganisms responsible for BSIs and sepsis and can vary based on geographic and relative resistance rates in particular areas. Nevertheless, the SSC do

recommend that blood cultures are drawn prior to antibiotic therapy being initiated wherever possible. It is well documented that early intervention in suspected BSIs with empiric antimicrobial therapy reduces mortality rates [110-112]. Yet, broad-spectrum antimicrobial therapy comes with a variety of unwanted side effects such as allergies to the drug, dysbiosis of the host microbiome (specifically the gut) and an increased risk in multi-drug resistant microbes as well as significant cost. The faster appropriate therapy can be provided the better the outcome for the patient and an economic ease for the healthcare providers, though to do this rapid and sensitive diagnosis needs to be achieved.

2.5.2. CEREBROSPINAL FLUID

Most hospitalisation of children with a significant fever will result in the child undergoing empirical antimicrobial treatment whilst their blood, urine and CSF are monitored for infection. The CSF should be clear and colourless and is usually obtained for diagnostic purposes by lumbar puncture, though can be obtained by suboccipital puncture or ventricular drainage. The CSF is a thin membrane of fluid which protects the brain and spinal cord. Meningitis is the swelling of these membranes, commonly caused by a virus or bacterial infection. Bacterial meningitis has a high mortality; with overall mortality 5-10% though with neonates this rises to 15-20%. In children aged 3-months or older the most frequent causes include *Neisseria meningitidis, Streptococcus pneumoniae* and *Haemophilus influenzae*, organisms which are usually found in the upper respiratory tract [113]. In children less than 28 days the most common causative organisms include *Streptococcus agalactiae*, *E. coli* and *Listeria monocytogenes*. CSF culture is considered the gold standard for the diagnosis of bacterial meningitis for a variety of reasons. Raised WBC and RBC counts, as well as glucose and protein profiles have not proven to be effective parameters in the diagnosis of meningitis as these can vary with age [113]. A variety of tests are performed on CSF including cell counting, Gram stains and measurement of lactate and glucose in the CSF. In 70% of bacterial meningitis, polymorphonuclear (PMNs) are seen in concentrations >300/µl and in 40% >2000/µl [114]. An increase in activated lymphocytes, monocytes, and macrophages is also observed. Gram stains and detection of bacterial antigens by latex agglutination can help diagnose bacterial meningitis rapidly. Yet, Gram stains are only informative in

~20-40% of cases as some bacterial can be difficult to visualise. Though the gold standard for diagnosis is CSF culture, and positive results are seen in ~70-85% of patients that have not had any antimicrobial therapy, these cultures can take up to 48 hours until identification [114]. The introduction of antibiotics not only decreases the effectiveness of CSF culture to 50% but also the Gram stain results drop to 40-60% effectiveness [114]. Fungal meningitis is less common than viral and bacterial and is mainly seen in critically ill and immunocompromised individuals [114]. These include patients with acquired immunodeficiency syndrome, immunosuppressive chemotherapy and patients having undergone organ transplantation. Other risk factors for the development of fungal infections include long-term antibiotic therapy and being of young age. A study showed that *Cryptococcus* was the most common causative of fungal meningitis (70%) with candidiasis causing 7.6% of infections, and that both had increased length of stay associated, at significant cost to the health care provider adding ~$100,000 per patient [115].

2.5.3. URINARY TRACT INFECTIONS

Urine is routinely measured in children with fever and suspected infection as this is the most common infection in childhood [116]. In pediatrics 80% of urinary tract infections (UTIs) are a result of *E. coli* infection with other common causes being Klebsiella, Proteus and Enterobacter. Again, the culture of urine is the gold standard in the diagnosis of UTIs. Urine in the bladder is considered sterile thus bacteria or fungi grown should be considered infection. It was found that urine cultures with less than 10^3 CFUs were almost always likely to be contamination, but those with 10^4 and 10^5 bacteria were likely infection, and over 10^5 CFU were almost certainly infection [116]. The cut offs for urine collected by noninvasive collection methods such as clean catch are 10^5 CFU/ml and for suprapubic aspiration are 10^2 CFU/ml. For samples obtained by a catheter 50,000 CFU/ml has been used as a cut off. Moreover, as contaminations are likely due to obtaining the urine sample from the genital tract it is usually considered a true infection if there is a presence of only one single organism as well as clinical signs of a UTI. Samples should be kept cool to prevent overgrowth of contamination. Urine is typically limited in nutrients which are needed for microbial growth. The presence of leukocyte esterase identifies the presence of WBCs in the

sample with its release assumed to be triggered by the leukocytes due to the presence of bacteria. The presence of nitrite is also a sign of bacterial infection as bacteria convert nitrate to nitrite, though this is not 100% sensitive as some bacteria do not convert nitrates [117].

PART I

THE USE OF MANNOSE-BINDING LECTIN IN THE RAPID DIAGNOSIS OF BLOOD STREAM INFECTIONS IN CHILDREN

AIMS

The aims of Part I:

1. Optimise and create an FcMBL pulldown method to be used in conjunction with MALDI-TOF MS for rapid diagnosis of infections in children;

2. Investigate the potential of the FcMBL pulldown method to enhance rapid diagnosis in the clinic;

3. Compare the FcMBL protocol to the current rapid diagnosis method for the identification of childhood infections at GOSH.

CHAPTER THREE

CURRENT METHODOLOGIES IN CLINICAL DIAGNOSTICS

Rapid and accurate diagnosis of infection is essential to all clinical microbiology laboratories. In the case of BSIs, the rapid identification of bacteria or fungi becomes even more critical. The longer a patient with a suspected BSI is waiting for microbiology results, the greater the delay in effective treatment with targeted antimicrobials, amplifying the risk of mortality and resistance development. The retrieval of pathogen from samples allows for confirmative diagnosis, as well as identification and susceptibility testing. In recent decades microbiology technology has advanced substantially, yet the techniques and protocols implemented in modern clinical diagnostic laboratories have remained largely unchanged since the introduction of susceptibility testing in the late 1990s. In Part I of this thesis, we study how the introduction of FcMBL beads – a genetically enhanced non-specific carbohydrate-binding lectin bound to magnetic beads – could shorten the time until positive diagnosis of BSIs with the use of MALDI-TOF mass spectrometry.

3.1. DIAGNOSING BLOOD STREAM INFECTIONS

At Great Ormond Street Hospital (GOSH) blood is collected in blood culture bottles and incubated in the BacT/Alert 3D (BACTEC) (bioMerieux) blood culture systems until a positive signal is produced. The blood culture bottles used at GOSH include the Peds Plus™ aerobic and the anaerobic lytic bottles (BD). Once a positive blood culture has been flagged by the machine, a Gram-stain is carried out aseptically and classed phenotypically as bacterial Gram-negative or Gram-positive, or fungal. A differentiation between bacilli and cocci, clusters, chains, and pairs are also observed and documented. The sample is then subcultured on to solid agar plates, typically blood agar CO_2, chocolate agar CO_2, blood agar ANO_2, or MacConkey O_2. Solid agar is incubated overnight or 16 hours. The laboratory then waits for subcultures to produce colonies large enough to identify and perform antimicrobial sensitivity testing. This subculturing process can be bypassed for immediate identification of the organism with the use of the Bruker Sepsityper kit, which isolates microbial pellets direct from the blood culture bottle that are large enough to be analysed directly. This is discussed later in this chapter in further detail.

3.1.1. CULTURE-DEPENDENT METHODS

Conventionally, biochemical testing on colonies grown from subcultured positively flagged blood cultures is the gold standard for the diagnosis of bacteraemia or fungaemia. Obtaining pure and single colonies is a time-consuming process, taking up to 72 hours for subcultured colonies to appear and a further 8-48 hours for conventional biochemical tests to be carried out. With the introduction of commercialised systems such as the MALDI-TOF MS, Multiplex PCR, and microarray technologies, turnaround time has been rapidly reduced, albeit at an increased financial cost (Table 2).

Table 2: Systems for diagnosis of pathogens in blood cultures dependent on microbial culture

Platform	**Manufacturer**	**Method**	**Turnaround**
MALDI-TOF MS	Bruker Daltonics, BioMerieux	Mass spectrometry	Less than 1 hour
QuickFISH™	AdvanDx USA	Fluorescence *in situ* hybridisation (FISH)	1 to 4 hours

3.1.2. CULTURE-INDEPENDENT METHODS

Though PCR approaches can provide rapid diagnoses of infections, one major issue is the relatively small concentration of microbial DNA in comparison to the large contamination of human DNA [118]. Currently, there are commercialised kits for identifying bloodstream fungal infections, such as the T2Candida Panel™ (T2 biosystems) yielding results as quickly as 3-4 hours; however, this PCR based technique only provides a diagnosis for fungal BSIs. Commercial kits are also available for the diagnosis of a large range of BSI with relatively short turnaround times (see Table 3). These are also PCR-based systems which do not require live pathogen, only the presence of DNA. Such PCR-based methods rely on the design and implementation of specific primers; if an organism is present for which there is not a corresponding primer, no detection will be made. In children this can be particularly challenging due to the wide range of infections they can suffer. Thus, PCR-based techniques require a broad range panel of PCR primers in order to be effective.

Table 3: Systems used for the diagnosis of microbes independent of microbial culture.

Platform	**Manufacturer**	**Method**	**Time**
MagicPlex™	Seegene, Seoul, Korea	PCR + multiplex RT PCR	3-5 hours
SeptiFast™	Roche, Switzerland	Broad range real-time PCR	3-5 hours
SepsiTest™	Molzym, Bremen Germany	PCR and sequencing	6 hours
16S sequencing	Illumina,	PCR and sequencing	>6 hours

3.2. MASS SPECTROMETRY

Mass spectrometry (MS) has its origins in experiments carried out by JJ Thompson in the early 20th century, who successfully separated ions of different masses. This led to the creation of the first mass spectrometer by his PhD student Francis Aston in 1919. MS allows for the accurate separation of atoms or molecules by their mass-to-charge ratio (*m/z*). MS comprises of three main components: an ionisation phase; a mass analyser; and an ion detection system. In modern MS systems computers are used to analyse and interpret the output data (Figure 12).

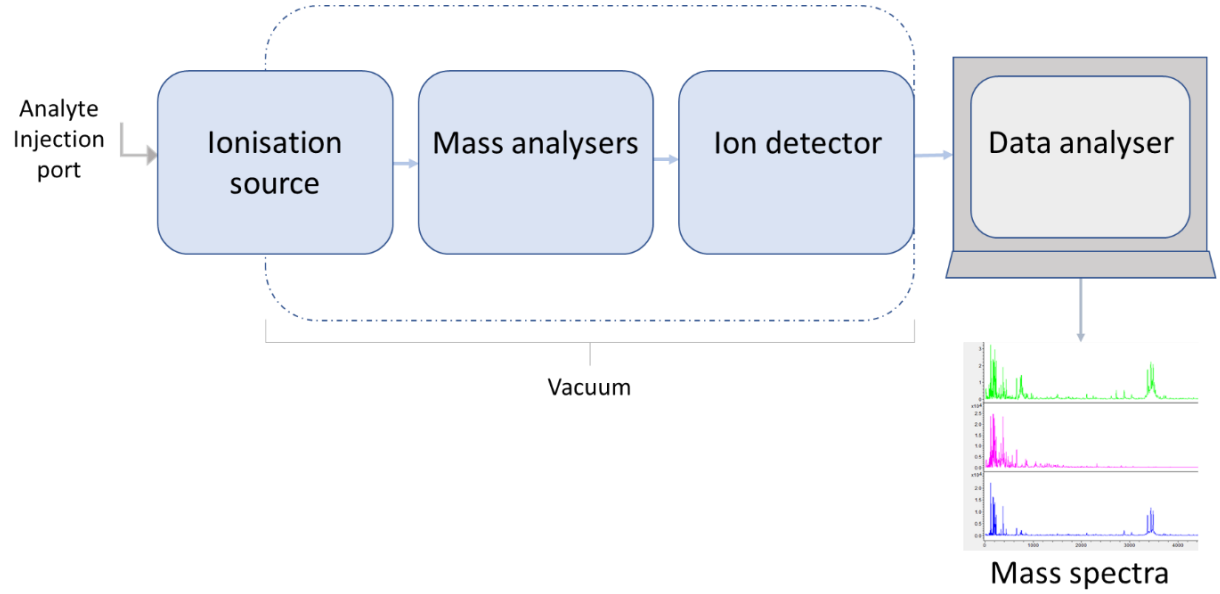

Figure 12: The basic setup of a mass spectrometer, comprising of an ionisation source, a mass analyser, an ion detector, and a data analyser.

In MS the analyte is accelerated by an electromagnetic field in the mass analyser, towards the ion detector, requiring that the particle obtain a charge. Ionisation is the process of molecules or atoms gaining or losing an electron and thus changing their charge, which can be carried out in a variety of ways. Classic ionisation techniques include electron impact (EI) and fast atom bombardment (FAB). Recently other forms of ionisation have been introduced, such as atmospheric pressure chemical Ionisation (APCI), electrospray ionisation (ESI) and matrix-assisted laser desorption ionisation (MALDI). MALDI-TOF MS, the technique used in our work, is discussed in detail later in this chapter.

3.2.1. MASS ANALYSERS:

Mass analysers stratify the analyte by their *m/z*. This is achieved through a variety of mechanisms:

3.2.1.1. QUADRUPOLE

Quadruple mass analysers consist of four cylindrical rods, arranged parallel to each other around a central axis. Each opposing rod pair is connected together electronically. A radio frequency and direct current are applied to the rods creating an oscillating electronic field that perturbs the ion trajectories. The stability of the ion when passing through the electronic field is determined by the *m/z*. The field is defined by the applied voltages, which can be altered by the user and thus set to accurately detect particular *m/z* as unstable ions will collide with the quadrupole rods and be filtered out.

3.2.1.2. TIME OF FLIGHT

Time of flight (TOF) analysers separate the ions by time with the use of a high voltage electrical field [119]. The velocity of the ions differentiates the *m/z* (Figure 13B), with the time of arrival at the detector providing the measurement. Particles with larger molecular weight (at fixed charge) have lower velocity and move slower through the tube.

3.2.1.3. MAGNETIC SECTOR

Magnetic sector mass analysers separate ions according to their momentum and their charge. Ions are fired into the magnetic sector, where the magnetic force bends the ions into an arc (Figure 13C). The *m/z* of the particles determines the radius of the arc they travel, and thus the spatial position where the ion hits the detector, providing the *m/z* measurement. The radius of the arc depends on the initial momentum, mass, and charge of the ion, and the magnetic field strength.

The ion detector measures the number of ions emerging from the analyser, giving an intensity value as well as the *m/z* (Figure 14).

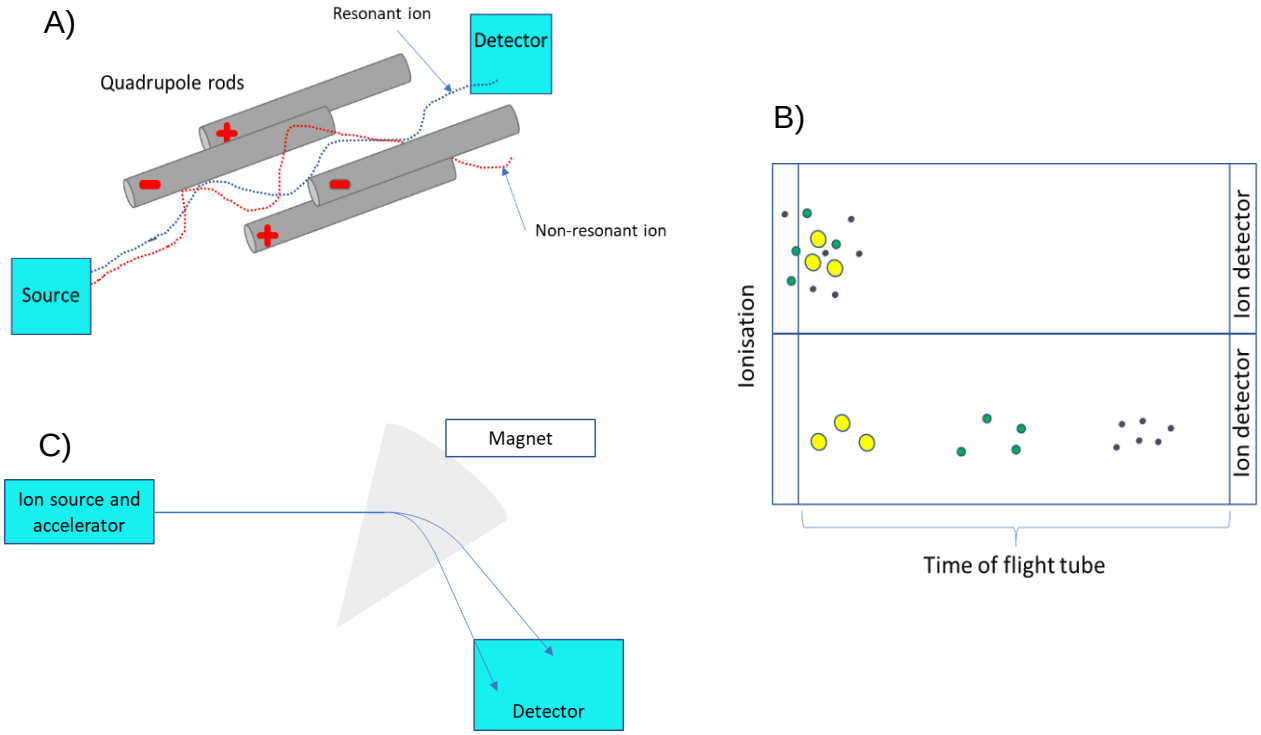

Figure 13: Schematic overview of mass analysers

A) In a quadrupole analyser, the red non-resonant ion is scattered and fails to reach the detector, while the blue resonant ion passes through. B) The TOF uses an electrical current to accelerate the ions towards the detector, with the lowest MW accelerating fastest. C) A magnetic sector mass analyser deflects the trajectory of the ions, with the radius of curvature largest for smaller ions.

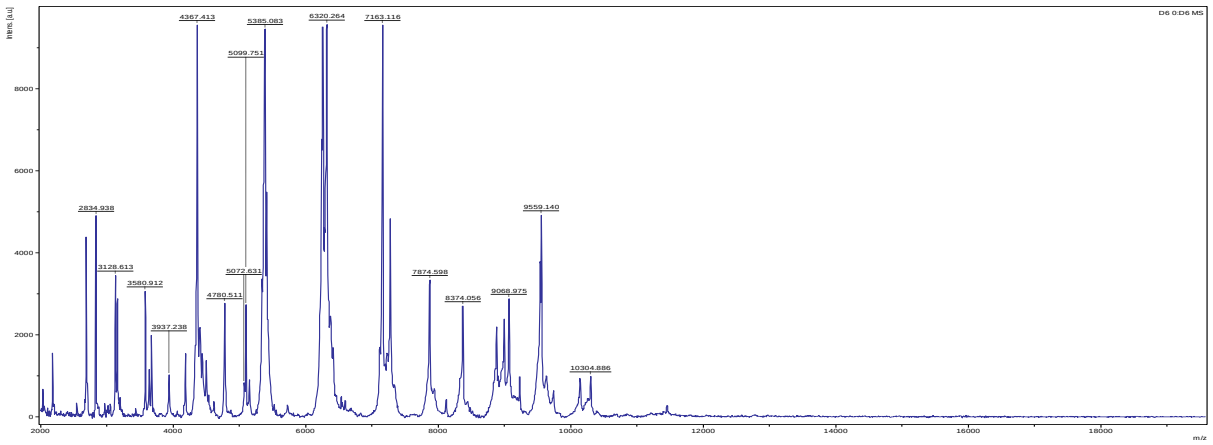

Figure 14: Typical mass spectra produced by MALDI-TOF MS technology for *E. coli* Schematic overview of mass analysers

3.2.2. MATRIX-ASSISTED LASER DESORPTION IONISATION (MALDI)

MALDI is a form of 'soft' ionisation which was first published in 1983 by Hillenkamp and Karas [120]. It is used mainly in conjugation with TOF analysers. An advantage is that a laser energy absorbing matrix is used to create ions from large molecules with minimal fragmentation. In the MALDI process a matrix is essential [121]. Once the sample is illuminated by an ultraviolet (UV) laser, the matrix absorbs the energy, and as the sample is vaporised the analytes are simultaneously ionised by proton transfer (Figure 15). Samples are co-crystallised with a matrix on a target plate, usually a ground or polished stainless-steel plate. MALDI ionisation allows for the analysis of non-volatile and large complex biomolecules such as lipids, proteins, and carbohydrates, as this soft ionisation technique results in complete molecular ions and minimal fragmentation compared to the other techniques mentioned. This soft ionisation is key for its use in microbial identification (Table 4). Also, due the nature of the matrix co-crystallising with the sample, sample plates may also be stored for future use under the correct conditions.

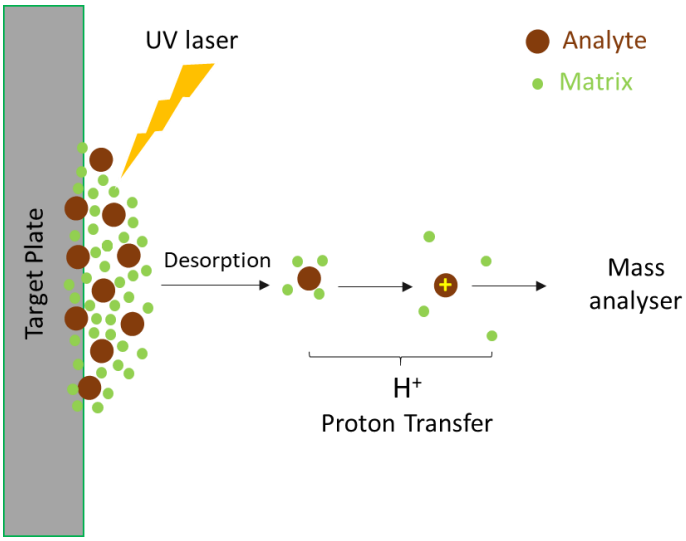

Figure 15: The MALDI ionisation process. Proton transfer from the matrix to the analyte happens after the high energy laser hits the target plate. The analytes are then propelled down the TOF tube towards the ion detector.

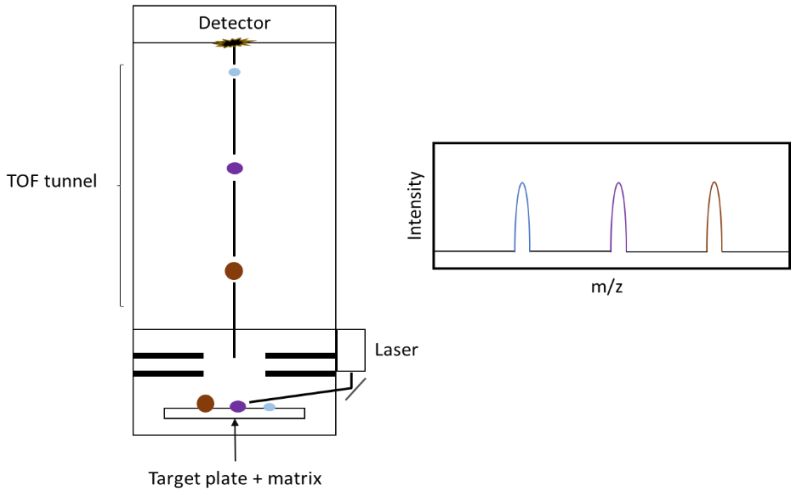

Figure 16: Schematic of a MALDI-TOF mass spectrometer (left). Right is the typical image of a mass spectra generated using MALDI-TOF MS

3.2.3. TANDEM MASS SPECTROMETRY

Tandem MS is the process of combining two or more mass analysers to increase the resolution and signal to noise ratio. Tandem MS is often referred to as MS/MS or MS^2. Different combinations of mass analysers can be used to create hybrid instruments. Sample molecules are ionised in the first mass spectrometer and separated by their *m/z*. Selected molecules are then filtered through to a second mass spectrometer and split into further fragments. By combining more than one mass analyser it makes it possible to separate and identify ions with similar *m/z* ratios by increasing the sensitivity.

3.2.4. MALDI-TOF MS VERSUS OTHER TECHNIQUES

There has been a considerable improvement in MALDI-TOF MS technology, allowing better performance over traditional methods including even the difficult to discriminate *Streptococcus mitis* group, with MALDI-TOF being able to distinguish *S. pneumoniae* from non-pneumococcal streptococci. Further, HACEK group discrimination was shown to be correctly identified by MALDI-TOF MS in more than 86% of isolates, versus 77% with biochemical testing [122]. With MALDI-TOF MS becoming more readily available and cheaper to run, as well as being user friendly, it has been suggested that a large laboratory could expect to save >50% on reagents if they switched to identification by MALDI-TOF MS compared to biochemical testing [123, 124].

Table 4: Comparison of different mass spectrometry techniques

	Sample type	**Sample preparation**	**Ionisation techniques**	**Applications**
GC-MS	Volatile and thermostable, typically of a small MW	Laborious/ expensive	EI and CI, both forms of harsh ionisation that results in substantial fragmentation	Substance detection e.g., accelerates, pesticides and drugs
LC-MS	Non-volatile and thermostable	Laborious/ expensive	ESI and APCI are both forms of harsh ionisation that results in substantial fragmentation	Metabolic profiling, environmental contamination and pharmaceutical
MALDI	Non-volatile and thermostable. Large molecular weight range	Easy, rapid, and cheap	MALDI is a form of soft ionisation which results in very little fragmentation thus larger macro molecules can be analysed	Protein identification, diagnosis of membrane associated cancers, microbiology and potentially drug resistance
Tandem MS	“ ”	Laborious	MALDI/ESI/APCI/EI/CI	Peptide sequencing, proteomics, biomarker identification

2.2.5. MALDI-TOF MS IN MICROBIOLOGY

Mass spectrometry analysis was once only a tool for the chemical sciences, but since the introduction of softer ionisation techniques such as ESI and MALDI it has now become a new and effective tool for analysing large biomolecules. MALDI-TOF MS is used in many clinical microbiology laboratories for the identification of microorganisms, particularly bacteria and fungi. Colonies are smeared onto the target plates and overlaid with a matrix. The proteins produce mass spectra for each sample to produce a “protein fingerprint” that is compared with a reference library of profiles, a process referred to as proteotyping. The microbial peaks consist of 70% ribosomal proteins, with ~30% being cell membrane and wall proteins. This means that discrimination between species with very similar ribosomal proteins such as the *Streptococcus* genus is difficult on the MALDI-TOF MS. This technique was first realised in two publications in 2010, demonstrating the use of MS in clinical microbiology [125, 126]. Compared to biochemical techniques, metabolic and immunological tests, MALDI-TOF MS is a cheaper, faster, and more accurate technique, and is speedily becoming a standard method of identification in many clinical microbiology laboratories. MALDI-TOF MS can be as quick as 30 minutes, as opposed to days with traditional techniques. This reduces the duration that patients are supplied with empirical antibiotics, rather than a more effective targeted antibiotic. Many studies have demonstrated that MALDI-TOF MS is as good as, if not better, at accurate pathogen identification in BSI than traditional techniques [127, 128]. He et al revealed that identification of bacteria in stool versus phenotypic methods could be sped up from 2-3 days to 30 minutes using MALDI-TOF MS [129].

3.2.4.1. MATRIX

Paramount to MALDI-TOF MS is a suitable matrix. Many matrices have been used with MALDI-TOF MS but the most successful for the microbiology field comes with α-Cyano-4-hydroxycinnamic acid (CHCA), 2,5-Dihydroxybenzoic acid (DHB) and Sinapinic acid. The matrix solution contains the matrix, water, organic solvents that contain ethanol, methanol or acetonitrile and an acid, usually trifluoroacetic acid (TFA) which dissolves the matrix. In the case of CHCA, the matrix is layered on top of the

sample on the target plate, where the solvents help break apart the microbial cell wall to release the intracellular proteins. As the solvent evaporates, the matrix co-crystallises, entrapping the sample [130]. When the sample is illuminated by the high energy laser, the matrix absorbs the energy and transfers this to the sample with which it is co-crystallised. This results in a charged ion which is able to vaporise and travel up the TOF toward the detector. HCCA is designed by Bruker and is a form of CHCA which has been patented, though the principles are the same.

3.2.4.2. BRUKER MALDI-TOF MS BIOTYPER

The ability of MALDI-TOF MS to identify microbes on a peptide mass fingerprint (PMF) led to the development of the MALDI-TOF MS Biotyper platform by Bruker Daltonics. The Bruker microFLEX™ machine is a compact benchtop MALDI-TOF MS which has a relatively small TOF tube that operates in linear or reflector mode as well as positive or negative ion mode (reflector and negative ion mode are model dependant). The linear positive bench top has a lower resolution due to the shorter TOF tube, though some machines have a reflector mode in which an ion mirror reflects the ions at an angle back down the tube toward the detector in order to increase the flight length and thus improve mass resolution. Using MALDI-TOF MS, only low mass peptides that ionise readily and are of high abundance can be observed. Proteins and biomarkers are presented on a spectrum defined by their MW, yet this does not identify the characteristics of the biomarker. Thus, the MicroFLEX does have difficulties in correctly identifying some species, in particular *S. pneumoniae* and *S. mitis* as well as *Shigella* and *E. coli* which are very closely related [131]. The Biotyper collects the mass spectra and runs it through an automated software to provide an identification. The Bruker Sirius is the most up to date model of Biotyper with a faster 200Hz smart beam laser compared to the previous 60Hz.

3.2.4.3. BIOMERIEUX VITEK MASS SPECTROMETER

Both the Bruker Biotyper and the VITEK are MALDI-TOF MS machines, though the VITEK machine uses the Myla™ software to analyse spectra [132]. A study by Jamal et al in 2014 demonstrated a slightly better performance in the detection of Gram-

positive cocci when using the Vitek MS over the Bruker Biotyper MS. However, a study in 2017 demonstrated slightly better results when using the Biotyper (82.0%) for identifying uncommon yeast species compared to the Vitek MS (73.4%) [133]. The VITEK provides scoring as a percentage of confidence with values between 60.0 and 99.9 being deemed reliable for species discrimination according to the manufacturer. The detection limit for the machine is 10^5 CFU/ml for bacteria and 10^4 CFU/ml for yeast according to the manufacturer, which is comparable to the Bruker Biotyper.

3.2.4.4. LIBRARY DEVELOPMENT

MALDI-TOF MS library development is essential for the accurate and rapid detection of microbial infection in clinical laboratories. Microbial isolates are processed to collect an average mass spectrum for a single strain. The greatest variation between bacterial and fungi species appears in the 2-20kDa *m/z* range, though MALDI-TOF MS can be used to measure proteins as large as 200,000 Daltons [134]. When a sample spectrum is collected and compared to saved libraries, a confidence score is provided. For each individual peak, the position, intensity, and frequency are calculated, and a log score of between 0 and 3 is provided by the Bruker Biotyper software. This is calculated by measuring three scores of the spectra against the library spectra. Firstly, the ratio of matched peaks to the total number of peaks in the unknown sample. Second, the ratio of matched peaks to the total number of peaks in the reference sample. Lastly, a score is given to relative intensities of matching peaks. Each score is given out of 10, which are multiplied together and then logged (Log10) to give a score between 0 and 3. Bruker recommend a log score of >1.70 for genus level and >2.0 for species level identification. Exceptions to this are when samples being analysed are direct from blood cultures using the Sepsityper kit (Bruker). Such samples can be run through a specialised algorithm known as the Bruker Sepsityper module. The cut off levels are then lowered to >1.60 and >1.90 for genus and species level identification respectively, which increases identification rates, though it has been noted this may introduce higher error rates. Each laboratory and institute should also ideally create additions to the commercial libraries to incorporate specific problem microbes for their patient population or geographical location. Though the libraries are extensive with ~4,000 species of ~700 genera in both the Biotyper and Vitex, they are still limited by

the number of bacteria and fungi recorded. The Biotyper also provides the log scores for two potential matches based on the library (Table 5). Some studies have described using the first organism match and the representative log scores for identification at species level whereas other studies have described confidence at species level if the two identified organisms match regardless of log scores.

Table 5: Identification examples found in the literature that use the MALDI-TOF MS for clinical identification of BSIs

	Organism match one	**Organism match two**	**Species ID?**
A	*E. coli* [1.83]	*E. coli* [1.80]	For some studies matching ID is enough for species identification despite log scores <2.00
B	*S.aureus* [1.90]	*S.simiae* [1.84]	No, both matches have log scores <2.00 and the two IDs do not match
C	*K. pneumoniae* [2.21]	*K. oxytoca* [1.99]	*K. pneumoniae* would be confirmed as the scores are >2.00 despite the second ID match

3.2.4.5. MALDI-TOF MS SAMPLE PREPARATION

Identifying microbes based on their whole cell PMF using MALDI-TOF MS has advanced diagnostic output. Though the direct profiling by whole cell PMF can be done with most pathogens, Gram-positive bacteria and yeast typically require additional preparation [135]. There are three main ways of preparing microbes for MALDI-TOF analysis: (a) a direct colony smear (DCS); (b) a DCS plus an overlay with 70% formic acid (FA); and (c) an extended protein extraction technique involving FA and acetonitrile (ACN). Gram-positive bacteria occasionally require additional acid breakdown to release the intracellular proteins due to their thicker cellular walls, i.e, method (b). FA breaks down the Gram-positive wall to release proteins and then the matrix is overlaid [136]. Other microbes with more intricate cell walls such as mycobacteria, yeast and *Nocardia* require additional and more complex extraction procedures prior to MALDI-TOF MS analysis to produce whole cell lysates. For *Nocardia*, Verroken et al., 2010 developed a technique involving ethanol protein extraction and resuspension of dried proteins in 70% FA and ACN prior to analysis

[137]. Of course, for samples such as mycobacterium, inactivation for the safety of laboratory staff is a priority. For yeast, many variations on FA techniques for extractions have been published, as FA appears to give the best results [128, 138]. The techniques involve incubation with ethanol and the addition of ACN, centrifugation, and the supernatant used for MALDI-TOF MS analysis. Others have shown success with mechanical methods using zirconia silica beads with ethanol, drying the pellet, and resuspending in 70% FA, and analysing the supernatant. Fungi of the *Penicillium* genus when intact or whole cell produce poor spectra but with resuspension in TFA plus glass bead disruption, discrimination between species was 100% accurate [139]. The FA and ACN approach in combination with the Sepsityper kit was found to be superior to DCS and the FA overlay technique for both Gram-negative and Gram-positive bacteria as well as fungi. This method involves removing host red and white blood cells via a short lysis step, a wash step, and then preparing the sample for application onto the MALDI-TOF plates for analysis. This requires adjustments to the libraries to account for the loss or addition of individual peaks.

3.2.5. RAPID PATHOGEN EXTRACTION TECHNIQUES

Though identification of pathogens via chromogenic media and biochemical testing is the gold standard, identification directly from the culture medium, i.e., blood or urine, would significantly reduce turnaround time. Companies such as Bruker Daltonics and Becton Dickinson (BD) have developed and commercialised rapid extraction kits. This usually involves the lysis of red and white blood cells from the sample, typically used for BSIs; however, this technique has also been used to look at identification of infection direct from urine samples [140-143]. The recently introduced BACpro® II kit (Nittobo Medical Co., Tokyo, Japan) also separates and removes the host-derived proteins and enhances aggregation of the bacteria by utilising cationic copolymers [142]. Still, an issue with direct MALDI-TOF MS analysis from blood cultures is that lower scores are achieved from clinical samples compared to pure cultures for solid agar and can be less reliable. However, the Sepsityper kit has a complimentary Sepsityper module on the MALDI Biotyper system (Bruker Daltonics) that was developed to improve the reliability. In a study conducted by Kayin et al 2019, it was shown that both the Sepsityper and BACpro® II method had some difficulties in

identifying particular Gram-positive bacteria, and all methods, including an inhouse method, had low identification rates for Streptococci and Enterococci [142]. Nevertheless, what the study did show was an average turnaround time of 30 minutes for the identification of the majority of bacterial strains with direct MALDI-TOF MS, compared to 18-48 hours using standard subculturing techniques.

3.2.6. Sensitivity and Specificity of the Sepsityper Protocol

Rapid isolation of microbes using these kits require whole cell bacteria or yeast and a sufficient number of live microbes in order to obtain a pellet large enough to analyse. This is achieved by performing the Sepsityper protocol on positively flagged blood culture bottles (Figure 17). The sensitivity of the protocol has been evaluated in several studies (Table 6 and Table 7). Gram-positive bacteria are more difficult to identify with the Sepsityper, with some studies showing as low as 58% species identification [144]. Nevertheless, a high accuracy for Gram-negative bacteria has been demonstrated, with sensitivity ranging from 66-100% [132, 143]. Yeast is also a problematic for the Sepsityper, with some studies showing identification rates as low as 57% to 81.7% [145]. Lysing host blood and centrifugation leaves behind host proteins which can interfere with the MALDI-TOF MS, thus reducing the identification accuracy. The Sepsityper comes at a cost compared to inhouse methods for direct MALDI-TOF MS; inhouse methods use the same concept as the Sepsityper kit, i.e., selective blood cell lysis and bacterial pelleting, though they are not standardised. Yet, a study by Martiny et al in 2012 demonstrated a 10-fold saving by using an in-house method compared to the Sepsityper kit as well as similar performance for genus identification of the two methods [141]. Compared to conventional techniques such as subculturing and biochemical testing, the Sepsityper has been shown to save 23–83 hours for Gram-negative and 34–51 hours for Gram-positive bacteria [146]. Another study found an overall reduction in time by 26.5 hours [143].

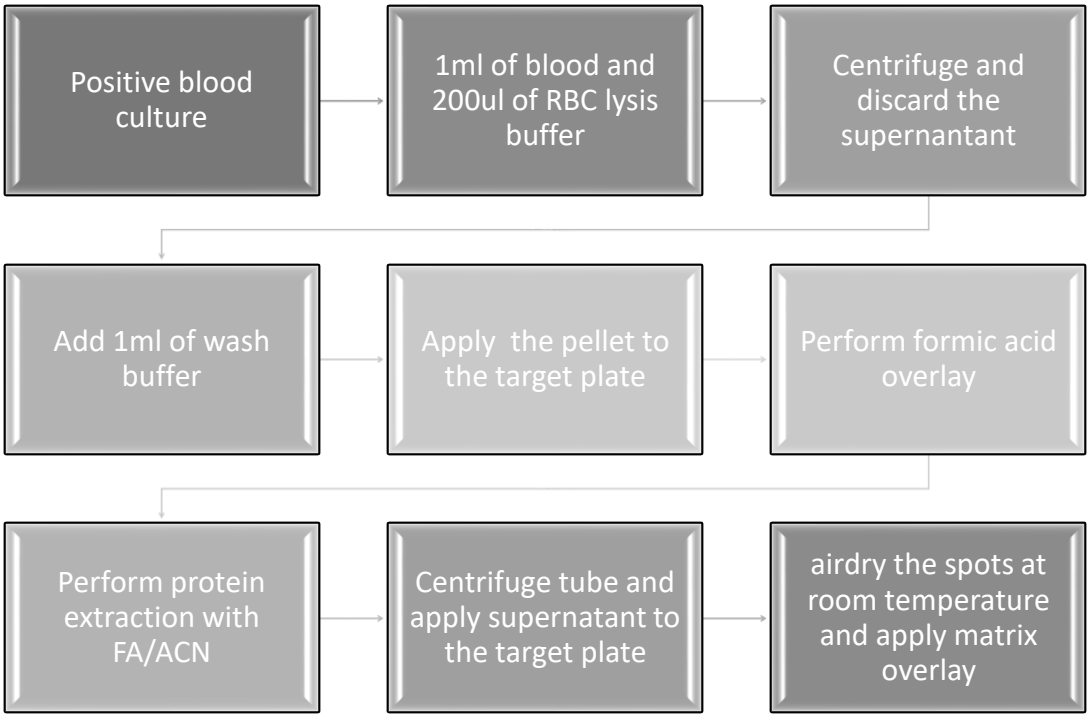

Figure 17: Schematic of the Sepsityper kit protocol (Bruker Daltonics). Positive blood cultures which flag on the BacTec have 1ml of blood removed with a needle and syringe. The RBC and WBC are lysed and centrifuged to wash away the debris leaving behind a microbial pellet. The pellet is then prepared for analysis on the MALDI-TOF MS. This can be down by allying a small amount of the pellet direct onto the target plate or by full protein extraction using formic acid and acetonitrile to release the proteins into the supernatant. The samples are then allowed to dry and the samples overlayed with matrix.

Table 6: Sensitivity of the Sepsityper method for Gram-positive and Gram-negative bacterial identification

Author	Gram-negative	Gram-positive	Overall Sensitivity	Log score cut off used
Meex [144]	82.5%	58%	67%	3 identical matches regardless of score
Buchan [146]	97.8%	80%	94.1%	>1.70 genus >2.00 species
Kayin [142]	91.8%	75.5%	68.3%	>1.70 genus >2.00 species
Loonen [147]	96%	64%	78%	>1.70 genus >2.00 species
Schubert [148]	89.8%	86.3%	86.5%	>1.50 species
Juiz [149]	95.8%	84.7%	87%	>1.70 genus >2.00 species
Kok [150]	79.7%	46.3%	59.5%	>1.70 genus >2.00 species
Lagace-Wiens [143]	100%	80%	88.5%	>1.50 genus >1.70 species
Martiny [141]	59.1%	74.3%	68.4%	>1.40 genus >1.60 species
Jamal [132]	66%	75.8%	75.6%	>2.00 species
Tadros & Petrich [151]	94.7%	66.7%	78%	>1.70 genus >2.00 species
Schieffer [152]	95.7%	81.7%	84%	>1.60 genus >1.80 species
	87.4%	**72.7%**	**77.9%**	

Table 7: Studies investigating the sensitivity of the Bruker Sepsityper kit for yeast identification

Author	Sensitivity	Log score cut off used
Young Jin Ko, 2020 [153]	(51/96) 53.1%	>1.70 genus >2.00 species
Yan et al 2011 [154]	(42) 100%	>1.9 species
Nonnemann et al 2013 [155]	(22) 77% species	>1.60 genus >1.80 species
Gorton et al 2014 [156]	(50) 76% genus 56% species	>1.60 genus >1.80 species
Nils G. Morgenthaler 2015 [157]	66%	>1.70 genus >2.00 species
Schubert et al 2011 [148]	(17) 70% species	>1.50 species
Buchan et al 2012 [146]	0% genus	>1.70 genus >2.00 species
Martinez et al 2014 [158]	(5) 60% genus 60% species	>1.60 genus >1.80 species
AM Bal, 2018 [159]	(25/40) 62.5% species	>1.70 genus >2.00 species
	62.7%	

3.2.7. WHOLE BLOOD LYSIS FOR MICROBIAL ENRICHMENT

The Sepsityper blood cell lysis contains an anionic surfactant to lyse the blood cells. A common anionic surfactant is sodium dodecyl sulphate (SDS); however, SDS is a strong detergent and likely to denature proteins which would subsequently be used for identification by MALDI-TOF MS. On the other hand, low SDS concentrations have been used successfully in inhouse lysis methods with positive results [160]. Long exposure and high concentrations may also impact negatively on the microbes within the blood. In contrast, saponin, of plant origin, lyses exclusively mammalian cells by targeting cholesterols within the cell membrane. Saponin and SDS are the two most common lysis agents seen in inhouse rapid lysis techniques. No significant difference between species level identification for the Sepsityper kit and an in-house saponin methods were found in two studies [144, 161].

3.2.8. THE USE OF MAGNETIC BEADS IN MASS SPECTROMETRY

An emerging technique is enrichment of samples via conjugated magnetic beads. These beads are able to bind to specific targets with high affinity, allowing the user to simply wash away any unwanted material. This enrichment of the target analyte allows for a purer and stronger signal which has driven the popularity of this technique. A recent work has demonstrated the use of magnetic beads for the direct quantification of peptides [162]. In this method the beads were added either directly to the target plate or mixed with HCCA, and the supernatant added direct the target plate. This was performed on a MALDI-TOF/TOF mass spectrometer (4700 Proteomics [Applied Biosystems]). Another study used weak cationic exchange magnetic beads to detect biomarkers for systemic lupus erythematosus also using MALDI-TOF MS [163]. They were able to profile serum proteomes from healthy and SLE patients and compare patten analysis for detection, similar to the principles behind microbe identification. The enrichment of microbial proteins and biomarkers from samples using magnetic beads is becoming more popular and promises to revolutionise modern diagnostics.

CHAPTER FOUR

METHODS & MATERIALS FOR PART I

4.1. FcMBL MATERIALS AND METHODS

4.1.1. MICROBE MAINTENANCE

Table 8: List of laboratory strain microbes

Organism
Escherichia coli NCTC 12241
Escherichia coli NCTC 29522
Escherichia coli NCTC 13476
Escherichia coli NCTC 10418
Staphylococcus aureus JE2 (USA 300)
Staphylococcus aureus NCTC 6571
Staphylococcus aureus NCTC 12493
Staphylococcus aureus NCTC 12973
Klebsiella pneumoniae NCTC 13438
Klebsiella pneumoniae NCTC 13442
Klebsiella pneumoniae NCTC 13443
Enterococcus faecalis NCTC 13379
Candida albicans NCPF 3939

A total of 21 strains were collected from GOSH that had previously been isolated from blood cultures and were implicated in candidemia: *Candida albicans* (6), *Candida glabrata* (3) *Candida parapsilosis* (3), *Candida auris* (3), *Candida tropicalis* (1), *Candida guilliermondii* (3), *Candida krusei (3), Candida kefyr (1)*. Streptococcal patient strains were also collected: *S. pneumoniae* (2), *S. anginosus* (2) and *Enterococcus faecalis* (2). *Escherichia coli* strains isolated from patients with meningitis were also collected from GOSH. Bacteria were stored in 20% glycerol stock at -80^{o}C and plated onto fresh LB, chocolate or blood agar plates and grown overnight for 16 hours at 37^{o}C at 5% CO_2.

4.1.2. MATERIALS AND REAGENTS

All products for bacterial growth and maintenance were purchased from Sigma unless specified otherwise. The mass spectrometry reagents including the water, acetonitrile and formic acid were purchased from Fluka Honeywell. The HCCA matrix, the mass spectrometry target plates, and bacterial testing standards (BTS) were purchased directly from Bruker Daltonics (Glasgow, UK). Blood culture bottles and blood collection sets were ordered from BD diagnostics (Wokingham, UK). HBSS with

calcium and magnesium ($HBSS^{++}$) and HBSS without ($HBSS^{--}$) were purchased from Gibco (Lincolnshire, UK).

4.1.3. GROWTH CURVES AND VIABILITY COUNTS

One colony was added to 5ml of BHI and incubated at 37°C, shaking at 290rpm overnight for 16 hours. In a fresh 50ml falcon, 5ml of BHI was inoculated with 200µl of the overnight culture and incubated until an OD600 reading of 0.2, 0.4, 0.6, 0.8 and 1 is achieved using the SPECTROstarNano (BMG LABTECH). Then 10-fold serial dilutions were prepared in BHI, and viability counts prepared. Using the Miles and Misra technique [164], 20µl of bacteria or yeast were plated onto LB or blood agar plates in triplicate, left to dry and incubated for 16 hours at 37°C [164].

4.1.4. BLOOD CULTURE SYSTEMS AND BLOOD CULTURE BOTTLES

Peripheral blood (PB) was collected into BD BACTEC™ Lytic Anaerobic medium and BD BACTEC™ Peds Plus™ Medium (BD). The Lytic bottles had 7ml of PB blood added and 3ml of PB was added to the Peds Plus™ unless specified otherwise. Bottles were incubated using the BD BACTEC™ FX blood culture system and growth determined by CO_2 production. Blood culture bottles were spiked with 10-30 CFU/ml and left on the BACTEC™ incubator until a positive blood culture was indicated. Blood was then extracted using a syringe and needle and added directly to 2ml screw cap tubes (Sarstedt, UK) for FcMBL processing or 1.5ml Eppendorfs for Sepsityper analysis (Figure 18).

4.1.5. PAEDIATRIC BLOOD SAMPLE COLLECTION

BACTEC™ clinical positive blood cultures had 1ml extracted using a syringe and needle and was added to a black screw cap tube with the sample number as reference.

4.1.6. CONVENTIONAL IDENTIFICATION METHODS

Simultaneously with blood samples being processed using rapid identification techniques, blood was also subcultured onto solid agar and incubated at 37°C until

colonies were visible. Colonies were smeared onto the MALDI-TOF MS target plate and overlaid with 1µl of fresh HCCA matrix. Samples were analysed on the Bruker Biotyper and analysed automatically with the Biotyper 3.1 software.

4.1.7. SEPSITYPER METHOD

Positive blood cultures were identified using the Sepsityper kit according to the manufacturers protocol (Figure 17). Briefly, 1ml of positive blood culture blood was removed using a syringe and needle and placed into a sterile 1.5ml Eppendorf tube. Then, 200µl of lysis buffer was added and the mixture vortexed for 10 seconds and centrifuged at 13,000*g* for 2 minutes. The pellet was resuspended with 1ml of wash buffer and centrifuged at 13,000*g* for 1 minute. The bacterial pellet was then extracted using FA/ACN, and 1µl of supernatant was layered onto the target plate and left to air dry.

4.1.8. FCMBL BEAD PULLDOWN PROTOCOL

Table 9: FcMBL method reagents and recipes

Reagent	**Recipes**	
HBSS Ca^{2+}		
FcMBL conjugated to magnetic beads	Wyss Institute	Accession code KJ710775
Dynabeads ™	Thermofisher	
Bead solution		
Per 1ml solution contains:	50µl FcMBL (1µM)	850µl of TBST Ca^{2+}
	100µl of 1M glucose	

FcMBL beads were prepared as described in Table 9 above with 1ml containing 5µg of beads. Samples were transferred to black screw cap tubes and incubated with 100µl of 5% saponin and 100µl of bead solution at 25ºC for 5 minutes rotating on a HULA shaker (Thermofisher Scientific) at 25RPM. Tubes were added to a magnetic holder (Thermofisher Scientific) until the beads were pulled to the side of the tube and washed thrice in 1ml of $HBSS^{++}$. The beads are then eluted in FA and ACN (10µl for bacteria and 20µl for yeast).

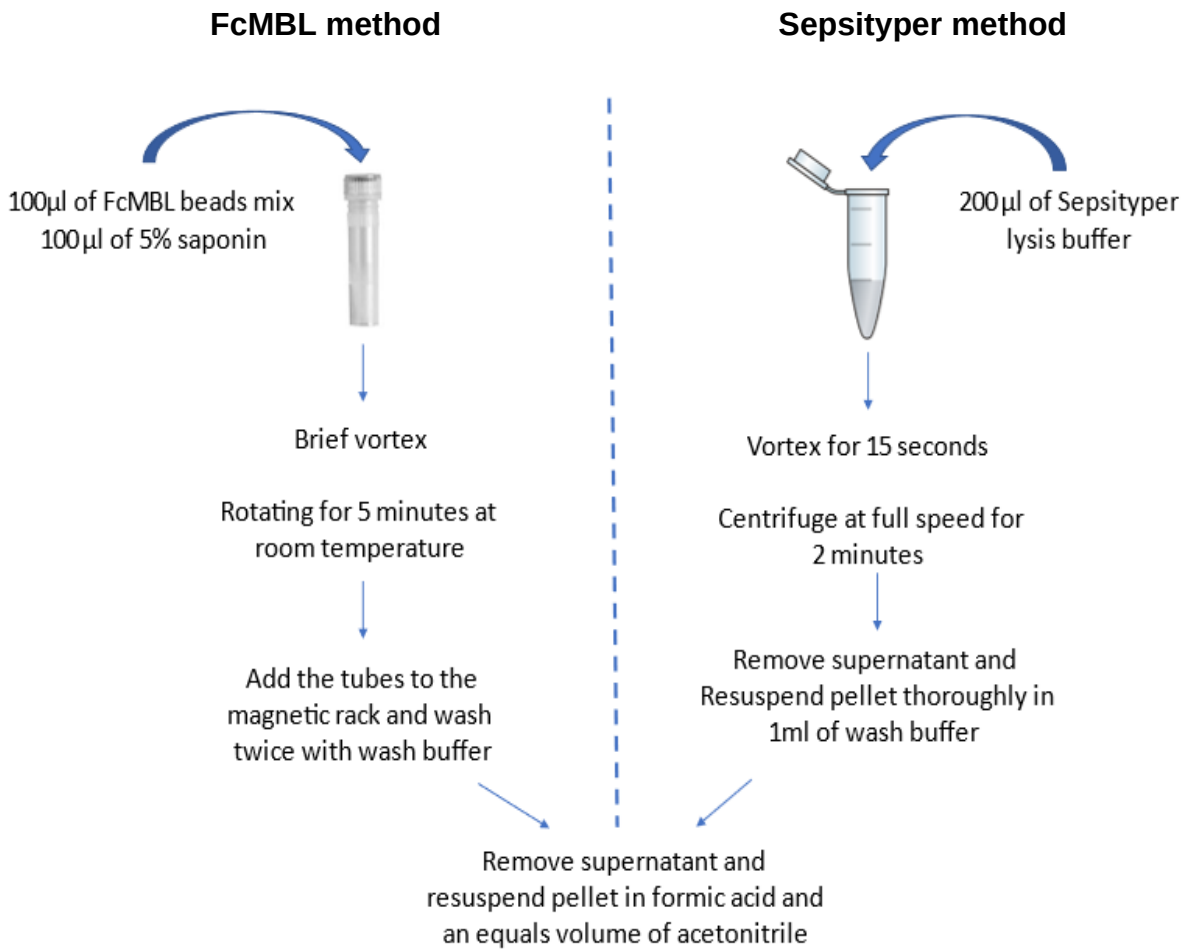

Figure 18: Comparison of the FcMBL and Sepsityper methods

4.1.9. Red Blood Cell lysis from positive blood cultures

Blood cell lysis was measured with healthy volunteer blood, both unspiked and spiked. Blood was processed with 200µl of 5% saponin unless specified otherwise. SDS or saponin was added to the blood prior to incubation on the HULA to find the optimal lysis protocol. The samples were then removed, added to the magnetic rack, and washed in 1ml of $HBSS^{++}$. The sample was prepared for MALDI-TOF MS by FA/ACN extraction. Determination of successful lysis was achieved by visualisation of the beads, MALDI-TOF MS scores, and bacterial viability counts.

4.1.10. FORMIC ACID AND ACETONITRILE PROTEIN EXTRACTION

Bacteria and yeast were extracted as described by Schulthess et al [165]. For FcMBL processed samples, beads were resuspended in 10µl of 70% FA for bacteria and 20µl for yeast and an equal volume of 100% ACN. Beads were then vortexed and added back into the magnetic rack. Once beads were pulled from the supernatant, 1µl was layered onto the target plate and left to air dry. Once dry, 1µl of fresh HCCA was layered onto the sample and again left to dry. For Sepsityper processed samples large pellets were resuspended in 50-80µl, vortexed briefly and then an equal volume of 100% ACN added and vortexed. Medium sized pellets are resuspended in 10-50µl and for small or non-visible pellets between 1-5µl resuspension volume was used.

4.1.11. DIRECT CULTURE OF FCMBL BEADS

Bacterial stocks were prepared such that 50µl of suspension would contain 10^0,10^1 and 10^2 bacteria. For control samples, 50µl of suspension was plated directly onto solid agar and counted. For FcMBL samples, the 50µl was added to 950µl of volunteer blood culture and the beads incubated and processed as described above (4.1.8) After the beads were processed with bacteria or fungi, FcMBL beads were resuspended in 100µl of fresh BHI, vortexed for 20 seconds and plated onto appropriate solid agar plates. Plates were incubated at 37^{o}C at 5% CO_2 for 16 hours and 28^{o}C for yeast samples before counting.

4.1.12. REDUCED CULTURE TIME EXPERIMENTS

Volunteers were bled into BACTEC™ blood culture bottles ~7-10ml for spiking experiments. The blood culture bottles were then spiked with ~10 CFU of pathogen and left to incubate on the BACTEC™. Samples were taken at regular intervals and processed for viability counts, processed with the FcMBL method and the Sepsityper method simultaneously. Success was characterised by whether significant microbial peaks were observed on the mass spec or identifications were made by the Bruker Biotyper software.

4.1.13. BLOOD AND FCMBL BEAD INCUBATION OPTIMISATION

Blood spiked with bacteria of known concentrations were incubated for various times with FcMBL beads and processed as mentioned. The beads were resuspended in 100µl BHI, vortexed for 20 seconds before being plated on appropriate agar. Viability counts were performed. Light microscope images of the blood cultures were taken at various time points to visualise blood cell lysis, bacterial location, and bead location.

4.1.14. MALDI-TOF MASS SPECTROMETRY

To analyse samples by MS, 1µl of supernatant was spotted onto disposable 96-spot MALDI target plates and left to dry. Once dry, 1µl of HCCA matrix was added to each spot and left to dry. Plates are kept free from dust for up to 24 hours before being analysed on the MALDI-TOF MS. The mass spectra (2-20kDa) were automatically acquired using Bruker's FlexControl software. Scores of >2.00 were considered sufficient for identification at species level and >1.70 for genus level, following the manufacturer's recommendation. For quality control and machine calibration, 1µl of Bruker's bacterial test standard (BTS) sample was added to each run. Blood was collected from 12 volunteers and processed with FcMBL beads as described, with and without microbes. Mass spectra were collected and overlaid using Flex Analysis software and common peaks were identified as blood background.

4.1.15. BIOFIRE FILMARRAY

To analyse the FcMBL beads 200µl of sputum was added directly to the BioFire cartridge and loaded directly into the machine. FcMBL beads were added to 200µl of the same sputum samples, washed and eluted in 200µl of HPLC-grade H_2O before being added to a BioFire cartridge. All experiments were performed in a CAT III laboratory.

4.1.16. QUANTITATIVE PCR (QPCR)

DNA was extracted from bacterial samples using the QIAmp DNA mini kit (Qiagen) according to manufacturer recommendations. The 16S qPCR was carried out using the QuantiTest SYBR Green PCR kit (Qiagen) as shown in Table 10 the following primers were used for amplification of the 16S gene: The forward (TCCTACGGGAGGCAGCAGT), reverse (GGACTACCAGGGTATCTAATCCTGTT).

Table 10: 16S qPCR reagent volumes and cycle requirements

Reagent	**Volume per sample**	
H_2O	8.5µl	
SYBR	12.5µl	
F primer	1µl	10pmol/µl working concentration
R primer	1µl	10pmol/µl working concentration
DNA template	2µl	1ng/µl
Temperature	**Time**	**Cycles**
95ºC	15 minutes	X1
94ºC	15 seconds	X45
58ºC	30 seconds	X45
72ºC	30 seconds	X45

4.1.17. DATA AND STATISTICAL ANALYSIS

MALDI-TOF MS data and raw spectra were collected from the machine and analysed using Flex Analysis 3.4 software. All spectra were smoothed, and baseline subtracted. All the graphs, calculations, and statistical analyses were performed using GraphPad Prism software version 7.0 (GraphPad Software, San Diego, CA, USA). A significance of $P<0.05$ was used for all analyses. Mann-Whitney *U* tests were performed to compare the median log scores for the Sepsityper and FcMBL methods. MS data were processed and analysed with FlexAnalysis 3.4 software.

We here outline the procedure by which the spectral similarities between the spiked Candida samples were calculated and visualised and refer to Appendix B for further details. The similarity of pairs of spectra were calculated by first mapping each spectrum into a normalised vector and then calculating the overlap (i.e., cosine similarity) of these “spectral vectors”. Spectral vectors are constructed by discretising the raw spectra into a finite number of bins and summing the intensity of all peaks in each bin. This accounts for slight measurement error and imperfection in the precise locations of the observed peaks. A data-driven approach was adopted for selecting the bin widths and positions. The spectral similarities between each pair of spiked samples were calculated, and used to generate clustered heatmaps, with sample clusters determined by an agglomerative clustering approach.

All investigations were performed in accordance with the Hospitals Research governance policies and procedures.

CHAPTER FIVE

OPTIMISATION OF THE FCMBL BEAD METHOD

This chapter details how the FcMBL bead method for BSI pathogen identification was optimised for use in clinical blood samples with the MALDI-TOF MS.

5.1. FcMBL OPTIMISATION AIMS

The aims of this chapter were to:

1. Develop and optimise an FcMBL bead-based method for microbial binding in clinical blood culture samples;

2. Establish the optimal MALDI-TOF MS sample preparation method for FcMBL-processed beads.

5.2. FcMBL OPTIMISATION RESULTS

5.2.1. BEAD FUNCTIONALITY

The functionality of the FcMBL beads were measured upon arrival from Boston, USA. To test the ability of the beads to bind to clinical isolates, experiments were performed using residual sputum from a patient at GOSH with confirmed respiratory tract infection by standard subculturing and MALDI-TOF MS analysis.

Neat sputum **FcMBL-processed sputum**

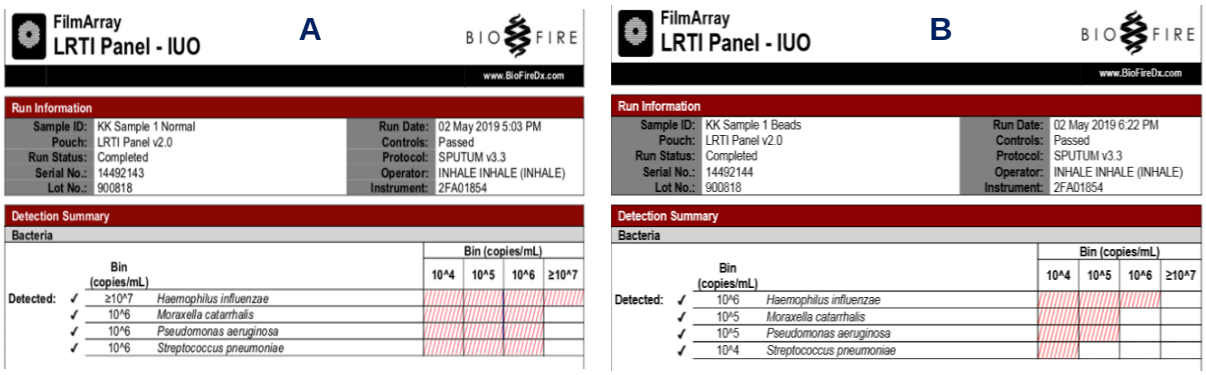

Figure 19: FcMBL beads bind respiratory pathogens within sputum as detected using the BioFire. Left had 200µl of neat sputum added to the cartridge and the right had 200µl of sputum processed by the FcMBL beads.

The FcMBL beads detected all of the microbes that detected in the unprocessed sputum sample using the BioFire FilmArray. Though the detection and quantification on the BioFire was an order of magnitude lower than the unprocessed, this could be explained as this is a PCR-based technique that can detect DNA from live and dead microbes. We observed that the FcMBL beads bind well to both Gram-negative and Gram-positive bacteria. Magnetic dynabeads without conjugated FcMBL were processed alongside and cultured on LB agar with no colonies grown. This as to ensure that binding was via the FcMBL component if the beads and not the biotin labels of the beads.

5.2.2. FcMBL ELUTION OPTIMISATION

Next, the elution volume of the FcMBL beads in H_2O was tested. MALDI-TOF MS analysis requires 1µl of sample to be layered onto the target plate; however, optimal results for elution of the beads were found to be with 200µl of MS-grade H_2O (Figure 21).

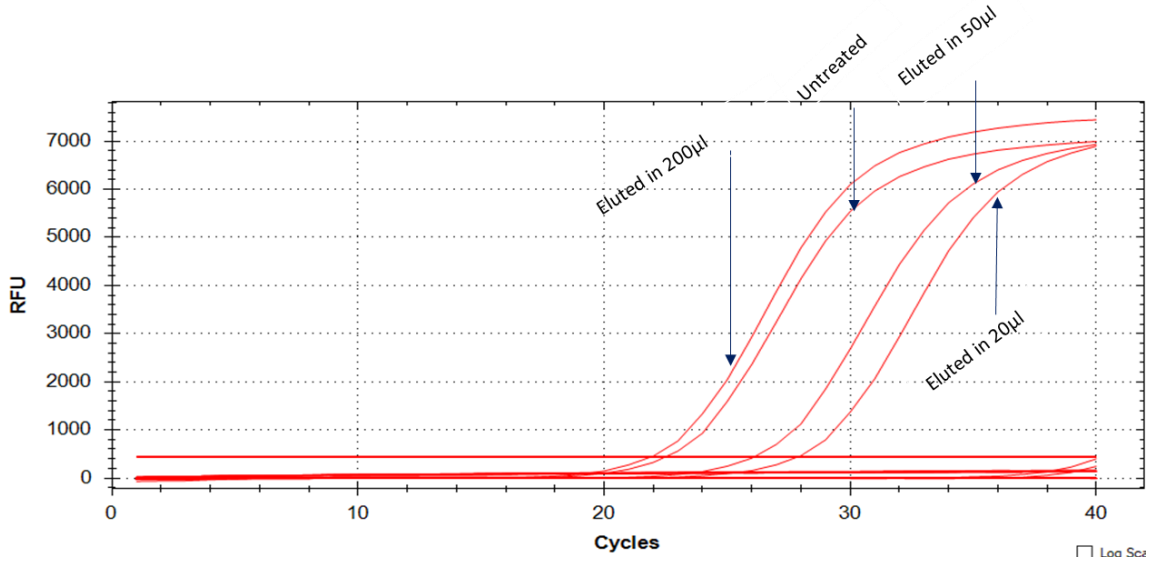

Figure 21: qPCR of the 16S rRNA gene after elution in different volumes of H_2O. The most effective volume was 200µl of H_2O and the least effective was the lower volume of 20µl.

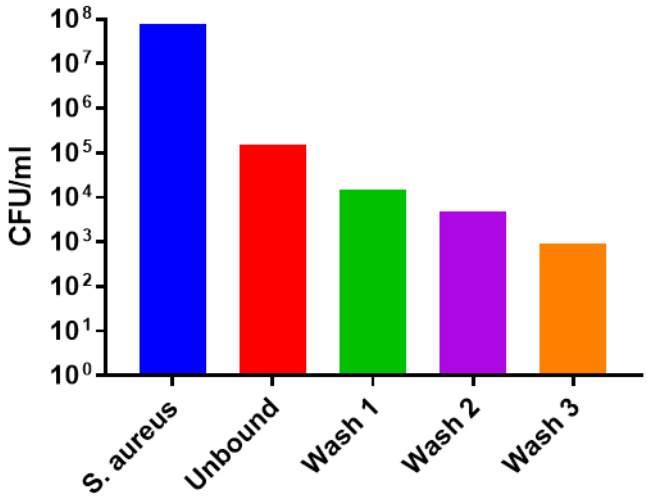

Figure 20: Bacterial loss during washing of FcMBL beads after capture of *S. aureus*. The total loss of the washes was <1% of the original concentration.

Eluting the beads in H_2O volumes below 200µl resulted in less bacteria being detected by 16S qPCR. This was validated in follow-up work carried out by Dr Mike Super's team at the Wyss Institute, Harvard (data not shown). In the same experiment the loss of bacteria during the washing stages was evaluated by viability counts. Aspirating the residual liquid from the first wash demonstrated that 10^5 bacteria were not captured by the FcMBL beads – compared to the 10^8 CFU captured – and the subsequent three washes lose <1% of the total captured (Figure 20). Similar results were seen for *E. coli* strains (3) and *K. pneumoniae* strains (3) as seen in Appendix A. These experiments were carried out to ensure that washing the beads was not removing the microbes bound to the beads.

EDTA is a chelator of calcium ions and was investigated as a potential eluent that could be added to the beads to remove carbohydrates bound to the MBL CRD, in order to use a lower volume.

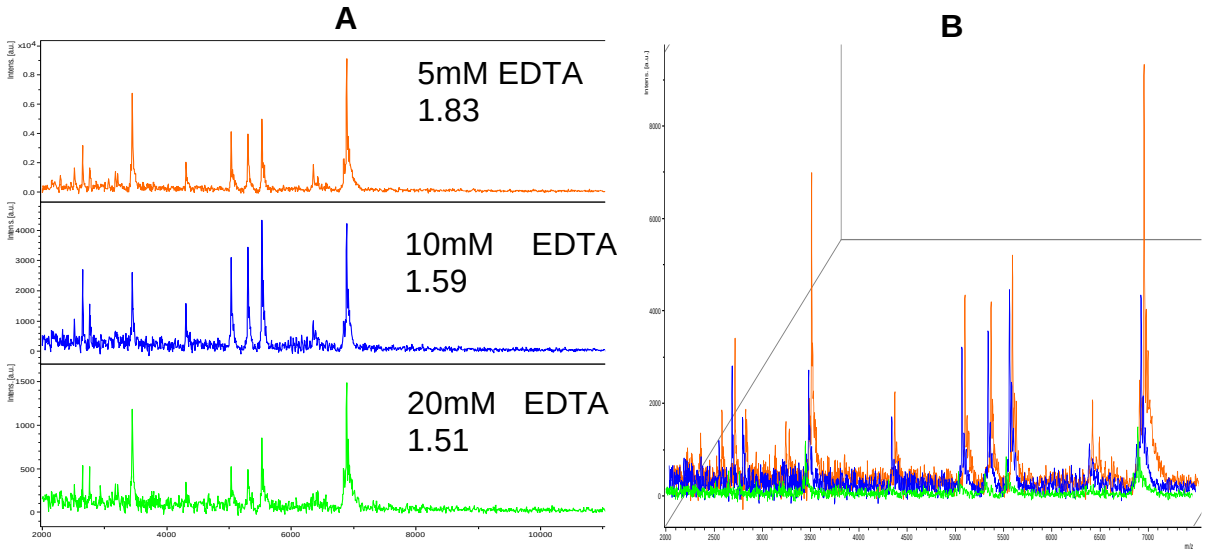

Figure 22: MALDI-TOF MS detection of *S. aureus* 12973 A) after elution of beads in various concentrations of EDTA. B) Spectral overlay of EDTA elutions

In Figure 22A, lower concentrations of EDTA (<10mM EDTA) resulted in higher log scores on the Biotyper despite similar peaks when the spectra were overlaid (Figure 22B). Concentrations larger than 10mM showed heavy precipitation of EDTA on the target plate when the acidic matrix was layered on top of the dried sample. Peak intensity decreases as the EDTA concentration increases (1,500a.u for 20mM vs 10,000a.u for 5mM). This drop in intensity could explain the similar peak patterns but lower log scores.

FA and ACN volumes were optimised by testing on bacteria of known concentration with and without processing using FcMBL beads. Log scores were higher when more FA was added for protein extraction. A) 10^9 *K. pneumoniae* processed by FcMBL beads. B) Unprocessed sample of 10^9 *K. pneumoniae* C) 10^8 bacteria processed with FcMBL beads. D) Unprocessed 10^8 *K. pneumoniae*. Larger volumes of FA and ACN increase the log scores for FcMBL processed samples (Figure 23). This increase in volume is more prominent in samples A and C. If too little FA is used when extracting direct from the beads, then little or no extraction occurs (Figure 23A), and the supernatant does not produce a reliable mass spectrum. Sample 21C shows a significant difference between 5µl of FA versus 20µl of FA with a *P* value of 0.0183 using a paired *t*-test.

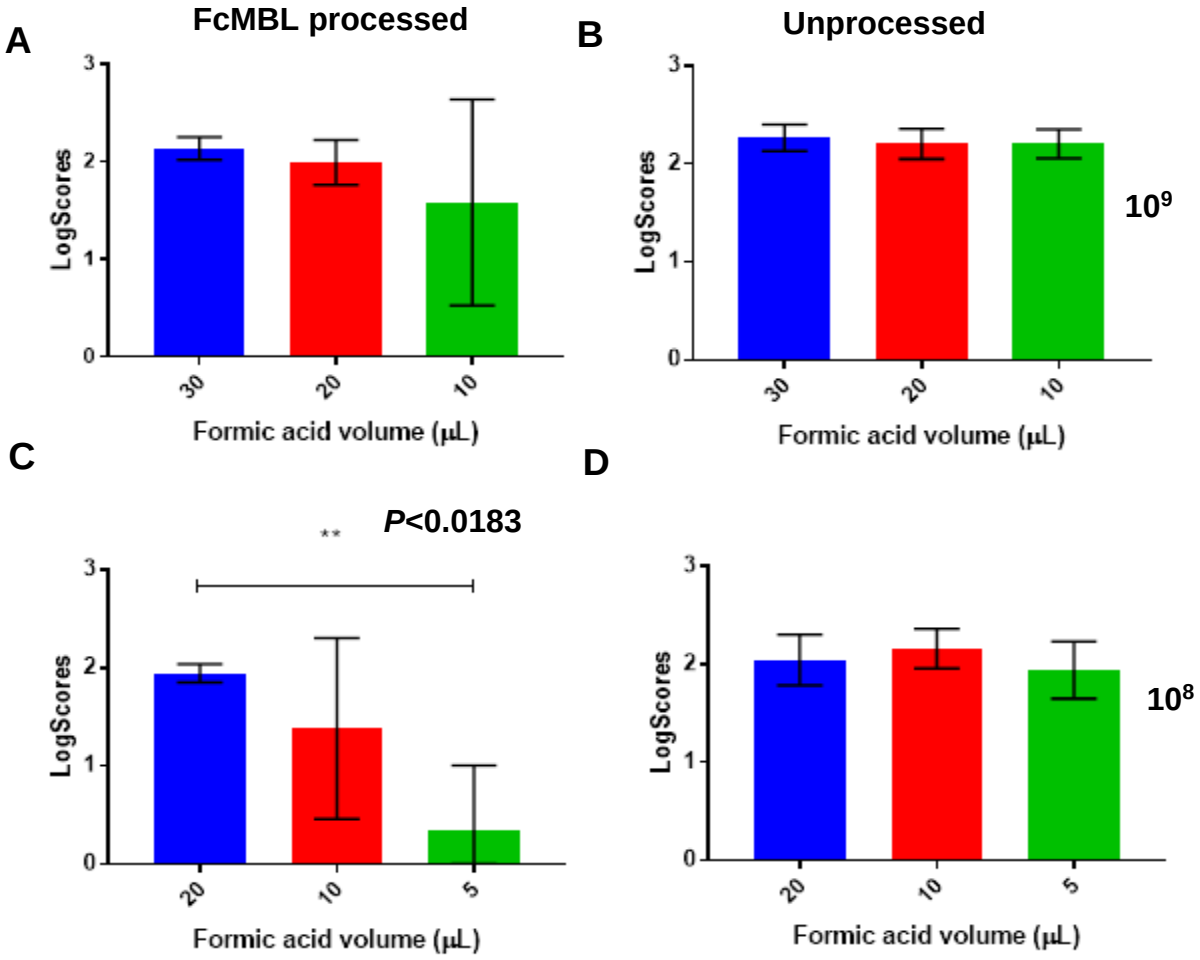

Figure 23: Formic acid volume optimisation using *Klebsiella pneumoniae* in HBSS^{++}. A and C on the left are from FcMBL processed samples. Images B and D are from unprocessed samples which were centrifuged. A and B were at concentrations of 10^9/ml and C and D were at 10^8/ml. For FcMBL processed samples a minimum of 10-20µl is needed for effective identification on the MALDI-TOF MS (*n=3*).

5.2.3. COMPARISON OF MALDI-TOF MS SAMPLE PREPARATION TECHNIQUES

Since elution of the beads in H_2O was found to only be successful with volumes above 50µl, we investigated the effect of FA and ACN extraction direct from the beads. Comparison of the different sample preparation techniques using three different bacteria at 10^7 CFU/ml in $HBSS^{++}$ was carried out (Table 11).

The spectral overlay of all the samples were similar and no obvious differences in peaks were observed (Figure 24). Increases in Biotyper log score values were seen for the FcMBL pulldown bacteria samples (D) that were eluted directly with FA/ACN, compared to the FcMBL processed samples that were first eluted in 200µl of water, centrifuged to pellet eluent and subsequent FA/ACN extraction (C). We found that FA/ACN extraction was faster (~30 minutes) than eluting in H_2O first.

Table 11: Comparison of MALDI-TOF MS log scores for the sample preparation techniques with *E. coli*, *K. pneumoniae* and *S. aureus* at 10^7/ml in HBSS (*n=1*).

Method		***E. coli***	***S. aureus***	***K. pneumoniae***
A	**DCS**	2.33	2.40	2.35
B	**70% FA overlay**	2.45	2.43	2.35
C	**Extended FA/ACN extraction after elution**	2.09	1.99	2.09
D	**Extended FA/ACN extraction direct from FcMBL beads**	2.21	2.03	2.40

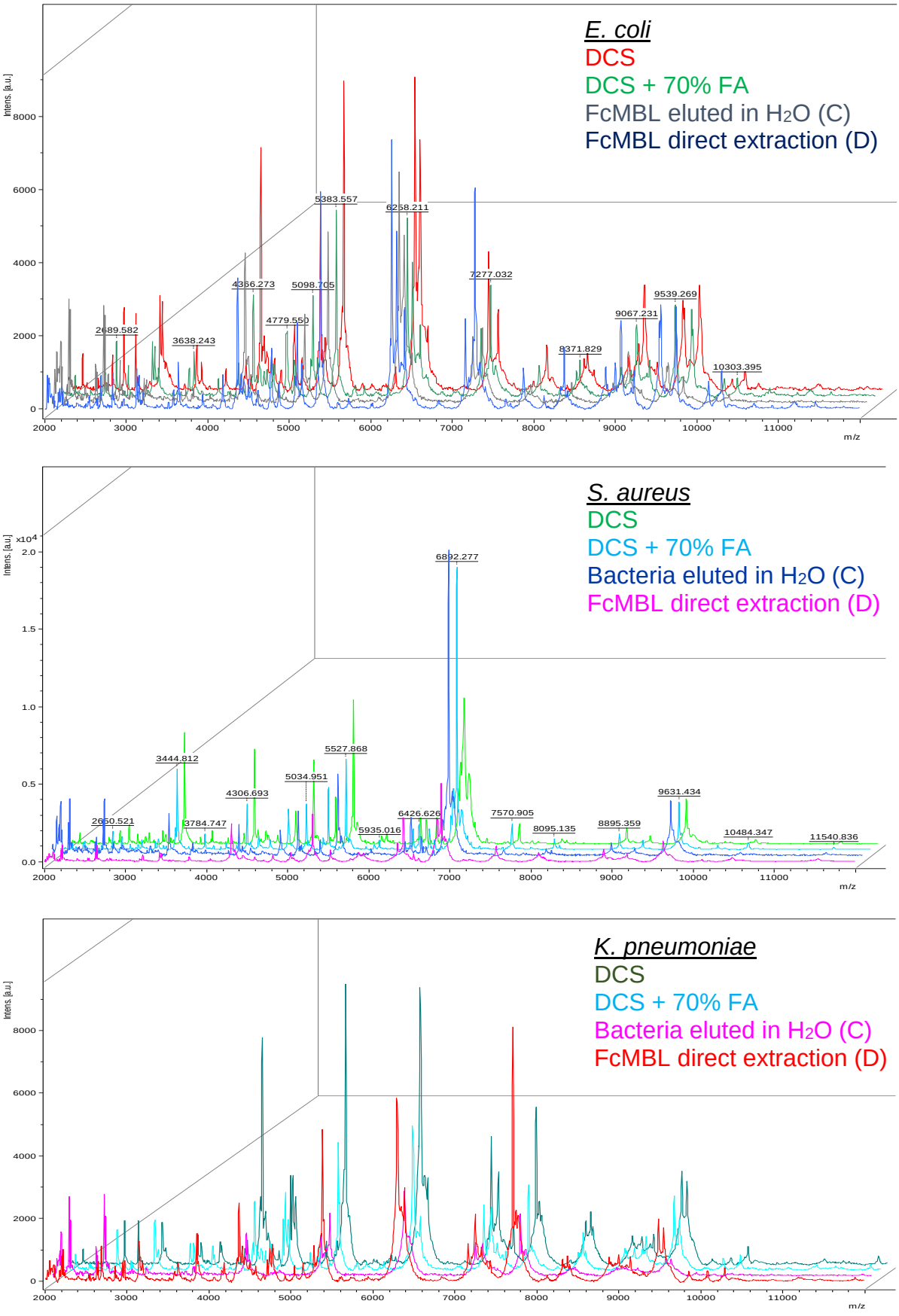

Figure 24: Spectral overlay of different MALDI-TOF MS sample preparation techniques. FcMBL direct extraction involves elution of the beads with FA and ACN.

OPTIMISATION OF FCMBL BEAD CAPTURE WITHIN PERIPHERAL BLOOD

5.2.4. BLOOD CELL LYSIS OPTIMISATION

Blood cell lysis buffers were investigated for their: A) ability to lyse whole blood; B) effect on bacterial integrity; and C) effect on the conjugated FcMBL molecule. A concentration of 10^8/ml of Gram-positive *S. aureus* was used.

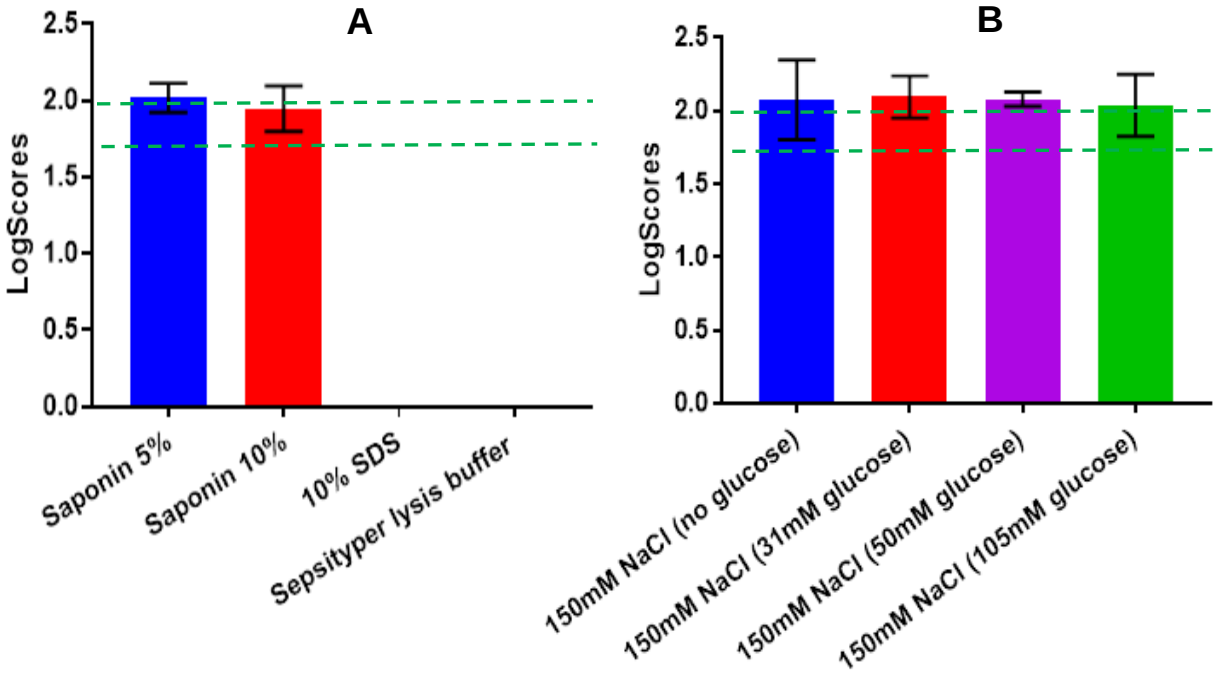

Figure 25: Comparison of different blood cell lysis reagents with the FcMBL protocol A) saponin vs SDS and the Sepsityper detergent B) 5% saponin with various salt and glucose concentrations using *S. aureus*. (*n*=3) [SD].

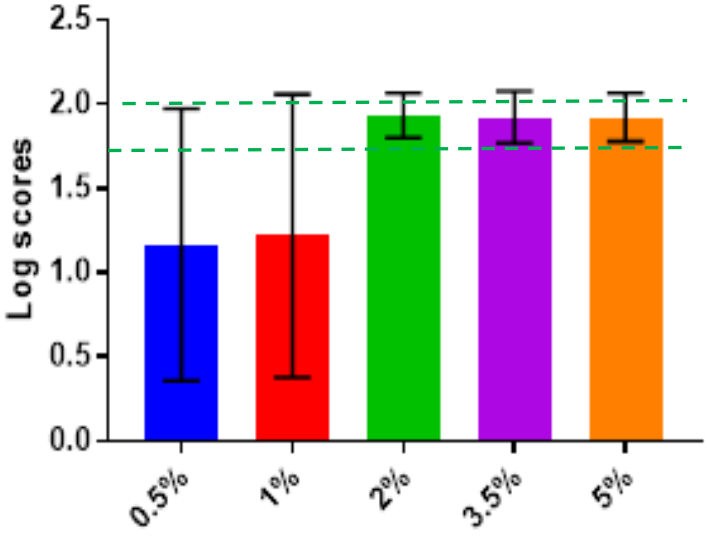

Figure 26: Comparison of blood cell lysis for bacterial isolation and detection by MALDI-TOF using a saponin gradient using *S. aureus*. (*n*=3) [SD].

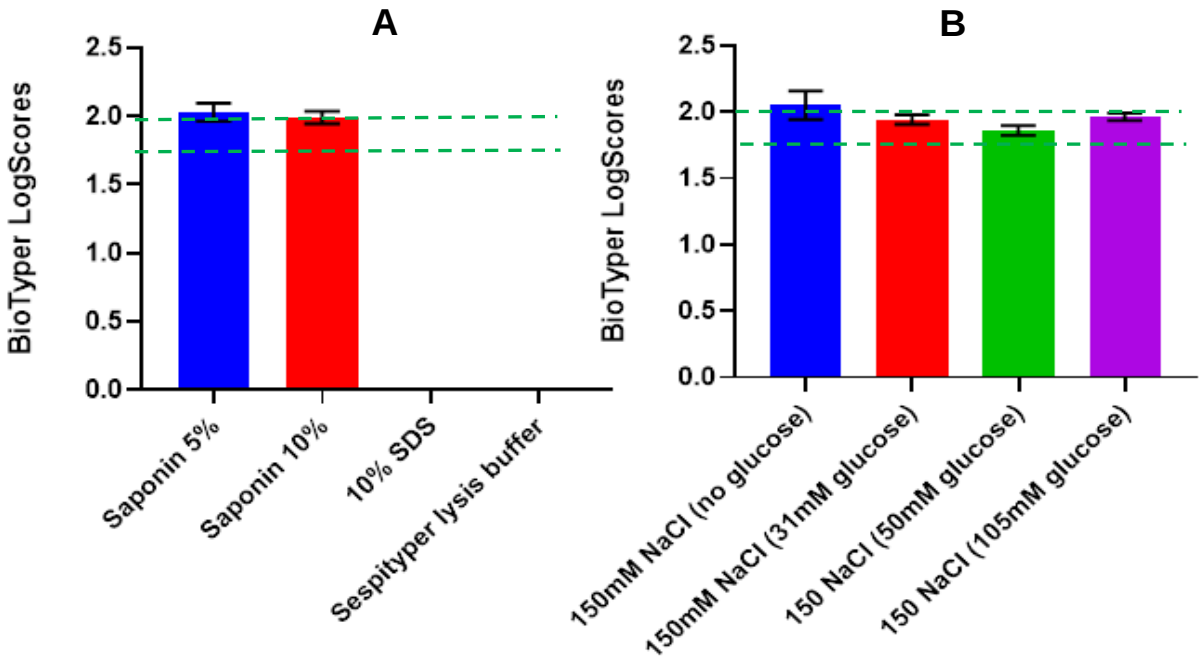

Figure 27: Comparison of different blood cell lysis reagents with the FcMBL protocol A) saponin vs SDS and the Sepsityper detergent B) 5% saponin with various salt and glucose concentrations using *E. coli*. (*n*=3) [SD].

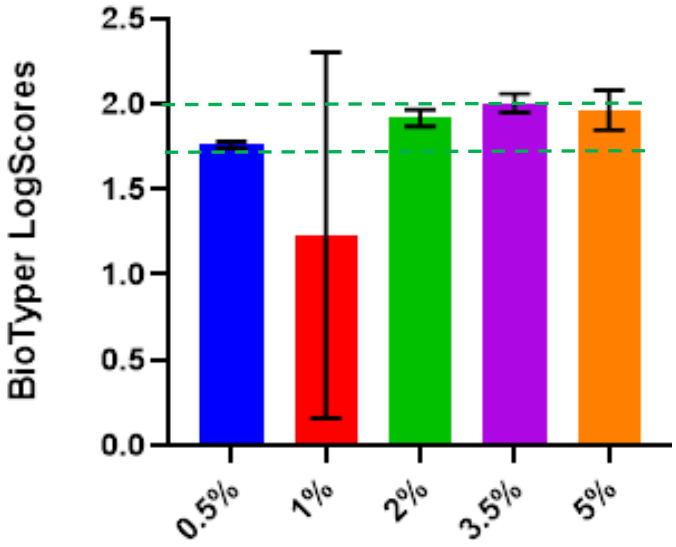

Figure 28: Comparison of blood cell lysis for bacterial isolation and detection by MALDI-TOF using a saponin gradient using *E. coli*. (*n*=3) [SD].

We observed that the FcMBL beads were ineffective if a strong detergent such as SDS or the Sepsityper lysis buffer was used (Figures 25A and 27A). We also see that 5% saponin is not significantly different to 10% saponin, and that adjusting salt and glucose concentrations did not increase bead recovery significantly. In an attempt find

the optimal saponin concentration we performed the assay with a saponin gradient (Figures 26 and 28). Less than 2% saponin was not enough to produce Biotyper log scores for *S. aureus* and was inconsistent for *E. coli* detection.

5.2.5. BLOOD AND FCMBL BEAD INCUBATION OPTIMISATION

To optimise the speed of the protocol, we investigated the time it takes for microbes to bind to the FcMBL beads within peripheral blood. Beads were incubated for various amounts of time with spiked blood, processed and plated on solid agar.

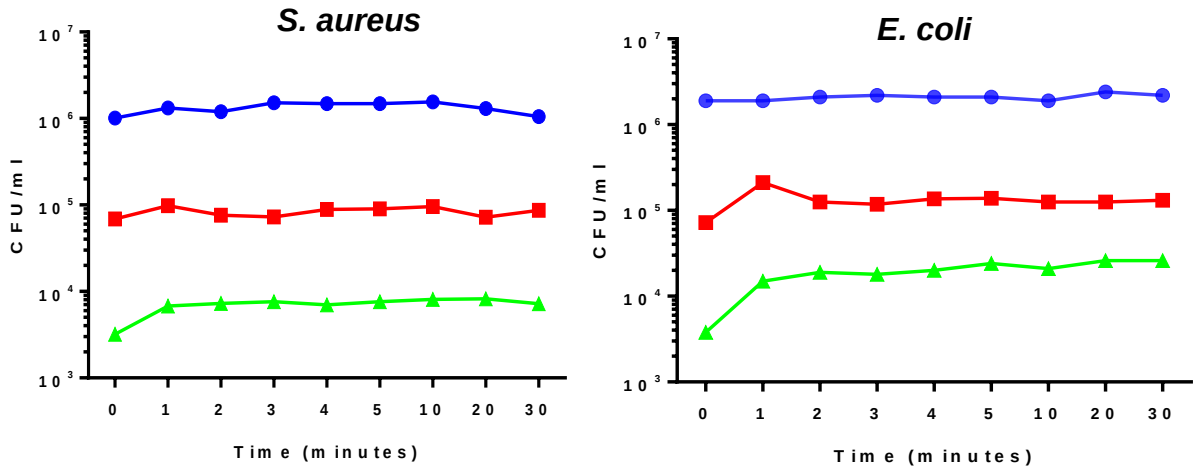

Figure 29: Rapid binding of FcMBL to *S. aureus* and *E. coli.* Blue shows the CFUs for concentrations of bacteria of 10^6/ml, red for 10^5/ml and green for 10^4/ml. (*n=1*)

To measure the efficiency and optimal binding time of the FcMBL beads, the beads were added to various concentrations of bacteria. The beads were then removed, washed briefly and vortexed in media to remove bacteria and plated on solid agar. No difference was observed in colony counts between incubation of the FcMBL beads with spiked blood for 5 minutes or 30 minutes (Figure 29). Five-minute incubations with the blood were sufficient time to capture bacteria. Binding was also observed when beads are added directly to the tubes and removed immediately. Once the bacterial concentration reaches approximately 10^6 the recovered bacteria concentration is the same for all time points in both Gram-positive and negative bacteria.

5.2.6. ENRICHMENT OF MICROBES USING FCMBL BEADS VS CENTRIFUGATION

The effectiveness of the beads was investigated by comparing unprocessed *E. coli* 10418 in a sterile PBS suspension at various concentrations (10^3–10^7 CFU/ml) with FcMBL-processed *E. coli* in PB of the same concentrations on the MALDI-TOF MS.

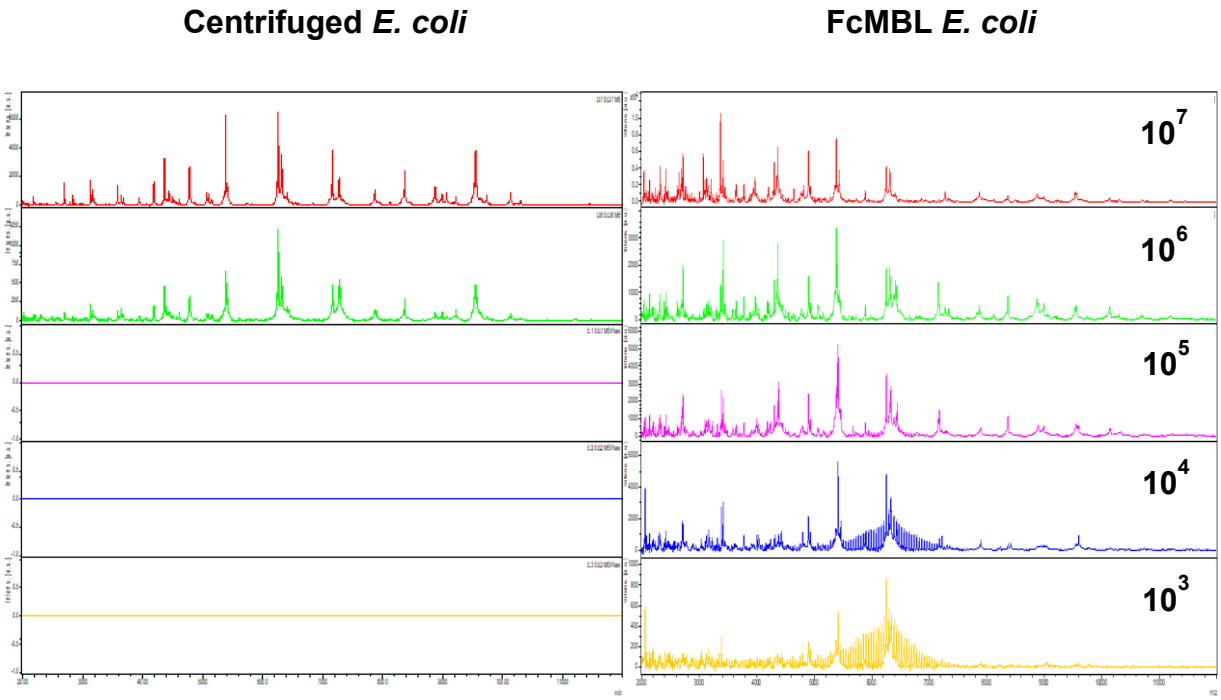

Figure 30: MALDI-TOF MS spectra of control samples (left) and FcMBL-processed samples (right). Bacteria were spiked in PB and processed with the FcMBL, and the control centrifuged samples were spiked into PBS.

Table 13: Biotyper log scores for the control centrifuged samples and the FcMBL-processed samples

	E. coli (unprocessed)	*E. coli* (FcMBL beads)
10^7	2.26	1.94
10^6	2.06	1.85
10^5	0.00	1.45
10^4	0.00	1.45
10^3	0.00	1.38

The Biotyper log scores for the 10^6 and 10^7 FcMBL-processed samples were lower than the centrifuged samples (Table 13). While the FcMBL-processed sample scores would have been sufficient for genus level identification (>1.70) they do not reach the Bruker recommendation for species level identification (≥2.00). Interestingly though, the FcMBL-processed samples provided peaks for analysis even down to 10^3 much below the $10^5/10^6$ required for the effective identification of microbes using MALDI-TOF MS technology. It was observed that though the log scores for FcMBL-processed samples at 10^4 and 10^5 were insufficient for identification using the Bruker algorithm, we observed a very close overlay with sufficient samples (Figure 30B).

5.2.7. RETRIEVAL OF BACTERIA FROM BLOOD CULTURES

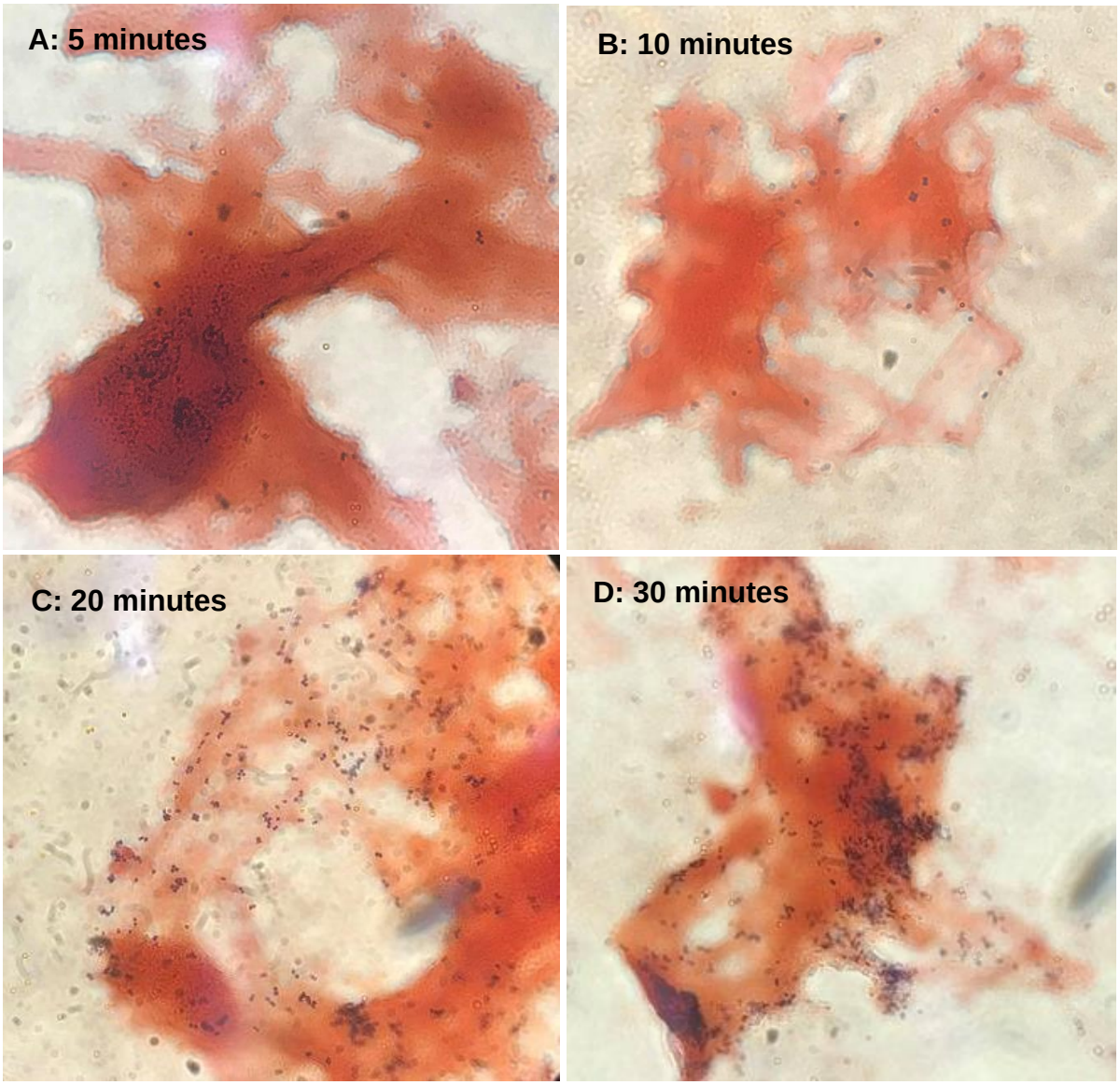

Figure 31: Gram-stain over time of blood cultures incubated with 10^7/ml *S. aureus* 12973 and FcMBL beads. The dark red areas are blood clots, and the purple stains are the *S. aureus* collecting within the clots.

S. aureus 12973 is coagulase positive, and the Gram-stain demonstrated that over 30 minutes of incubation more of the bacteria becomes trapped in blood clots within the sample (Figure 31). Some beads were seen inside the clots; however, this number remained similar throughout the incubation. This clotting was only observed when high doses of bacteria were spiked into fresh healthy donor blood.

FcMBL bead plating direct onto solid agar plates permits microbial growth (Figure 32). Using *E. coli, K. pneumoniae* and *S. aureus*, similar results were obtained for both the unprocessed and FcMBL processed samples, suggesting that the FcMBL beads permit (and do not hinder) direct culture of bacteria on solid agar. Moreover, FcMBL allows for enrichment of microbes from samples as observed in Figure 32 below. Paired *t*-tests showed no differences between the two methods.

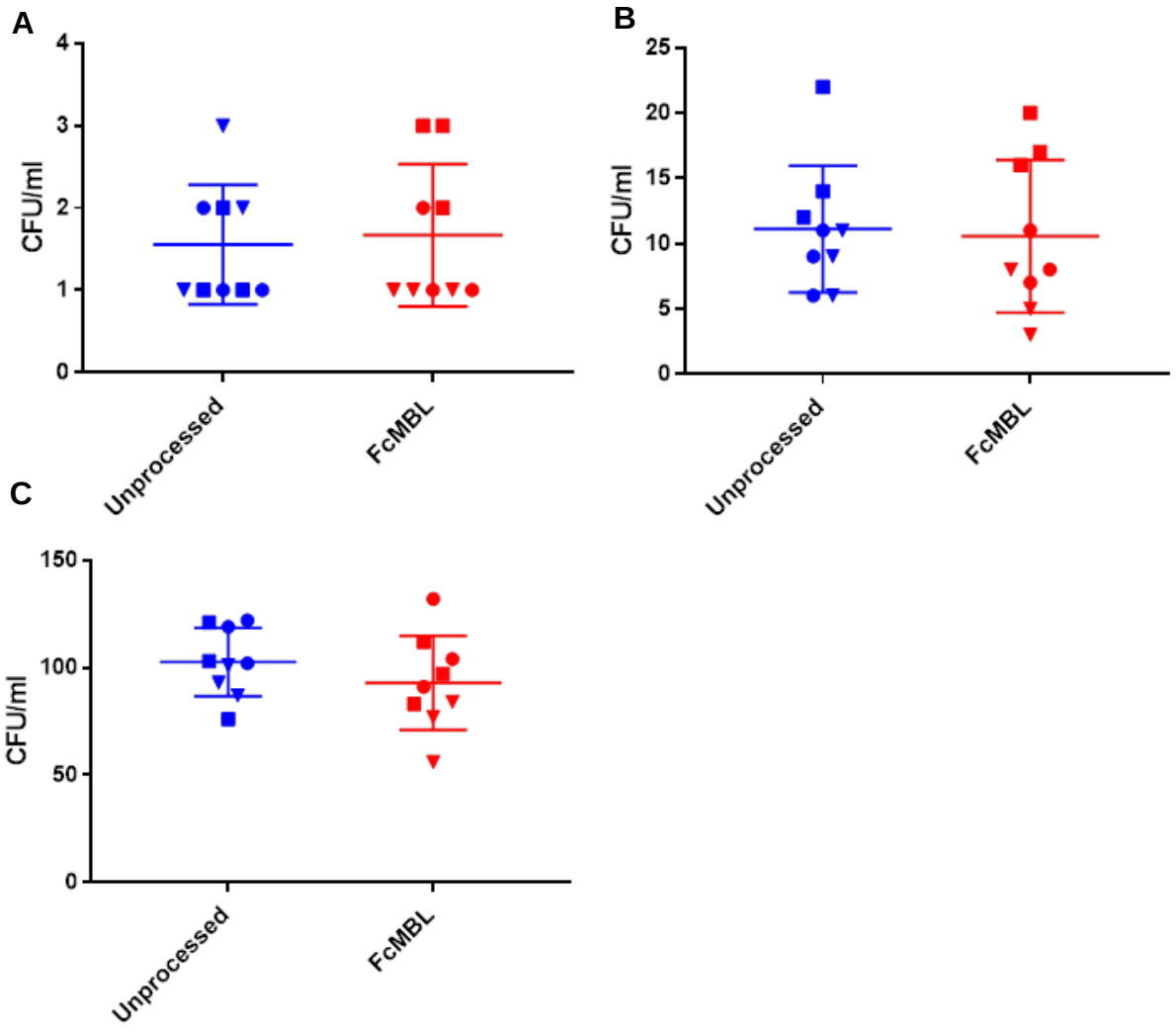

Figure 32: FcMBL beads permit growth of bacteria captured from blood cultures direct onto solid agar even at low concentrations of 10^0/ml, 10^1/ml and 10^2/ml (red). Unprocessed samples were plated directly without being added to blood as a control (blue).

5.2.8. BLOOD ONLY BACKGROUND PEAKS

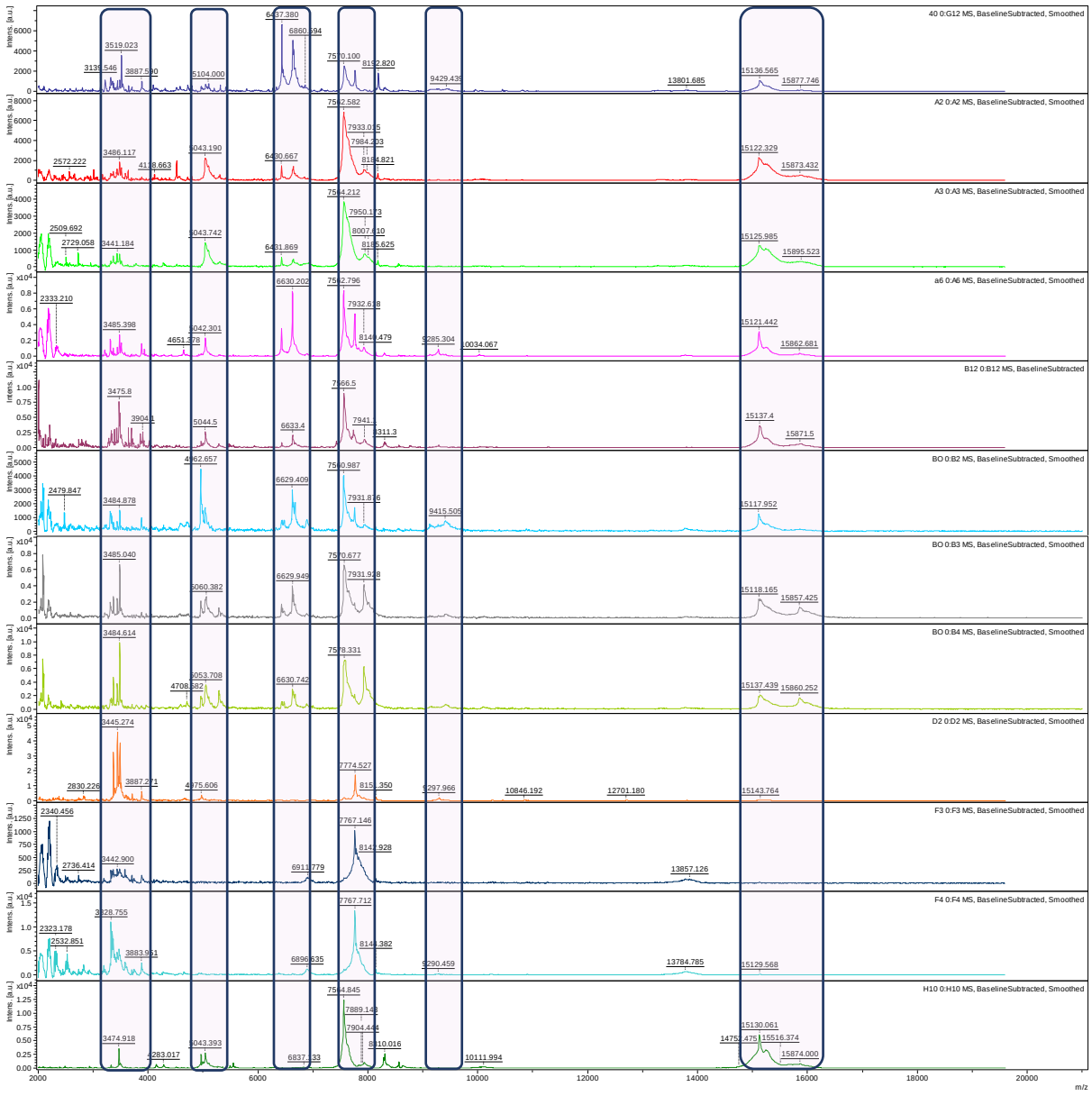

Figure 33: Spectra of FcMBL-processed blood only samples from various volunteer blood donors. Beads were eluted with 10µl of 70% FA and 10µl 100% ACN.

Blood-only spectra contain six specific areas where peaks are likely to appear. However, we find that when bacteria or yeast are also present, the blood only peaks are removed. This loss of blood only peaks is more prominent when acetonitrile is added (Figure 34 and 35).

5.2.8.1. ACETONITRILE INCREASES LOG SCORES FOR GRAM-NEGATIVE BACTERIA

Blood cultures that flagged positive were processed with the FcMBL method and the effects of formic acid and acetonitrile on log scores and mass spectra quality were measured.

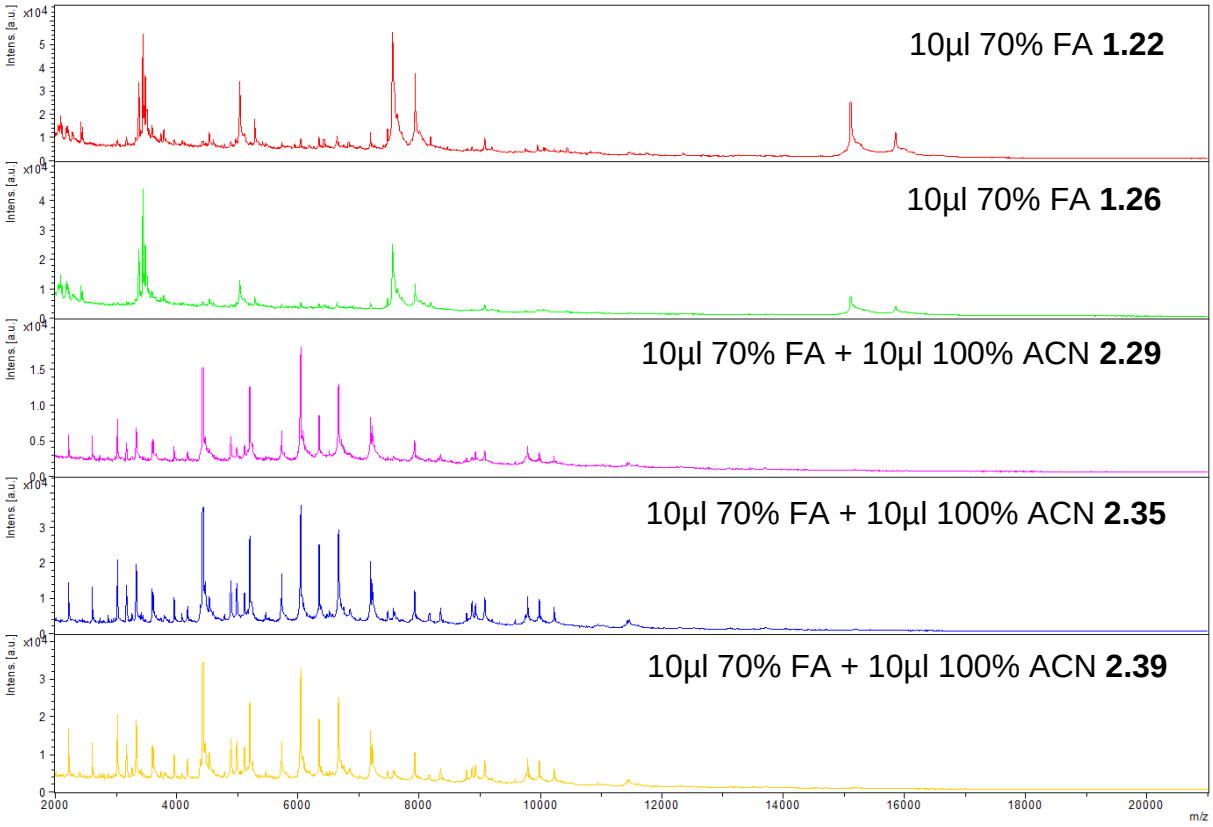

Figure 34: The effects of 100% ACN treatment were investigated for *Pseudomonas aeruginosa*. The first two samples show that FA alone produces low log scores and produces a similar background to blood-only. The last three MS show an increase in log scores once ACN is added and a decrease in blood-only background with an increase in microbial peaks

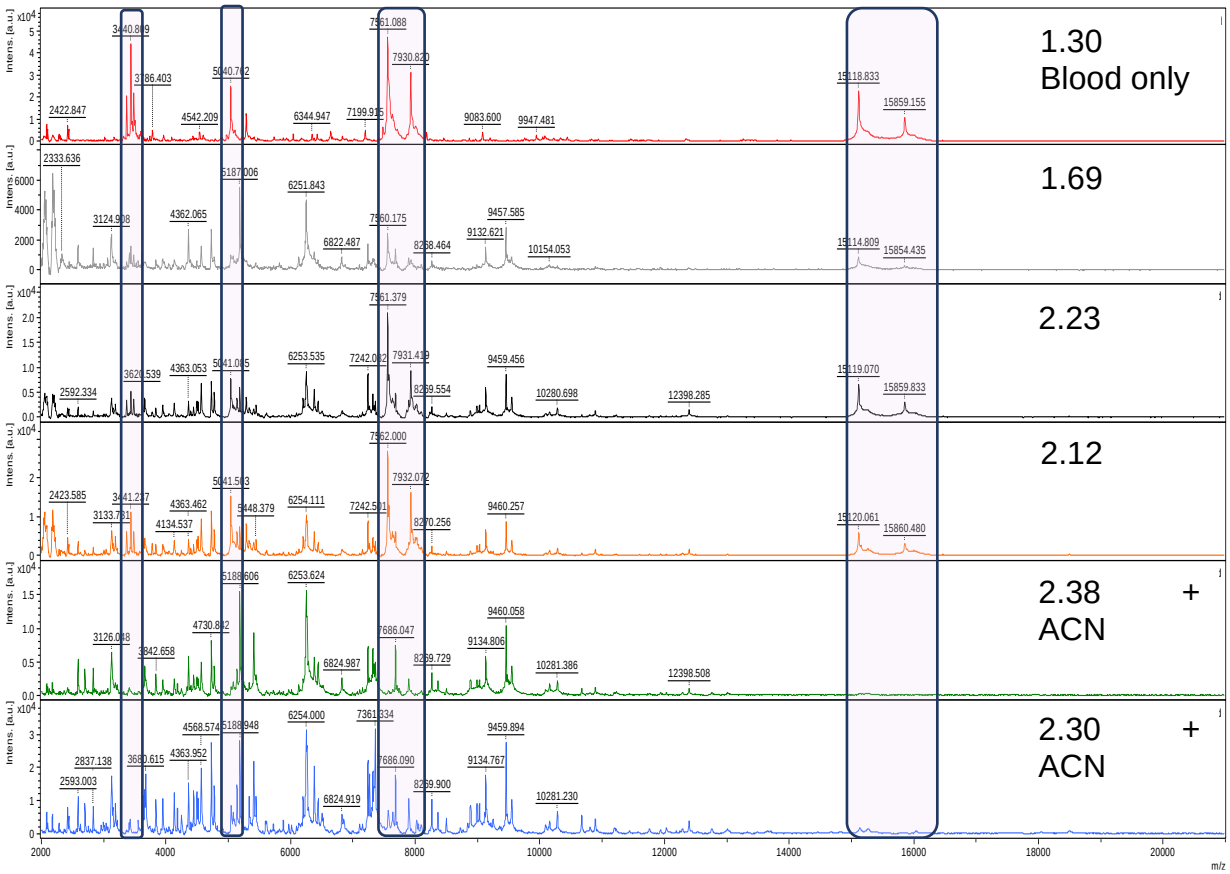

Figure 35: Effects of acetonitrile on *Klebsiella pneumoniae* spectra and Biotyper log scores. The first spectra are blood only processed. The second, third and fourth are FA only samples and the fifth and six spectra are samples processed with both FA and ACN

The effects of acetonitrile on Biotyper log scores and mass spectra blood background can also be seen with *Klebsiella* (Figure 35). At least four distinct blood only peaks can be seen missing in the two spectra produced by the addition of acetonitrile. Biotyper log scores also increase with the addition of ACN. Interestingly, though FA alone resulted in species level identification for the *K. pneumoniae*, this was not the same for the *P. aeruginosa* (Figure 34). These figures indicate that the addition of ACN drastically reduces the blood background peaks from MS, which correspondingly reduces background peaks for analysis.

5.2.8.2. YEAST DETECTION OPTIMISATION

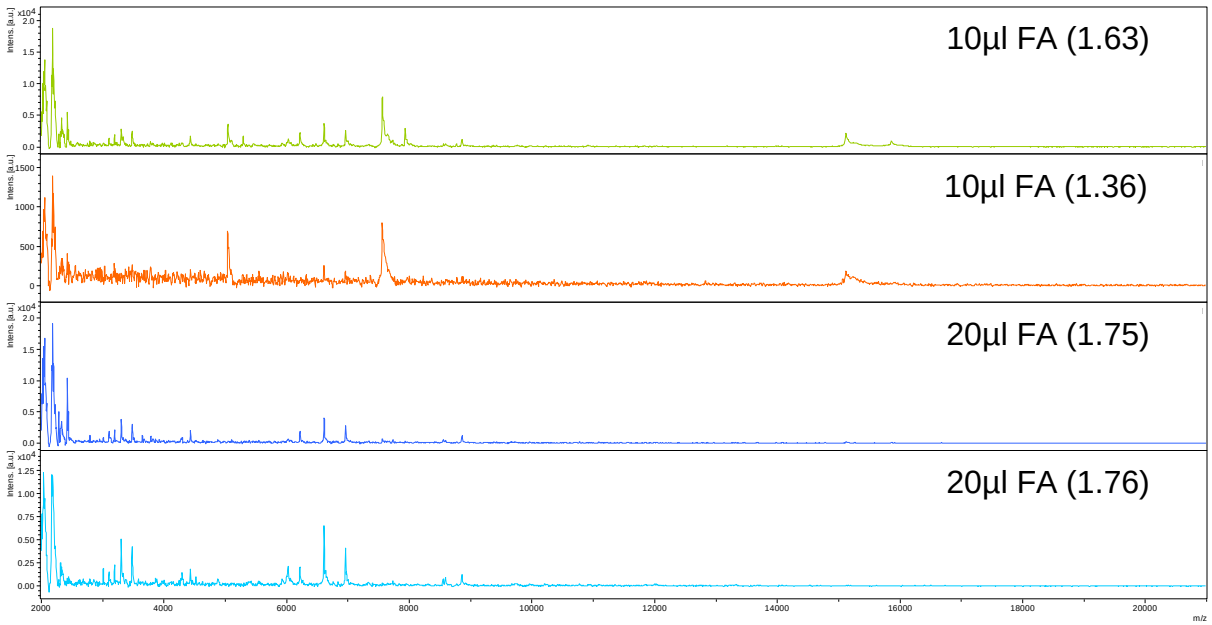

Figure 36: Comparison of 10µl 70% FA and 20µl 70% FA for the elution of *Candida glabrata* from FcMBL beads. The first two MS show blood only background peaks with minimal yeast peaks. Whereas an increased volume of FA in the last two spectra show a decrease in background and increase in yeast specific peaks. All samples had an equal volume of ACN added.

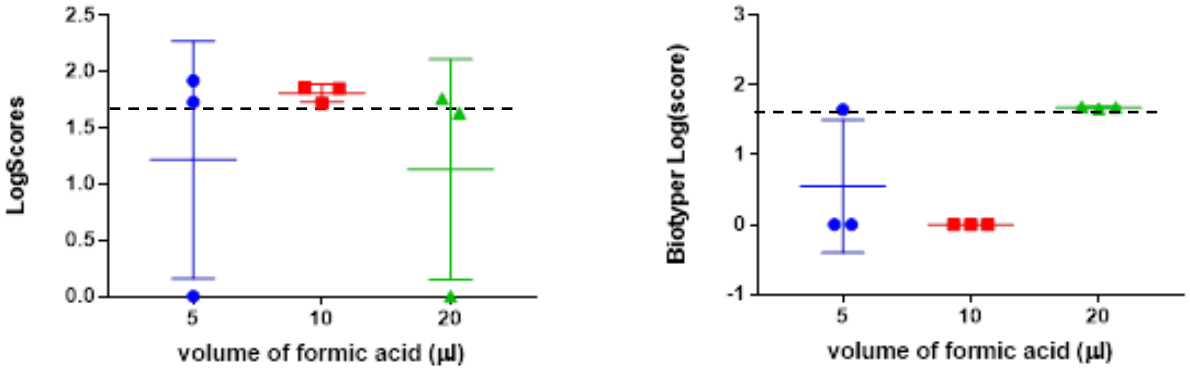

Figure 37: Formic acid volume extraction optimisation for A) *Candida albicans* and B) *Candida parapsilosis.* FA volumes below 5µl were insufficient for both species and 10µl was ineffective for *C. parapsilosis* however, 20µl was successful 5 of the 6 times. All samples had an equal volume of ACN added. The dashed line indicates genus level identification threshold.

An increase in FA volume to 20µl compared to 10µl FA for bacterial elution solves the extraction problem for yeast. Figure 36 compares two *Candida glabrata* mass spectra for each of when 10µl or 20µl of FA is added. In the latter two we see the loss of blood only peaks around ~7500Da and the increase in *C. glabrata* specific peaks around ~3,000-4,000 and 6,000–7,000Da. We also observed the most consistent results in Biotyper log scores when 20µl of FA was used to breakdown the yeast (Figure 37).

5.3. CHAPTER FIVE DISCUSSION

In this chapter a viable method for the capture and pulldown of whole cell bacteria was optimised for the detection of BSIs using MALDI-TOF MS. The optimised protocol can be applied to clinical blood bottles and is evaluated for clinical use later in this thesis.

We first tested the stability of the bead batches to ensure their functionality by using the BioFire FilmArray. We tested their ability to bind clinical pathogens using sputum isolated from a patient suffering with CF. Compared to the control sample, less detection of the bacteria was observed with the FcMBL method, though this could be explained by the presence of DNA in the sputum enhancing the quantification in sputum only control.

We observed a difficulty in releasing bacteria from the beads in a suitable volume for MS. To overcome this, we considered adding the FcMBL beads directly to the MALDI-TOF MS. The present literature in this regard is scant, as a lot of magnetic bead works are performed using larger MALDI-TOF MS machines that are not suitable for clinical work. Due to concerns that magnetic beads would interfere with the machine we dismissed the prospect of directly plating them onto the target plate and instead investigated alternative methods including the calcium ion chelator EDTA. However, due to heavy precipitation of EDTA on the target plate surface and low log scores with EDTA concentrations above 10µg/ml, ETDA elution was ruled out. We optimised the elution of the beads, investigating the lowest volumes to elute the beads by using 16S qPCR. We showed that volumes of H_2O below 200µl were sub-optimal for elution of the bacteria from the beads. Yet 200µl was determined to be too dilute, resulting in no peaks observed when 1µl of the eluent was analysed by MALDI-TOF MS. We instead investigated protein extraction techniques direct from the processed beads. FA can break down the biotin-streptavidin bond as well as degrade the cellular wall of both Gram-positive bacteria and yeast we optimised FA and ACN volume for extraction from FcMBL beads. Figure 36 shows that if too little FA is added to the beads, no extraction takes place, and no peaks are observed. A minimum of 10µl of FA is required for complete extraction, with higher Biotyper log scores observed for beads as well as centrifuged samples when FA volume is increased. For Candida samples we observed that a minimum of 20µl of FA is required for complete extraction, likely due to the thicker cellular wall (Figure 36 and 37). We compared different methods of

sample preparation including direct smearing, overlaying with FA and extended protein extraction using FA and ACN. It was determined that it was possible to extract proteins from microbes bound to the beads and subsequently use the supernatant for analysis by MALDI-TOF MS without having to add the beads directly. We showed that the beads yielded higher Biotyper log scores after extraction compared to unprocessed control samples, likely due to the enrichment from the beads.

We also counted the bacteria in the washes during the processing protocol to establish how well the beads were able to maintain binding during the washes and determine the suitability of different wash buffers. We observed less than 1% of the total *S. aureus* added was lost during washing. This strong binding demonstrated by the small loss of bacteria when washing was also observed during elution optimisation. After processing the beads with a vigorous elution method, the FcMBL beads still permitted a considerable amount of bacterial growth on solid agar, suggesting that the beads were not fully decomplexed. As the bacteria were bound so effectively to the beads, we investigated the ability of the beads to permit bacterial growth on solid agar. This method would potentially allow for the rapid binding and isolation of whole cell bacteria and direct subculture from suspected BSIs. We show that MBL was indeed successful at capturing and culturing even 10^0 bacteria from spiked blood.

We further showed that blood samples spiked with low concentrations of *E. coli* and *S. aureus* and then processed with FcMBL magnetic beads grew similar numbers of colonies to the unprocessed samples, suggesting a very high capture efficiency. The ability of the beads to do this could have significant impact on clinical diagnostics. If bacteria can be captured directly from blood samples as low as 10^0 and subcultured directly, then the average 24 hours to 5 days wait for positive blood culture could be bypassed, positively impacting patient management.

Complete cell lysis without disrupting the beads needed to be achieved for the FcMBL protocol. An issue with incomplete host cell lysis is that the beads can become contaminated with host residue, regardless of the bacterial load, providing a negative read on the MALDI-TOF MS (i.e., no peaks detected). We investigated the two most common in-house lysis buffer reagents, saponin and SDS. Saponins target only mammalian cells, perforating the cell membrane, whereas SDS solubilises the cellular membrane and denatures proteins during the process. Though SDS is faster at solubilising cell walls and membranes the concern was its effect on the FcMBL protein and if this would disrupt the beads binding abilities - Figure 25 and 27 compared

saponin and SDS buffers. Saponin was also tested with various salt and glucose concentrations concluding salt and glucose concentrations make no impact. Moreover, despite significant blood lysis observed with the SDS buffer, the beads were unable to detect any bacteria and no peaks were observed for any of the runs. This is most likely due to denaturation of the FcMBL protein and the streptavidin/biotin bonds.

Control samples (centrifuged at 13,000*g*) were only able to detect *E. coli* at 10^7 and 10^6, with no peaks observed at lower concentrations. In contrast, the processed samples detected bacterial peaks even down to 10^3, albeit with scores too low for bacterial identification using the Bruker bio-database.

Lastly, blood or FcMBL specific background was investigated as some samples displayed lower log scores than the controls, suggesting FcMBL background was interfering with the algorithm. Moreover, lower log scores were demonstrated when low volumes of FA were used to elute the beads which resulted in non-microbial background peaks – blood only samples from 10 volunteers were analysed and similar peak pattens were found. However, it is important to note that these peaks were only seen when no bacteria or yeast were present. We have shown that FA and ACN in appropriate volumes extract microbial proteins which outcompete the background signals. Another reason the peaks may disappear is that the matrix has a higher affinity to bind to microbial analytes more readily, leading to enhanced excitation for microbial analytes than blood or FcMBL-specific analytes. Regardless, appropriate protein extraction with FA/ACN directly from the FcMBL beads is effective at identifying microbes from blood with MALDI-TOF MS technology

To summarise, this chapter has demonstrated a developed and optimised protocol using FcMBL coated beads to rapidly bind and enrich infected blood samples for MALDI-TOF MS analysis.

CHAPTER SIX

CLINICAL EVALUATION OF THE FCMBL METHOD

BSIs are associated with high morbidity and mortality rates and these rates continue to increase the longer the time before effective treatment is provided [110, 166]. In order for effective treatment to be prescribed a diagnosis has to be made. The Bruker Sepsityper kit allows for the rapid isolation of microbes from biological samples including blood and urine, reducing the diagnostic turnaround time from 18-48 hours down to 30 minutes, yet the kit is less effective for particular organisms, particularly yeast. This technique requires a positive blood culture as well as separate libraries based on individual pathogens isolated directly from host.

FcMBL-conjugated beads provide a broad range binding of microbes including whole cell and fragmented microbes, with a higher affinity for binding yeast. The FcMBL beads promise a rapid, broad range and sensitive microbial detection platform complementary to the Sepsityper kit. In this chapter we compare the feasibility, sensitivity, and specificity of an FcMBL bead-based Sepsityper method to the standard commercial kit.

6.1. AIMS

1. Develop and evaluate the performance of an FcMBL bead-based method for rapid identification of BSIs in the clinic using MALDI-TOF MS.

2. Compare the speed, sensitivity, and specificity of the FcMBL method to the standard commercial Bruker Sepsityper kit on clinical paediatric blood samples.

3. Compare the efficiency of both methods in the detection of Gram-negative and Gram-positive bacteria and yeast.

6.2. RESULTS

6.2.1. MICROBIAL BINDING AND DETECTION PROPERTIES OF FCMBL

Firstly, we have shown that the magnetic FcMBL method takes approximately 15 minutes, including a protein extraction from the beads prior to adding the sample to the target plate. This is comparable to the standard Sepsityper method, which takes approximately 10-20 minutes. However, both of these methods are much faster than conventional methods of subculturing onto solid agar which can take significantly longer, approximately 18-48 hours. We also demonstrate that the FcMBL beads bind a range of clinically important microbes, including yeast and provide a distinct mass spectrum which can be used to distinguish species (Figure 38).

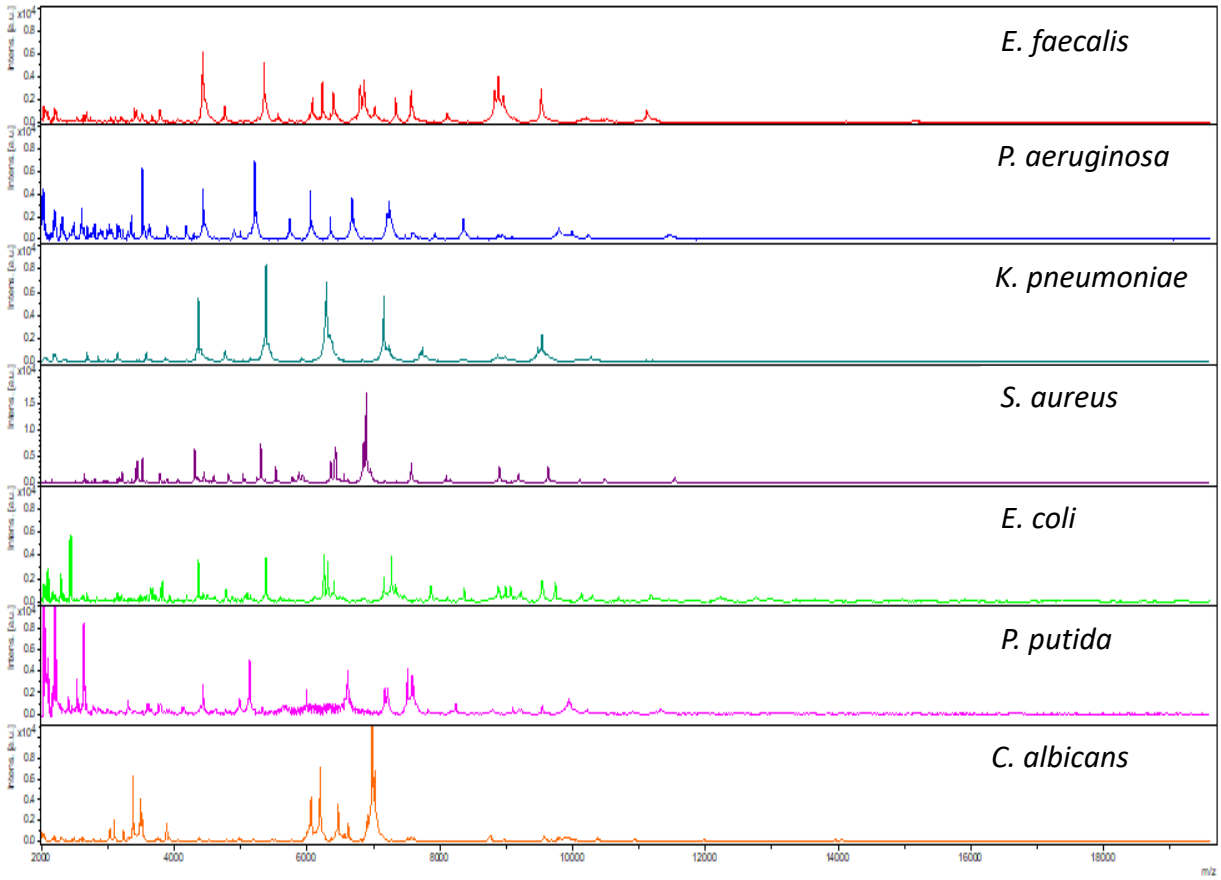

Figure 38: MALDI-TOF MS spectra of bacteria and yeast captured and eluted from FcMBL-processed beads

To evaluate the consistency of the method across different patients and strains we investigated the ability for the FcMBL beads to identify specific *Candida* or bacterial strains in multiple blood samples from multiple donors. *Candida albicans*, *Streptococcus anginosus* and *Klebsiella pneumoniae* patient isolates were spiked into blood culture bottles from three volunteers. Each blood sample was processed in triplicate. We observed similar log scores between replicates as well as between donors (Table 14).

Table 14: Inter-run variability of Biotyper log scores for the FcMBL method between blood donors

	Donor one	**Donor two**	**Donor three**	**Average [SD]**
Candida albicans				
1	1.73	1.75	1.95	**1.83 [0.0692]**
2	1.86	1.81	1.83	
3	1.85	1.80	1.90	
Streptococcus anginosus				
1	1.71	1.86	1.77	**1.75 [0.0600]**
2	1.70	1.70	1.74	
3	1.71	1.76	1.84	
Klebsiella pneumoniae				
1	2.28	2.05	1.74	**2.05 [0.185]**
2	2.34	2.06	2.01	
3	2.00	2.11	1.87	

6.2.2. FcMBL DETECTION OF CLINICAL PAEDIATRIC BLOOD CULTURE SAMPLES

Paediatric blood culture samples were analysed using the FcMBL method after achieving positivity on the BACTEC™ blood culture incubator. A total of 66 individual patient strains were tested; some had multiple bottles tested if both aerobic and anaerobic blood cultures flagged positive, resulting in a total of 70 samples tested. This comprised of 25 anaerobic and 45 aerobic blood cultures. We observed high levels of Staphylococci, particularly coagulase-negative Staphylococci (30%). Streptococci and Enterococci were the cause of 11%, and 7% were caused by yeast. We see that the FcMBL beads have a high efficiency for Gram-negative and Gram-positive bacteria, and an even higher efficiency for yeast (Table 15). Table 16 shows the log scores for and the number of samples for each pathogen type. We observed higher log scores for Gram-negative bacteria than Gram-positive bacteria and yeast (Figure 39).

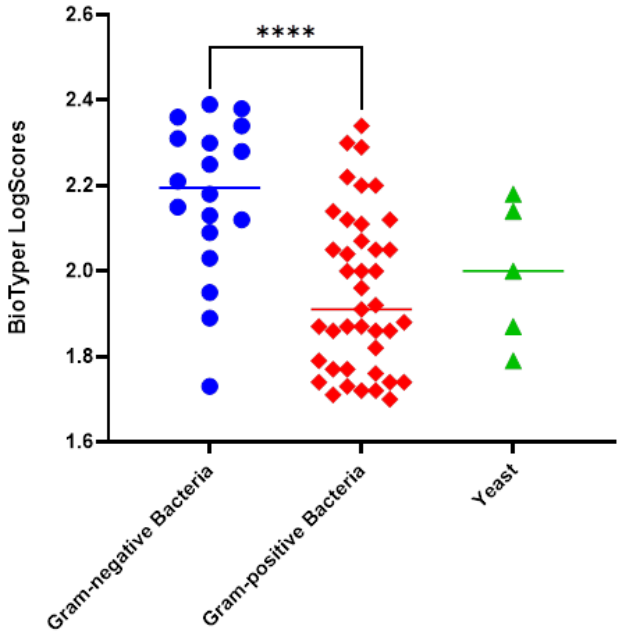

Figure 39: Comparison of the Biotyper log scores produced from eluting FcMBL beads incubated in patient BC samples. *n*=70. Mann-Whitney *U* test. *P*=0.0001

Table 15: FcMBL efficiency (% of log scores >1.70) with clinical samples

Gram-negative	Gram-positive	Yeast
20/21	41/44	5/5
95.2%	93.2%	100%

Table 16: MALDI-TOF MS identification of paediatric samples using FcMBL beads

Species	**No. patient strains**	**No. FcMBL positive**	**Bruker Biotyper log score range**
Staphylococcaceae			
Staphylococcus aureus	6	6	1.72 – 2.22
Staphylococcus epidermidis	9	8	1.73 – 1.92
Staphylococcus haemolyticus	2	2	1.77 – 1.82
Staphylococcus hominis	2	2	2.05
Staphylococcus equorum	1	1	1.70
Staphylococcus capitis	1	1	2.29
Streptococcaceae			
Streptococcus oralis	3	2	0.00 – 2.20
Streptococcus mitis	1	0	0.00
Streptococcus parasanguinis	2	3	1.87 – 2.34
Streptococcus perosis	1	1	2.00
Streptococcus pneumoniae	2	3	2.04 - 2.13
Streptococcus salivarius	1	1	2.08
Enterococcaceae			
Enterococcus faecium	4	4	1.71 – 2.30
Enterococcus faecalis	3	4	2.00 – 2.11
Enterobacteriaceae			
Escherichia coli	2	1	0.00 - 1.95
Enterobacter bugandensis	1	1	2.34
Enterobacter cloacae group	2	3	1.73 – 2.09
Raoultella ornithinolytica	1	2	2.12 - 2.18
Klebsiella oxytoca	2	3	2.03 - 2.39
Klebsiella pneumoniae	4	4	2.21 – 2.31
Other species			
Micrococcus luteus	1	1	1.96
Stenotrophomonas maltophilia	3	3	2.15 - 2.28
Burkholderia cepacia	1	1	2.13
Pseudomonas aeruginosa	2	2	2.34 - 2.36
Clostridium perfringens	1	1	1.86
Actinomyces graevenitzii	1	1	1.88
Yeast			
Candida glabrata	1	1	2.00
Candida albicans	1	1	1.79
Candida parapsilosis	2	2	1.87 - 2.18
Wickerhamomyces anomalus	1	1	2.14
Total samples tested	**66**	**66/70**	**94.3%**

6.2.3. FcMBL versus The Sepsityper for rapid identification of Microbes

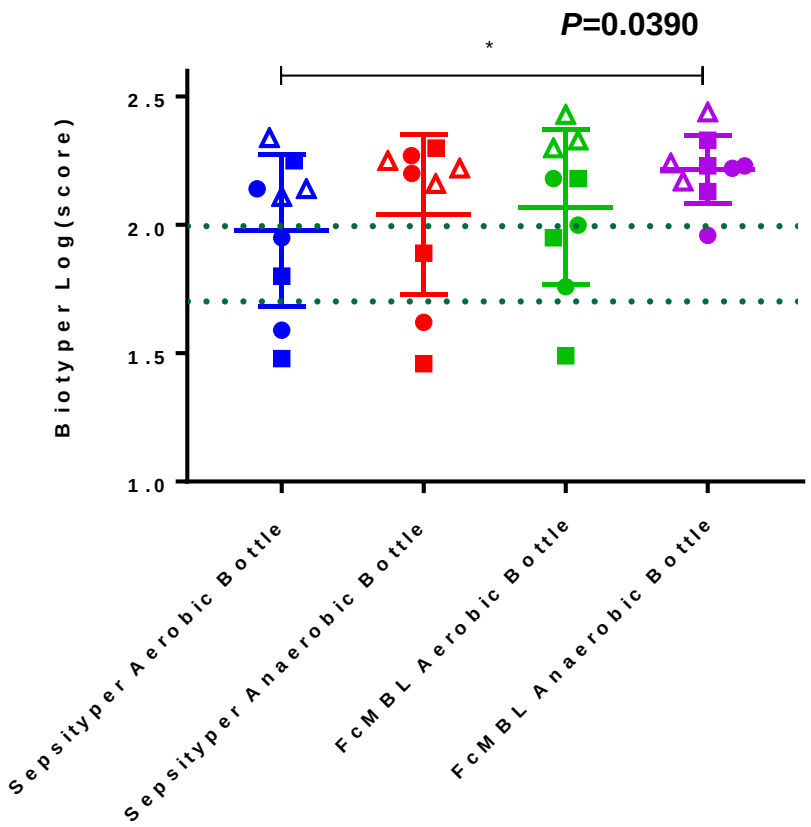

Figure 40: Comparison of Identification log scores from the Bruker Biotyper for the Sepsityper and FcMBL method on bacterial spiked BCs. Squares represent *S. aureus*, circles; *E. coli*, and triangles; *K. pneumoniae*

Laboratory strains of *E. coli*, *S. aureus* and *K. pneumoniae* were used initially to compare the two rapid isolation methods: the Sepsityper and the FcMBL beads (Figure 40). We found that both methods were able to identify most of the strains. The Sepsityper method performed on spiked aerobic blood cultures had the lowest log scores failing to identify one Gram-negative and a Gram-positive with only 56% above species level identification (>2.00) and 78% above genus level (>1.70). The FcMBL method in the anaerobic blood culture bottles demonstrated the highest log scores with 89% above the threshold for species identification and 100% above genus. No significant differences were found between the two methods and the same bottle types.

Due to the low numbers of candidemia in the clinical population at the time of this study, spiked volunteer blood samples were prepared to investigate and compare the performance of the two methods in candidemia identification (Table 17).

All 24 of the candidemia samples tested were identified using the FcMBL method, compared to 17 (70.8%) using the Sepsityper. An increased level of species identification was seen with the FcMBL method, with 37.5% reaching >2.00, compared to 25% with the Sepsityper method. A Mann-Whitney *U* test between the levels that hit the genus level threshold was carried out with no significance seen between the two methods (Figure 41).

Despite only 37.5% reaching species level threshold with the FcMBL method, both organism matches were for the correct species. We suspect this reduced confidence in the score is due to the presence of FcMBL-specific background peaks that are not accounted for in the standard sample libraries. To explore this possibility, we post-processed the spectra to truncate the *m/z* range where many of these background peaks are observed and performed a cluster analysis on the processed (truncated) and unprocessed samples (see Figures 42 and 43).

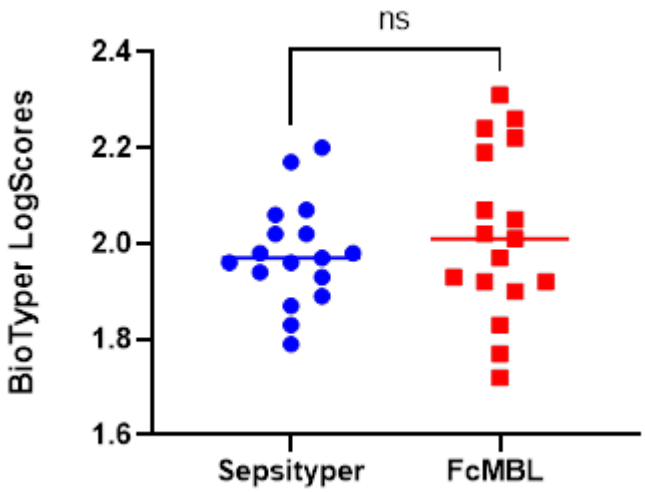

Figure 41: FcMBL method versus the Sepsityper method for the detection of yeast in positive spiked blood cultures using MALDI-TOF MS. *n*=17. Mann-Whitney *U* *P*=0.5089

Table 17: Comparison of Biotyper log scores between the Sepsityper and FcMBL rapid identification methods for fungemia.

	STANDARD BIOTYPER MODULE	
ORGANISM	**SEPSITYPER LOG SCORE**	**FCMBL LOG SCORE**
C. albicans		
1	1.66	**1.81**
2	-	**1.86**
3	1.83	**1.97**
4	**2.06**	1.83
5	1.36	1.74
6	1.87	**1.90**
C. kefyr		
1	1.98	**2.31**
2	**2.17**	2.02
3	1.98	**2.24**
C. krusei		
1	1.93	**2.05**
C. auris		
1	-	**1.87**
2	1.13	**1.92**
3	1.89	**2.19**
C. glabrata		
1	-	**1.93**
2	1.97	**2.26**
3	**2.20**	1.92
C. tropicalis		
1	**2.02**	1.93
C. parapsilosis		
1	-	**1.72**
2	1.96	**2.07**
3	1.96	**2.22**
4	**2.07**	1.77
C. guilliermondii		
1	1.94	**2.01**
2	1.79	**1.92**
3	**2.02**	1.72
% Genus level	17/24 (70.8%)	100%
% Species level	6/24 (25%)	9/24 (37.5%)
Total identified	**17**	**24**

Clustering analysis was performed on the spectral similarities between each pair of sample spectra for each of the truncated and untruncated spectra (Figures 42 and 43). Stronger clustering of the Candida species can be seen at the reduced *m/z* range of 2400–7400. The *Candida tropicalis* and *Candida albicans* appear to cluster closer than the other Candida species, whereas there are clear subcultures of *Candida glabrata* and *Candida auris*. These data suggest that removing background noise from the analysis through the use of libraries tailed for the FcMBL method increases species clustering and is a potential method for increasing species identification using the FcMBL method.

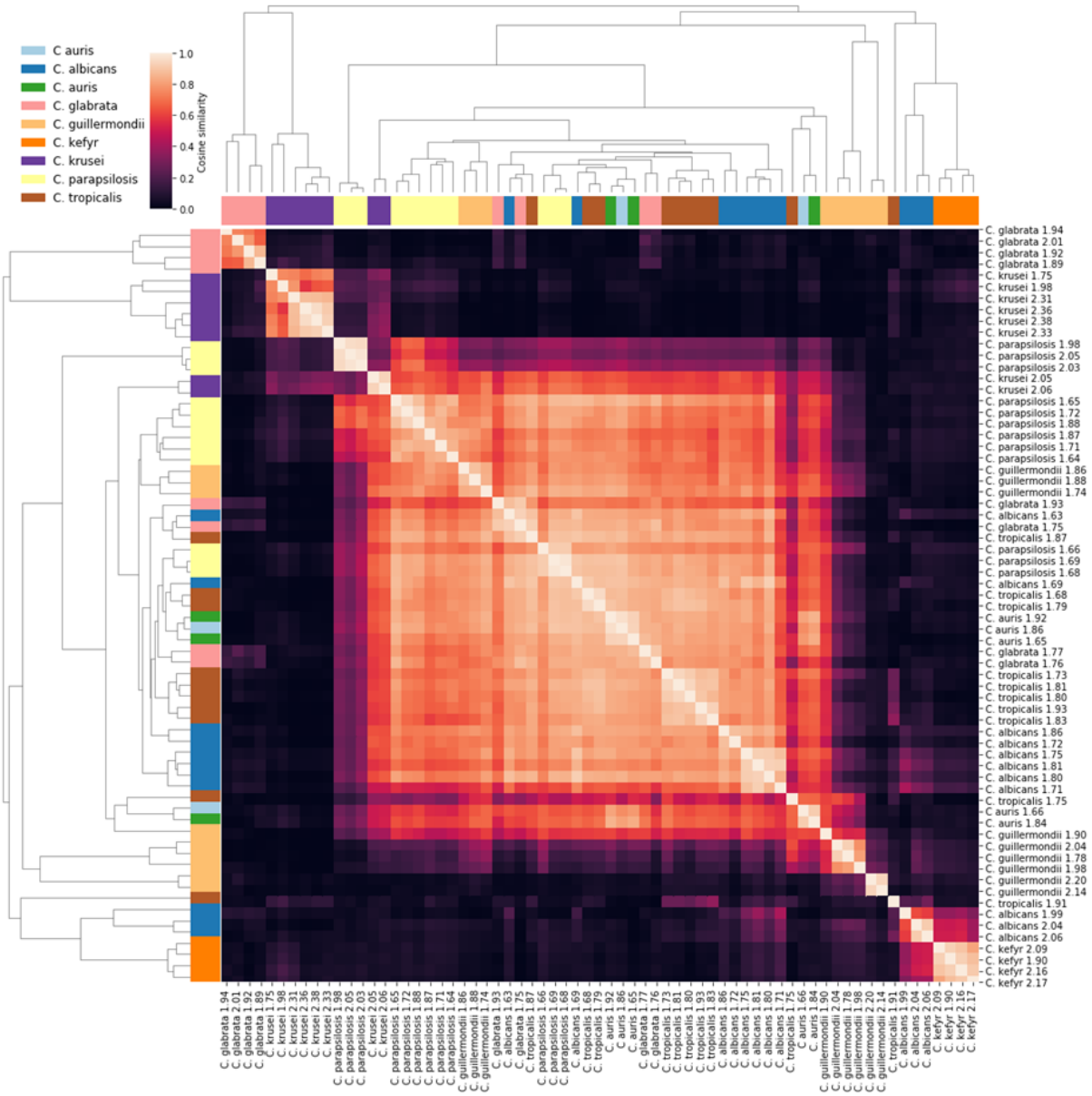

Figure 42: Heatmap of spectral similarities with dendrogram clustering analysis for FcMBL candida mass spectra (2,000-20,000*m/z*)

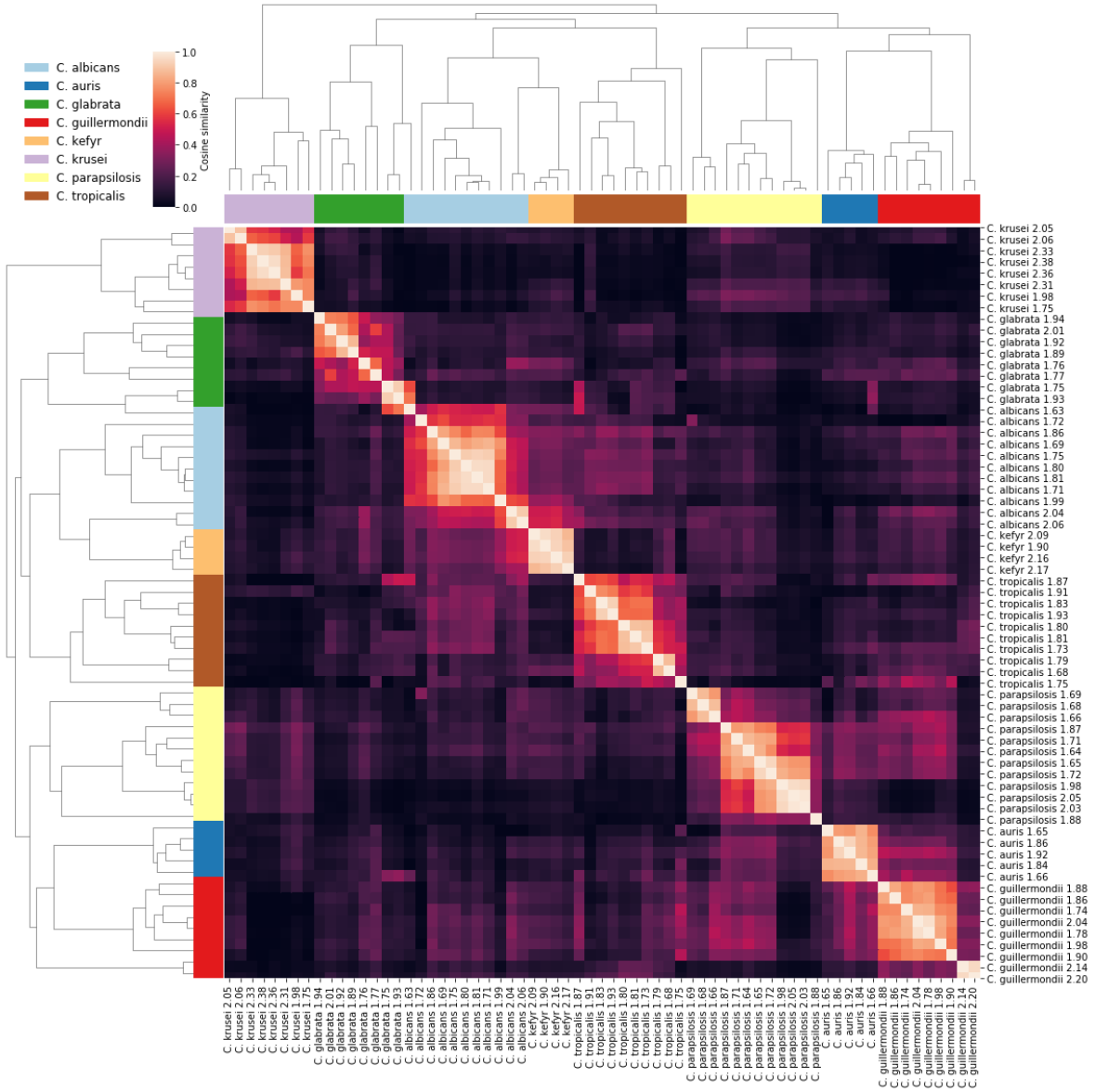

Figure 43: Heatmap of spectral similarities with dendrogram clustering analysis for FcMBL candida mass spectra (2,500-7,400*m/z*).

Following the success of the FcMBL method compared to the Sepsityper in laboratory strain isolation from blood we compared the methods on clinical samples from GOSH (Table 18). We observed that the FcMBL method was able to identify 100% of samples to genus level, compared to 68% for the Sepsityper kit. Note that not all the samples tested had a parallel Sepsityper analysis for comparison. We observe that the FcMBL was highly effective at detecting yeast despite failure of the Sepsityper kit performed by the clinical microbiology staff at GOSH on the same samples.

The Sepsityper also failed to detect four *S. epidermidis*, one *S. salivarius*, one *S. pneumoniae* and one *S. maltophilia* infection. These were infections that were identified with the FcMBL method, albeit mostly only to genus level. Interestingly, yeast was often not identified with the Sepsityper method (33%), and rare pathogens such as *Wickerhamomyces anomalus* were detected by the FcMBL method but not the Sepsityper.

We also looked at the Biotyper log scores for both the Sepsityper and the FcMBL beads that had made positive identifications for both the Sepsityper and the FcMBL method (Figure 44). We see no significant difference between the log scores of the samples which reached the threshold (≥1.70). We also see a slight increase in the number of species level detected with the FcMBL method compared to the Sepsityper, with 48% and 40% respectively.

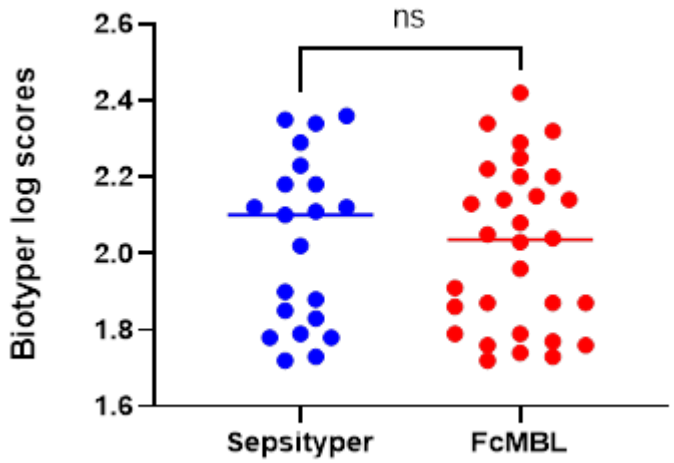

Figure 44: Comparison of Bruker Biotyper log scores for the FcMBL method and Sepsityper kit for clinical blood cultures. *n*=21. Mann-Whitney *U* test *P*=0.7942

Table 18: Bruker Biotyper log score comparison of the FcMBL and Sepsityper method for clinical paediatric samples for GOSH

Species	Sepsityper method	FcMBL method
Staphylococcus aureus	**2.29**	2.04
Staphylococcus aureus	2.10	**2.22**
Staphylococcus aureus	**2.18**	2.05
Staphylococcus aureus	**2.34**	2.14
Coagulase-negative staphylococci		
Staphylococcus epidermidis	**1.78**	1.73
Staphylococcus epidermidis	Failed	**1.74**
Staphylococcus epidermidis	Failed	**1.76**
Staphylococcus epidermidis	Failed	**1.87**
Staphylococcus epidermidis	Failed	**1.76**
Staphylococcus epidermidis	**2.23**	1.86
Staphylococcus capitis	1.72 (*S. hominis*)	**2.29**
Streptococcaceae		
Streptococcus oralis	1.83 (*S. mitis*)	**2.20**
Streptococcus oralis	**1.88** (*S. pneumoniae*)	1.87
Streptococcus mitis	1.78 (*S. pnuemoniae*)	**2.20**
Streptococcus mitis	**2.02**	1.72
Streptococcus pneumoniae	**2.35**	1.91
Streptococcus pneumoniae	Failed	**1.77**
Streptococcus salivarius	Failed	**2.08**
Other species		
Escherichia coli	2.36	2.42
Enterococcus faecium	**2.11**	1.79
Enterobacter bugandensis	1.73 (*E. cloacae*)	**2.34**
Klebsiella oxytoca	**2.18**	2.03
Klebsiella pneumoniae	2.12	**2.32**
Micrococcus luteus	1.90	**1.96**
Stenotrophomonas maltophilia	Failed	**2.25**
Stenotrophomonas maltophilia	2.12	**2.15**
Burkholderia cepacia	1.79	**2.13**
Yeast		
Wickerhamocytes anomalus	Failed	**2.14**
Candida albicans	Failed	**1.79**
Candida parapsilosis	1.85	**1.87**
% Identification to genus	**21/30 (70%)**	**30/30 (100%)**
% Identification to species	**12/30 (40%)**	**16/30 (53%)**

6.2.4. INVESTIGATION OF THE BACTERIAL CONCENTRATIONS AFTER POSITIVITY

As we observed that two Streptococci were not identified with the FcMBL method, we tested clinical isolates for autolysis once they hit the stationary phase. This could explain why FcMBL beads were unable to bind and produce enough spectra to reach the threshold for identification on the Biotyper. We used *S. pneumoniae* and *S. anginosus* as a control for autolysis. Clinical isolates of Streptococci were spiked into blood culture bottles and incubated until positive on the BacTec. Samples were tested at 0, 4, 8, 16, 24 and 48 hours after positivity to see if this affected the FcMBL method efficiency. We observed no significant autolysis in any of the strains nor in any of corresponding log scores (Table 19 and 20). Interestingly, we do not see much growth in the bacteria during this time despite being stored at 37^{o}C during this period (Table 19).

Table 19: CFUs of *Streptococcus* strains after being indicated positive on the BacTec

	Hours post positive result					
	0	**4**	**8**	**16**	**24**	**48**
S. anginosus	2.0×10^8	2.1×10^8	1.8×10^8	1.7×10^8	1.7×10^8	1.1×10^8
S. anginosus	2.3×10^8	2.1×10^8	2.1×10^8	2.0×10^8	2.1×10^8	1.9×10^8
S. pneumoniae	1.3×10^8	1.4×10^8	1.7×10^8	1.3×10^8	1.0×10^8	9.3×10^7
S. pneumoniae	1.9×10^8	2.0×10^8	2.1×10^8	2.0×10^8	2.1×10^8	2.1×10^8

Table 20: MALDI-TOF MS log scores for *Streptococcus* strains after positivity

	Hours post positive result					
	0	**4**	**8**	**16**	**24**	**48**
S. anginosus	1.78	1.79	1.74	2.03	2.01	1.94
S. anginosus	2.02	2.04	2.04	1.97	1.96	1.94
S. pneumoniae	1.94	1.96	2.04	2.01	1.92	1.86
S. pneumoniae	1.93	1.85	1.76	1.86	1.72	1.91

6.2.5. IMPLEMENTING THE FCMBL METHOD TO DETECT MICROBES FROM BCS REMOVED EARLY FROM THE BACTEC INCUBATOR

Blood culture bottles were removed prior to positivity to investigate the enrichment of FcMBL beads. We found FcMBL was not able to detect *E. coli* prior to positivity, nor was the Sepsityper (Figure 45). Yet, the FcMBL method was able to detect *S. aureus* and *C. albicans* prior to positivity with 5 hours and 17.5 hours saved respectively. The Sepsityper also detected the *S. aureus* prior to positivity with 1 hour saved. Though it should be noted that there was a bacterial pellet observed when testing at the 24th hour yet this did not reach the threshold for identification on the machine.

Table 21: Comparison of the FcMBL method and the Sepsityper kit for the detection of pathogens from blood culture bottles prior to positivity on the BacTec. Time to positive identification (TTPI) and time to positivity (TTP) on the BacTec. (*n*=2)

	Attempt one			**Attempt two**		
	Hours					
	TTPI	TTP	Time saved	TTPI	TTP	Time saved
	S. aureus					
FcMBL	24	29	5	28	33	5
Sepsityper	28	29	1	32	33	1
	E. coli					
FcMBL	28	27	0	24	21.5	0
Sepsityper	28	27	0	24	21.5	0
	C. albicans					
FcMBL	24	42	18	28	45	17
Sepsityper	48	42	0	48	45	0

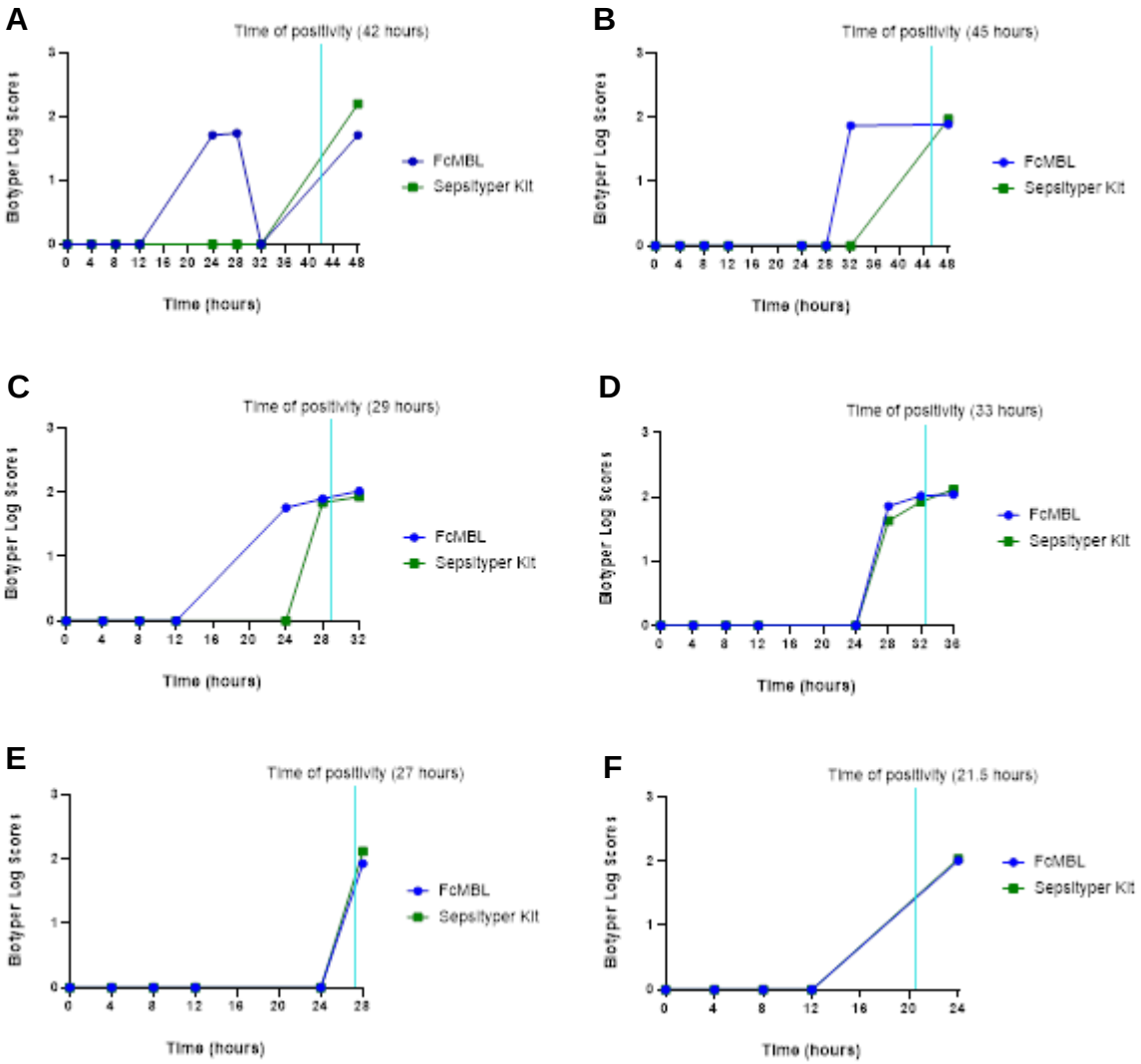

Figure 45: Early removal of spiked blood culture bottles for the early detection of pathogens comparing the Bruker Sepsityper kit and the FcMBL method. A) and B) *Candida albicans*, C) and D) *Staphylococcus aureus* E) and F) *Escherichia coli*. (*n*=2)

6.3. CHAPTER SIX DISCUSSION

The FcMBL method, introduced in this thesis and evaluated in this chapter, has a duration of approximately 15 minutes, comparable to the Sepsityper method. Both methods are rapid and require minimal handling, a necessity to reduce the workload and pressure of clinical microbiology laboratories. A further benefit of the FcMBL method is that it could feasibly be automated, which would increase its suitability within the clinic.

We showed in this chapter that the beads bind rapidly to patient samples, including Gram-positive and Gram-negative bacteria and yeast. The Sepsityper and FcMBL methods were both effective at detecting Gram-positive and Gram-negative bacterial infections *in vitro* with laboratory strains (Figure 40). However, laboratory strains can grow rapidly and often lack similarity with patient strains, particularly in their carbohydrate expression. Therefore, we also applied the methods to patient samples, in order to ascertain their relative performance in practical and realistic settings. We observed that FcMBL was very effective at binding and detecting Gram-negative (95.2%) and Gram-positive bacteria (93.2%).

One *S. oralis* and a *S. mitis* group were unable to be detected by the beads despite being cultured and identified by clinical routine methods. This may have been due to the beads not binding to the organism or due to the death of the organism. To test this, we cultured two *S. anginosus* and two *S. pneumoniae* in volunteer blood on the BACTEC™ until positive. Of the 4 samples we tested we did not observe any significant autolysis or death of the *Streptococcus* even 48 hours after becoming positive. There were no significant changes in log scores either and all samples were able to be detected at every time point meaning we were unable to assess the effects of autolysis on the FcMBL capture method.

Recent years have seen increases in antifungal resistance rates with the CDC reporting that 7% of Candida handled in their labs were resistant to fluconazole, a first line defence [163]. Due to the low efficiency of the Sepsityper for yeast identification and the effectiveness demonstrated by the FcMBL method for clinical identification of

yeast we carried out further study by spiking blood cultures using previous isolates of candidemia. We observed a strong affinity of the FcMBL beads for Candida (100%), compared to the Sepsityper which has ~50% efficiency according to both the literature and our study (Table 17).

We observed that regardless of how much yeast was bound to the FcMBL beads the log scores were quite low for many of the samples (<2.00) and so investigated the possibility of FcMBL-specific background interfering with the log scores. We produced heatmaps of the similarities of measured spectra from Candida samples with full mass range (2,000–20,000*m/z*) and truncated range to incorporate only the 2,400-7,400*m/z* peaks (Figures 42 and 43). We demonstrated much clearer clustering of individual Candida species once the mass range was shortened. This is likely because many FcMBL-specific background peaks, not accounted for by the libraries, were excluded. This is validated by a 2021 study using a similar construct to ours, FcMBL@Fe3O4, which explains that the protein background peaks from functional proteins bound to beads can affect the log scores and identification rates [167]. They found using a chelator of Ca^{2+} (EDTA) to remove bound bacteria from the proteins rather than smearing the samples and beads onto the plate resulted in higher identification rates for *E. coli* and *S. aureus*. They demonstrated that the FcMBL proteins and beads can produce spectra which can affect the accuracy of identification which can cause errors when comparing the spectra to the standard bacterial spectra database.

We suggest that FcMBL beads can be used to rapidly identify yeast infections in blood samples that have failed to be identified by the Bruker Sepsityper kit. We also propose to alter the mass range that is detected or analysed for known yeast samples as shown in Figure 43 to increase the discriminative power of the beads and overcome the potential background noise issues that arise. Moreover, we assessed the consistency of the beads' performance, essential if the beads were to be introduced as clinical procedure. Using clinical isolates, we tested the reproducibility of the FcMBL method for the detection of *Streptococcus anginosus* (Gram-positive), *Klebsiella pneumoniae* (Gram-negative) and *Candida albicans* (yeast) in volunteer blood. We found that the FcMBL method was able to produce similar log scores for each sample even within different volunteer bloods.

To summarise, the data presented in this chapter demonstrates a strong potential for the FcMBL method to be introduced as a rapid diagnostic tool to aid clinical microbiologists identify positive blood cultures, in particular yeast which is currently limited with current methods. We have shown the beads bind rapidly to a variety of different bacteria and yeast in blood cultures and can be straightforwardly eluted with cheap and readily available reagents that the clinical microbiology staff are already familiar with. Using MALDI-TOF MS technology the FcMBL method was able to identify more BSIs than the Sepsityper kits, especially candidemia. Overall, the FcMBL method presented here poses a potential alternative or adjunct method for rapid diagnosis in clinical microbiology aiding in reduced economic burden as well as mortality and morbidity in childhood.

PART II

INVESTIGATING THE ROLE OF MANNOSE-BINDING LECTIN IN THE PREVENTION AND TREATMENT OF INFECTIONS IN CHILDHOOD

Part II of this thesis considers the role of MBL as a therapeutic in the prevention or treatment of infections, including bacterial and viral infections.
Because the two chapters utilise very distinct methods, we cover these *in situ* within the chapters where relevant.

AIMS

1. To examine the ability of MBL to prevent and treat bacterial biofilm infections.

2. To investigate the role played by MBL in the severity and progression of SARS-CoV-2, with a particular focus on the novel disease Paediatric Multisystem Inflammatory Syndrome - temporally associated with SARS-CoV-2 (PIMS-TS).

CHAPTER SEVEN

THE ROLE OF MBL IN THE PREVENTION AND TREATMENT OF MRSA BIOFILM INFECTIONS

Bacterial biofilms pose a persistent, expensive problem for health care establishments. Biofilms produce a protective extracellular layer that reduces the effectiveness of antibiotic therapy and immune clearance and increases the likelihood of resistance. Bacterial biofilms develop readily on inserted medical devices such as prosthetic heart valves, shunts, and prosthetic joints, almost always resulting in the eventual removal of the infected implemented device. With ever increasing antibiotic resistance a need for alternative and less toxic methods of biofilm prevention and eradication are required.

7.1. BACTERIAL BIOFILMS

A particularly troublesome problem oft-encountered in the clinic, biofilms are communities of pathogens that attach and become encased in an extracellular matrix (ECM) produced by microbial cells within the mass. The ECM consists of lipids, proteins, extracellular DNA, and exopolysaccharides [168]. These sessile communities are found in a variety of environments such as soil and plant tissues, as well as in a variety of chronic bacterial infections. Biofilm infections exhibit resistance to host defences including opsonisation, phagocytosis and complement deposition. They are notorious for having increased resistance towards antimicrobials, with particular antibiotics exhibiting a minimum inhibitory concentration (MIC) up to three orders of magnitude greater to treat a biofilm infection than compared to planktonic infection [5]. This recalcitrance engenders persistent and relapsing infections, even in the face of typically adequate antimicrobial dosage, and increases the risk of sepsis. The mechanisms for their resistance have gradually been discovered over the years, revealing that changes in their metabolism are essential [169]. The figure below describes the lifecycle of a biofilm, from its initial attachment to either a biotic or abiotic surface to the eventual maturation and dispersion back into the host environment (Figure 46) [170].

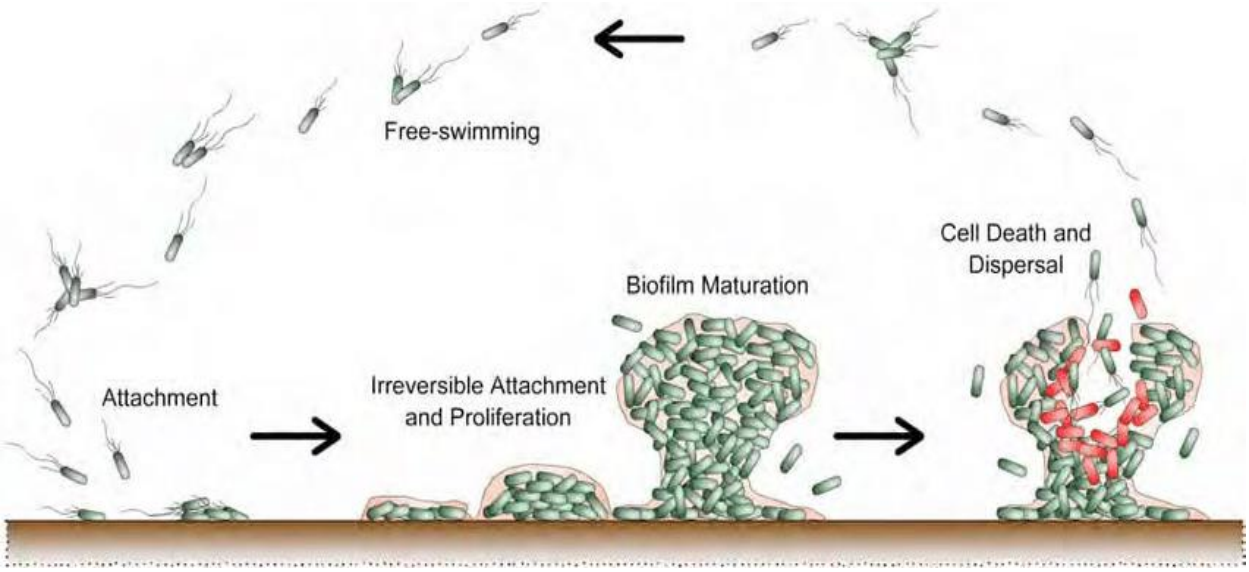

Figure 46: Biofilm lifecycle taken from Barraud et al 2009

7.2. BIOFILM INFECTIONS

Surface-associated biofilm infections display specific and characteristic properties distinct from planktonic bacteria. It was known that indwelling devices could attract bacterial infections more easily, but it was not until 1982 that scanning electron microscopy (SEM) provided evidence of *S. aureus* biofilm infection on an endocardial pacemaker [171]. Biofilms can be detected in a range of environments including oral and respiratory structures such as the adenoids. For example, consider cystic fibrosis, an autosomal recessive disease which leads to abnormal electrolyte transport leading to an accumulation of viscous sections in the respiratory, digestive, and reproductive tracts. As these secretions build up in the lung they lead to obstructions and infections, the most common being *H. influenzae* and *P. aeruginosa*. *P. aeruginosa* biofilms are a particular issue due to their increased resistance to all major classes of antibiotics and common presence in ventilated new-borns. Indwelling devices such as shunts, artificial valves, pacemakers, and ventilators are all at risk of serious biofilm infections. Biofilm infections are not only difficult to treat but also a significant expense for healthcare providers. A study investigating the cost of chronic wounds in the UK surmised that biofilms infections cost the National Health Service (NHS) between £4.5 - £5.1 billion in 2012-2013 [172].

7.2.1. BIOFILMS AND THE IMMUNE SYSTEM

It is generally accepted that the immune response initiated during biofilm infection is ineffective. This is due to a variety of mechanisms which regulate the micro-environment of the biofilm. The ECM produced by the community act as an antibody net, absorbing the majority of antibody released by the host before it can bind directly to the pathogen, impairing opsonophagocytosis [173]. The ECM also captures complement proteins, specifically C5a, which prevents complement activation. The negative charge of the biomass attracts positively charged antimicrobial peptides, also inhibiting alternative pathway activation.

The ECM poses other problems for the host such as high-level toxin accumulation, which may negatively affect host cells [174]. Toxins produced by biofilms lyse white blood cells and the resulting debris is incorporated into the biomass, which continues to grow over time. As antibiotics diffuse through the ECM, the concentration drops,

with the lowest concentration at bottom of the biofilm. As a result, antibiotic concentrations need to be increased in biofilm related infections, though the concentrations required may not always be physiologically practical with some infections requiring up to 10^3 times the usual dose [175]. An infiltration of T cells and polymorphonuclear neutrophils (PMN) into biofilm sites has been documented, and it was thought that they may contribute to the progression of biofilm infection due to 'frustrated phagocytosis' [173]. However, work by Meyle et al demonstrated that PMNs migrated towards Staphylococcal biofilms, degrading and phagocytosing the biofilms [176].

7.2.2. BIOFILM CULPRITS

Recently the World Health Organisation (WHO) classified methicillin-resistant *Staphylococcus aureus* (MRSA) as one of twelve priority pathogens which threaten human health [177]. In this chapter, the majority of the work has been carried out using *Staphylococcus aureus* JE2 (USA300), an MRSA. Due to the rapid increase in antibiotic resistance in recent years, with insufficient antibiotics being introduced to replace them, alternative therapies are urgently needed. WHO have suggested that failure to address antibiotic resistance could lead to over 10 million deaths by 2050 [178]. MRSA was first identified in 1961, just two years after Methicillin was first introduced in 1959 – and has ever since been a problem in nosocomial infections worldwide. Resistance is conferred by the *mecA* gene, which encodes the penicillin-binding protein (PBP2A) that has a decreased affinity for β-lactam antibiotics. It is responsible for a variety of health care issues including soft tissue infections, pneumonia, infections of the bone and heart valves, and septicaemia [179].

7.3. AIMS

1. Investigate the potential role of MBL therapy in the prevention of MRSA biofilm infections to enhance their neutrophil-mediated destruction

7.4. BIOFILM METHODS

7.4.1. MBL MIXTURES

Both human plasma derived and recombinant MBL were gifted by Professor Steffen Thiel and Professor Jens Jensenius of Aarhus University, Denmark. Recombinant MBL (rMBL) was produced by Enzon Pharmaceuticals in HEK cell lines. Plasma-derived human MBL (pdMBL) was produced by the Statens Serum Institut (SSI) in Denmark. For some experiments MBL was heat inactivated at 70ºC for 30 minutes.

7.4.2. BIOFILM MICROTITER PLATE AND CHAMBER SLIDE ASSAYS

Biofilm formation by MRSA strain JE2 (from Dr Sean Nair, The Eastman Institute) was quantified using the microwell plate method described by Christensen et al. and Manago et al [180, 181]. Bacterial stocks were streaked onto trypticase soy agar plates and incubated for 16 hours at 37ºC. Single colonies were picked, and bacteria were grown for 16 hours in brain heart infusion (BHI) then diluted 1:200 in BHI (Oxoid) with 1% glucose (Sigma), and 200µl were incubated in 96-well flat-bottom polystyrene microwell plates (Sarstedt) at 37ºC for 24 hours without shaking, sealed with an aeroseal. Bacterial growth was measured at OD600 for total biofilm and planktonic bacterial growth. The media was removed by pipetting, and the remaining biofilms were washed with sterile PBS, heat-fixed at 60°C for 1 hour and then stained with 100µl of 0.1% (w/v) crystal violet (CV) solution (Sigma) for 10 minutes at room temperature (RT). Plates were washed with dH_2O thrice, emptied and left to air-dry for 15 minutes. Biofilms were quantified by eluting the CV stain with 250µl of 33% acetic acid and then measuring the absorbance at 590nm (SPECTROstar Nano Plate reader).

7.4.3. BIOFILM PREVENTION ASSAYS

S. aureus JE2 biofilms were generated as above, with various concentrations of pdMBL and rMBL (20, 10 and 5µg/ml) added to the 1:200 dilution before plating. MBL was also coated onto microtiter plates overnight at 4ºC at 10µg/ml in PBS, before a 1:200 dilution of bacteria was added to the plates. OD600 and biofilms were measured as described above.

7.4.4. GROWTH CURVES AND VIABILITY COUNTS

To measure bacterial growth, fresh overnight cultures were diluted 1:200 and incubated with 20µl of 4mg/ml AlamarBlue. Measurements of 530/590nm were taken every 10 minutes for 13 hours using a Fluoroskan Ascent Microplate Fluorometer (ThermoLabsystems). Growth curves were plotted using GraphPad Prism Version 7.0. For viability counts fresh colonies were picked and grown in BHI for 16 hours at 37^{o}C and were diluted in fresh BHI and grown until OD600 0.1. Bacteria were then diluted 1:20 and serial dilutions of bacteria were performed in a microtiter plate until 10^{7}. Using the Miles and Misra technique 20µl of bacteria were plated onto LB plates in triplicate, left to dry and incubated for 16 hours at 37^{o}C.

7.4.5. CELL CULTURE

A549 cells were maintained in Roswell Park Memorial Institute 1640 medium (Invitrogen) containing 10% fetal bovine serum (FBS; Hyclone), penicillin (100 U/ml), and streptomycin (100 mg/ml).

7.4.6. BACTERIAL ADHERENCE ASSAYS

A549 cells were seeded at 1 ml of 2×10^{5} cells without antibiotics into the centre of a 24-well TC plate. Cells were incubated overnight at 37^{o}C and 5% CO_2. Bacteria were also cultured overnight by inoculating one colony into 5ml of BHI and incubated at 37^{o}C with shaking at 290rpm. The cells were inspected for at least 90% confluency, washed in warm HBSS and 1ml of fresh medium with 10% FBS, with no antibiotics added. Fresh medium was also added to three wells without any cells. Bacterial cultures corresponding to 1×10^{6} CFU/ml were prepared to represent a multiplicity of infection (MOI) of 5:1. Bacteria were centrifuged and resuspended to ensure a purer sample. Bacterial culture was added to the wells and incubated at 37^{o}C for 3 hours with 5% CO_2. The media was then removed from the wells gently and the infected wells washed thrice with warm HBSS. Cells were then lysed with 100µl of 1% Triton X-100 at room temperature for 10 minutes then 900µl of LB medium was added. The suspension is homogenised by gently pipetting up and down. Serial 10-fold dilutions are prepared, and viability counts performed as described above.

7.5. MBL AND BIOFILM TREATMENT

7.5.1. NEUTROPHIL ISOLATION

Peripheral blood was obtained in EDTA vacutainers (BD) and mixed with 2% Dextran (Sigma) in a 50ml falcon (1ml/6ml of blood) and left to settle for 30-60 minutes to separate the red blood cells from the buffy coat. Percoll solutions of 80% and 56% (GE Healthcare) were made fresh for each experiment for the Percoll gradients. Each gradient had 2.5ml of 80% Percoll on the bottom layer with 5ml of 56% Percoll layered on top. Buffy coat is then added to the Percoll gradient, centrifuged for 22 minutes at 190*g*, with the brake off. Using a Pasteur pipette the neutrophil layer is removed from between the 80% and 56% gradient and added to a 50ml falcon then washed twice with warm HBSS (Life Technologies) without calcium and magnesium ($HBSS^{--}$). Cells were then counted using a haemocytometer. Cells were pelleted and resuspended in 500µl $HBSS^{--}$ with 1µl of Calcein red/orange (10µM) (Thermofisher), a fluorescent dye, and incubated at 37^{o}C for 30 minutes before being washed and resuspended at 2×10^{6}/ml in $HBSS^{++}$.

7.5.2. SERUM COLLECTION

Serum was obtained by bleeding volunteers into serum tubes (BD), waiting for clot formation, and spinning the vacutainer at 180*g* for 10 minutes. Serum is kept on ice until use or frozen immediately at -80^{o}C.

7.5.3. NEUTROPHIL-MEDIATED BIOFILM DESTRUCTION ASSAYS

Biofilms grown on glass coverslips were washed in sterile PBS and incubated at RT with 5µM of Cell Trace CFSE (Thermofisher) for 15 minutes. Biofilms were then washed twice with PBS and left at RT for 5 min and washed a further two times. Biofilms were then placed in $HBSS^{++}$ with 10% human serum, 10µg/ml pdMBL or 10µg/ml rMBL, and were incubated with 2×10^{6}/ml neutrophils at 37^{o}C for 30 minutes. Biofilms were gently washed, and neutrophils removed by washing with sterile PBS. Neutrophils were then washed, fixed with 4% PFA and quenched with CV before being analysed by FACS. The biofilms were washed gently with sterile PBS before being fixed with 4% PFA and mounted onto microscope glass slides using anti-fade mounting media. Slides were stored at 4^{o}C until analysis on the spinning disk.

7.5.4. FLOWCYTOMETRY ANALYSIS

Neutrophils were gated using FFC and SSC on the CytoFLEX (Beckman) and analysed using the FITC channel to investigate the phagocytosis of biofilm. Neutrophils that were not exposed to biofilm were used as a negative control for phagocytosis. FlowJo v8 was used for analysis of the FACS data and geometric means were extracted for analysis.

7.5.5. CONFOCAL LASER-SCANNING MICROSCOPY

Biofilms slides were analysed using the UltraVIEW VoX Spinning Disk Confocal microscope (PerkinElmer). Z-stack imaging was performed with a 20× objective using two lasers (495nm and 690nm). Briefly, the step size was 0.7µm and then consecutive cross-section images (XYZ) were acquired from the top to the bottom. 3D reconstruction was built up using Imaris software and analysis was performed using Fiji and Icy.

7.5.6. SCANNING ELECTRON MICROSCOPY

Neutrophil-mediated biofilm destruction experiments were set up as described above, after fixation with 4% PFA biofilms, and were then prepared for SEM by Mark Turmaine (UCL). Briefly, biofilms were post fixed in 1% oso4(osmium tetraoxide)/1.5% potassium ferroncyanine K4Fe (CN)6 in 0.1m cacodylate buffer at 3^{o}C for 30 minutes. Samples were washed in 0.1m cacodylate buffer and rinsed with H_2O. Specimens were dehydrated in graded ethanol-water series to 100% ethanol. The samples were then dried and mounted onto aluminium stubs. Samples were then coated in a thin layer of Au/Pd (approximately 3nm thick) using a Gatan ion beam coater. The images were then viewed and recorded with a Jeol 7401 FEGSEM.

7.5.7. WESTERN BLOTTING AND COOMASSIE BLUE STAINING

To test the stability and oligomerisation of the products after shipping, Western blotting was performed at various dilutions. Gradient SDS-Polyacrylamide gel electrophoresis (4-20%) of MBL under non-reducing conditions was performed. MBL was visualised using anti-MBL antibody (Clone: HYB 131-01) and enhanced chemiluminescence (ECL) (Thermofisher). Images were taken on a ChemiDoc XRS (BioRad).

7.6. STATISTICS

Statistical analysis was performed in Prism 7.04, GraphPad and a significance level of $P<0.05$ was used for all analyses. A paired *t*-test was used to compare the significance between the MBL mixtures in the biofilm prevention assays and the adhesion assays.

7.7. BIOFILM RESULTS

7.7.1. PLASMA-DERIVED MBL AND RECOMBINANT MBL STRUCTURE

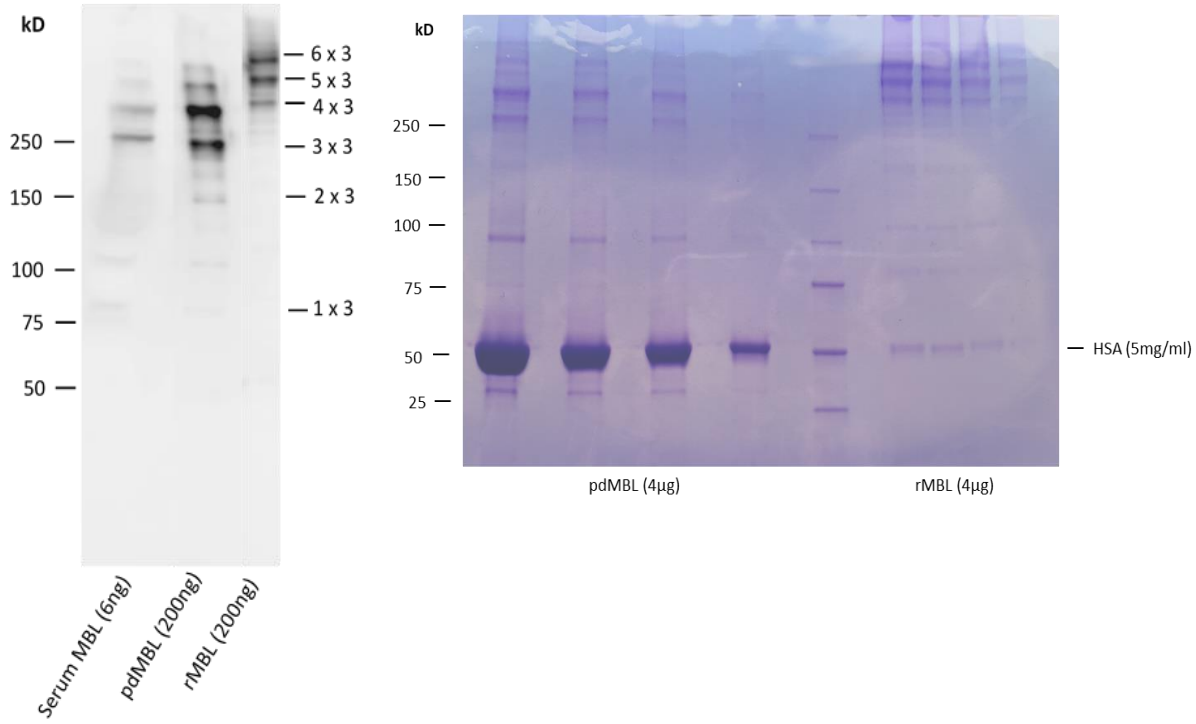

Figure 47: Western blot (left) and Coomassie blue analysis (right) of the plasma derived MBL and recombinant MBL received from Denmark that were used in the experiments

Western blotting demonstrated that the shipment of the mixtures from Denmark to the UK as well as their long-term storage had not compromised their structures. It shows the pdMBL has the majority of its MBL in the trimer and tetramer formation, with some pentamers and hexamers as expected (Figure 47). The recombinant MBL is slightly different, with the majority being pentamers and hexamers and a smaller amount of tetramer. The Coomassie blue stain shows a relatively pure recombinant MBL sample compared to the plasma derived MBL sample. The large bands seen at approximately 45kDa are human serum albumin (HSA) which was used to stabilise the MBL protein which is also safe and commonly used in the clinic.

7.7.2. THE ROLE OF MBL IN THE PREVENTION OF MRSA BIOFILM FORMATION

We first invesitgated biofilm formation by SEM. MRSA biofilms were cultured for 24 hours on glass coverslips before being prepared for SEM imagining. Extracellular matrix was observed on all samples (Figure 48).

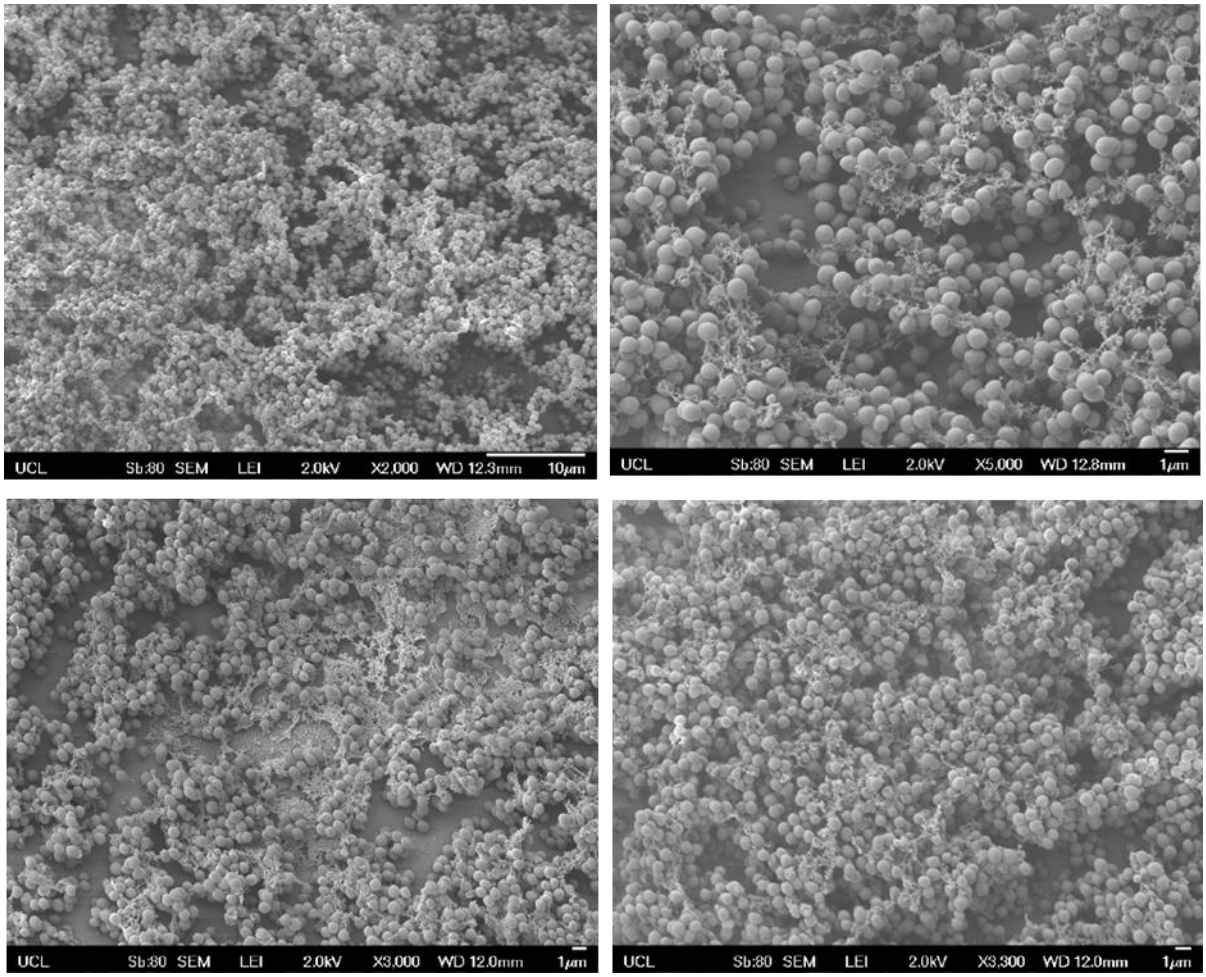

Figure 48: SEM images of MRSA biofilms

We then used microtiter plate biofilm assays incubated with pdMBL and rMBL to measure biofilm growth. The rMBL did not show any significant effect on OD600 levels or the biofilm quantity. Conversely the pdMBL did show significant disruption of biofilm formation in a dose-dependent manner (Figure 49). A significant reduction in biomass can be observed at 10µg/ml and 20µg/ml of pdMBL. An average of 30% reduction compared to controls when 20µg/ml pdMBL is added, while a 10% reduction was seen in the 5µg/ml samples, and a 15% reduction in the 10µg/ml samples. Biomass reduction was significantly greater with 20µg/ml of pdMBL than 5µg/ml (*P*=0.0053). Biomass disruption is measured using crystal violet to quantify biomass.

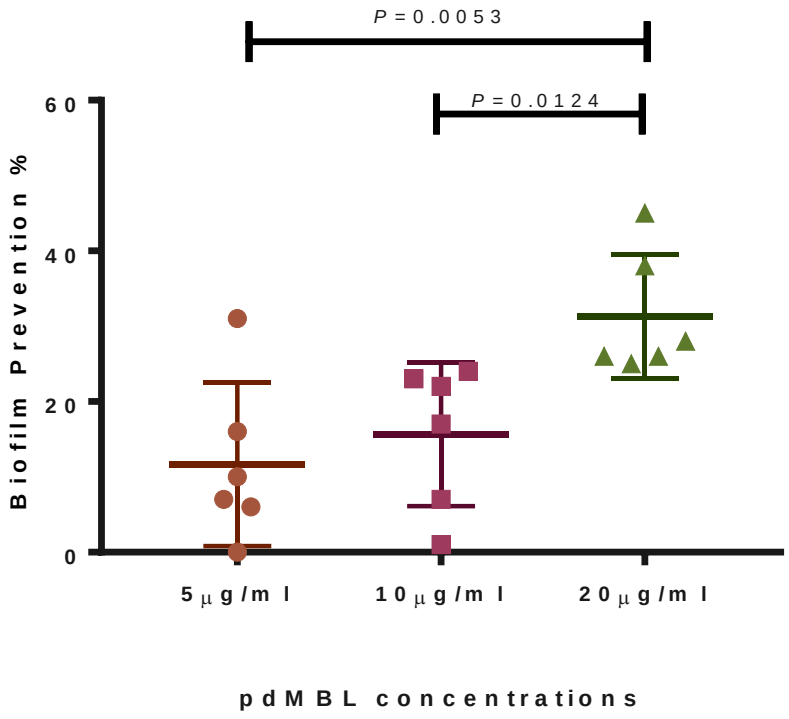

Figure 49: pdMBL decreases biomass in a dose dependent manner

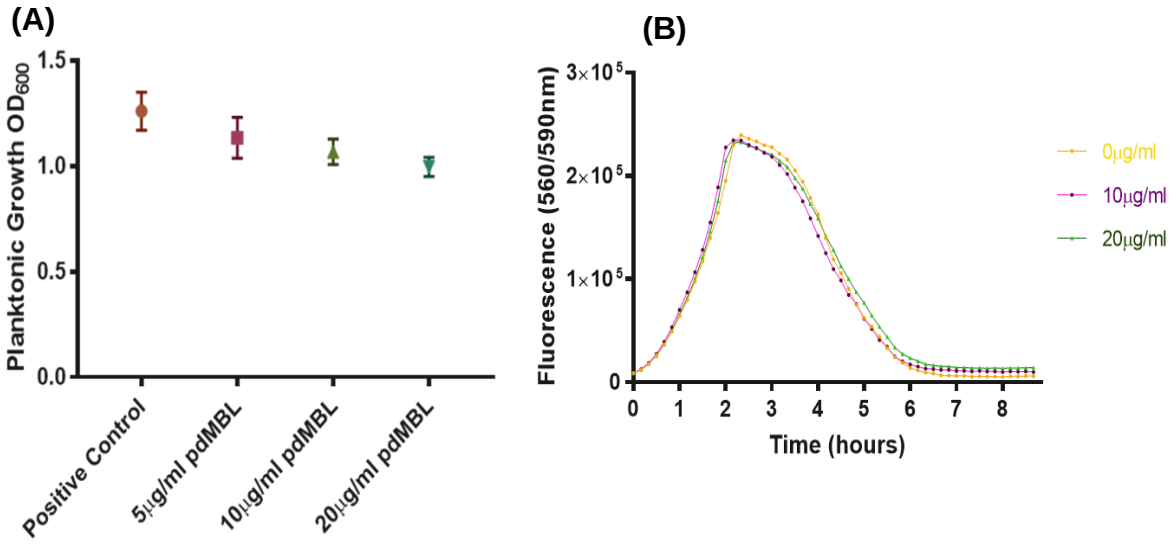

Figure 50: (A) Planktonic growth of MRSA after a 24-hour incubation with pdMBL is reduced when observed using spectrophotometry techniques (B) Alamar blue assay of MRSA demonstrating no changes in metabolism when in the presence of increasing concentrations of pdMBL

We investigated the reduced OD600 observed in Figure 50A assuming this may be due to reduced bacterial growth induced due to incubation with MBL mixtures. Using an alamar blue (resazurin) assay we investigated the metabolism of the cells during incubation with MBL, finding that no differences were observed. Light microscope images demonstrate increased light transmission due to significant aggregation of bacteria with pdMBL (Figure 51).

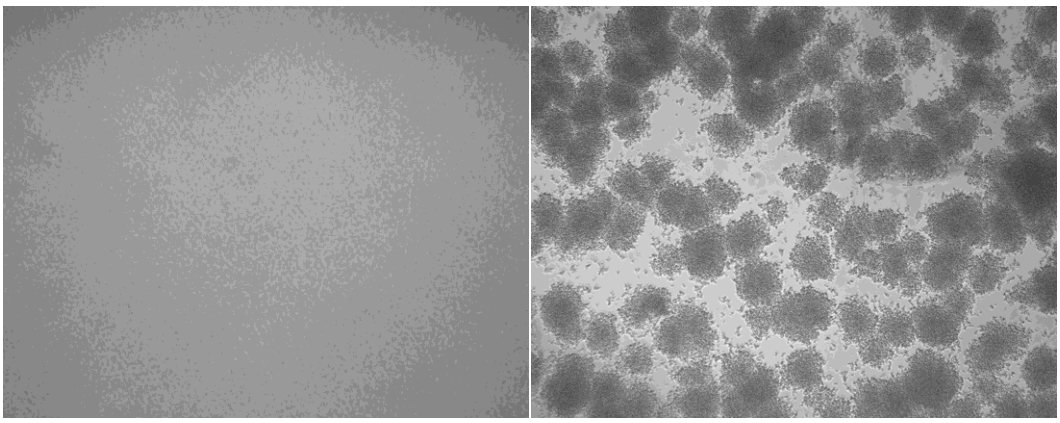

0µg/ml 10µg/ml pdMBL

Figure 51: Light microscope images of aggregation of MRSA after incubation with pdMBL for 5 hours

Due to the enhanced aggregation we decided to investigate precoating tissue culture plates with MBL, which had no effect on MRSA biofilm formation, with similar quantities of biomass seen in all conditions (Figure 52).

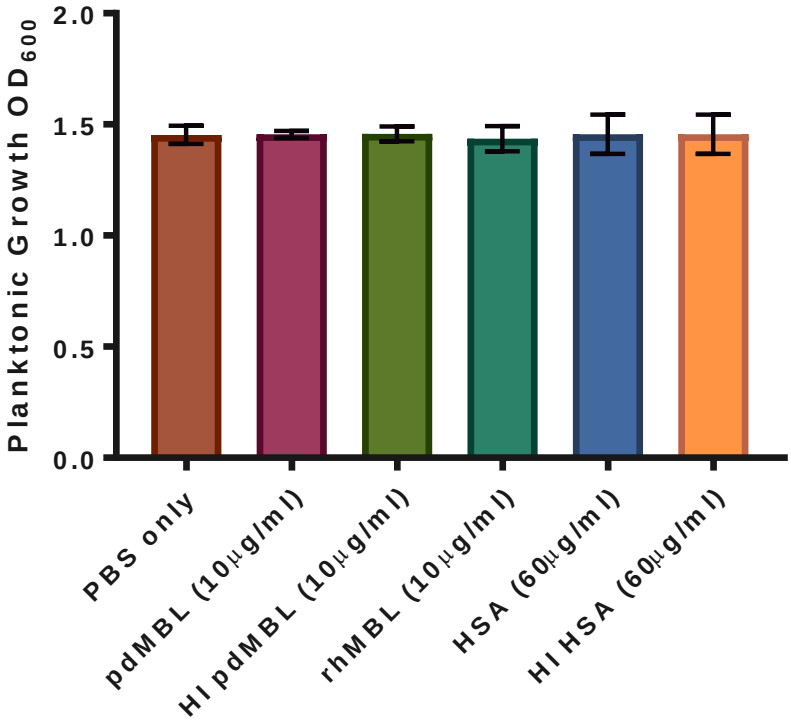

Figure 52: Effects of pdMBL and rMBL on MRSA biofilm formation when coated onto 96 well TC plates (*n*=3)

The reduction of biofilm formation on the microtiter plates led us to investigate the effects MBL would have on the reduction of bacterial adherence to epithelial cell lines (Figure 53). A paired *t*-test showed no significance in the reduction of the binding of either *E. coli* or *S. aureus* to the surface of the epithelium, though a slight reduction was observed.

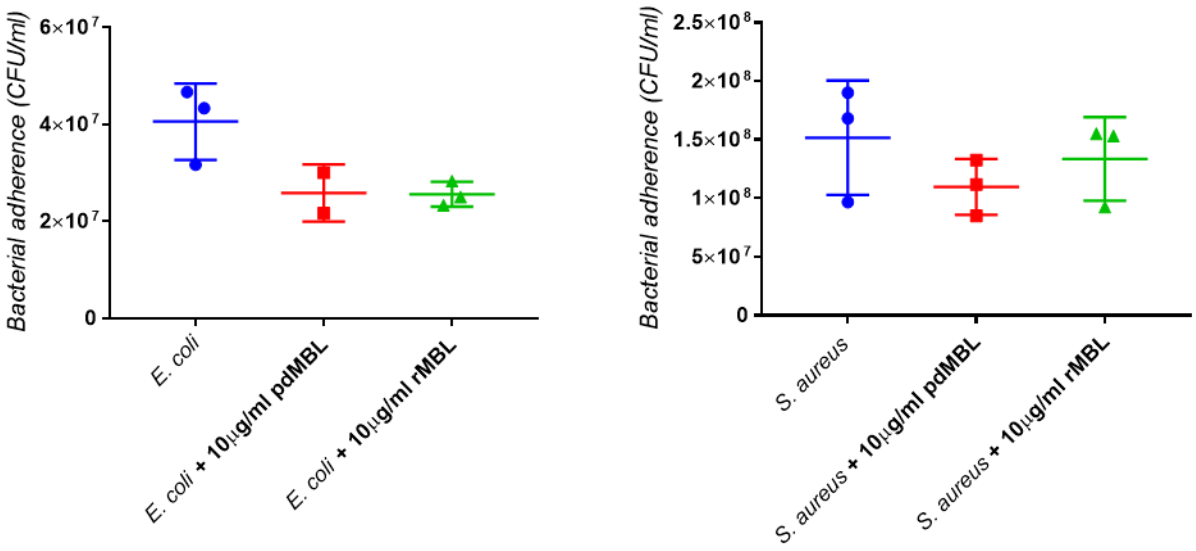

Figure 53: The effects of pdMBL and rMBL on bacterial adherence to epithelial cell line A549 cells (*n*=3)

7.7.3 NEUTROPHIL-MEDIATED DESTRUCTION OF MRSA BIOFILMS *IN VITRO*

Next the effects of MBL on neutrophil mediated biofilm destruction were investigated.

Isolated neutrophils were incubated for 30 minutes on CFSE labelled MRSA biofilms. The biofilms were then gently washed to remove lose neutrophils and then fixed. Control samples demonstrated some destruction by the neutrophils, though the pdMBL samples expressed much more destruction with increased ‘halo patches’ around the neutrophils (Figure 54C). Figure 54 are representative images of three replicate experimental sets of confocal images. Neutrophils can be seen in red, though if they have gorged on biofilm, they become bright green due to CSFE intake, making the red stain less visible. Some bright green neutrophils can be seen in Figure 54B, where they were incubated with HSA as a control; however, compared to Figures 54C and 54D there are considerably less neutrophils remaining on or in the biofilm.

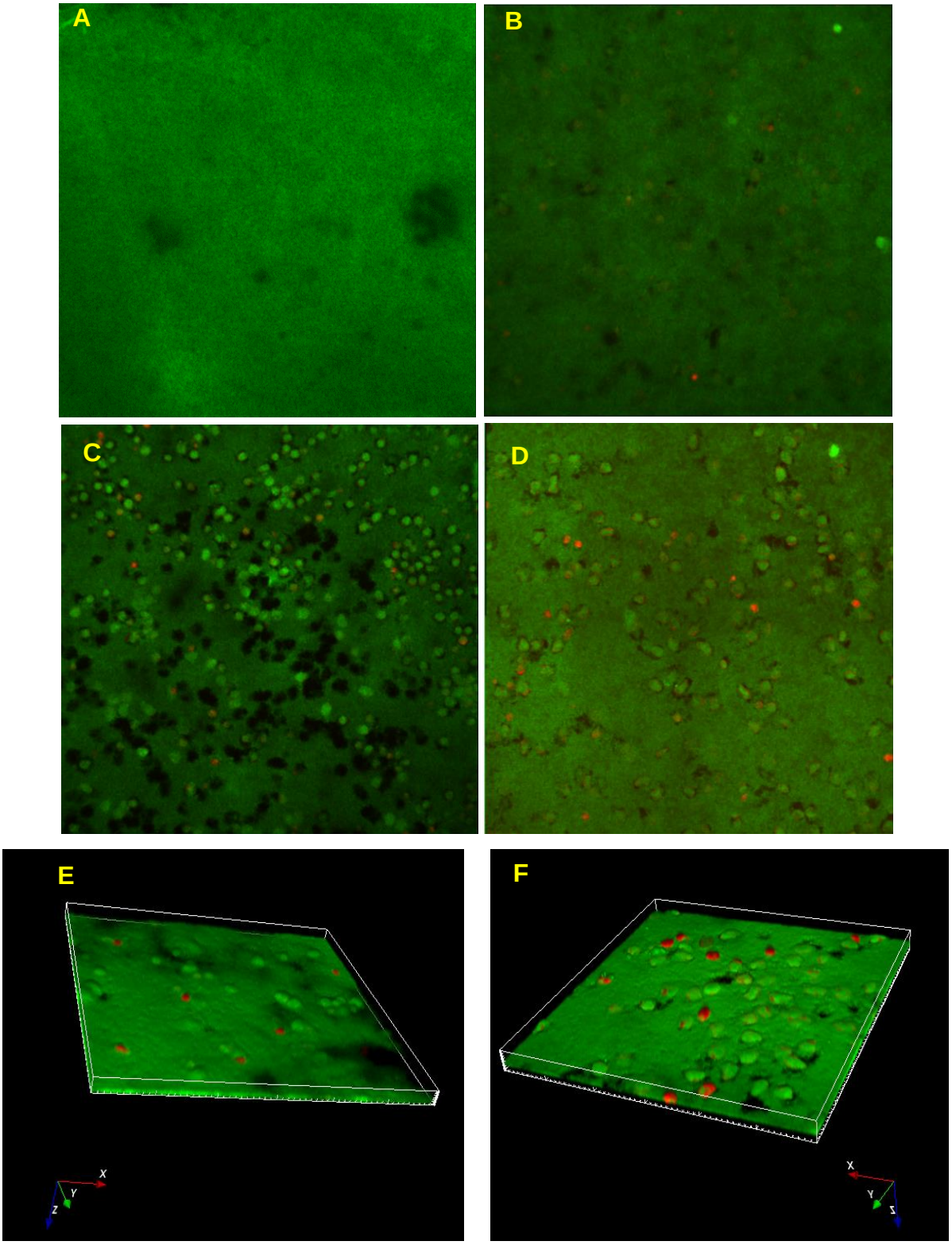

Figure 54: Control sample (A) shows CFSE-labelled biofilm only and image (B) shows biofilms incubated with neutrophils and HSA. (C) shows biofilms incubated with pdMBL and rMBL (D). 3D representation of *S. aureus* JE2 biofilm (green) and neutrophils (red). (E) Shows neutrophils within the biofilm in 10% serum conditions and (F) represents 10% serum conditions substituted with 10µg/ml of pdMBL.

The ‘halo effect’ seen in the confocal microscopy images was investigated further. Phagocytosis of the CFSE stained MRSA biofilms were measured by flow cytometry. An increase in phagocytosis can be seen in the samples supplemented with 10µg/ml of pdMBL compared to non-supplemented samples (Figure 55). Unfortunately, due to time constraints and COVID-19 restrictions the data displayed in the above graph was carried out only for is of *n*=2.

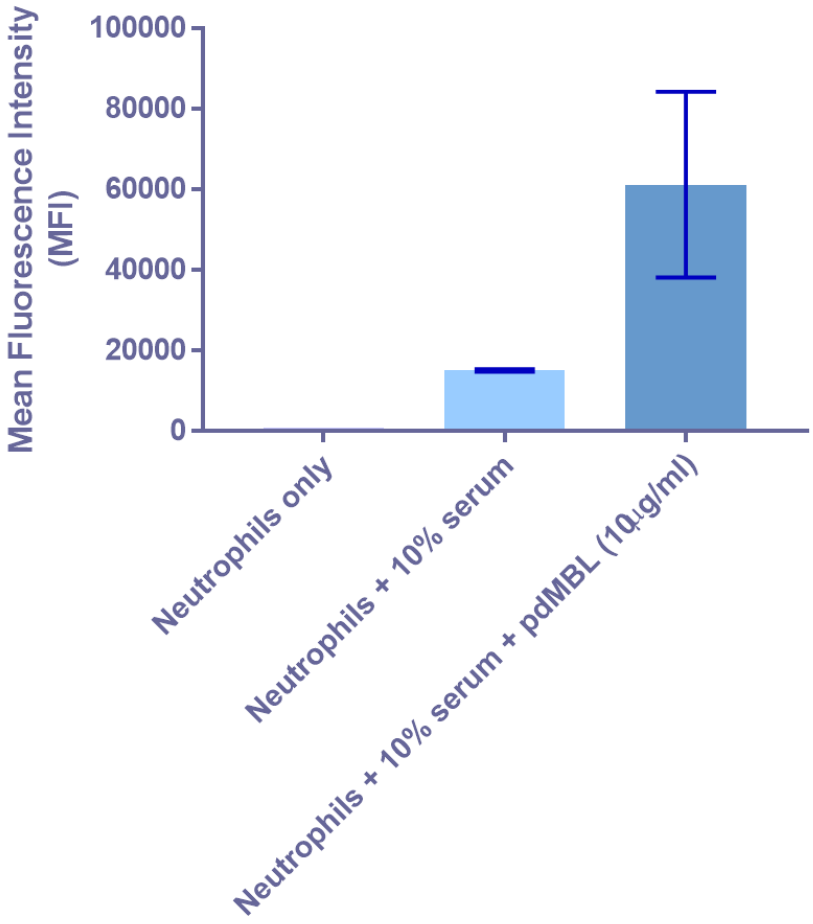

Figure 55: The measurement of phagocytosis of CFSE labelled MRSA biofilms by neutrophils with and without the presence of pdMBL (*n*=2)

7.8. BIOFILM DISCUSSION

Biofilm infections bear a significant cost to healthcare providers worldwide. Developed countries with advanced surgical treatments such as heart valve replacements and shunts experience a particularly significant biofilm burden. Moreover, children who are MBL deficient are more likely to develop infections such as sepsis and pneumonia, both of which are commonly caused by biofilm infections. The extensive and effective abilities for microbes to protect themselves from the host and anti-microbial therapies mean that these infections are extremely difficult – if not impossible – to treat without removal of the infected area. Resistance is also much more likely to appear in biofilm infections due to the impenetrability of the anti-microbial agent at significant concentrations. The increased resistance risk in an era of global anti-microbial resistance as well as the significant cost and mortality rates means new approaches and therapies are essential for the imminent future.

We hypothesised that MBL plays a role in preventing biofilm formation by mopping up planktonic bacteria and enhancing immune responses in the infected area, preventing the formation of biofilms. Heretofore, no work had yet investigated the role of MBL in the prevention of the treatment of biofilm infections.

In our work, the effects of both pdMBL and rMBL on bacterial growth and metabolism were investigated. While at first it appeared that MBL reduced the growth of MRSA during the biofilm assays due to reduction in the OD590 (Figure 50A), investigations into the metabolic rate of the bacteria showed that MBL does not affect the growth of the bacteria (Figure 50B). Upon closer inspection we determined that the bacteria were aggregating and forming small clumps due to the MBL, permitting more light transmission, and thus reducing the OD590. We looked at the effects of this aggregation on MRSA biomass formation, and demonstrated that MBL could bind, aggregate, and reduce biofilm formation of MRSA (Figure 51). The assay did not involve complement or immune cells, thus measuring only the blocking capabilities of the MBL CRDs. We found that pdMBL was effective at reducing the biomass of MRSA, with reductions of 10-35% with 5µg/ml and 20µg/ml respectively. This extreme aggregation most likely prevented the MRSA from binding to the tissue culture plate surface. The tight clumping may also have induced different gene expression, resulting in less biomass, though this hypothesis requires further exploration.

Due to the reduction in biomass as MBL was added, we looked at the effect of MBL in preventing the binding of bacteria to the epithelium using *E. coli* and *S. aureus* (Figure 53). We see a reduced ability for MBL to prevent the adhesion of Gram-negative and Gram-positive bacteria to the surface of the epithelium; however, this is not significant and is most likely due to flaws in the setup of the experiment, in particular too large a concentration of initial bacterial spike. We saw that MBL is not neutralising but only blocking as bacterial growth can still occur (Figure 53B). This blocking effect could be limited by dose, suggesting that a concentrations of 10µg/ml MBL is not high enough for high bacterial concentrations. However, due to time and COVID-19 restrictions we were unable to repeat and refine these experiments.

We also investigated the role of MBL in the clearance of establish biofilm infections, focusing mainly on the role of MBL on neutrophil-mediated destruction of MRSA biofilms. We investigated the effect of MBL on enhancing the neutrophil response to MRSA biofilms. Neutrophils were incubated with biofilms for 30 minutes before being removed, washed, and analysed by flow cytometry to measure phagocytosis of the biomass (Figure 55). We saw an increase in fluorescence from the neutrophils incubated with pdMBL, suggesting much more phagocytosis had occurred than without MBL. This was corroborated by the biofilm confocal images of the sample experiments (Figure 54). The images show the accumulation of more neutrophils on the biofilm surface with the MBL samples than in the controls. They also show darker spots (‘halos’) around the neutrophils which represent damaged biofilm, as well as holes where the neutrophils have washed away. The MBL enhanced the phagocytic abilities of the neutrophils which may explain why larger patches of the biofilm are destroyed, though this may also be explained by other enhanced functions of the neutrophils. For example, MBL may enhance the release of antimicrobial agents such as reactive oxygen species (ROS). This would explain the halos seen around the neutrophils and could be explained by both enhanced phagocytosis and antimicrobial production.

The pitfalls of this chapter lie mainly on the lack of repeats. This was due to the restrictions imposed during the outbreak of the 2020 pandemic. We also planned to further investigate the effect of MBL on neutrophil function, beyond the destruction of biofilm via phagocytosis to also measure changes in neutrophil receptor expression by flow cytometry and cytokine release by ELISA (Figure 56). We would have looked into the production of inflammatory cytokines and ROS to measure the effect of MBL on neutrophil immune defence. This chapter hoped to further investigate MBL therapy as an ancillary therapy to antimicrobial therapy, measuring synergy between the two. One such experiment would have looked at the determining the MICs for bacteria with and without the presence of MBL. Alas, time constraints, restrictions imposed due to the COVID-19 pandemic, and renewed research priorities prevented these plans from being realised before completion of this thesis.

To conclude, the work in this chapter demonstrates the potential of MBL to bind and prevent bacterial adhesion and thus biofilm formation. Bacterial adhesion to the epithelium in the lungs is associated with biofilm formation and is why individuals with impaired ciliary movement such as CF patients have recurrent chronic infections. Having sufficient MBL levels or MBL therapy may protect individuals who are at risk of infection, such as those who have just undergone invasive surgeries. We see enhanced phagocytosis of biofilms when MBL is present, which could be used to assist antimicrobial therapies for such infections. Considering higher doses of antimicrobials are required for biofilm infections, if enhanced immune responses could be generated by MBL this may be a useful adjunct to antimicrobial therapy.

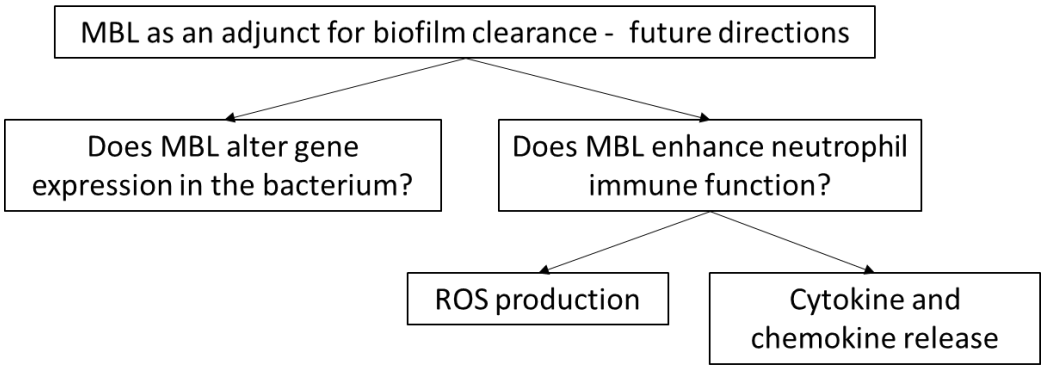

Figure 56: Future directions investigating MBL as an adjunct for biofilm clearance

CHAPTER EIGHT

THE ROLE OF MANNOSE-BINDING LECTIN IN SARS-COV-2 AND PIMS-TS

SARS-CoV-2 is a novel coronavirus with the first clinical test detected at the end of 2019 in Wuhan, China. Reports suggest a small proportion of those who become infected go on to develop the severe disease known as COVID-19. The aetiology is yet to be fully uncovered though it is suggested that a mix of genetic and environmental differences in our immune system, influence the progression into severe disease. MBL deficiency is the most common immunodeficiency, with a higher prevalence of deficiency in the Black African and Asian community. Recently, a novel inflammatory syndrome known as paediatric inflammatory multisystem syndrome temporarily associated with SARS-CoV-2 (PIMS-TS) has been observed across the globe. Evidence suggests the same ethnicities more likely to have low or deficient MBL have an increased likelihood for worse outcomes after SARS-CoV-2 infection and for PIMS-TS. From this we hypothesised that MBL plays a role in the prevention of PIMS-TS. In this chapter we explore this hypothesis.

8.1. CORONAVIRUSES

Prior to 2019, there were four human coronaviruses in circulation, none of which were particularly virulent, and causing only mild cold like symptoms. Though, 2002 witnessed the development of the SARS-CoV-1 epidemic in China and approximately 11 years later came the development of the Middle Eastern Respiratory Syndrome-CoV (MERS) epidemic. Both of these coronaviruses demonstrated a previously unseen enhanced virulence. A global pandemic began in 2019 with the emergence and spread of the SARS-CoV-2. The virus spread rapidly around the world, developing mutations which increased the rate of transmission [182]. These coronaviruses can be fatal, with 10%, 27% and 5% mortality rates respectively [183]. The viruses are spread via respiratory droplets and can live on surfaces for weeks [184]. The aetiology of these viruses is yet to be fully understood.

8.1.1. SEVERE ACUTE RESPIRATORY SYNDROME CORONAVIRUS-2

In 2019, the outbreak of a global pandemic strain of coronavirus was observed, detected due to a rise and cluster of pneumonias in Wuhan, China. This new coronavirus and its associated disease COVID-19 spread rapidly across the globe. SARS-CoV-2 was responsible for over one million deaths globally within 10 months of being first identified. It was quickly realised that SARS-CoV-2 had higher infectivity and disease severity in the Black African and Asian minority ethnic (BAME) community, with one study showing prevalence in people of Black (17.3%) and Asian (11.9%) ethnicities compared to 5% Caucasian ethnicity [185]. It was also noted that infection was more severe in older populations with 18% of over 80-year-olds hospitalised for SARS-CoV-2 infection compared to 1% of 20–30-year-olds [186]. Lower numbers of children have been hospitalised, with only 0.9% of children in the UK, 2% in China and 1.7% in North America [187].

SARS-CoV-2 is an enveloped, positive single-stranded RNA virus. Genes *S, E, M* and *N* encode for the structural proteins and the *ORF* gene encodes for non-structural proteins. The Spike protein (S-protein) also contains the receptor binding domain (RBD) which is essential for the initial viral attachment. Gene fragments express structural and non-structural proteins. The virus is covered in many glycosylated S-proteins that are capable of binding to the host cell receptor angiotensin-converting

enzyme 2 (ACE-2) mediating viral entry. The glycoproteins expressed on the viral surface are PAMPs and are recognised by PRMs of the innate immune system. Though this initial response appears crucial in disease progression early on, if out of control, it may cause excessive tissue damage. In COVID-19 patients the damage in the lung appears to be due to dysregulation of the immune response rather than just viral replication [49].

8.1.2. COVID-19

Coronavirus disease 2019 (COVID-19) is a severe contagious disease caused by SARS-CoV-2. Symptoms of SARS-CoV-2 infection typically include fever, cough, sore throat, headache as well as fatigue and breathlessness, though approximately a third of those afflicted with SARS-CoV-2 have no symptoms at all [188]. However, a small group of the population progress to severe infection, including difficulty breathing, acute respiratory distress syndrome, and septic shock with an exaggerated inflammatory response. The patients may go on to develop pulmonary disease, cardiac, hepatic, renal or thrombotic disease. Interestingly, males appear to be more affected than females and this is most likely due to hormone profile differences [189]. Severe COVID-19 infection presents as systemic hyper-inflammation and coagulation which can severely affect multiple organs. Also, in severe cases, some patients may be intubated to support breathing and can go on to develop hyperinflammation, also known as a cytokine storm. Also observed are high levels of IL-6 and CRP in patients with respiratory failure, with one study demonstrating improved survival rates for those on anti-cytokine therapy [190]. Interestingly, one study found that in severe COVID-19 RNAemia was detected in the blood. RNAemia detection in non-survivors was 56% compared to 13% in survivors [191]. Also, a twofold increase in mortality was documented in COVID-19 with patients suffering from hypertension, the most common treatment for which are ACE inhibitors which can increase the ACE-2 receptor expression.. Moreover, ACE-2 is expressed in the lungs, kidneys, and gastrointestinal tract as well as the endothelium.

8.1.3. THE CLEARANCE OF SARS-COV-2

Just like bacterial infections such as sepsis, viral infections need to be safely cleared to remove PAMPs which can still invoke immune responses even after the death of

the microbe. It has been shown that MBL binds and neutralises PAMPs from a variety of microbes, even showing a clear involvement in the prevention of Gram-negative bacterial sepsis despite the binding of MBL to Gram-negative whole cell bacteria being weak compared to Gram-positive bacteria or yeast [193]. A study using FcMBL found that only 35% of *E. coli* isolates were bound when whole cell, but after fragmentation this increased to 93% [19]. SARS-CoV-2 infection has been shown to clear on average within 1-2 weeks of testing positive by PCR, though viral proteins such as the N and S proteins have been found in patients' GI and hepatic organs 9-180 days post-infection [194, 195]. Plus, persistence of SARS-CoV-2 proteins has be found in CD16+ monocytes in post-acute COVID-19 up to as much as 15 months post-infection [196]. Other studies have demonstrated the potential for the nucleocapsid and spike proteins to induce IL-6 in monocytes and macrophages [197, 198]. The S-protein has been shown to elicit a variety of the symptoms seen in COVID-19 including neurological disorders due to effects in the brain as well as downregulation of the ACE-2 receptor on the endothelium [198, 199]. One theory that has been put forward for severe infection and inflammation is the viral protein fragmentation theory [200]. The theory is based on the idea that the SARS-CoV-2 S-protein can initiate cell signalling events without the need of the other viral components. This theory would further implicate a role of the innate proteins in the binding and neutralisation of the viral fragments to reduce prolonged inflammation and potentially prevent the onset of PIMS-TS.

8.1.4. PAEDIATRIC INFLAMMATORY MULTISYSTEM SYNDROME (PIMS)

Paediatric inflammatory multisystem syndrome temporally associated with SARS (PIMS-TS) is a novel condition affecting children below the age of 18-years-old. These children develop significant systemic inflammation with symptoms including fever, abdominal pain, and potential cardiac involvement, and were confirmed to have had SARS-CoV-2 infection either by PCR, serology or known exposure. Moreover, recent reports have shown that PIMS-TS rates are prevalent 2-5 weeks after COVID-19 infections spike [201]. The post-infectious disease presents similar to Kawasaki disease (KD). Children present with fever and inflammation including neutrophilia, lymphopenia, and elevated CRP levels. There is also evidence of single and multi-organ dysfunction with other complications. The syndrome can be fatal and needs to be treated immediately and appropriately. Again, the Black African and Asian

community are at higher risk of developing PIMS-TS compared to the Caucasian community [202]. In regard to the treatment of PIMS-TS, early intervention with IVIG is recommended and or with high dose glucocorticoids [203]. However, approximately 30-80% do not respond to IVIG and require further therapy to control the inflammation, as also observed in KD [204-208]. Additional dosing with methylprednisolone and IVIG has been suggested for patients not responding to the initial doses. For these reasons a clearer understanding of the progression between SARS-CoV-2 initial infection and the development of PIMS-TS is needed to provide more effective treatments.

8.2. KAWASAKI DISEASE

KD is an acute febrile illness which can occur in early childhood, though it is rare. The majority of cases (>80%) occur before 5 years and after 6 months of age [209]. Characterisation includes a fever that lasts longer than 5 days with acute vasculitis of the small and medium blood vessels which can cause significant damage to the coronary artery, subsequently making KD the leading cause for acquired heart disease in the developed world. Though the presentation of KD does not differ between ethnicity, Northeast Asians are 20 times more likely to acquire KD than Caucasian ethnicities [210]. Black children were more likely to suffer KD than Caucasian children yet more importantly were more likely to have severe outcomes and treatment failure than Caucasian counterparts [211]. No definitive causative agent has been found, though it is believed to be due to an infectious agent due to the increased incidences during winter and other seasonal peaks in tropical climates [212]. The fact that most babies are protected from KD in the first few months of life and once they reach adulthood suggests that adults have been exposed to the causative agent, protecting babies via maternal IgG transfer. It is important to note that though originally PIMS-TS was described as a ‘Kawasaki-like’ disease it has since been shown to be distant from KD but with many similar clinical features [213].

8.2.1. THE ROLE OF MANNOSE-BINDING LECTIN IN KAWASAKI DISEASE

Little research has been done into the role of MBL in KD, though studies have revealed some interesting results. A study in Japan found that the heterozygote -54 codon

polymorphism was significant in the KD cohort (49% versus 36.5% in healthy controls) [214]. However, murine studies investigating the role of MBL in KD vasculitis found MBL in the aortic root contributed to exacerbated vasculitis and complement deposition [215]. Moreover, wildtype MBL genotypes were described as potentially being an increased risk for developing coronary aortic lesions in older children with KD [216]. Though, as discussed previously, MBL may likely play a role in the prevention of inflammatory diseases such as KD, but once the disease progresses its protective functions may result in more injury to the host.

8.3. COMPLEMENT IN SARS-COV-2

Complement activation has been previously linked to acute repository distress syndrome as well as respiratory failure in other diseases [217, 218]. The involvement of complement in lung injury has also been found by histopathological studies of post-mortem biopsies of COVID-19 patients [219]. C3 deficient mice infected with SARS-CoV-1 have been shown to have less severe respiratory inflammation compared to control mice [218]. Moreover, one study showed that complement activation by MASP-2 and thrombotic microangiopathies are active in COVID-19, and that MASPS 1 and 2 can bind directly to the spike and nucleocapsid proteins of SARS-CoV-2 [220]. MASPs have been shown to play key roles in the complement and coagulation cascade [221]. Interestingly, anticoagulant therapies in COVID-19 have been shown to reduce dysfunction coagulation [222]. It has been shown that MASP-2 interacts with SARS-CoV-1, MERS-CoV and SARS-CoV-2 to induce the complement cascade. One study suggested that MBL and MASPs are important during the incubation stage of SARS-CoV-2, though it is important to note that MBL is only in the lung of chronically infected patients with only a slight increase in MBL levels during acute infection [70, 223]. Another study found MBL and pentraxin 3 (PTX3) were positively associated with mortality within the ICU for COVID-19 [191]. PTX3 and MBL were shown to bind to SARS-CoV-2 recombinant proteins in a study measuring protein interactions and the virus. Recombinant MBL and PTX3 were shown to bind to the spike protein and nucleocapsid respectively [224]. Within the same study interactions between SARS-CoV-2 and pentraxins including CRP and serum amyloid component were measured but no binding observed. Other PRMs of the lectin family were measured including

collectin 11, collectin 12, collectin 13 and the lung surfactant SP-A and SP-D as well as the three ficolins (1, 2 and 3). No binding was observed to the spike proteins except for MBL. It is also worth noting that MBL has been found to bind the glycosylation sites conserved on both the SARS-CoV-1 and SARS-CoV-2 spike proteins [75, 224]. Cq1 of the classical pathway was also found to not bind any SARS-CoV-2 proteins including the envelope, spike and nucleocapsid. On the other hand, a 2021 study in Brazil demonstrated that variants within a cohort of patients hospitalised due to SAR-CoV-2 were more likely to carry *MBL2* variants that result in higher MBL serum levels [225]. The role of MBL is hard to decipher due to the contradictory literature available, however, it is most likely that MBL's role is in the protection of systemic microbial spread during infection and the regulation of inflammation, particularly post-infection. It is important to regulate safe clearance of microbial fragments and proteins to maintain homeostasis. However, if disease continues, the previously protective role now becomes reversed, with MBL then enhancing complement deposition and enhancing the immune response to the detriment of the host.

8.4. THE ROLE OF LECTINS IN SARS-COV-2 INFECTION

The literature describing a highly mannose and mannan coated spike protein on SARS-CoV-2 is what lead to the hypothesis that MBL would bind and neutralise the virus. A publication in 2021 demonstrated that mutations at codon 54 which are associated with lower MBL serum levels were a higher risk for the development and severity of COVID-19 infection similar to that demonstrated in KD [214, 226]. The study had 284 cases versus 100 controls (10.9% deficient –BB genotype and 1%). Yet, another study showed no differences in deficiency or MBL levels between healthy and severe COVID-19 cohorts [219]. It was also found that MBL deficiency caused by the B allele mutation rs1800450 was a risk factor of severe COVID-19 [227]. One study demonstrated that MBL as well as FCN-2 and collectin-11 are capable of binding to recombinant S and N-proteins of SARS-CoV-2 and initiate complement [220]. Another case study investigated a lack of seroconversion in a 30-year-old female with MBL deficiency (<50ng/ml). No seroconversion was observed after the first infection and only seen 8 weeks after the second infection months after the first, despite IgG generation being typically observed 2 weeks after initial infection [228]. Prominent

activation of both the alternative and LP in severe COVID-19 has been observed, as well as systemic complement activation and consumption which has been associated with in-hospital mortality [229]. Yet, despite this, Sinkovitis et al demonstrated no difference in LP activity between those with severe and less severe COVID-19 patients [229]. A possible role for the lectin proteins may be in neutralisation of the virus during early infection. The range of lectins as well as lung surfactants may contribute to first line defences preventing the virus entering the cells, though recent data suggests that SP-A and SP-D are unable to bind the virus [224]. MBL, amongst other serum lectins, may contribute to reduced thromboinflammation by preventing the virus binding or interacting with the endothelium. This may also be achieved by causing aggregation of immunostimulatory fragments of virus and enhancing controlled clearance via opsonophagocytosis. Yet, various studies have previously demonstrated high or normal MBL levels may contribute to increased thrombosis [218, 225]. This conflicting literature is why more research into MBL as well as other innate molecules is needed in order to fully understand their roles in infection and inflammation and resolve these dichotomies.

8.5. ANTI-COMPLEMENT THERAPEUTICS

A significant amount of evidence has been published showing that SARS-CoV-2 infection drives an inflammatory response by the host innate immune system which results in coagulation and thrombosis. This starts in the lung and can move to other organs, which can result in multiorgan failure [230]. Various attempts to regulate inflammation with anti-cytokine therapies and anti-thrombosis targets have been tested [231]. Due to the recent associations with high complement deposition seen in the tissues of severe COVID-19 patients during PM, a recent surge in anti-complement therapies have begun. Though it should be noted that high complement in the lungs of COVID-19 patients may contribute to exacerbated damage, one study found that no secondary infections were seen in a cohort of COVID-19 patients, compared to 80% of H1N1 cases [225]. However, though less coinfections were documented early on in the pandemic more recent studies have been made available suggesting that 27.7% of COVID-19 patients requiring mechanical ventilation suffer coinfections [232]. Studies involving MERS-CoV found that anti-C5a drugs decrease the severity of

disease in mouse models [233]. Moreover, treatments with C5 blockers including eculizumab, found an increase in lung function and an inverse correlation with CRP and IL-6 levels [234]. The blocking of essential immune pathways may result in increased infections and further systemic inflammation due to BSIs including sepsis. This was the case in a study blocking C5 in severe COVID-19 patients, with one patient developing an occult and fatal *Klebsiella* infection [235]. Another study found an increase in infections such as ventilator-associated pneumonias and bacteraemias during a clinical trial of eculizumab [236]. Interestingly, unlike the C3 and C5 inhibitors, disruption of the MASP-2 pathway would not lead to interference of the classical pathway and could result in reduced thrombosis. Additionally, attempts to block the alternative pathway with a C1 inhibitor (icatibant) was trialled on 30 patients with no significant effects observed [237]. It was noted however that icatibant was safe for use and had a positive impact on the lung severity.

Here, we investigate the role of MBL in the neutralisation of SARS-CoV-2 and its potential role in the development of PIMS-TS disease (Figure 57).

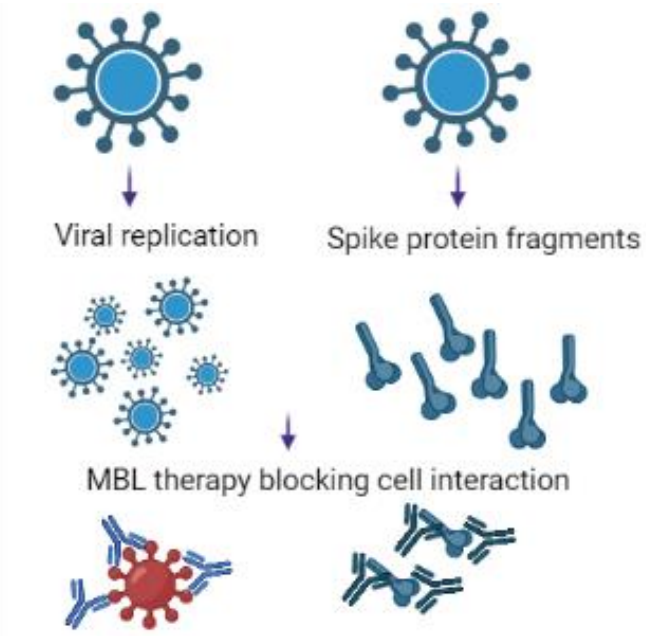

Figure 57: MBL therapy theory; MBL blocks whole cell SARS-CoV-2 and secreted S-proteins from interacting with the ACE-2 receptor preventing cell signalling and inflammation (adapted from Suzuki 2020 [196]).

8.6. AIMS

With only a small portion of the population at risk of developing PIMS-TS we hypothesised that this was due to commonly shared genetic influencers of viral and inflammatory control. As SARS-CoV-2 is a novel virus, it can be assumed that there is a lack of an effective adaptive immunity and thus MBL's role in clearing and regulating inflammation as an innate molecule found to bind to the S-protein would be crucial. Higher levels of deficiency are seen in the BAME community, up to 30%, and current literature suggests that the same communities with higher rates of MBL deficiencies are more at risk of severe COVID-19 and PIMS-TS development [238].

We hypothesise that MBL plays a key role in the control of established respiratory viral infection and in the clearance of viral debris post-infection. The severe hyper inflammation observed in both COVID-19 and PIMS-TS is important to understand in order to provide more effective treatments. To understand this further we set out the following aims:

1. Investigate serum MBL levels in PIMS-TS patients relative to control groups

2. Investigate correlations between age of PIMS-TS onset and MBL serum levels

3. Investigate patient ethnicities and likelihood of MBL serum levels and disease

4. Investigate how MBL serum levels impact the clinical outcomes in PIMS-TS

5. Investigate the neutralising abilities of pdMBL and rMBL on SARS-CoV-2

8.7. METHODS & MATERIALS

All reagents were purchased from Sigma, UK unless stated otherwise.

8.7.1. MEASURING MANNOSE-BINDING LECTIN SERUM LEVELS

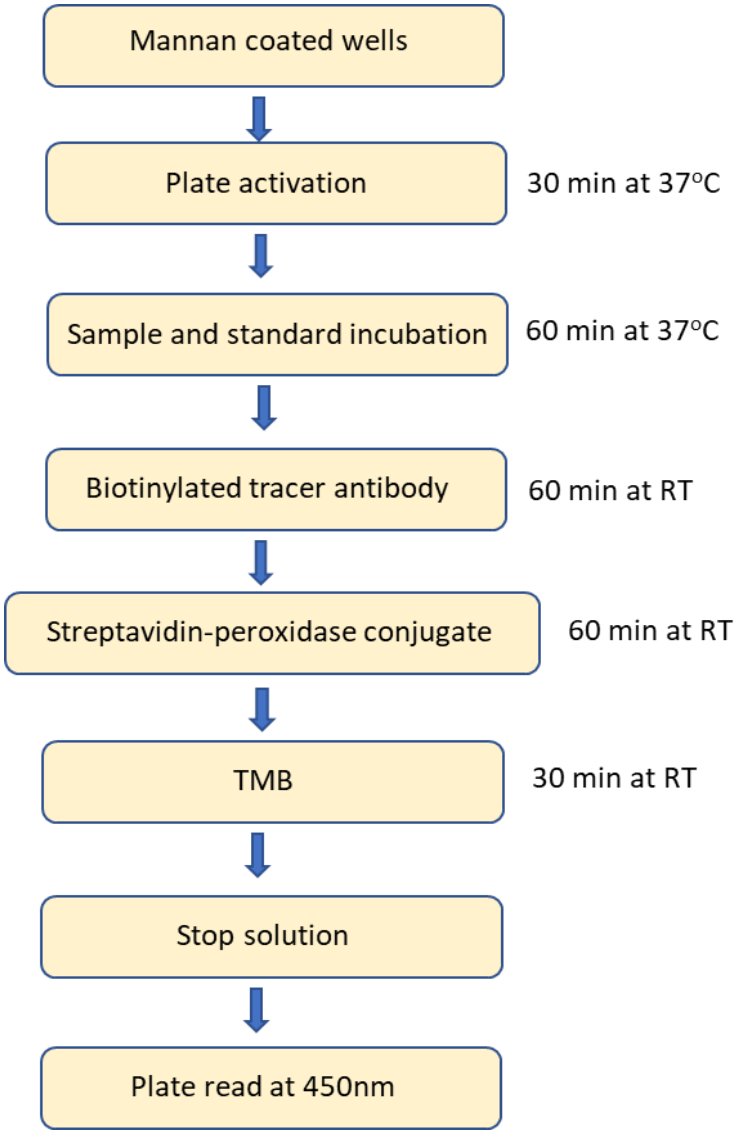

Figure 58: Hycult MBL ELISA protocol overview

Plasma was isolated and frozen immediately at -80°C. Determination of the oligomerised MBL concentration of the samples was measured using ELISA (Human MBL HK323, Hycult Biotech). The linear range of the assay is 0.41–100ng/ml when plasma is diluted 1:100 in the sample diluent provided by the manufacturer.

8.7.2. PATIENT SELECTION

Children and teenagers admitted to GOSH with suspected PIMS-TS had plasma samples taken as routine and MBL levels were investigated as part of routine diagnostics. Children were confirmed to be PIMS-TS cases by the clinicians at GOSH according to the Royal College of Paediatrics and Child Health advice guidelines for clinicians [239] . Diagnosis of PIMS-TS describes the following: a child with persistent fever, inflammation, and evidence of single or multiple organ failure. This also included elevated CRP levels, lymphopaenia and neutrophilia. Other causes for such presentation were excluded such as KD, bacterial infection, or sepsis. A SARS-CoV-2 PCR test can be negative or positive. A total of 39 patients which met these criteria were chosen from GOSH between December 2020 and June 2021. A further 146 were collected from PIMS-TS patients who were admitted to GOSH from July 2021 to January 2022 with details of their clinical data during active disease. A total of 75 PIMS-TS samples were collected form the DIAMONDS study. A total of 260 PIMS-TS patients were analysed in this study. As the data analysis was retrospective and no additional data were collected beyond those required for standard medical care, a full ethics review under the terms of the Governance Arrangements of Research Ethics Committees in the UK was not required. Great Ormond Street Hospital for Children, NHS Foundation Trust, Research and Development approved the study (R&D number 20IR39).

8.7.2.1. DIAMONDS STUDY

Paediatric samples were donated by the DIAMONDS study in order to investigate MBL levels. The DIAMONDS study includes 11 EU countries and recruits paediatric patients on admission to hospital with fever or inflammation. The aims of the DIAMONDS study are to determine host gene expression towards illness and to discover biomarkers of illness to rapidly diagnose illness when patients are admitted to hospital. A total of 324 samples were received from the study including 75 PIMS-TS samples. A total of 63 bacterial infection, 50 viral infection, 27 COVID-19 affected children and 77 unknown but assumed bacterial or viral infections were collected. A total of 26 samples were excluded from analysis due to lack of demographic data, being above the age of 18-years-old, or duplication of patients.

8.7.3. MBL MIXTURES

In vitro assays investigating the role of MBL during SARS-CoV-2 infection were carried out with three individual MBL mixtures. The first being pdMBL (Denmark), the second rMBL (Statens State Institut) and third rMBL carrier free (rMBL CF) (Bio-techne, Oxford). Western blotting and Coomassie blue staining were carried out for the pdMBL and rMBL mixtures (methods in section 7.4.1.).

8.7.4. VERO-E6 CELL MAINTENANCE

Vero-E6 cells (kidney epithelium cells from the African green monkey) were maintained in DMEM with 10% FBS and 1% Pen/Strep (Fisher, UK) in TC treated flasks at 37^{o}C in 5% CO_2. Cells were detached using trypsin 0.05%/EDTA (Fisher) for ~5 minutes. Cells were washed and resuspended in DMEM and seeded in a 1:10 ratio.

8.7.5. PLAQUE ASSAYS

Vero-E6 cells were seeded at 1.15-1.5×10^5 cells per ml in 24-well TC treated plates in DMEM and incubated overnight. Cells were then transported to the CAT III facility and aspirated and incubated with 200µl of 10-fold serially diluted viral inoculum in OptiMEM (Gibco). Plates were incubated for 1 hour at 37^{o}C in 5% CO_2. Inoculum was removed and 350µl of overlay (2.4% Avicell cellulose solution in ddH_2O) in 2 times minimal essential media (MEM) was added to each well. Plates were incubated at 37^{o}C in 5% CO_2 for 48 hours. The plates were then removed from the incubator and the overlay aspirated. Wells were then fixed with 200µl of 2% PFA and 2% glutaraldehyde (Polyscience) for 20 minutes at room temperature. The fixative was then aspirated off and 200µl of crystal violet (8% crystal violet + 20% ethanol) added to each well for 10 minutes at room temperature. Plates were then washed under the tap and left to air dry. Plaques were then counted and plaque forming units (PFUs) calculated.

8.7.6. MANNOSE-BINDING LECTIN NEUTRALISATION CONCENTRATION CURVE

Concentration curves investigating the neutralising effect of MBL were performed as above for all three mixtures of rMBL and pdMBL with a linear concentration range from 20µg/ml to 0.062µg/ml.

8.7.7. MANNOSE-BINDING LECTIN NEUTRALISATION ASSAYS

Vero-E6 cells were cultured and maintained in DMEM with 10% FBS and 1% Pen/strep at 37ºC in 5% CO_2. Cells were seeded in 96 well culture plates at 4×10^5 per well in 300µl volumes of media. Cells were cultured for 24 hours to reach confluency. Virus stocks were thawed and diluted to ~100 PFU per well in MEM. MBL mixtures of pdMBL and rMBL were diluted in OptiMEM and incubated with the virus at a 1:1 ratio. Control and media only samples were prepared at the same time. All samples were incubated at 37ºC for one hour. Media were removed from the Vero cells and 60µl of sample was added to each well in triplicate. Wells were topped up with 120µl of fresh media and incubated at 37ºC for 48 hours. The media was removed from the wells, and cells fixed and stained with CV and air dried. Images of the plates were taken before being washed with dH_2O thrice, emptied and left to air-dry for 15 minutes. Neutralisation was quantified by eluting the crystal violet with 250µl of 33% acetic acid and measuring the absorbance at 590nm (SPECTROstar Nano Plate reader, BMG Labtech).

8.7.7.1. MBL COMPETITION ASSAYS

EDTA was used to outcompete SARS-CoV-2 to the CRD of MBL to establish the exact mechanism for the MBL neutralisation. EDTA was used at a linear concentration of 10mM-2.5mM.

8.7.8. STATISTICAL ANALYSIS

Statistical analysis was performed in Prism 7.04, GraphPad. Shapiro-Wilk tests were used for testing the normality of MBL serum level distributions. Mann-Whitney *U* tests were used to compare the MBL serum level distributions between binary groups. Wilcoxon signed-rank tests were used to compare between MBL levels during active PIMS-TS and convalescence. Kruskal-Wallis tests were performed to test whether MBL serum level distributions vary by ethnicity within the patient cohorts. Spearman's rank tests were performed for analysis between age and MBL serum levels. Paired *t*-tests were used to investigate variations between the MBL mixtures in the neutralisation and plaque assays. A significance level of $P<0.05$ was used for all analyses.

8.8. SARS-CoV-2 Results

8.8.1. Patient demographics

Table 22: Patient demographics for the DIAMONDS and GOSH patients. IQR=Interquartile range, Demographic data was unavailable for 3 of the PIMS-TS patients.

		PIMS-TS	Viral	Bacterial	Unknown	COVID-19	Total
Total		260	50	63	77	27	
Age (years) median		10	6	9	7	12	
Gender	Female, n (%)	96 (37)	20 (40)	23 (37)	43 (56)	8 (30)	190
	Male, n (%)	161 (63)	30 (60)	40 (63)	34 (44)	19 (70)	284
Ethnicity (%)	Arabic	10 (4)	3 (6)	4 (6)	6 (8)	-	
	Black African	53 (21)	13 (26)	17 (27)	15 (19)	2 (7)	
	Mixed (Black & Caucasian)	36 (14)	3 (6)	3 (5)	2 (3)	1 (3.5)	
	European Caucasian	60 (23)	20 (40)	22 (35)	37 (48)	15 (56)	
	East Asian	-	1 (2)	2 (3)	-	-	
	South Asian	55 (21)	4 (8)	6 (10)	9 (12)	4 (15)	
	West Asian	1 (0.4)	2 (4)	1 (1.5)	3 (4)	-	
	Other	45 (18)	4 (8)	8 (13)	5 (6)	5 (19)	
MBL serum levels	Median [IQR]	557 [77 – 2188]	1571 [338 – 2882]	970 [113 - 2896]	1841 [215 - 3302]	1104 [219 – 2903]	
	Deficient <100ng/ml (%)	73 (28)	2 (4)	15 (23)	11 (14)	5 (19)	106
	Low <500ng/ml (%)	125 (48)	14 (28)	24 (38)	25 (32)	7 (44)	195
	Sufficient >500ng/ml (%)	135 (61)	36 (72)	39 (62)	52 (68)	15 (56)	277

Shapiro-Wilk normality testing indicated a significant deviation of the MBL serum levels from a normal distribution for the PIMS-TS data set (*P*=0.0001) and combined data set of all disease states (*P*=0.0001) (Figure 59). Due to the significant deviation from normal distributions, we use non-parametric tests on this data.

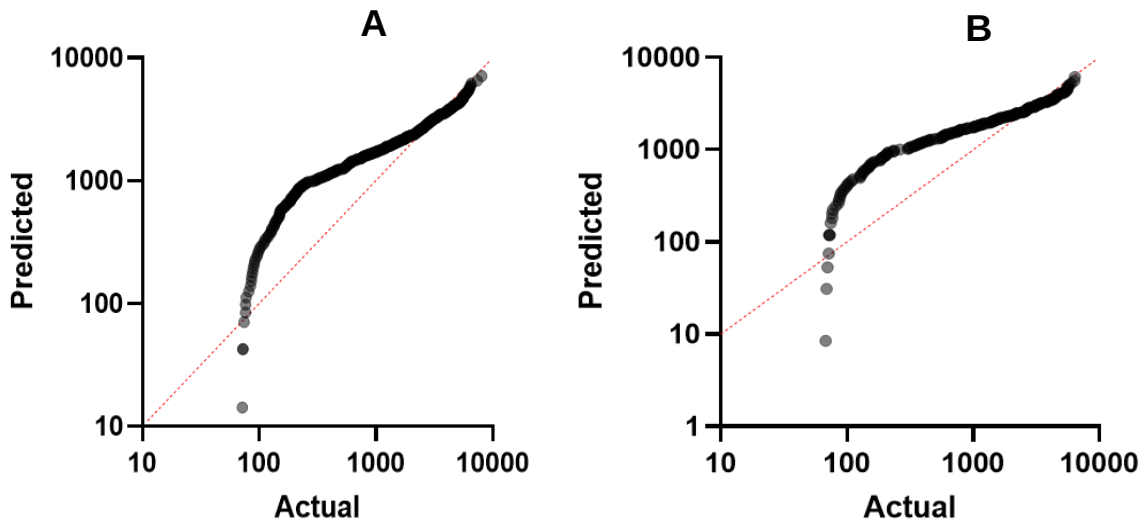

Figure 59: Normality testing using the Shapiro-Wilk test for MBL distribution in A) PIMS-TS patients (*n*=260) and B) all data including PIMS-TS, bacterial, viral, unknown, and COVID-19 infections (*n*=474).

MBL levels in females and males of the PIMS-TS cohort and all the data were compared by a Mann-Whitney *U* test, with no significant differences observed *P*=0.9826 (Figure 60).

Variations in the MBL levels of the PIMS-TS patients according to ethnicity (Figure 61) and age (Figure 62) were investigated. Age and MBL levels did not demonstrate any significant correlation in our cohorts (*P*=0.2016). We observe in the PIMS-TS cohort that White European (23%) were the predominantly affected cohort with South Asian (21%) and Black African (21%) closely following, with the median MBL levels shown for each ethnicity in Table 23. A Kruskal-Wallis test was performed showing no significant difference between the different MBL levels and ethnicities in our cohort (Figure 61).

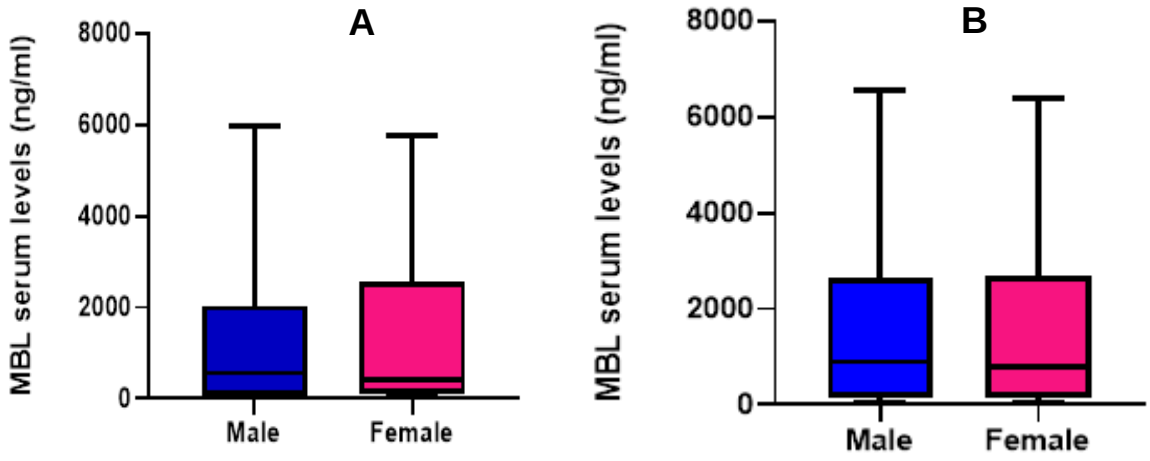

Figure 60: Mannose-binding lectin serum levels in females versus males of A) the PIMS patient cohort *n*=161 males and 96 females B) the whole patient cohort *n*=284 males and 190 females. Mann-Whitney *U* tests showed no significance A) *P*=0.9826 B) *P*=0.8940

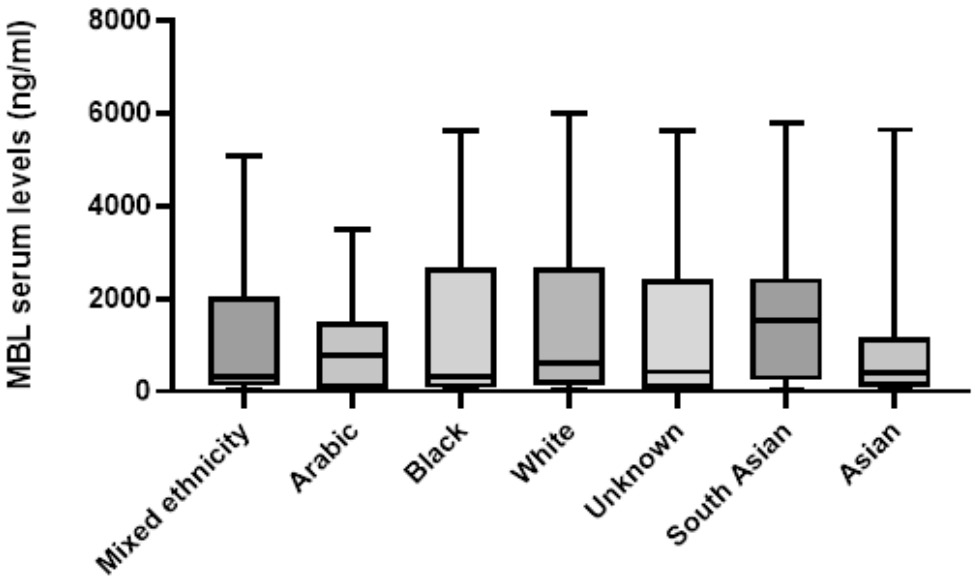

Figure 61: Ethnicity median MBL serum levels in the total PIMS-TS patient cohort. Kruskal-Wallis test showed no significance (*P*=0.4630). *n*=260

Table 23: MBL serum levels in the various ethnicities within the PIMS-TS cases

	Mixed ethnicity	**Arabic**	**Black**	**Caucasian**	**South Asian**	**Asian**	**Unknown**
n	27	10	52	57	41	26	47
Median (ng/ml)	306.2	774.4	328.4	600.6	425.6	1513	411.9

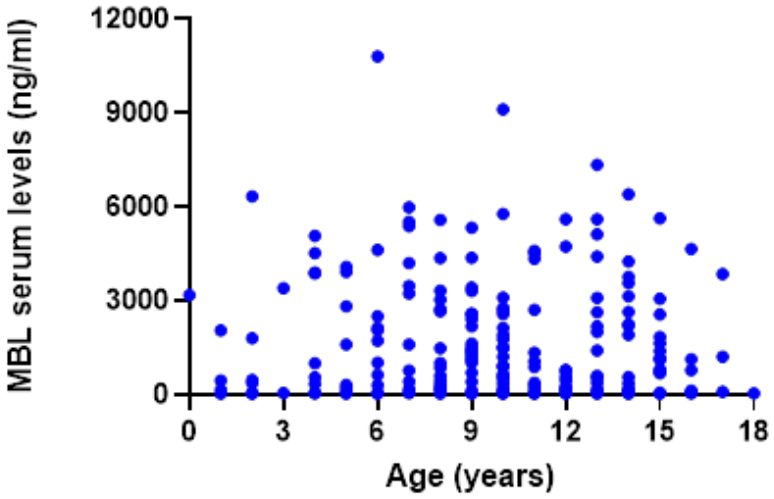

Figure 62: Scatter plot showing the distribution of MBL levels against age for the PIMS-TS cohort. A Spearman's rank test was performed with no significant correlation (*P*= 0.2016).

8.8.2. MBL SERUM LEVELS IN DISEASE

Median MBL levels were investigated for all disease types (Figure 63). Low MBL level have long been an established risk factor in the development of severe bacterial infections. In the absence of a healthy control cohort, we use a bacterial infection cohort as a control, as well as COVID-19 patients who acquired SARS-CoV-2 infection but did not go on to develop PIMS-TS.

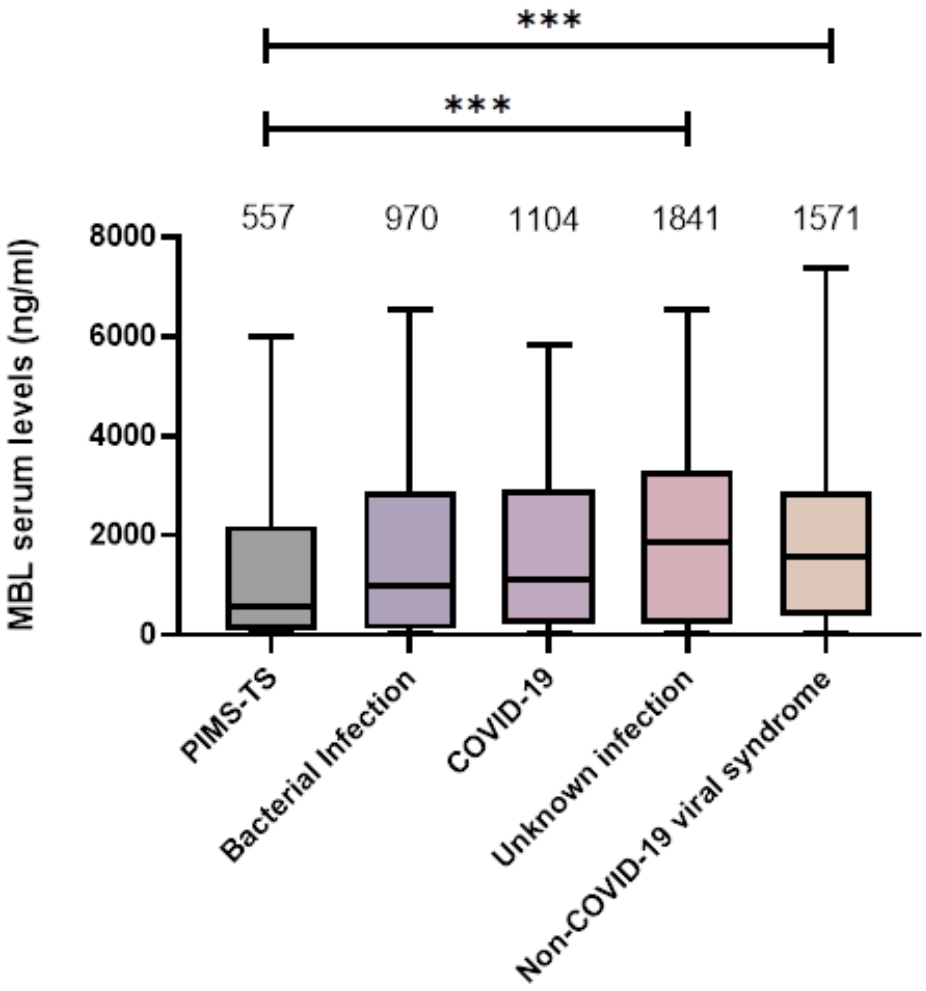

Figure 63: MBL serum levels during active disease including PIMS-TS, Bacterial infection, COVID-19, unknown bacterial or viral infection and non-COVID-19 related viral syndrome.

Mann-Whitney *U* tests showed no significant deviation between the distribution of MBL levels in PIMS-TS cohort and the bacterial infected (P=0.6864) and COVID-19 (P=0.2016) cohorts. Significant deviation was seen between the PIMS-TS cohort and the unknown bacterial or virally infected cohort (n=77, P=0.0007) and the non-COVID-

19 viral syndrome cohort (*n*=50, *P*=0.0008), which persists following Bonferroni multiple testing correction. Median, IQR, and range of MBL levels are shown on the graph for each disease. Of the patients analysed at GOSH, 47 had convalescence data for comparison (Figure 64). We investigated the MBL levels during and after disease, firstly due to MBL being named an acute phase protein, and secondly to determine whether the patients with apparent MBL deficiency were indeed truly deficient or were instead consuming their MBL during active disease. A Wilcoxon signed-rank test was performed to assess this, and a significant drop in MBL levels after active PIMS-TS was observed (*P*=0.0074). Convalescent samples were taken between 12 weeks and 6 months after discharge.

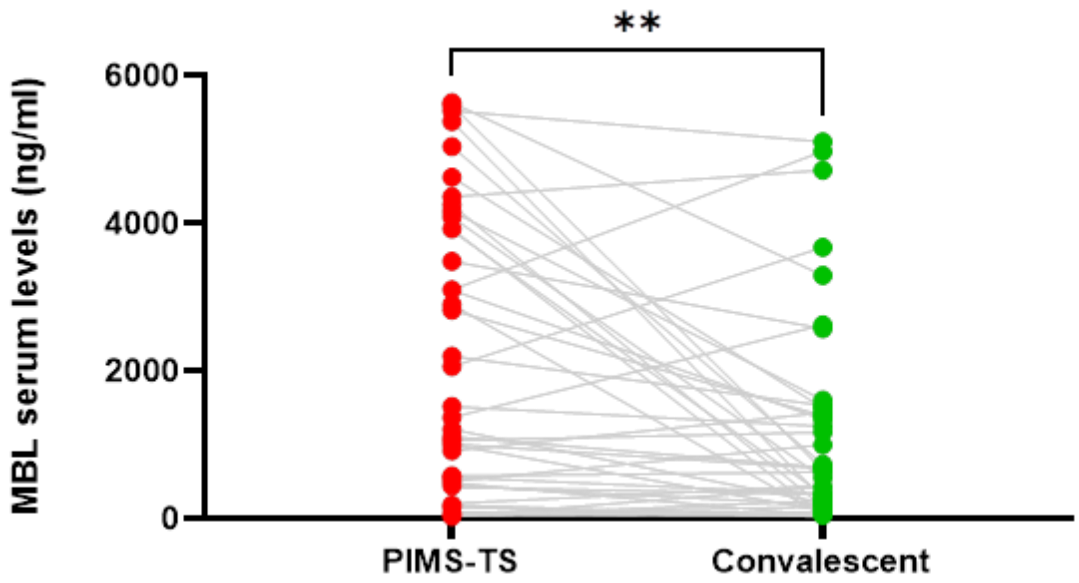

Figure 64: MBL serum levels of PIMS-TS patients during active disease and convalescence. Data from GOSH. *n*=47 pairs. Wilcoxon test showed a significant difference with a *P*=0.0074

8.8.3. THE ROLE OF MBL AND CLINICAL FEATURES DURING PIMS-TS

Table 24: Clinical data analysed for PIMS-TS patients from GOSH. Comparisons were made between the categories of MBL low (<500ng/ml) and MBL normal (>500ng/ml). MWU = Mann-Whitney *U* test. (*n*=140)

Clinical Marker	Role in disease	Median	IQR	Test	Result	P value
ALT	Liver damage	34.5	8.00 - 63.5	MWU	NS	0.0550
Creatinine	Kidneys	52.0	39.0 - 76.8	MWU	NS	0.9493
Conjunctivitis (Y/N) (MBL levels)	Associated with PIMS-TS	-	-	MWU	NS	0.2808
CRP (peak)	Inflammatory marker	278	203 - 339	MWU	NS	0.2318
D-dimer (peak)	Blood clots	3665	2219 - 7028	MWU	NS	0.8148
Duration of admission (days)	Severity	9	7.00 - 11.0	MWU	NS	0.8058
ECG changes (Y/N) (MBL levels)	Heart damage	-	-	MWU	NS	0.8736
ECHO changes (Y/N) (MBL levels)	Heart damage	-	-	MWU	NS	0.8931
Ferritin (peak)	Liver disease	845	455 - 1663	MWU	NS	0.5108
Fibrinogen (peak)	Higher chance of blood clots	5.60	4.53 - 6.70	MWU	NS	0.5074
ICU (days)	Severity	2.31	0.925 - 3.57	MWU	NS	0.1655
Inotropic support (Y/N) (MBL levels)		-	-	MWU	NS	0.2514
NT-proBNP	Heart failure	13759	3550 - 29792	MWU	NS	0.7512
Troponin (peak)	Heart damage	138	40.8 - 379	MWU	NS	0.4022

None of the clinical markers in Table 24 showed a statistically significant variation with categorisation of MBL levels, even prior to the application of multiple testing correction to the significance levels.

8.9. *IN VITRO* ASSAYS INVESTIGATING MBL AND SARS-COV-2

Using the microtiter plate assay, the neutralisation of SARS-CoV-2 using MBL was investigated (Figure 65). A paired *t*-test showed a significant difference between the viral control and pdMBL (*P*=0.0115), with a significant reduction in Vero-E6 cell death when the virus is incubated with pdMBL. We also see a possible reduction in cell death when the virus is incubated with rMBL, though not statistically significant (*P*=0.1643). (*n*=5).

Neutralisation concentration curves were established in Figure 66, with pdMBL displaying enhanced neutralisation of SARS-CoV-2 over the recombinant MBL mixtures, with 50% neutralisation between 1.2-2.5µg/ml, compared to 2.5-5µg/ml and 5-10µg/ml required for rMBL and rMBL CF respectively.

Competition assays with EDTA were also established, almost completely inhibiting the neutralising effect of the rMBL mixtures (Figure 67). Neutralisation of ~75% was observed for pdMBL of a similar EDTA concentration (5-10mM).

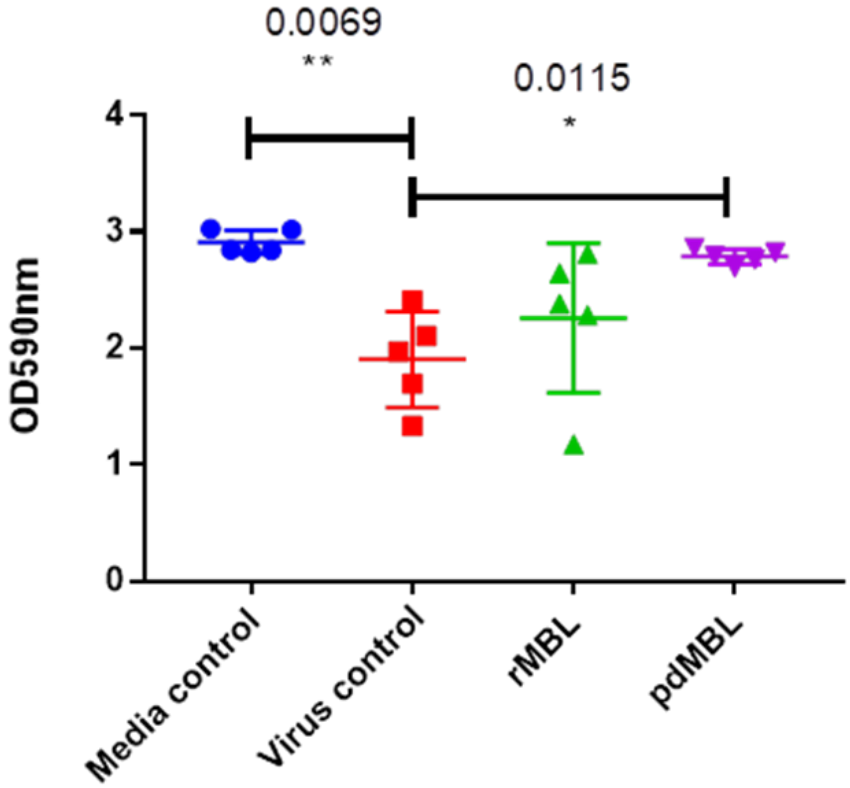

Figure 65: MBL (10µg/ml) neutralises SARS-CoV-2 in Vero-E6 cells.

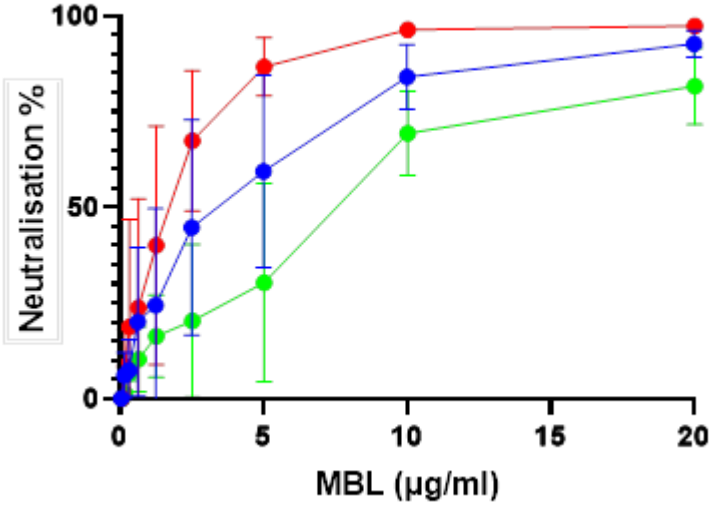

Figure 66: Concentration curves for the MBL mixtures rMBL (blue), pdMBL (red) and rMBL CF (green). (*n*=3).

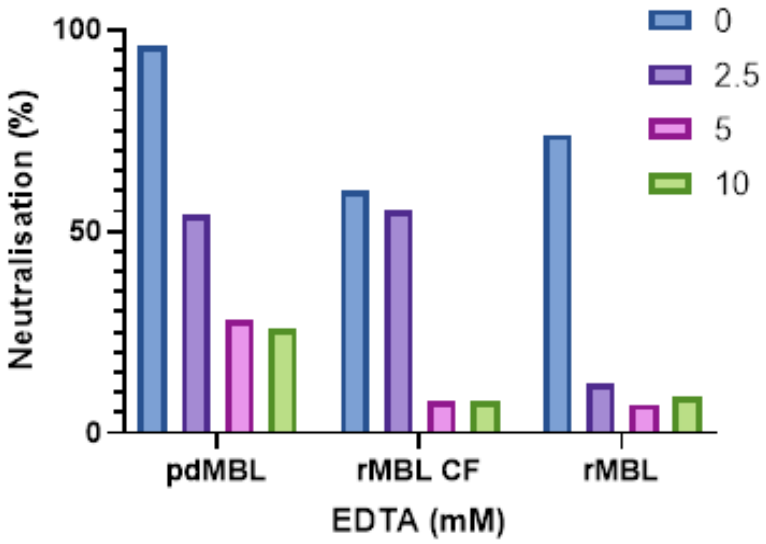

Figure 67: Competition assay with EDTA to measure neutralisation of SARS-CoV-2 by MBL mixtures. (*n*=1)

8.10. SARS-CoV-2 Discussion

PIMS-TS is a serious novel disease affecting individuals of or under the age of 18-years-old. Due to the bias of COVID-19 and PIMS-TS affecting the BAME community and the higher rates of MBL deficiency in these communities we hypothesised that MBL deficiency may the reason for this increased risk of severe disease resulting from SARS-CoV-2 infection. In 2005 it was also established that severe sufferers of SARS-CoV-1 had lower MBL serum levels [240]. It has also been demonstrated that low MBL serum levels may be associated in the dysregulation of inflammation in Kawasaki disease, a disease similar to PIMS-TS.

To investigate this, we collected serum from patients at GOSH and from the DIAMONDS biobank. We measured phenotypic MBL levels in these patients and analysed this alongside their demographic data e.g., sex, age, and ethnicity. Firstly, we found that MBL levels in children 10 years-of-age or above suffering from PIMS-TS were significantly lower than those younger in age. The significance of which is easier to understand when we look at other inflammatory diseases such as KD which predominantly effects children under the age of 10-years-old.

In our PIMS-TS GOSH population we found that 70% of children over 10-years-old were deficient for MBL compared to only 30% of children below 10-years-old. This led us to expand or patient population and collect more numbers from the DIAMONDS study. Though, with the additional patients we no longer observed a difference between age and MBL levels (Figure 63). We also did not observe a link between MBL levels and MBL deficiency in the different ethnicities in our disease populations despite previous reports of higher levels of low and deficient MBL in the Black and Asian populations (Figure 60). Moreover, no significant differences were observed between males and females (Figure 59).

Along with this, clinical data was also collected for 140 of the PIMS-TS patients which included various markers of clinical severity (Table 25). Of these markers, 14 of these were selected for testing based on what is established already in the MBL literature. Before multiple testing correction was applied no significance was found between MBL levels and clinical severity.

In spite of that, significant differences in MBL levels were observed between PIMS-TS and virally infected patients (P=0.0008) and the unknown bacterial and virally

infected patients (*P*=0.0007). Yet, no significant differences were seen between the cohort severely affected by COVID-19 and the bacterially infected cohort. Nevertheless, low MBL serum levels and an increased risk of severe bacterial infection in children has long been established and may be the reason for no significant difference between the two. On top of that, the number of COVID-19 patient controls was low (*n*=27) giving low statistical power.

We also wanted to ensure that MBL levels during PIMS-TS correlated to MBL levels during convalescence and that low MBL levels were not a result of consumption during active inflammatory disease. For this 47 of the GOSH patients had convalescent samples to compare (Figure 62). A Wilcoxon test showed a significant difference with a *P*=0.0074, with the MBL deficient patients remaining deficient and the majority of the high MBL levels dropping significantly.

To investigate further whether MBL deficiency could be a risk factor for PIMS-TS development after SARS-CoV-2 infection we investigated binding of MBL to the virus. We note that a similar study was carried out independently at the same time by another group [224]. Our work differs from these other approaches through the use of the clinically approved and tested mixtures of pdMBL and rMBL. Both plasma derived MBL and recombinant MBL were used in the assays.

Using the microtiter plate assay, neutralisation of SARS-CoV-2 was clearly visible in samples incubated with pdMBL (*P*=0.0115). Samples incubated with rMBL also show some potential inhibition of viral entry, though not as strongly as with pdMBL, and not reaching the threshold for statistical significance (*P*=0.1643) (Figure 65). Due to the relatively high values for the virus control produced using this experimental procedure, we decided to investigate MBL neutralisation by using plaque assays (Figure 66). We found that EDTA reduced the neutralising effect of the MBL mixtures, having the most effect on the recombinant mixtures, with pdMBL still having some neutralising effect at concentrations >5mM.

Previous work at ICH has shown that MBL is in the lung of chronically infected patients, but at lower levels in acutely infected patients. Due to this we hypothesise that the neutralisation of SARS-CoV-2 by MBL may play a larger role in the dissemination of whole or fragmented virus in the blood stream. In COVID-19 patients on the ICU, SARS-CoV-2 RNA copies in the plasma are commonly observed [241]. A study conducted in 2021 showed the MBL deficiency-causing B allele (rs1800450) to

be associated with more severe disease and likelihood of pneumonia [227]. Stravalaci et al found disruptive MBL alleles including rs5030737, rs1800450 and rs1800451 had a significant predisposing effect in an Italian cohort. However, Hultström et al found no association with low producing MBL gene mutations (including rs1800450) on the clinical severity of COVID-19 in a Swedish cohort. As mentioned above we see no clinical impact with MBL serum levels on PIMS-TS severity only lower levels in this cohort compared to other disease cohorts.

To summarise, we found the following;

- Lower median MBL levels in PIMS-TS patients compared to controls
- However, no significant correlation was found between low MBL levels and heightened markers of clinical severity in PIMS-TS patients
- MBL neutralises SARS-CoV-2 entry into the epithelium *in vitro*
- EDTA inhibits the neutralising effects of recombinant MBL mixtures
- EDTA does not fully inhibit the neutralisation effects of pdMBL

CHAPTER NINE

THESIS DISCUSSION

9.1. THESIS DISCUSSION

This thesis considered two distinct avenues for the clinical use of MBL. Part I explored the broad range binding properties of MBL and the potential use of genetically engineered magnetic FcMBL beads for use within clinical diagnostics. Part II focused on the immune activation properties of MBL, firstly by investigating MBL's ability to enhance the immune response toward chronic MRSA biofilm infections, and secondly by investigating the association of MBL levels with SARS-CoV-2, in particular PIMS-TS, and assessing SARS-CoV-2 neutralisation with various MBL structures (Figure 68).

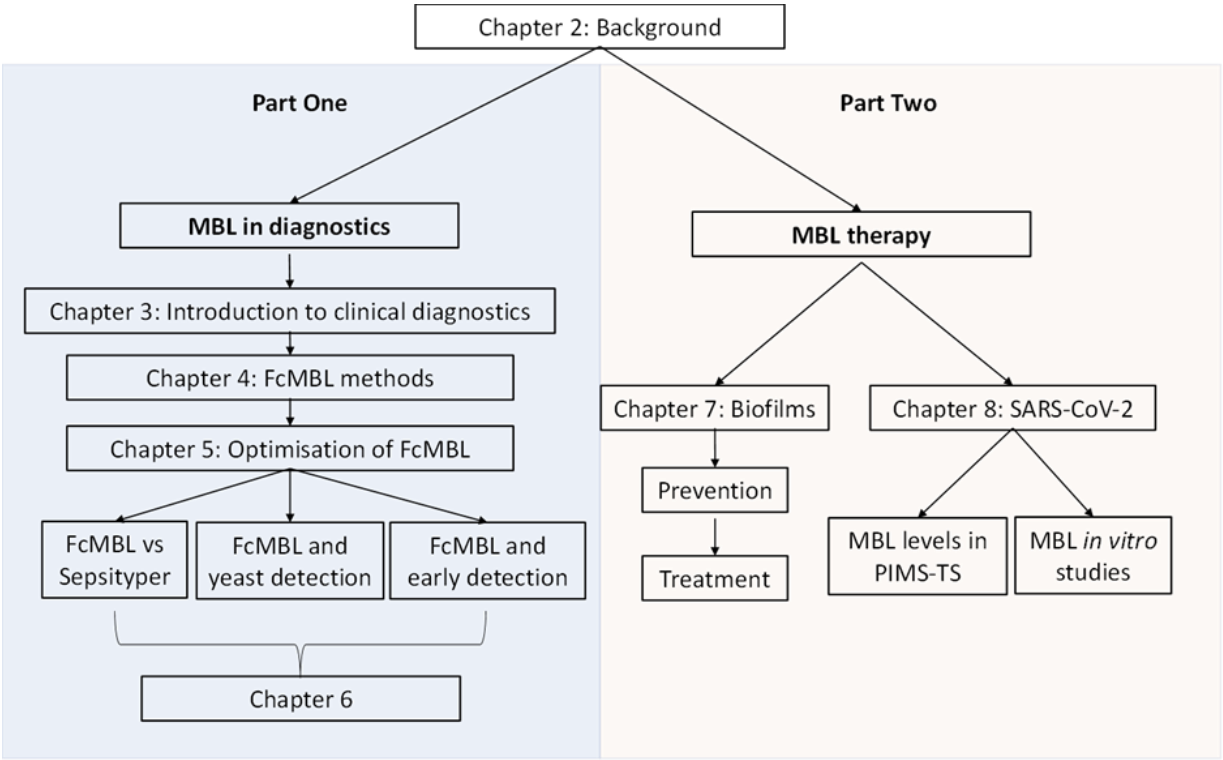

Figure 68: Thesis overview

9.2. PART I: MBL IN CLINICAL DIAGNOSTICS

Part I detailed an optimised protocol for the use of FcMBL beads to capture and identify blood pathogens with MALDI-TOF MS. The protocol was optimised for clinical samples by reducing incubation time to only 5 minutes and using reagents already present in a microbiology laboratory. We chose the MALDI-TOF MS benchtop as these machines are most readily available to clinical diagnostic laboratories. The FcMBL method developed and optimised in this thesis was reduced to ~15 minutes total, on par with the currently used Bruker Sepsityper kit. We were also able to demonstrate that the FcMBL beads bind a wide range of clinically significant bacteria and yeast.

9.2.1. FCMBL IS MORE EFFECTIVE AT THE RAPID DETECTION OF MICROBES FROM POSITIVE BLOOD CULTURES THAN THE BRUKER SEPSITYPER

The FcMBL method was more efficient at the detection of yeast and Gram-positive bacteria than the Bruker Sepsityper kit, which is currently the only available rapid diagnosis kit for clinical microbiology laboratories. The FcMBL method was also highly effective for the detection of Gram-negative bacteria. The FcMBL method shows a potential to be combined in clinical use alongside the Sepsityper as an ancillary tool for rapid identification, with an emphasis on Gram-positive bacteria and yeast. The Sepsityper has a higher efficiency for Gram-negative bacteria than for Gram-positive bacteria and fungi, and thus the use of these two methods in tandem would increase the efficiency of rapid detection for a broad range of infections within the microbiology clinic.

9.2.2. FCMBL CAN IDENTIFY MICROBES FROM BLOOD CULTURE SAMPLES PRIOR TO POSITIVITY

Our work has also shown the ability of the FcMBL to detect microbes in blood culture bottles prior to them flagging as positive on the blood culture machine. This could be useful in particular cases where patients need urgent care or are not responding to standard antimicrobials. The longer patients are left on broad-spectrum antimicrobials, the greater the risk of developing resistance, as well as unwanted side effects from toxic antimicrobials.

9.2.3. THE REMOVAL OF FCMBL-SPECIFIC BACKGROUND FROM MASS SPECTRA INCREASES SPECIES LEVEL CONFIDENCE

We have shown that the FcMBL method is more effective at yeast detection than the Sepsityper; this may be due to either less non-specific background, or the enrichment power of the FcMBL beads. Though yeast and fungal infections are less common than bacterial, they still carry a significant burden to healthcare establishments and patients, exacerbated by their detection difficulty. MBL naturally possesses a strong affinity to mannan, which is more highly expressed on the surface of both yeast and fungi, while a lack of MBL has been associated with recurrent fungal infections. The implementation of FcMBL beads into clinical diagnostics could help reduce the clinical burden presented by these infections. We found with the FcMBL method was consistently able to identify to genus level, but often did not reach species level confidence. We hypothesised that this was due to FcMBL-specific background in the mass spectrum interfering with the Bruker algorithm. Through a crude method that removed many of these background peaks by truncating the spectra, we demonstrated an increased degree of species level clustering. Thus, the development of FcMBL-specific libraries to be used in conjunction with the FcMBL method should allow for increased species level confidence.

9.2.4. FCMBL STUDY LIMITATIONS

This study was a proof-of-concept and was limited to a relatively small size of samples. Given that we also had a small number of clinical yeast samples, we expanded our zoo of samples with spiked candida samples, though it should be noted that the use of such spiked samples with healthy blood is different to clinical samples and may provide biased results. We also observed a small number of Gram-negative bacterial infections compared to Gram-positive. As MBL binding to Gram-negative bacteria has been shown to be less effective, a larger study of Gram-negative bacteria would be necessary. As we did not have the time to develop FcMBL-specific libraries, we could not validate the expected increase in species level confidence with an altered algorithm.

9.3. PART II: MBL AS A THERAPEUTIC

9.3.1. MBL AIDS IN THE PREVENTION AND TREATMENT OF MRSA BIOFILMS *IN VITRO*

Biofilm infections often result in significant cost and prolonged antimicrobial therapy, increasing the risk of resistance development and unwanted side effects in the patients. Biofilms dampen the host immune response by creating an inhibitory microenvironment. The first chapter of Part II of this thesis focused on the abilities of both naturally occurring and recombinant MBL to tackle MRSA biofilms, which constitute a significant threat to global health. We observed that MBL was effective at preventing MRSA biofilms *in vitro,* with pdMBL demonstrating better results than its rMBL counterpart. This higher efficiency is most likely due to the higher levels of aggregation of MRSA by pdMBL. This aggregation may influence quorum sensing, or disrupt the ability of the bacteria to interact with the surface and thus reduce their ability to form biofilms. This ability to disrupt the initial binding or influence biofilm formation may be useful in the prevention of biofilm infection post-surgery when the patient has received an artificial device, such as a prosthetic heart value or shunt.

9.3.2. MBL RECONSTITUTION ENHANCES NEUTROPHIL-MEDIATED BIOFILM DESTRUCTION

We show enhanced neutrophil-mediated destruction of biofilms with the use of pdMBL and rMBL mixtures. *In vitro* experiments established; the formation of significant MRSA biofilms visualised using SEM, they also demonstrated that pdMBL showed a greater increase in neutrophil-mediated biofilm destruction than rMBL as observed with confocal microscopy as well as FACS. It was initially believed that neutrophils or other immune cells could not attack and destroy biofilm. We now know that these cells do; however, the microenvironment dampens this response significantly and reduces the complement factors required to induce the complement pathway. Nevertheless, with the increase in opsonophagocytosis and biofilm destruction we see that MBL therapy, alongside standard antimicrobial therapies, may be beneficial in the control and eradication of biofilm infections.

9.3.3. MBL SERUM LEVELS IN PIMS-TS

The final chapter of this thesis investigates the potential role(s) of MBL in the progression of PIMS-TS. We found that median MBL serum levels are lower in a cohort of PIMS-TS patients than the control sets. This may prove to be a risk factor in the development of PIMS-TS after acquiring SARS-CoV-2 infection. We also demonstrated significant neutralisation of the virus with pdMBL mixtures, with less neutralisation observed for recombinant mixtures. MBL is not present in the lungs of heathy individuals, rising slightly in acute illness with high levels observed in chronic illness [70], suggesting the role of MBL during initial infection would be limited. We therefore theorised MBL would play a more key role in viral control within the lung during established infection, and the clearance and neutralisation of whole virus or viral PAMPs within the blood. To first establish if MBL played a role in the progression into PIMS-TS we looked at the serum levels of PIMS-TS patients and compared them to cohorts of children with viral, bacterial, and COVID-19 infections. We found that the lowest median levels were observed in PIMS-TS, followed by the bacterially infected cohort. Just as low levels of MBL have long been associated with increased risk and severity of bacterial infections in children, we believe that low or non-functional MBL levels may also be a risk factor in the development of PIMS-TS. We also investigated whether MBL levels influence the clinical features or severity of PIMS-TS. To do this we measured the MBL levels of PIMS-TS patients and performed a statistical analysis to see if any associations emerged. Yet, we observed no significant correlation with clinical severity for patients with low or deficient MBL levels. With PIMS-TS bearing similarities to other inflammatory disease states such as Kawasaki disease, understanding what, if any, role MBL plays in the prevention or progression of these diseases would enhance the treatment options for these children. The low MBL levels found in these patients warrants further study into MBL and PIMS-TS.

9.3.4. MBL BINDS AND BLOCKS SARS-CoV-2 ENTRY *IN VITRO*

To establish if MBL can actually bind SARS-CoV-2 and what effect this may have, MBL neutralisation assays were performed. With significant neutralisation observed for the pdMBL mixture, we prepared competition assays designed to outcompete the

CRD of MBL using EDTA, a chelator of calcium which is essential for CRD binding to its antigen. This was done to assess whether the neutralisation observed was due to the CRD blocking the S-protein from interacting with the ACE-2 receptor, or due to the addition of MASPs found bound to the pdMBL structures. We found that EDTA decreased the neutralisation exhibited by the MBL structures, suggesting that the neutralisation effects were associated with the CRD of MBL. We found this reduction in the neutralisation of all mixtures, with a greater reduction observed for the recombinant MBL mixtures. Unlike the recombinant mixtures, pdMBL still had some neutralising effect even at the higher concentrations of EDTA (≥5mM). This could be explained by the greater neutralising effect of the pdMBL already demonstrated, or due to the possible interaction of MASP-2 or other complement associated proteins bound to the pdMBL structure. Additional experiments investigating the role of MASP-2 and other conjugated proteins would be required to fully decipher this.

9.3.5. MBL THERAPY STUDY LIMITATIONS

MBL therapy was investigated in conditions which did not permit the activation of the lectin complement pathway. It would be important to understand how MBL therapy would influence complement activation, and the subsequent consequences of that *in vivo*. The study was limited also by the restrictions established during the COVID-19 pandemic, which were behind the lack of repeats in chapter seven. In chapter eight additional PIMS-TS and cohort controls would be highly useful in enhancing the statistical power of our analysis, as would data on the MBL levels of a genuinely healthy control set of patients. We also assessed the neutralisation properties of the MBL mixtures in the absence of complement factors, which again would be of importance when translating into a clinical treatment. The lack of complete blocking of neutralisation demonstrated with the competition assays using EDTA, may be due to the interference of associated complement proteins in the mixture, in particular the MASP-2 protein, which has been shown to bind SARS-CoV-2. The study would be enhanced with an experimental design that could measure the individual roles of the protein and structures found within the pdMBL mixture.

9.4. FINAL CONCLUSIONS

To conclude, the work and research completed in this thesis suggests MBL's role in disease presents a double-edged sword, providing protection during the early stages, with the role reversed if chronic infection persists. It has been suggested that low levels of MBL result in susceptibility to infection, especially during infancy, but that sufficient MBL levels increase host damage after either trauma such as I/R, or infection by initiating a potent complement response. We show that genetically modified MBL structures can be useful in the enrichment of microbes from clinical samples and thus enhances rapid diagnosis of infection. We also demonstrated favourable results *in vitro* for MBL therapy against bacterial and viral infections. Still, *in vivo* MBL therapy would have to be tightly regulated and its impact assessed for various diseases.

9.5. FUTURE WORKS

9.5.1. MBL IN DIAGNOSTICS

Part I of this thesis introduced the FcMBL method for BSI pathogen identification. Before the introduction of this method into the clinic, more clinically diverse samples would have to be assessed including a larger range of fungi and yeast. This could be followed by a larger scale clinical trial performed alongside the Bruker Sepsityper in clinical diagnostic laboratories (Figure 69), providing access to a much larger set of patient samples.

The method would also benefit from an FcMBL-specific library that would account for potential background signals from the FcMBL molecule itself, and thus improve the confidence of genus and species level identification.

As shown, FcMBL can capture as low as 10^0 bacteria. It would be exciting to see, using clinical samples, if this could bypass the need to culture samples on the BACTEC™ by simply capturing the low concentration of viable microbes and plating the beads directly onto solid media. For identification and AST only a small number of colonies are required; if FcMBL beads were used to enrich the blood cultures prior to incubation, providing colonies after 24-48 hours, this would offer an extreme time saving for the microbiology clinic.

Furthermore, a study of FcMBL binding and recognition of moribund or microbial fragments would be interesting. Establishing specific peak patterns for various microbes commonly known to cause disease would revolutionise clinical microbiology. Moreover, extending the method to samples taken from CSF and urine, which have relatively less background compared to blood, could provide further enhancement. This would be revolutionary in the detection of various infections such as meningitis, with CSF commonly having a low concentration of viable microbes for culture due to the nature of the infection or the early administration of antimicrobials. To do this would require the building of a complete FcMBL PAMP-specific library as well as its validation. The detection of PAMPs would require changes to the mass spectrometry protocol and algorithm. With the emergence of new and more sensitive MS technology this could become a possibility in the future, and with the enrichment properties of MBL these two technologies should be investigated in conjunction. We suspect one crux in this direction would be the removal of the PAMPs from the beads, as MBL has a higher affinity for PAMPs than whole cell. We found that the best way to detect the whole cell

microbes from the positive blood cultures was to extract them after washing but whilst they were still bound to the beads using the supernatant for analysis. This was because the FcMBL molecule bound strongly to the microbes. We believe a potential workaround would be to design an FcMBL molecule that could be more readily removed from the magnetic bead, rather than attempts to dissociate the PAMPs from the FcMBL protein or find a new method of elution.

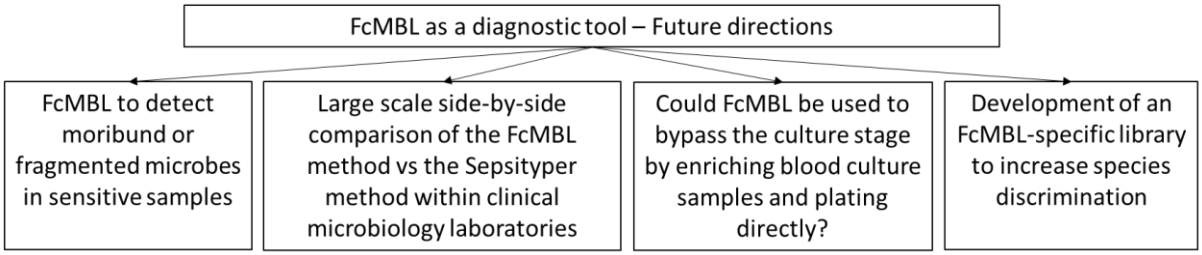

Figure 69: FcMBL as a diagnostic tool - future directions

9.5.2. MBL IN THE TREATMENT OF BIOFILM INFECTIONS

In Part II of this thesis, antimicrobial checkerboards investigating synergy between MBL, and antibiotics were proposed due to the aggregating effect and reduction of biofilm observed with MBL. We propose that MBL therapy may reduce the concentration of antibiotic needed to clear biofilm infections, either due to the aggregation or enhancement of the immune response at the site of infection.

This leads to the investigation of the neutrophil response in conjunction with MBL therapy. We observed an increase in neutrophil-mediated biofilm destruction but did not get the chance to explore the mechanisms further. With evidence of MBL trafficking throughout the phagosome, we propose that MBL may influence the neutrophil response pathways, enhancing ROS production, cytokine release, and receptor expression. This could be further explored using migration assays, ELISAs, and flow cytometry. This would provide further insight into how MBL influences bacterial infection control. Work in 2008 demonstrated that phagocytosis of *S. aureus* bound to MBL by macrophages interacted with toll-like receptor 2 to traffic the bacteria through the phagosome enhancing the immune response [242]. This was observed in mice with an increase in pro-inflammatory cytokines observed in MBL wild-type mice compared to knockout mice.

If MBL therapy were to enhance the hosts immune response this could overcome the inhibitory effect, and along with the antimicrobial therapy, help treat biofilm infections more effectively. MBL is a natural protein which poses a limited risk to humans. While the literature suggests high MBL levels are associated with an increased risk in various diseases and autoimmune diseases, this corresponds to high levels sustained over a person's lifetime, as opposed to brief, targeted bursts. Investigations into short term high level MBL therapy would need to be investigated to measure safety, particularly in vulnerable children.

9.5.3. MBL FOR THE TREATMENT OF SARS-COV-2 RELATED DISEASES

Finally, the work on MBL and SARS-CoV-2 could be further enhanced (Figure 70). Firstly, the introduction of SARS-CoV-2 variants would provide further clarity on the binding sites of the various MBL structures, as well as the potency of MBL therapy in the future. Viruses adapt rapidly and escape immune recognition, with mutations seen commonly within the binding site of antibodies. Understanding MBL's ability to control important variants of SARS-CoV-2 could provide a useful tool in understanding the innate immune response in the control of SARS-CoV-2 infection.

We also suggest assessing the impact of MASP-2 on the pdMBL mixture using a MASP-2 inhibitor. This would provide quantitative evidence of the effects of MASP-2 on virus control. This would also be key in understanding how MBL therapy would influence the immune response, as high complement activation appears to detrimental to the host in severe SARS-CoV-2 infection.

Furthermore, various works have demonstrated that the S-protein of SARS-CoV-2 can elicit some of the symptoms seen in COVID-19, including neurological consequences. One way to advance the hypothesis of this thesis would be to assess the MBL binding and neutralisation of viral PAMPs, in particular the S-protein. This would be achieved with recombinant S-proteins and N-proteins or fragmented virus. The impact of these viral proteins on the immune response would be assessed and compared to MBL incubated controls. If MBL were able to block the effects of the S-protein on the downregulation of the ACE-2 receptor within the circulatory system, this could prove significant in the reduction of hypertension in severe COVID-19 patients

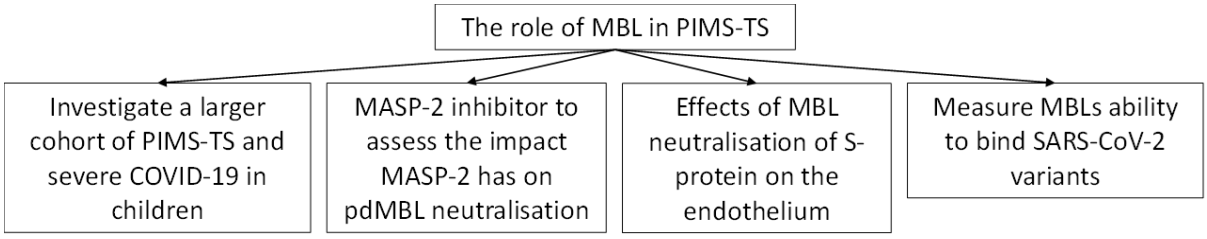

Figure 70: The role of MBL in SARS-CoV-2 infection - Future directions

APPENDICES

APPENDIX A. FCMBL OPTIMISATION DATA

1. Direct subculturing

Table 25: The number of colonies counted on solid LB agar after direct plating of the FcMBL beads compared to unprocessed

Bacteria	Method	Bacterial concentration								
		10^0	10^1	10^2	10^3	10^4	10^5	10^6	10^7	10^8
S. aureus (12973)	Unprocessed	1	9	121	x	x	x	x	x	x
	FcMBL	1	7	97	x	x	x	x	x	x
S. aureus (12493)	Unprocessed	2	22	103	x	x	x	x	x	x
	FcMBL	3	17	112	x	x	x	x	x	x
S. aureus (6571)	Unprocessed	1	11	122	x	x	x	x	x	x
	FcMBL	1	8	104	x	x	x	x	x	x
E. coli (10418)	Unprocessed	1	6	76	x	x	x	x	x	x
	FcMBL	2	11	83	x	x	x	x	x	x
E. coli (12241)	Unprocessed	2	14	102	x	x	x	x	x	x
	FcMBL	2	20	91	x	x	x	x	x	x
E. coli (13476)	Unprocessed	1	12	119	x	x	x	x	x	x
	FcMBL	3	16	132	x	x	x	x	x	x
K. pneumoniae (13438)	Unprocessed	3	9	87	x	x	x	x	x	x
	FcMBL	1	3	56	x	x	x	x	x	x
K. pneumoniae (13443)	Unprocessed	1	6	93	x	x	x	x	x	x
	FcMBL	1	5	77	x	x	x	x	x	x
K. pneumoniae (13443)	Unprocessed	2	11	101	x	x	x	x	x	x
	FcMBL	1	8	84	x	x	x	x	x	x

2. Assessing washing of FcMBL beads after microbial capture to test binding efficiency *K. pneumoniae* and *E. coli* washes

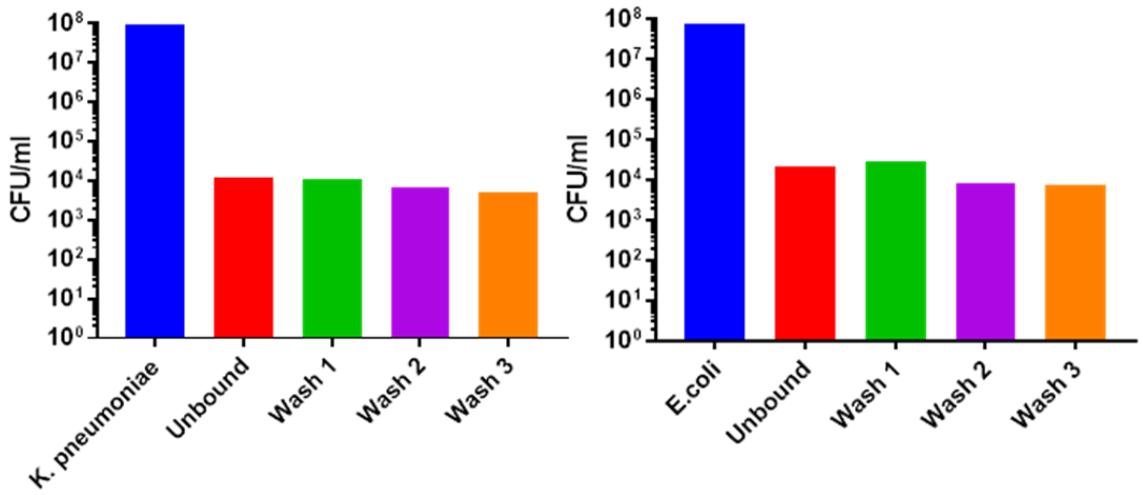

Figure 71: CFUs for FcMBL bead washing with *K. pneumoniae* and *E. coli*

APPENDIX B. FCMBL HEATMAP AND CLUSTERING METHODS

Spectral similarities between pairs of spectra were determined using cosine similarity. To account for slight imperfections in the precise location of the observed peaks in the MS we discretised the raw spectra for each sample into B bins, with any pair of peaks in a given bin differing by at most Δ. Thus, Δ encodes the assumed level of measurement precision. To ensure stability of the binning a data-driven approach was adopted, wherein all peaks were assigned to bins via agglomerative clustering using the furthest-neighbour criterion [243, 244] with a distance threshold of Δ, ensuring that each bin has width Δ or less. The intensities of peaks assigned to the same bin were then summed to produce a "spectral vector" of dimension B for each sample. Finally, the spectral similarity between two samples is given by the cosine similarity between their spectral vectors. The cosine similarity of two vectors $a \text{ and } b$ of dimension B is given by $S(a,b) = \sum_{j=1}^{B} a_j\, b_j / \left(\sqrt{\sum_{j=1}^{B} a_j^2}\,\sqrt{\sum_{j=1}^{\mathrm{B}} b_j^2}\right)$.

The spectral similarities between all spiked samples were calculated and visualised via clustered heatmaps (Figures 42 and 43), where sample clusters were inferred via agglomerative clustering based on the spectral similarities using the group-average criterion [244]. Since this method yields a hierarchy of sample clusters, an 'optimal' ordering of samples was determined wherein the sum of similarities between adjacent samples is minimised [245], and the rows and columns of the heatmaps were arranged as per the optimal ordering. Consequently, the quality of clusters induced by cosine similarity with respect to species identification can be judged by observing whether samples of the same species appear contiguously in the optimal ordering, i.e., adjacent to each other in the heatmap visualisations.

Because the real precision is unknown, an 'optimal' value of Δ was determined by calculating the optimal ordering for a range of values of Δ, and selecting the Δ with optimal ordering closest to a 'perfect' ordering where all samples from a given species appear contiguously. This requires defining a distance between orderings. Let X_i be the set of samples of species i and s be the total number of species, $n_i = |X_i|$ be the number of samples of species i, and y_u^{α} be the position of sample u in an ordering α. Let the sum of pairwise absolute differences in sample positions of species i in ordering α be denoted by $f_i(\alpha) = \frac{1}{2}\sum_{(u,v)\in {X_i}^2} |y_u^{\alpha} - y_v^{\alpha}|$. It can be shown that this

function is minimised if and only if α is a perfect ordering with respect to species i, with value $f_i(\alpha) = n_i(n_i^2 - 1)/6$. We define the distance between two orderings α, β as $d(\alpha, \beta) = \sum_{i=1}^{s} |f_i(\alpha) - f_i(\beta)|$. It can be shown that d is a pseudometric on the space of sample orderings, satisfying symmetry and the triangle inequality. Then, the scoring function $g(\alpha) = \sum_{i=1}^{s} (f_i(\alpha) - n_i(n_i^2 - 1)/6)$ measures the distance of an ordering from a perfect ordering, with $g(\alpha) = 0$ if and only if α is a perfect ordering, wherein samples of any given species are contiguously positioned. Meanwhile $g(\alpha) > 0$ indicates that samples of some species are interleaved with samples from other species in the ordering α. Consequently, the optimal value of Δ is the one that induces an ordering α with the smallest $g(\alpha)$. Note that more than one Δ may induce the same smallest score, in which case we select the minimum Δ attaining this score. Figures 42 and 43 depict heatmaps with optimal values $\Delta = 7$ and $\Delta = 8$, respectively, optimised over $\Delta \in \{1,2,\ldots,100\}$. We remark that $\Delta = 8$ induces a perfect ordering in Figure 43.

Agglomerative clustering was performed using *SciPy* [246] and heatmaps were generated using *seaborn* [247] and *Matplotlib* [248], in *Python*.

REFERENCES

1. Everard, M.L., *Paediatric respiratory infections.* Eur Respir Rev, 2016. **25**(139): p. 36-40.
2. Haque, M., et al., *Health care-associated infections - an overview.* Infect Drug Resist, 2018. **11**: p. 2321-2333.
3. Kollef, M.H., et al., *The intensive care medicine research agenda on multidrug-resistant bacteria, antibiotics, and stewardship.* Intensive Care Med, 2017. **43**(9): p. 1187-1197.
4. Morris, D.E., D.W. Cleary, and S.C. Clarke, *Secondary Bacterial Infections Associated with Influenza Pandemics.* Front Microbiol, 2017. **8**: p. 1041.
5. Hoiby, N., et al., *The clinical impact of bacterial biofilms.* Int J Oral Sci, 2011. **3**(2): p. 55-65.
6. Potera, C., *ANTIBIOTIC RESISTANCE: Biofilm Dispersing Agent Rejuvenates Older Antibiotics.* Environmental Health Perspectives, 2010. **118**(7): p. A288-A288.
7. Ricklin, D., et al., *Complement: a key system for immune surveillance and homeostasis.* Nature Immunology, 2010. **11**(9): p. 785-797.
8. van Schaarenburg, R.A., et al., *The production and secretion of complement component C1q by human mast cells.* Molecular Immunology, 2016. **78**: p. 164-170.
9. Super, M., et al., *Association of low levels of mannan-binding protein with a common defect of opsonisation.* The Lancet, 1989. **334**(8674): p. 1236-1239.
10. Garred, P., et al., *A journey through the lectin pathway of complement-MBL and beyond.* Immunol Rev, 2016. **274**(1): p. 74-97.
11. Holmskov, U., S. Thiel, and J.C. Jensenius, *Collections and ficolins: humoral lectins of the innate immune defense.* Annu Rev Immunol, 2003. **21**: p. 547-78.
12. Kjaer, T.R., et al., *Oligomerization of Mannan-binding Lectin Dictates Binding Properties and Complement Activation.* Scand J Immunol, 2016. **84**(1): p. 12-9.
13. Keizer, M.P., et al., *Substitution of Mannan-Binding Lectin (MBL)-Deficient Serum With Recombinant MBL Results in the Formation of New MBL/MBL-Associated Serine Protease Complexes.* Front Immunol, 2018. **9**: p. 1406.
14. Harboe, M. and T.E. Mollnes, *The alternative complement pathway revisited.* J Cell Mol Med, 2008. **12**(4): p. 1074-84.
15. Wirthmueller, U., et al., *Properdin, a positive regulator of complement activation, is released from secondary granules of stimulated peripheral blood neutrophils.* J Immunol, 1997. **158**(9): p. 4444-51.
16. Noris, M. and G. Remuzzi, *Overview of complement activation and regulation.* Semin Nephrol, 2013. **33**(6): p. 479-92.
17. Tegla, C.A., et al., *Membrane attack by complement: the assembly and biology of terminal complement complexes.* Immunol Res, 2011. **51**(1): p. 45-60.

18. Super, M., et al., *Association of low levels of mannan-binding protein with a common defect of opsonisation.* (0140-6736 (Print)).
19. Seiler, B.T., et al., *Broad-spectrum capture of clinical pathogens using engineered Fc-mannose-binding lectin enhanced by antibiotic treatment.* F1000Res, 2019. **8**: p. 108.
20. Cartwright, M., et al., *A Broad-Spectrum Infection Diagnostic that Detects Pathogen-Associated Molecular Patterns (PAMPs) in Whole Blood.* EBioMedicine, 2016. **9**: p. 217-227.
21. Sumiya, M., et al., *Molecular basis of opsonic defect in immunodeficient children.* The Lancet, 1991. **337**(8757): p. 1569-1570.
22. Guo, N., et al., *The human ortholog of rhesus mannose-binding protein-A gene is an expressed pseudogene that localizes to chromosome 10.* Mamm Genome, 1998. **9**(3): p. 246-9.
23. Garred, P., et al., *Mannose-binding lectin and its genetic variants.* Genes Immun, 2006. **7**(2): p. 85-94.
24. Lipscombe, R.J., et al., *High frequencies in African and non-African populations of independent mutations in the mannose binding protein gene.* Human Molecular Genetics, 1992. **1**(9): p. 709-715.
25. Sorensen, C.M., et al., *Hormonal regulation of mannan-binding lectin synthesis in hepatocytes.* Clin Exp Immunol, 2006. **145**(1): p. 173-82.
26. Steffensen, R., et al., *Detection of structural gene mutations and promoter polymorphisms in the mannan-binding lectin (MBL) gene by polymerase chain reaction with sequence-specific primers.* Journal of Immunological Methods, 2000. **241**(1): p. 33-42.
27. Ezekowitz, R.A., *Role of the Mannose-Binding Lectin in Innate Immunity.* The Journal of Infectious Diseases, 2003. **187**(Supplement_2): p. S335-S339.
28. Unterberger, C., et al., *Stat3 is involved in control of MASP2 gene expression.* Biochemical and biophysical research communications, 2008. **364**: p. 1022-5.
29. Feinberg, H., et al., *Crystal structure of the CUB1-EGF-CUB2 region of mannose-binding protein associated serine protease-2.* (0261-4189 (Print)).
30. Thiel, S., et al., *A second serine protease associated with mannan-binding lectin that activates complement.* Nature, 1997. **386**(6624): p. 506-10.
31. Degn, S.E., et al., *Mannan-binding lectin-associated serine protease (MASP)-1 is crucial for lectin pathway activation in human serum, whereas neither MASP-1 nor MASP-3 is required for alternative pathway function.* J Immunol, 2012. **189**(8): p. 3957-69.
32. Héja, D., et al., *Monospecific inhibitors show that both mannan-binding lectin-associated serine protease-1 (MASP-1) and -2 Are essential for lectin pathway activation and reveal structural plasticity of MASP-2.* J Biol Chem, 2012. **287**(24): p. 20290-300.
33. Megyeri, M., et al., *Quantitative characterization of the activation steps of mannan-binding lectin (MBL)-associated serine proteases (MASPs) points to the central role of MASP-1 in the initiation of the complement lectin pathway.* J Biol Chem, 2013. **288**(13): p. 8922-34.
34. Dong, M., et al., *Conformational changes in mannan-binding lectin bound to ligand surfaces.* J Immunol, 2007. **178**(5): p. 3016-22.
35. Beltrame, M.H., et al., *MBL-associated serine proteases (MASPs) and infectious diseases.* Molecular immunology, 2015. **67**(1): p. 85-100.
36. Boldt, A.B., et al., *A dual role for Mannan-binding lectin-associated serine protease 2 (MASP-2) in HIV infection.* Mol Immunol, 2016. **78**: p. 48-56.

37. Andrade, F.A., et al., *Serine Proteases in the Lectin Pathway of the Complement System.* Proteases in Physiology and Pathology, 2017: p. 397-420.
38. Gulla, K.C., et al., *Activation of mannan-binding lectin-associated serine proteases leads to generation of a fibrin clot.* Immunology, 2010. **129**(4): p. 482-95.
39. Møller-Kristensen, M., et al., *Levels of mannan-binding lectin-associated serine protease-2 in healthy individuals.* J Immunol Methods, 2003. **282**(1-2): p. 159-67.
40. Thiel, S., et al., *Deficiency of mannan-binding lectin associated serine protease-2 due to missense polymorphisms.* Genes Immun, 2007. **8**(2): p. 154-63.
41. Ytting, H., et al., *Biological variation in circulating levels of mannan-binding lectin (MBL) and MBL-associated serine protease-2 and the influence of age, gender and physical exercise.* Scand J Immunol, 2007. **66**(4): p. 458-64.
42. Ameye, L., et al., *M-ficolin levels are associated with the occurrence of severe infections in patients with haematological cancer undergoing chemotherapy.* Clin Exp Immunol, 2012. **167**(2): p. 303-8.
43. Matricardi, P.M., R.W. Dal Negro, and R. Nisini, *The first, holistic immunological model of COVID-19: Implications for prevention, diagnosis, and public health measures.* Pediatr Allergy Immunol, 2020.
44. Degn, S.E., et al., *MAp19, the alternative splice product of the MASP2 gene.* J Immunol Methods, 2011. **373**(1-2): p. 89-101.
45. Kang, I., et al., *Mannan-binding lectin (MBL)-associated plasma protein present in human urine inhibits calcium oxalate crystal growth.* FEBS Lett, 1999. **462**(1-2): p. 89-93.
46. Liu, J.L., C. Cao, and Q.J. Ma, *[Study on interaction between SARS-CoV N and MAP19].* Xi Bao Yu Fen Zi Mian Yi Xue Za Zhi, 2009. **25**(9): p. 777-9.
47. Palaniyar, N., et al., *Nucleic acid is a novel ligand for innate, immune pattern recognition collectins surfactant proteins A and D and mannose-binding lectin.* J Biol Chem, 2004. **279**(31): p. 32728-36.
48. Ogden, C.A., et al., *C1q and mannose binding lectin engagement of cell surface calreticulin and CD91 initiates macropinocytosis and uptake of apoptotic cells.* J Exp Med, 2001. **194**(6): p. 781-95.
49. Casadevall, A. and L.-a. Pirofski, *In fatal COVID-19, the immune response can control the virus but kill the patient.* Proceedings of the National Academy of Sciences, 2020. **117**(48): p. 30009.
50. Ghiran, I., et al., *Complement receptor 1/CD35 is a receptor for mannan-binding lectin.* J Exp Med, 2000. **192**(12): p. 1797-808.
51. Møller-Kristensen, M., et al., *Deficiency of mannose-binding lectin greatly increases susceptibility to postburn infection with Pseudomonas aeruginosa.* J Immunol, 2006. **176**(3): p. 1769-75.
52. Berger, S.P., et al., *Association between mannose-binding lectin levels and graft survival in kidney transplantation.* Am J Transplant, 2005. **5**(6): p. 1361-6.
53. Huh, J.W., et al., *Association of mannose-binding lectin-2 genotype and serum levels with prognosis of sepsis.* Critical care (London, England), 2009. **13**(6): p. R176-R176.
54. Dzwonek, A.B., et al., *The role of mannose-binding lectin in susceptibility to infection in preterm neonates.* (0031-3998 (Print)).

55. Garred, P., et al., *Diallelic polymorphism may explain variations of the blood concentration of mannan-binding protein in Eskimos, but not in black Africans.* Eur J Immunogenet, 1992. **19**(6): p. 403-12.
56. Bellamy, R., et al., *Mannose binding protein deficiency is not associated with malaria, hepatitis B carriage nor tuberculosis in Africans.* Qjm, 1998. **91**(1): p. 13-8.
57. Davies, J.C., et al., *Impaired pulmonary status in cystic fibrosis adults with two mutated MBL-2 alleles.* Eur Respir J, 2004. **24**(5): p. 798-804.
58. Garred, P., et al., *Mannose-binding lectin (MBL) therapy in an MBL-deficient patient with severe cystic fibrosis lung disease.* Pediatr Pulmonol, 2002. **33**(3): p. 201-7.
59. Terai, I. and K. Kobayashi, *Perinatal changes in serum mannose-binding protein (MBP) levels.* Immunol Lett, 1993. **38**(3): p. 185-7.
60. Thiel, S., et al., *Ontogeny of human mannan-binding protein, a lectin of the innate immune system.* Pediatric Allergy and Immunology, 1995. **6**(1): p. 20-23.
61. Schlapbach, L.J., et al., *Differential role of the lectin pathway of complement activation in susceptibility to neonatal sepsis.* Clin Infect Dis, 2010. **51**(2): p. 153-62.
62. Roy, S., et al., *MBL genotype and risk of invasive pneumococcal disease: a case-control study.* The Lancet, 2002. **359**(9317): p. 1569-1573.
63. Neth, O., et al., *Deficiency of mannose-binding lectin and burden of infection in children with malignancy: a prospective study.* The Lancet, 2001. **358**(9282): p. 614-618.
64. Shi, L., et al., *Mannose-binding lectin-deficient mice are susceptible to infection with Staphylococcus aureus.* The Journal of experimental medicine, 2004. **199**(10): p. 1379-1390.
65. Eisen, S., A. Dzwonek, and N.J. Klein, *Mannose-binding lectin in HIV infection.* Future Virol, 2008. **3**(3): p. 225-233.
66. Ji, X., H. Gewurz, and G.T. Spear, *Mannose binding lectin (MBL) and HIV.* Mol Immunol, 2005. **42**(2): p. 145-52.
67. Michelow, I.C., et al., *High-dose mannose-binding lectin therapy for Ebola virus infection.* J Infect Dis, 2011. **203**(2): p. 175-9.
68. Ji, X., et al., *Mannose-binding lectin binds to Ebola and Marburg envelope glycoproteins, resulting in blocking of virus interaction with DC-SIGN and complement-mediated virus neutralization.* J Gen Virol, 2005. **86**(Pt 9): p. 2535-2542.
69. Ezekowitz, R.A., et al., *A human serum mannose-binding protein inhibits in vitro infection by the human immunodeficiency virus.* J Exp Med, 1989. **169**(1): p. 185-96.
70. Fidler, K.J., et al., *Mannose-binding lectin is present in the infected airway: a possible pulmonary defence mechanism.* Thorax, 2009. **64**(2): p. 150-5.
71. Kase, T., et al., *Human mannan-binding lectin inhibits the infection of influenza A virus without complement.* Immunology, 1999. **97**(3): p. 385-392.
72. Chang, W.-C., et al., *Lack of the pattern recognition molecule mannose-binding lectin increases susceptibility to influenza A virus infection.* BMC Immunology, 2010. **11**(1): p. 64.
73. Ling, M.T., et al., *Mannose-binding lectin contributes to deleterious inflammatory response in pandemic H1N1 and avian H9N2 infection.* The Journal of infectious diseases, 2012. **205**(1): p. 44-53.

74. Tu, X., et al., *Functional polymorphisms of the CCL2 and MBL genes cumulatively increase susceptibility to severe acute respiratory syndrome coronavirus infection.* J Infect, 2015. **71**(1): p. 101-9.
75. Ip, W.K., et al., *Mannose-binding lectin in severe acute respiratory syndrome coronavirus infection.* (0022-1899 (Print)).
76. Zhou, Y., et al., *A single asparagine-linked glycosylation site of the severe acute respiratory syndrome coronavirus spike glycoprotein facilitates inhibition by mannose-binding lectin through multiple mechanisms.* J Virol, 2010. **84**(17): p. 8753-64.
77. Neglia, L., et al., *Specific contribution of mannose-binding lectin murine isoforms to brain ischemia/reperfusion injury.* Cell Mol Immunol, 2020. **17**(3): p. 218-226.
78. Auriti, C., et al., *Mannose-Binding Lectin: Biologic Characteristics and Role in the Susceptibility to Infections and Ischemia-Reperfusion Related Injury in Critically Ill Neonates.* J Immunol Res, 2017. **2017**: p. 7045630.
79. Guttormsen, H.K., et al., *Deficiency of mannose-binding lectin greatly increases antibody response in a mouse model of vaccination.* Clin Immunol, 2009. **130**(3): p. 264-71.
80. Jordan, J.E., M.C. Montalto, and G.L. Stahl, *Inhibition of Mannose-Binding Lectin Reduces Postischemic Myocardial Reperfusion Injury.* Circulation, 2001. **104**(12): p. 1413-1418.
81. Magro, C., et al., *Complement associated microvascular injury and thrombosis in the pathogenesis of severe COVID-19 infection: A report of five cases.* Transl Res, 2020. **220**: p. 1-13.
82. Fidler, K.J., et al., *Increased incidence and severity of the systemic inflammatory response syndrome in patients deficient in mannose-binding lectin.* Intensive Care Med, 2004. **30**(7): p. 1438-45.
83. Pagowska-Klimek, I., et al., *Mannose-binding lectin (MBL) insufficiency protects against the development of systemic inflammatory response after pediatric cardiac surgery.* Immunobiology, 2016. **221**(2): p. 175-81.
84. Garred, P., et al., *Association of mannose-binding lectin polymorphisms with sepsis and fatal outcome, in patients with systemic inflammatory response syndrome.* J Infect Dis, 2003. **188**(9): p. 1394-403.
85. Walsh, M.C., et al., *Mannose-binding lectin is a regulator of inflammation that accompanies myocardial ischemia and reperfusion injury.* J Immunol, 2005. **175**(1): p. 541-6.
86. Jack, D.L., et al., *Mannose-binding lectin regulates the inflammatory response of human professional phagocytes to Neisseria meningitidis serogroup B.* (0022-1899 (Print)).
87. Sprong, T., et al., *Mannose binding lectin enhances IL-1beta and IL-10 induction by non-lipopolysaccharide (LPS) components of Neisseria meningitidis.* (1043-4666 (Print)).
88. Chaka, W., et al., *Cryptococcus neoformans and cryptococcal glucuronoxylomannan, galactoxylomannan, and mannoprotein induce different levels of tumor necrosis factor alpha in human peripheral blood mononuclear cells.* (0019-9567 (Print)).
89. Miller, M., et al., *A FAMILIAL, PLASMA-ASSOCIATED DEFECT OF PHAGOCYTOSIS: A New Cause of Recurrent Bacterial Infections.* The Lancet, 1968. **292**(7559): p. 60-63.

90. Summerfield, J.A., *Clinical potential of mannose-binding lectin-replacement therapy.* Biochem Soc Trans, 2003. **31**(Pt 4): p. 770-3.
91. ClinicalTrials.gov. *Recombinant Human Mannose-Binding Lectin (MBL) in Treating Young Patients With MBL Deficiency and Fever and Neutropenia*. 2009 [cited 2022 10/10/2022]; Available from: https://clinicaltrials.gov/ct2/show/NCT00886496.
92. Bicart-See, A., et al., *Rapid Isolation of Staphylococcus aureus Pathogens from Infected Clinical Samples Using Magnetic Beads Coated with Fc-Mannose Binding Lectin.* PLoS One, 2016. **11**(6): p. e0156287.
93. Kang, J.H., et al., *An Engineered Human Fc-Mannose-Binding-Lectin Captures Circulating Tumor Cells.* Adv Biosyst, 2017. **1**(7): p. e1700094.
94. Akers, K.S., et al., *653. Diagnosis of Burn Sepsis Using the FcMBL ELISA: A Pilot Study in Critically Ill Burn Patients.* 2019(2328-8957 (Electronic)).
95. Park, K.H., et al., *Human serum mannose-binding lectin senses wall teichoic acid Glycopolymer of Staphylococcus aureus, which is restricted in infancy.* J Biol Chem, 2010. **285**(35): p. 27167-75.
96. Fang, Y.L., et al., *An integrated microfluidic system for early detection of sepsis-inducing bacteria.* Lab Chip, 2021. **21**(1): p. 113-121.
97. Maharaj, B., Y. Coovadia, and A.C. Vayej, *An investigation of the frequency of bacteraemia following dental extraction, tooth brushing and chewing.* Cardiovasc J Afr, 2012. **23**(6): p. 340-4.
98. Formanek, P.E. and D.F. Dilling, *Advances in the Diagnosis and Management of Invasive Fungal Disease.* Chest, 2019. **156**(5): p. 834-842.
99. Singer, M., et al., *The Third International Consensus Definitions for Sepsis and Septic Shock (Sepsis-3).* JAMA, 2016. **315**(8): p. 801-10.
100. Henderson, K.L., et al., *The changing aetiology of paediatric bacteraemia in England and Wales, 1998-2007.* J Med Microbiol, 2010. **59**(Pt 2): p. 213-219.
101. Laupland, K.B. and D.L. Church, *Population-based epidemiology and microbiology of community-onset bloodstream infections.* Clinical microbiology reviews, 2014. **27**(4): p. 647-664.
102. Isaacman, D.J., et al., *Effect of number of blood cultures and volume of blood on detection of bacteremia in children.* The Journal of Pediatrics, 1996. **128**(2): p. 190-195.
103. Schelonka, R.L., et al., *Volume of blood required to detect common neonatal pathogens.* (0022-3476 (Print)).
104. Kellogg, J.A., J.P. Manzella, and D.A. Bankert, *Frequency of low-level bacteremia in children from birth to fifteen years of age.* J Clin Microbiol, 2000. **38**(6): p. 2181-5.
105. Kellogg, J.A., et al., *Frequency of low level bacteremia in infants from birth to two months of age.* (0891-3668 (Print)).
106. Green, N., et al., *Quantifying the Burden of Hospital-Acquired Bloodstream Infection in Children in England by Estimating Excess Length of Hospital Stay and Mortality Using a Multistate Analysis of Linked, Routinely Collected Data.* J Pediatric Infect Dis Soc, 2015. **4**(4): p. 305-12.
107. Guest, J.F., et al., *Modelling the annual NHS costs and outcomes attributable to healthcare-associated infections in England.* BMJ Open, 2020. **10**(1): p. e033367.
108. Sudhir, U., et al., *Significance of serum procalcitonin in sepsis.* Indian journal of critical care medicine : peer-reviewed, official publication of Indian Society of Critical Care Medicine, 2011. **15**(1): p. 1-5.

109. Martin, G.S., et al., *The epidemiology of sepsis in the United States from 1979 through 2000.* N Engl J Med, 2003. **348**(16): p. 1546-54.
110. Ferrer, R., et al., *Empiric Antibiotic Treatment Reduces Mortality in Severe Sepsis and Septic Shock From the First Hour: Results From a Guideline-Based Performance Improvement Program*.* Critical Care Medicine, 2014. **42**(8).
111. Dellinger, R.P., et al., *Surviving Sepsis Campaign: international guidelines for management of severe sepsis and septic shock, 2012.* Intensive Care Med, 2013. **39**(2): p. 165-228.
112. Levy, M.M., et al., *Surviving Sepsis Campaign: association between performance metrics and outcomes in a 7.5-year study.* Intensive Care Med, 2014. **40**(11): p. 1623-33.
113. Brouwer, M.C., A.R. Tunkel, and D. van de Beek, *Epidemiology, diagnosis, and antimicrobial treatment of acute bacterial meningitis.* Clinical microbiology reviews, 2010. **23**(3): p. 467-492.
114. Torzewski, M. and K.J. Lackner, *Cerebrospinal fluid cytology: a highly diagnostic method for the detection of diseases of the central nervous system.* LaboratoriumsMedizin, 2016. **40**(3).
115. Charalambous, L.T., et al., *Prevalence, healthcare resource utilization and overall burden of fungal meningitis in the United States.* Journal of medical microbiology, 2018. **67**(2): p. 215-227.
116. Robinson, J.L., et al., *Urinary tract infections in infants and children: Diagnosis and management.* Paediatrics & child health, 2014. **19**(6): p. 315-325.
117. Dadzie, I., et al., *The Effectiveness of Dipstick for the Detection of Urinary Tract Infection.* Can J Infect Dis Med Microbiol, 2019. **2019**: p. 8642628.
118. Opota, O., et al., *Blood culture-based diagnosis of bacteraemia: state of the art.* (1469-0691 (Electronic)).
119. Singhal, N., et al., *MALDI-TOF mass spectrometry: an emerging technology for microbial identification and diagnosis.* Front Microbiol, 2015. **6**: p. 791.
120. Karas, M., D. Bachmann, and F. Hillenkamp, *Influence of the wavelength in high-irradiance ultraviolet laser desorption mass spectrometry of organic molecules.* Analytical Chemistry, 1985. **57**(14): p. 2935-2939.
121. Zhang, S., et al., *A novel strategy for MALDI-TOF MS analysis of small molecules.* J Am Soc Mass Spectrom, 2010. **21**(1): p. 154-60.
122. Bizzini, A., et al., *Matrix-assisted laser desorption ionization-time of flight mass spectrometry as an alternative to 16S rRNA gene sequencing for identification of difficult-to-identify bacterial strains.* (1098-660X (Electronic)).
123. Tan, K.E., et al., *Prospective evaluation of a matrix-assisted laser desorption ionization-time of flight mass spectrometry system in a hospital clinical microbiology laboratory for identification of bacteria and yeasts: a bench-by-bench study for assessing the impact on time to identification and cost-effectiveness.* (1098-660X (Electronic)).
124. Tran, A., et al., *Cost Savings Realized by Implementation of Routine Microbiological Identification by Matrix-Assisted Laser Desorption Ionization-Time of Flight Mass Spectrometry.* (1098-660X (Electronic)).
125. Bizzini, A. and G. Greub, *Matrix-assisted laser desorption ionization time-of-flight mass spectrometry, a revolution in clinical microbial identification.* Clin Microbiol Infect, 2010. **16**(11): p. 1614-9.
126. van Veen, S.Q., E.C. Claas, and E.J. Kuijper, *High-throughput identification of bacteria and yeast by matrix-assisted laser desorption ionization-time of flight*

mass spectrometry in conventional medical microbiology laboratories. J Clin Microbiol, 2010. **48**(3): p. 900-7.
127. La Scola, B. and D. Raoult, *Direct identification of bacteria in positive blood culture bottles by matrix-assisted laser desorption ionisation time-of-flight mass spectrometry.* PLoS One, 2009. **4**(11): p. e8041.
128. Stevenson, L.G., et al., *Evaluation of matrix-assisted laser desorption ionization-time of flight mass spectrometry for identification of clinically important yeast species.* J Clin Microbiol, 2010. **48**(10): p. 3482-6.
129. He, Y., et al., *Mass spectrometry biotyper system identifies enteric bacterial pathogens directly from colonies grown on selective stool culture media.* J Clin Microbiol, 2010. **48**(11): p. 3888-92.
130. Horneffer, V., et al., *Localization of Analyte Molecules in MALDI Preparations by Confocal Laser Scanning Microscopy.* Analytical Chemistry, 2001. **73**(5): p. 1016-1022.
131. Martiny, D., et al., *Comparison of the Microflex LT and Vitek MS systems for routine identification of bacteria by matrix-assisted laser desorption ionization-time of flight mass spectrometry.* J Clin Microbiol, 2012. **50**(4): p. 1313-25.
132. Jamal, W., M.J. Albert, and V.O. Rotimi, *Real-time comparative evaluation of bioMerieux VITEK MS versus Bruker Microflex MS, two matrix-assisted laser desorption-ionization time-of-flight mass spectrometry systems, for identification of clinically significant bacteria.* BMC Microbiol, 2014. **14**: p. 289.
133. Lee, H.S., et al., *Comparison of the Bruker Biotyper and VITEK MS Matrix-Assisted Laser Desorption/Ionization Time-of-Flight Mass Spectrometry Systems Using a Formic Acid Extraction Method to Identify Common and Uncommon Yeast Isolates.* Ann Lab Med, 2017. **37**(3): p. 223-230.
134. Liu, H., et al., *Universal sample preparation method for characterization of bacteria by matrix-assisted laser desorption ionization-time of flight mass spectrometry.* Appl Environ Microbiol, 2007. **73**(6): p. 1899-907.
135. Ilina, E.N., et al., *Direct bacterial profiling by matrix-assisted laser desorption-ionization time-of-flight mass spectrometry for identification of pathogenic Neisseria.* J Mol Diagn, 2009. **11**(1): p. 75-86.
136. McElvania Tekippe, E., et al., *Optimizing identification of clinically relevant Gram-positive organisms by use of the Bruker Biotyper matrix-assisted laser desorption ionization-time of flight mass spectrometry system.* J Clin Microbiol, 2013. **51**(5): p. 1421-7.
137. Verroken, A., et al., *Evaluation of matrix-assisted laser desorption ionization-time of flight mass spectrometry for identification of nocardia species.* J Clin Microbiol, 2010. **48**(11): p. 4015-21.
138. Theel, E.S., et al., *Dermatophyte identification using matrix-assisted laser desorption ionization-time of flight mass spectrometry.* J Clin Microbiol, 2011. **49**(12): p. 4067-71.
139. Hettick, J.M., et al., *Discrimination of Penicillium isolates by matrix-assisted laser desorption/ionization time-of-flight mass spectrometry fingerprinting.* Rapid Communications in Mass Spectrometry, 2008. **22**(16): p. 2555-2560.
140. Oviano, M., et al., *Rapid direct detection of carbapenemase-producing Enterobacteriaceae in clinical urine samples by MALDI-TOF MS analysis.* J Antimicrob Chemother, 2017. **72**(5): p. 1350-1354.
141. Martiny, D., A. Dediste, and O. Vandenberg, *Comparison of an in-house method and the commercial Sepsityper kit for bacterial identification directly from positive blood culture broths by matrix-assisted laser desorption-ionisation*

time-of-flight mass spectrometry. Eur J Clin Microbiol Infect Dis, 2012. **31**(9): p. 2269-81.
142. Kayin, M., et al., *Comparison of rapid BACpro(R) II, Sepsityper(R) kit and in-house preparation methods for direct identification of bacteria from blood cultures by MALDI-TOF MS with and without Sepsityper(R) module analysis.* Eur J Clin Microbiol Infect Dis, 2019. **38**(11): p. 2133-2143.
143. Lagace-Wiens, P.R., et al., *Identification of blood culture isolates directly from positive blood cultures by use of matrix-assisted laser desorption ionization-time of flight mass spectrometry and a commercial extraction system: analysis of performance, cost, and turnaround time.* J Clin Microbiol, 2012. **50**(10): p. 3324-8.
144. Meex, C., et al., *Direct identification of bacteria from BacT/ALERT anaerobic positive blood cultures by MALDI-TOF MS: MALDI Sepsityper kit versus an in-house saponin method for bacterial extraction.* J Med Microbiol, 2012. **61**(Pt 11): p. 1511-1516.
145. Bidart, M., et al., *An in-house assay is superior to Sepsityper for direct matrix-assisted laser desorption ionization-time of flight (MALDI-TOF) mass spectrometry identification of yeast species in blood cultures.* Journal of clinical microbiology, 2015. **53**(5): p. 1761-1764.
146. Buchan, B.W., K.M. Riebe, and N.A. Ledeboer, *Comparison of the MALDI Biotyper system using Sepsityper specimen processing to routine microbiological methods for identification of bacteria from positive blood culture bottles.* J Clin Microbiol, 2012. **50**(2): p. 346-52.
147. Loonen, A.J., et al., *An evaluation of three processing methods and the effect of reduced culture times for faster direct identification of pathogens from BacT/ALERT blood cultures by MALDI-TOF MS.* Eur J Clin Microbiol Infect Dis, 2012. **31**(7): p. 1575-83.
148. Schubert, S., et al., *Novel, improved sample preparation for rapid, direct identification from positive blood cultures using matrix-assisted laser desorption/ionization time-of-flight (MALDI-TOF) mass spectrometry.* The Journal of molecular diagnostics : JMD, 2011. **13**(6): p. 701-706.
149. Juiz, P.M., et al., *A comparative study of two different methods of sample preparation for positive blood cultures for the rapid identification of bacteria using MALDI-TOF MS.* Eur J Clin Microbiol Infect Dis, 2012. **31**(7): p. 1353-8.
150. Kok, J., et al., *Identification of bacteria in blood culture broths using matrix-assisted laser desorption-ionization Sepsityper™ and time of flight mass spectrometry.* PLoS One, 2011. **6**(8): p. e23285.
151. Tadros, M. and A. Petrich, *Evaluation of MALDI-TOF mass spectrometry and Sepsityper Kit™ for the direct identification of organisms from sterile body fluids in a Canadian pediatric hospital.* Can J Infect Dis Med Microbiol, 2013. **24**(4): p. 191-4.
152. Schieffer, K.M., et al., *Multicenter evaluation of the Sepsityper™ extraction kit and MALDI-TOF MS for direct identification of positive blood culture isolates using the BD BACTEC™ FX and VersaTREK(®) diagnostic blood culture systems.* J Appl Microbiol, 2014. **116**(4): p. 934-41.
153. Ko, Y.J., J.K. Kook, and C.K. Lee, *In-house method for direct bacterial identification in positive blood culture broths using microfiltration, bead beating, and matrix-assisted laser desorption/ionization time-of-flight mass spectrometry.* (1872-8359 (Electronic)).

154. Yan, Y., et al., *Improved identification of yeast species directly from positive blood culture media by combining Sepsityper specimen processing and Microflex analysis with the matrix-assisted laser desorption ionization Biotyper system.* Journal of clinical microbiology, 2011. **49**(7): p. 2528-2532.
155. Nonnemann, B., T. Tvede M Fau - Bjarnsholt, and T. Bjarnsholt, *Identification of pathogenic microorganisms directly from positive blood vials by matrix-assisted laser desorption/ionization time of flight mass spectrometry.* (1600-0463 (Electronic)).
156. Gorton, R.L., et al., *Comparative analysis of Gram's stain, PNA-FISH and Sepsityper with MALDI-TOF MS for the identification of yeast direct from positive blood cultures.* (1439-0507 (Electronic)).
157. Morgenthaler, N.G. and M. Kostrzewa, *Rapid identification of pathogens in positive blood culture of patients with sepsis: review and meta-analysis of the performance of the sepsityper kit.* (1687-918X (Print)).
158. Martinez, R.M., et al., *Evaluation of three rapid diagnostic methods for direct identification of microorganisms in positive blood cultures.* (1098-660X (Electronic)).
159. Bal, A.M. and M. McGill, *Rapid species identification of Candida directly from blood culture broths by Sepsityper-MALDI-TOF mass spectrometry: impact on antifungal therapy.* (2042-8189 (Electronic)).
160. Shalel, S., S. Streichman, and A. Marmur, *The mechanism of hemolysis by surfactants: effect of solution composition.* J Colloid Interface Sci, 2002. **252**(1): p. 66-76.
161. Yonetani, S., et al., *Direct identification of microorganisms from positive blood cultures by MALDI-TOF MS using an in-house saponin method.* International Journal of Infectious Diseases, 2016. **52**: p. 37-42.
162. Burlina, F., et al., *A direct approach to quantification of the cellular uptake of cell-penetrating peptides using MALDI-TOF mass spectrometry.* Nat Protoc, 2006. **1**(1): p. 200-5.
163. Huang, Z., et al., *MALDI-TOF MS combined with magnetic beads for detecting serum protein biomarkers and establishment of boosting decision tree model for diagnosis of systemic lupus erythematosus.* Rheumatology, 2009. **48**(6): p. 626-631.
164. Miles, A.A., S.S. Misra, and J.O. Irwin, *The estimation of the bactericidal power of the blood.* J Hyg (Lond), 1938. **38**(6): p. 732-49.
165. Schulthess, B., et al., *Evaluation of the Bruker MALDI Biotyper for identification of Gram-positive rods: development of a diagnostic algorithm for the clinical laboratory.* J Clin Microbiol, 2014. **52**(4): p. 1089-97.
166. Cattoir, L., et al., *Improving timelines in reporting results from positive blood cultures: simulation of impact of rapid identification on therapy on a real-life cohort.* Eur J Clin Microbiol Infect Dis, 2018. **37**(12): p. 2253-2260.
167. Sun, J., et al., *Releasing bacteria from functional magnetic beads is beneficial to MALDI-TOF MS based identification.* Talanta, 2021. **225**: p. 121968.
168. Dakheel, K.H., et al., *Methicillin-Resistant Staphylococcus aureus Biofilms and Their Influence on Bacterial Adhesion and Cohesion.* Biomed Res Int, 2016. **2016**: p. 4708425.
169. Wan, N., et al., *Bacterial Metabolism During Biofilm Growth Investigated by 13C Tracing.* Frontiers in Microbiology, 2018. **9**: p. 2657.

170. Barraud, N., et al., *Nitric oxide-mediated dispersal in single- and multi-species biofilms of clinically and industrially relevant microorganisms.* Microb Biotechnol, 2009. **2**(3): p. 370-8.
171. Marrie, T.J., J. Nelligan, and J.W. Costerton, *A scanning and transmission electron microscopic study of an infected endocardial pacemaker lead.* Circulation, 1982. **66**(6): p. 1339-41.
172. Guest, J.F., et al., *Health economic burden that wounds impose on the National Health Service in the UK.* BMJ Open, 2015. **5**(12): p. e009283.
173. Bhattacharya, M., et al., *Staphylococcus aureus biofilms release leukocidins to elicit extracellular trap formation and evade neutrophil-mediated killing.* Proc Natl Acad Sci U S A, 2018. **115**(28): p. 7416-7421.
174. Johansson, A., et al., *Protease inhibitors, the responsible components for the serum-dependent enhancement of Actinobacillus actinomycetemcomitans leukotoxicity.* (0909-8836 (Print)).
175. Mah, T.-F., *Biofilm-specific antibiotic resistance.* Future Microbiology, 2012. **7**(9): p. 1061-1072.
176. Guenther, F., et al., *Phagocytosis of Staphylococci Biofilms by Polymorphonuclear Neutrophils: S. aureus and S. epidermidis Differ with Regard to Their Susceptibility Towards the Host Defense.* The International Journal of Artificial Organs, 2009. **32**(9): p. 565-573.
177. Craft, K.M., et al., *Methicillin-resistant Staphylococcus aureus (MRSA): antibiotic-resistance and the biofilm phenotype.* Medchemcomm, 2019. **10**(8): p. 1231-1241.
178. Organisation, W.H., *No time to wait: Securing the future from drug-resistant infections*. 2019. p. https://www.who.int/publications/i/item/no-time-to-wait-securing-the-future-from-drug-resistant-infections.
179. Gordon, R.J. and F.D. Lowy, *Pathogenesis of methicillin-resistant Staphylococcus aureus infection.* Clin Infect Dis, 2008. **46 Suppl 5**: p. S350-9.
180. Christensen, G.D., et al., *Adherence of coagulase-negative staphylococci to plastic tissue culture plates: a quantitative model for the adherence of staphylococci to medical devices.* Journal of clinical microbiology, 1985. **22**(6): p. 996-1006.
181. Manago, K., et al., *Biofilm Formation by and Accessory Gene Regulator Typing of Methicillin-Resistant Staphylococcus aureus Strains Recovered From Patients With Nosocomial Infections.* Infection Control & Hospital Epidemiology, 2006. **27**(2): p. 188-190.
182. Kirby, T., *New variant of SARS-CoV-2 in UK causes surge of COVID-19.* The Lancet Respiratory Medicine, 2021. **9**(2): p. e20-e21.
183. Huang, Y., et al., *Structural and functional properties of SARS-CoV-2 spike protein: potential antivirus drug development for COVID-19.* Acta Pharmacol Sin, 2020. **41**(9): p. 1141-1149.
184. Riddell, S., et al., *The effect of temperature on persistence of SARS-CoV-2 on common surfaces.* Virology Journal, 2020. **17**(1): p. 145.
185. Ward, H., et al., *SARS-CoV-2 antibody prevalence in England following the first peak of the pandemic.* Nat Commun, 2021. **12**(1): p. 905.
186. Clark, A., et al., *Global, regional, and national estimates of the population at increased risk of severe COVID-19 due to underlying health conditions in 2020: a modelling study.* The Lancet Global Health, 2020. **8**(8): p. e1003-e1017.

187. Swann, O.V., et al., *Clinical characteristics of children and young people admitted to hospital with covid-19 in United Kingdom: prospective multicentre observational cohort study.* Bmj, 2020.
188. Elliott, J., et al., *Predictive symptoms for COVID-19 in the community: REACT-1 study of over 1 million people.* PLOS Medicine, 2021. **18**(9): p. e1003777.
189. Bwire, G.M., *Coronavirus: Why Men are More Vulnerable to Covid-19 Than Women?* SN comprehensive clinical medicine, 2020. **2**(7): p. 874-876.
190. Cron, R.Q., *COVID-19 cytokine storm: targeting the appropriate cytokine.* The Lancet Rheumatology, 2021. **3**(4): p. e236-e237.
191. Gutmann, C., et al., *SARS-CoV-2 RNAemia and proteomic trajectories inform prognostication in COVID-19 patients admitted to intensive care.* Nat Commun, 2021. **12**(1): p. 3406.
192. Bumiller-Bini, V., et al., *MASPs at the crossroad between the complement and the coagulation cascades - the case for COVID-19.* Genet Mol Biol, 2021. **44**(1 Suppl 1): p. e20200199.
193. Dzwonek, A.B., et al., *The role of mannose-binding lectin in susceptibility to infection in preterm neonates.* Pediatr Res, 2008. **63**(6): p. 680-5.
194. Rhee, C., et al., *Duration of Severe Acute Respiratory Syndrome Coronavirus 2 (SARS-CoV-2) Infectivity: When Is It Safe to Discontinue Isolation?* Clinical Infectious Diseases, 2021. **72**(8): p. 1467-1474.
195. Cheung, C.C.L., et al., *Residual SARS-CoV-2 viral antigens detected in GI and hepatic tissues from five recovered patients with COVID-19.* Gut, 2022. **71**(1): p. 226.
196. Patterson, B.K., et al., *Persistence of SARS CoV-2 S1 Protein in CD16+ Monocytes in Post-Acute Sequelae of COVID-19 (PASC) up to 15 Months Post-Infection.* Front Immunol, 2021. **12**: p. 746021.
197. Karwaciak, I., et al., *Nucleocapsid and Spike Proteins of the Coronavirus SARS-CoV-2 Induce IL6 in Monocytes and Macrophages—Potential Implications for Cytokine Storm Syndrome.* Vaccines, 2021. **9**(1).
198. Lei, Y., et al., *SARS-CoV-2 Spike Protein Impairs Endothelial Function via Downregulation of ACE 2.* Circ Res, 2021. **128**(9): p. 1323-1326.
199. Buzhdygan, T.P., et al., *The SARS-CoV-2 spike protein alters barrier function in 2D static and 3D microfluidic in-vitro models of the human blood-brain barrier.* Neurobiol Dis, 2020. **146**: p. 105131.
200. Suzuki, Y.J., *The viral protein fragment theory of COVID-19 pathogenesis.* Med Hypotheses, 2020. **144**: p. 110267.
201. White, M., et al., *Paediatric inflammatory multisystem syndrome temporally associated with SARS-CoV-2 (PIMS-TS): the Evelina Experience.* Arch Dis Child, 2020. **105**(11): p. 1025-1027.
202. Whittaker, E., et al., *Clinical Characteristics of 58 Children With a Pediatric Inflammatory Multisystem Syndrome Temporally Associated With SARS-CoV-2.* JAMA, 2020. **324**(3): p. 259-269.
203. Schlapbach, L.J., et al., *Best Practice Recommendations for the Diagnosis and Management of Children With Pediatric Inflammatory Multisystem Syndrome Temporally Associated With SARS-CoV-2 (PIMS-TS; Multisystem Inflammatory Syndrome in Children, MIS-C) in Switzerland.* Front Pediatr, 2021. **9**: p. 667507.
204. Davies, P., et al., *Association Between Treatments and Short-Term Biochemical Improvements and Clinical Outcomes in Post-Severe Acute Respiratory Syndrome Coronavirus-2 Inflammatory Syndrome.* Pediatric critical

care medicine : a journal of the Society of Critical Care Medicine and the World Federation of Pediatric Intensive and Critical Care Societies, 2021. **22**(5): p. e285-e293.
205. Pouletty, M., et al., *Paediatric multisystem inflammatory syndrome temporally associated with SARS-CoV-2 mimicking Kawasaki disease (Kawa-COVID-19): a multicentre cohort.* (1468-2060 (Electronic)).
206. Feldstein, L.R., et al., *Multisystem Inflammatory Syndrome in U.S. Children and Adolescents.* N Engl J Med, 2020. **383**(4): p. 334-346.
207. Toubiana, J., et al., *Kawasaki-like multisystem inflammatory syndrome in children during the covid-19 pandemic in Paris, France: prospective observational study.* BMJ, 2020. **369**: p. m2094.
208. Ramcharan, T., et al., *Paediatric Inflammatory Multisystem Syndrome: Temporally Associated with SARS-CoV-2 (PIMS-TS): Cardiac Features, Management and Short-Term Outcomes at a UK Tertiary Paediatric Hospital.* (1432-1971 (Electronic)).
209. Harnden, A., M. Takahashi, and D. Burgner, *Kawasaki disease.* BMJ, 2009. **338**: p. b1514.
210. Holman, R.C., et al., *Racial/ethnic differences in the incidence of Kawasaki syndrome among children in Hawaii.* Hawaii medical journal, 2010. **69**(8): p. 194-197.
211. Padilla, L.A., et al., *Kawasaki Disease and Clinical Outcome Disparities Among Black Children.* The Journal of pediatrics, 2021. **229**: p. 54-60.e2.
212. Burns, J.C., et al., *Seasonality of Kawasaki disease: a global perspective.* PloS one, 2013. **8**(9): p. e74529-e74529.
213. Roarty, C. and T. Waterfield, *Review and future directions for PIMS-TS (MIS-C).* Archives of Disease in Childhood, 2022: p. archdischild-2021-323143.
214. Sato, S., et al., *Association of mannose-binding lectin gene polymorphisms with Kawasaki disease in the Japanese.* International journal of rheumatic diseases, 2009. **12**(4): p. 307-310.
215. Nakamura, A., et al., *Involvement of mannose-binding lectin in the pathogenesis of Kawasaki disease-like murine vasculitis.* Clin Immunol, 2014. **153**(1): p. 64-72.
216. Biezeveld, M.H., et al., *Polymorphisms in the mannose-binding lectin gene as determinants of age-defined risk of coronary artery lesions in Kawasaki disease.* (0004-3591 (Print)).
217. Sun, S., et al., *Inhibition of complement activation alleviates acute lung injury induced by highly pathogenic avian influenza H5N1 virus infection.* Am J Respir Cell Mol Biol, 2013. **49**(2): p. 221-30.
218. Gralinski, L.E., et al., *Complement Activation Contributes to Severe Acute Respiratory Syndrome Coronavirus Pathogenesis.* mBio, 2018. **9**(5).
219. Holter, J.C., et al., *Systemic complement activation is associated with respiratory failure in COVID-19 hospitalized patients.* Proc Natl Acad Sci U S A, 2020. **117**(40): p. 25018-25025.
220. Ali, Y.M., et al., *Lectin Pathway Mediates Complement Activation by SARS-CoV-2 Proteins.* Frontiers in Immunology, 2021. **12**.
221. Hess, K., et al., *Effects of MASP-1 of the complement system on activation of coagulation factors and plasma clot formation.* PLoS One, 2012. **7**(4): p. e35690.
222. Ranucci, M., et al., *The procoagulant pattern of patients with COVID-19 acute respiratory distress syndrome.* J Thromb Haemost, 2020. **18**(7): p. 1747-1751.

223. Gao, T., et al., 2020.
224. Stravalaci, M., et al., *Recognition and inhibition of SARS-CoV-2 by humoral innate immunity pattern recognition molecules.* Nature Immunology, 2022.
225. Malaquias, M.A.S., et al., *The role of the lectin pathway of the complement system in SARS-CoV-2 lung injury.* Transl Res, 2021. **231**: p. 55-63.
226. Medetalibeyoglu, A., et al., *Mannose binding lectin gene 2 (rs1800450) missense variant may contribute to development and severity of COVID-19 infection.* Infect Genet Evol, 2021: p. 104717.
227. Speletas, M., et al., *MBL deficiency-causing B allele (rs1800450) as a risk factor for severe COVID-19.* Immunobiology, 2021. **226**(6): p. 152136.
228. Hayes, B., J. Stanley, and B.P. Peppers, *COVID-19 Recurrence Without Seroconversion in a Patient With Mannose-Binding Lectin Deficiency.* Allergy Rhinol (Providence), 2021. **12**: p. 21526567211024140.
229. Sinkovits, G., et al., *Complement Overactivation and Consumption Predicts In-Hospital Mortality in SARS-CoV-2 Infection.* Frontiers in Immunology, 2021. **12**.
230. Pellegrini, D., et al., *Microthrombi as a Major Cause of Cardiac Injury in COVID-19: A Pathologic Study.* (1524-4539 (Electronic)).
231. van de Veerdonk, F.L., et al., *A guide to immunotherapy for COVID-19.* Nat Med, 2022. **28**(1): p. 39-50.
232. Kreitmann, L., et al., *Early bacterial co-infection in ARDS related to COVID-19.* Intensive Care Medicine, 2020. **46**(9): p. 1787-1789.
233. Jiang, Y., et al., *Blockade of the C5a-C5aR axis alleviates lung damage in hDPP4-transgenic mice infected with MERS-CoV.* Emerging microbes & infections, 2018. **7**(1): p. 77-77.
234. Mastellos, D.C., et al., *Complement C3 vs C5 inhibition in severe COVID-19: Early clinical findings reveal differential biological efficacy.* Clinical immunology (Orlando, Fla.), 2020. **220**: p. 108598-108598.
235. Zelek, W.M., et al., *Complement Inhibition with the C5 Blocker LFG316 in Severe COVID-19.* Am J Respir Crit Care Med, 2020. **202**(9): p. 1304-1308.
236. Annane, D., et al., *Eculizumab as an emergency treatment for adult patients with severe COVID-19 in the intensive care unit: A proof-of-concept study.* EClinicalMedicine, 2020. **28**: p. 100590.
237. Mansour, E., et al., *Safety and Outcomes Associated with the Pharmacological Inhibition of the Kinin-Kallikrein System in Severe COVID-19.* Viruses, 2021. **13**(2).
238. *<DIALLELIC POLYMORPHISM MAY EXPLAIN VARIATIONS OF THE BLOOD CONCENTRATION OF MANNAN-BINDING PROTEIN IN ESKIMOS, BUT NOT IN BLACK AFRICANS.pdf>.*
239. RCPCH. *Paediatric multisystem inflammatory syndrome temporally associated with COVID-19 (PIMS) - guidance for clinicians.* 2020 [cited 2021 17th March 2021]; Available from: https://www.rcpch.ac.uk/resources/paediatric-multisystem-inflammatory-syndrome-temporally-associated-covid-19-pims-guidance
240. Ip, W.K., et al., *Mannose-binding lectin in severe acute respiratory syndrome coronavirus infection.* J Infect Dis, 2005. **191**(10): p. 1697-704.
241. Hogan, C.A., et al., *High Frequency of SARS-CoV-2 RNAemia and Association With Severe Disease.* Clinical infectious diseases : an official publication of the Infectious Diseases Society of America, 2021. **72**(9): p. e291-e295.
242. Ip, W.K., et al., *Mannose-binding lectin enhances Toll-like receptors 2 and 6 signaling from the phagosome.* J Exp Med, 2008. **205**(1): p. 169-81.

243. Johnson, S.C., *Hierarchical clustering schemes.* Psychometrika, 1967. **32**(3): p. 241-254.
244. Lance, G.N. and W.T. Williams, *A General Theory of Classificatory Sorting Strategies: 1. Hierarchical Systems.* The Computer Journal, 1967. **9**(4): p. 373-380.
245. Bar-Joseph, Z., D.K. Gifford, and T.S. Jaakkola, *Fast optimal leaf ordering for hierarchical clustering.* Bioinformatics, 2001. **17**(suppl_1): p. S22-S29.
246. Virtanen, P., et al., *SciPy 1.0: fundamental algorithms for scientific computing in Python.* Nature Methods, 2020. **17**(3): p. 261-272.
247. Waskom, M., *seaborn: statistical data visualization.* The Journal of Open Source Software, 2021. **6**: p. 3021.
248. Hunter, J.D., *Matplotlib: A 2D Graphics Environment.* Computing in Science & Engineering, 2007. **9**(3): p. 90-95.